

Scientific Report  
2007-2009



SCUOLA  
NORMALE  
SUPERIORE  
PISA

*Coordinamento e revisione*

Pasqualantonio Pingue  
Chiara Spinelli

*Progetto grafico e realizzazione*

Gianfranco Adornato  
Marina Berton  
Michele Fiaschi  
Andrea Freccioni  
Daniele Leccese  
Bruna Parra

*Stampa*

Bandecchi e Vivaldi

## Table of contents

Introduction	3
NEST Staff	5
NEST Students/Graduates	7
Research activity	9
SAW-driven electron dynamics in nanostructures	13
Terahertz quantum cascade lasers	17
Transport phenomena in self-assembled nanowires	21
Selective control of quantum Hall edge-channel trajectories by scanning gate microscopy	25
Evidence for a first-order quantum phase transition of excitons in semiconductor bilayers	29
Intersubband polaritonics	31
Quantum properties of hybrid and superconducting structures	35
Probing collective modes of correlated states of few electrons in quantum dots	39
Low-dimensional In-based semiconductor systems	41
Graphene and artificial graphene	43
Electronic states and quantum transport in graphene ribbons	47
Interferometry and entanglement detection at the nanoscale	51
Solid-state quantum information	55
Silicon-Germanium heterostructures for optoelectronic devices	59
Thermal properties at the nanoscale: cooling and nonequilibrium	63
Quantum transport in hybrid normal-superconductor nanostructures	67
Surface-acoustic-wave driven lab-on-chip technologies	71
Monitoring brain function by <i>in vivo</i> 2-photon microscopy	75
E <sup>+</sup> GFP: protein nanodevices tailored for intracellular biosensing	79
Nanotechnology for guided cell differentiation	83
Fluorescent proteins for multiphoton and super-resolution imaging	87
Modeling macro-biomolecules	91
Nanotechnology for intracellular delivery and targeting of drugs, nanoreporters and nanoactuators	95
Cold Atoms	99
New experimental techniques	101
Differential Near Field Scanning Optical Microscope (DNSOM)	103
Growth of semiconductor nanowires	105
NEST facilities	107
Publications	113



## Scientific Report 2007-2009

NEST, the National Enterprise for nanoScience and nanoTechnology, is an interdisciplinary research and training centre where physicists, chemists and biologists investigate scientific issues at the nanoscale. It was jointly established by Scuola Normale Superiore and Istituto Nazionale per la Fisica della Materia (now part of the Consiglio Nazionale delle Ricerche) in 2001 and is located in the San Silvestro building (<http://www.laboratorionest.it/gallery>).

NEST was designed with the twofold objective to support the educational program of Scuola Normale in nanoscience and to join efforts with CNR for the establishment of an advanced research center in nanoscience and nanotechnology. This concentration of resources allows NEST scientist and students to address a rather broad range of research activities that span from semiconductor/superconductor nanostructure design, growth and experimental investigation, to single-molecule studies in live cells and tissues. Despite this broad scope, NEST scientists adopt a unified approach thanks to the close cultural integration of its multidisciplinary teams which is peculiar to nanoscience. Funding was provided by a range of institutions and agencies under a variety of projects and collaboration programs. Scuola Normale Superiore, Consiglio Nazionale delle Ricerche, and Fondazione Monte dei Paschi di Siena deserve a special mention for their institutional support that was instrumental in giving NEST scientists the competitive edge to successfully participate to a number European and Italian calls and ensure a lively, rapidly-developing environment.

In 2009, the last year covered by this report, the NEST initiative was further strengthened by the partnership with the Istituto Italiano di Tecnologia. IIT established within the San Silvestro facility its IIT@NEST, Center for Nanotechnology Innovation and approved a significant five-year funding program that will much expand the scope and intensity of nanoscience research at NEST. I am confident that the next Activity Report will show the positive impact of this institutional partnership.

In a way this report closes a first phase of the NEST program and represent the fulfillment of the goals jointly set by SNS and INFN in 2001: the following pages show the main achievements of these last three years.

Prof. Fabio Beltram  
Director  
Laboratorio NEST



## NEST Staff

DIRECTOR	Fabio Beltram	SNS
CHIEF OPERATING OFFICER	Pasqualantonio Pingue	SNS
SECRETARIAT	Paola Crasta	SNS
	Daniela Lalli	SNS
	Patrizia Pucci	CNR
	Antonella Sagramoni	SNS
RESEARCH DIRECTORS/FULL PROFESSORS	Rosario Fazio	SNS
	Giuseppe Grosso	CNR
	Lucia Sorba	CNR
	Alessandro Tredicucci	CNR
SENIOR SCIENTISTS/ASSOCIATE PROFESSORS	Daniele Arosio	CNR
	Stefan Heun	CNR
	Vittorio Pellegrini	CNR
	Gianmichele Ratto	CNR
	Francesco Tafuri	CNR
	Mauro Tonelli	CNR
SCIENTISTS	Ranieri Bizzarri	SNS
	Marco Cecchini	CNR
	Alessandro Cresti	SNS
	Fabrizio Dolcini	SNS
	Emilio Doni	CNR
	Aldo Ferrari	SNS
	Francesco Giazotto	CNR
	Vittorio Giovannetti	SNS
	Stefano Luin	SNS
	Riccardo Nifosi	CNR
	Vincenzo Piazza	SNS
	Marco Polini	SNS
	Walter Rocchia	SNS
	Stefano Roddaro	SNS
	Michela Serresi	SNS
	Fabio Taddei	CNR
	Valentina Tozzini	CNR
	Stefano Veronesi	CNR

<i>NEST Staff</i>		
TECHNOLOGISTS	Franco Carillo	SNS
	Daniele Ercolani	SNS
TECHNICAL STAFF	Pietro Barnini	SNS
	Paolo Faraci	SNS
	Bruno Guidi	SNS
	Claudio Lelli	SNS
	Riccardo Pallini	CNR
POST-DOCTORAL FELLOWS	Amit Agarwal	SNS
	Aji Anappara Akhileswaran	SNS
	Alberto Albanese	SNS
	David Barate	SNS
	Igor Batov	SNS
	Subhajit Biswas	SNS
	Detlef Born	SNS
	Riccardo Degl'innocenti	SNS
	Armida Di Fenza	SNS
	Cesar Pascual Garcia	SNS
	Richard Green	SNS
	Sokratis Kalliakos	SNS
	Biswajit Karmakar	SNS
	Silvia Landi	SNS
	Lukas Mahler	SNS
	Didier Nicholas	SNS
	Daniela Parisi	SNS
	Elena Putignano	SNS
	Orlando Quaranta	CNR
	Ranjana Sahai	SNS
Giovanni Signore	CNR	
Achintya Singha	CNR	
Michele Virgilio	CNR	
Jihua Xu	SNS	

## NEST Undergraduate / Graduate students

2007-2008-2009

Lorenzo Albertazzi	SNS
Pietro Amat	SNS
Andrea Arcangeli	Università di Pisa
Leonardo Bartoloni	SNS
Mara Barucco	SNS
Alice Bolcioni	SNS
Marco Brondi	SNS
Andrea Callegari	SNS
Francesco Cardarelli	SNS
Cosimo Mauro	SNS
Daniele Costantini	Università di Pisa
Giorgio De Simoni	SNS
Giuseppe De Vito	SNS
Fabio Deon	SNS
Alessandro Farace	SNS
Steven Forti	Università di Trento
Simone Gasparinetti	SNS
Marco Gibertini	SNS
Ef시오 Gigliotti	Università di Pisa
Sarah Goler	SNS
Sebastian Grubel	Università di Göttingen
Roberta Guldani	SNS
Sara Guidi	SNS
Giacomo Lanza	SNS
Ang Li	SNS
Emanuela Ligarò	Università di Pisa
Tonia Losco	SNS
Laura Marchetti	SNS
Matilde Marchi	SNS
Luca Masini	SNS
Davide Massarotti	Università di Napoli
Riccardo Metere	Università di Pisa
Sandro Meucci	Università di Pisa
Domenico Montemurro	SNS
Michele Montinaro	Università di Pisa

---

*NEST Undergraduate / Graduate students*

---

Gianpaolo Papari	Università di Napoli
Nicola Paradiso	SNS
Sebastiano Peotta	SNS
Andrea Pescaglino	Università di Pisa
Giovanni Pizzi	SNS
Sanghamitra Pradhan	SNS
Alessandro Principi	Università di Pisa
Giulia Privitera	SNS
Rosario Elio Profumo	Università di Pisa
Stefano Pugnetti	SNS
Diego Rainis	SNS
Fernanda Ricci	SNS
Lorenzo Romeo	SNS
Cinzia Rotella	Università di Pisa
Fabrizio Salomone	SNS
Diego Scarabelli	SNS
Ugo Siciliani de Cumis	SNS
Daniela Stornaiuolo	Università di Napoli
Barbara Storti	SNS
Elia Strambini	SNS
Sebastian Sulis Sato	SNS
Stefano Tirelli	Università di Pisa
Andrea Tomadin	SNS
Fabio Trovato	SNS
Andrea Ursic	SNS
Stefano Valentini	SNS
Giuseppe Valletta	SNS
Valerio Voliani	SNS

## Research activity

SAW-driven electron dynamics in nanostructures	13
Terahertz quantum cascade lasers	17
Transport phenomena in self-assembled nanowires	21
Selective control of quantum Hall edge-channel trajectories by scanning gate microscopy	25
Evidence for a first-order quantum phase transition of excitons in semiconductor bilayers	29
Intersubband polaritonics	31
Quantum properties of hybrid and superconducting structures	35
Probing collective modes of correlated states of few electrons in quantum dots	39
Low-dimensional In-based semiconductor systems	41
Graphene and artificial graphene	43
Electronic states and quantum transport in graphene ribbons	47
Interferometry and entanglement detection at the nanoscale	51
Solid-state quantum information	55
Silicon-Germanium heterostructures for optoelectronic devices	59
Thermal properties at the nanoscale: cooling and nonequilibrium	63
Quantum transport in hybrid normal-superconductor nanostructures	67
Surface-acoustic-wave driven lab-on-chip technologies	71
Monitoring brain function by <i>in vivo</i> 2-photon microscopy	75
E <sup>n</sup> GFP: protein nanodevices tailored for intracellular biosensing	79
Nanotechnology for guided cell differentiation	83
Fluorescent proteins for multiphoton and super-resolution imaging	87
Modeling macro-biomolecules	91
Nanotechnology for intracellular delivery and targeting of drugs, nanoreporters and nanoactuators	95
Cold Atoms	99



## SAW-driven electron dynamics in nanostructures

The acoustoelectric effect is the manifestation of the transport of charge carriers in a piezoelectric semiconductor by means of surface acoustic waves (SAWs). Lattice deformations induced by SAWs in a piezoelectric substrate generate potential waves that can drag electrons resulting in a net dc current or voltage [1] also in an intrinsic medium if electrons are fed into the device by an appropriate injector [2]. In one-dimensional (1D) devices, this effect gives rise to acoustoelectric current quantization [3]: control over the 1D-constriction width allows the accurate determination of the number of electrons packed in each SAW-potential minimum down to single-electron transport. The demonstration of quantized acoustoelectric effect led to the proposal of several innovative devices: converting the flux of individual SAW-driven electrons in a flux of photons by injecting them into a two-dimensional hole gas, would realise an almost ideal single-photon source for quantum-cryptography applications. Additionally, manipulation of single electrons in 1D systems can be exploited to implement scalable quantum-information-processing circuits with solid-state devices. At NEST we are exploring these approaches aiming at the realisation of a high-repetition-rate single-photon source [4] and a solid-state Hadamard gate based on a three-terminal Aharonov-Bohm ring which is investigated in the linear-transport regime.

### SAW-driven single-photon source

Our scheme (Fig. 1a) is based on a  $n$ - $i$ - $p$  planar junction defined in a quantum well in a GaAs/AlGaAs heterostructure: SAWs, propagating from the  $n$ -side of the device to the  $p$ -side drive electrons along the  $i$ -region towards the  $p$ -region where radiative recombination occurs. A 1D constriction will allow controlling the acoustoelectric current down to the single electron regime. In this condition at most one photon per SAW cycle is generated. A  $n$ -region and a  $p$ -region are induced by  $n$ -type and  $p$ -type Ohmic contacts and two top gates that allow inducing in the QW a two-dimensional electron gas (2DEG) and a two-dimensional hole gas (2DHG). The central sections of the gates (Fig. 1a) incorporate narrow structures (NSs) to select a privileged area for  $n$ - $i$ - $p$  conduction that can be electrostatically controlled by a pair of lateral gates (LGs). An interdigitated transducer (IDT), with a resonance frequency of 3.018 GHz, generates SAWs that propagates from the  $n$  to the  $p$  side of the device.

Acoustoelectric transport was probed at 5 K by injecting a constant current into one

of the  $n$ -type contact (the  $n$ -source) while measuring the current flowing out from another contact (the  $n$ -drain). A 2DHG was also induced in the  $p$ -region and a current injected between the  $p$ -source and the  $p$ -drain.

At the IDT resonance, carrier transfer between the two regions is observed as a negative peak in the  $n$ -drain current (Fig. 2a). The electrons transferred into the 2DHG region recombine with holes resulting in a positive peak in the  $p$ -drain current and in an electroluminescence (EL) signal due to electron-hole radiative recombination. Spatially-resolved snapshots of EL emission

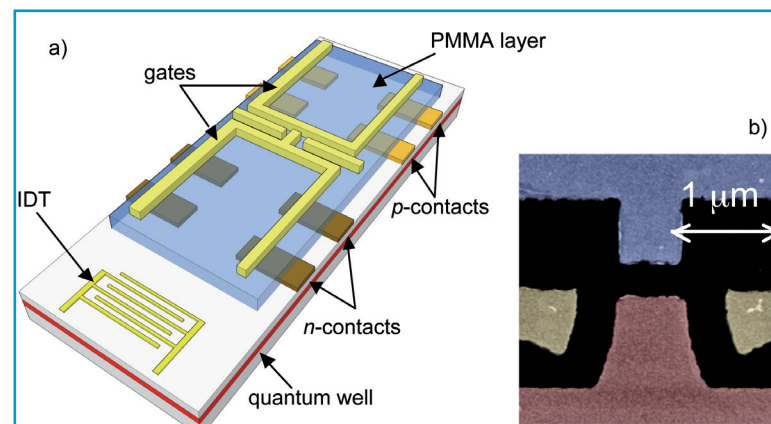


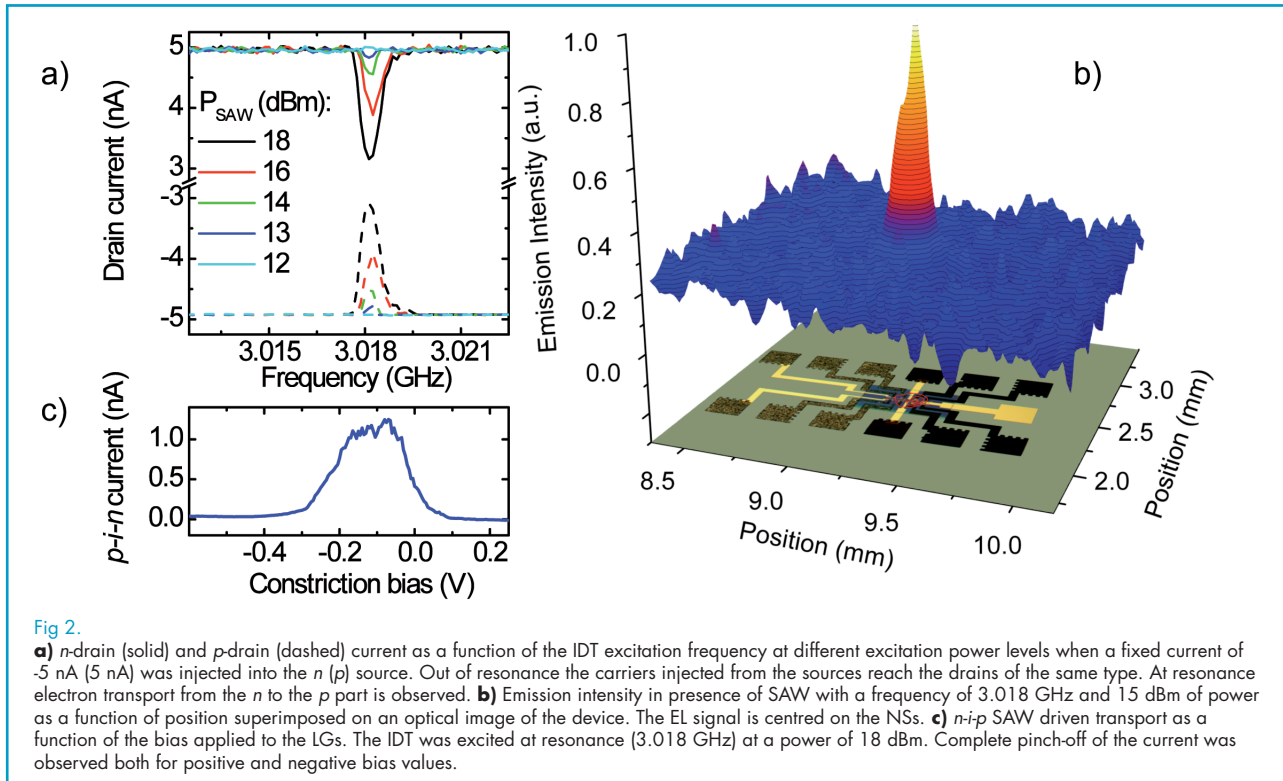
Fig. 1  
a) Schematic view of the SAW-based single photon source. SAWs, generated by the interdigitated transducer (IDT), extract electrons from the  $n$ -type region and drag them to the  $p$  region where radiative recombination occurs. The 1D constriction in the central part of the device allows controlling the current. b) coloured SEM image of the SAW-based device. The red (blue) region is the gate that controls the  $n$ -type ( $p$ -type) side of the junction. Yellow areas are the lateral gates that allow tuning the 1D constriction width.

Vincenzo Piazza

v.piazza@sns.it

#### Collaborators

F. Beltram  
G. Biasiol  
G. De Simoni  
L. Sorba  
E. Strambini



confirm that emission occurs from the NSs (Fig. 2b). Figure 2c shows that the constriction can be narrowed down to complete acoustoelectric-current pinch-off by means of the LGs.

Device optimization is currently being carried out to demonstrate single-photon operation.

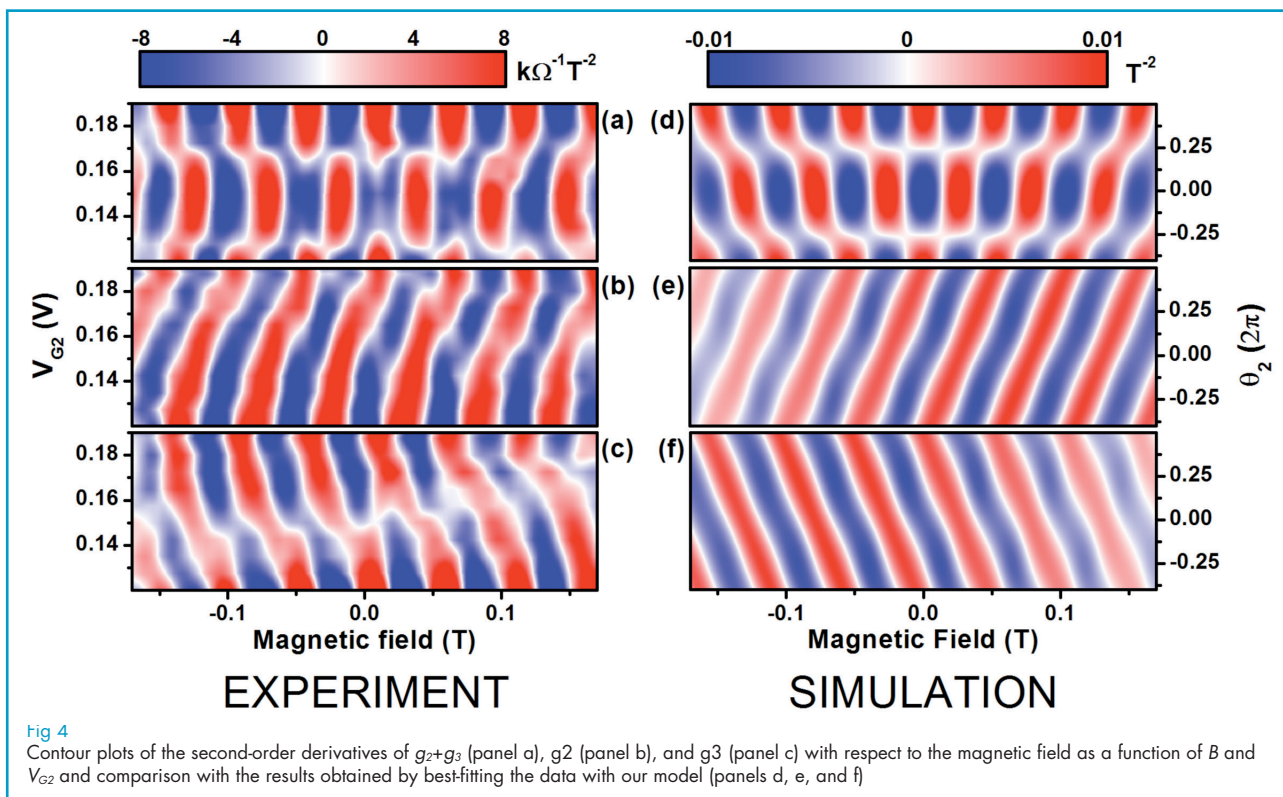
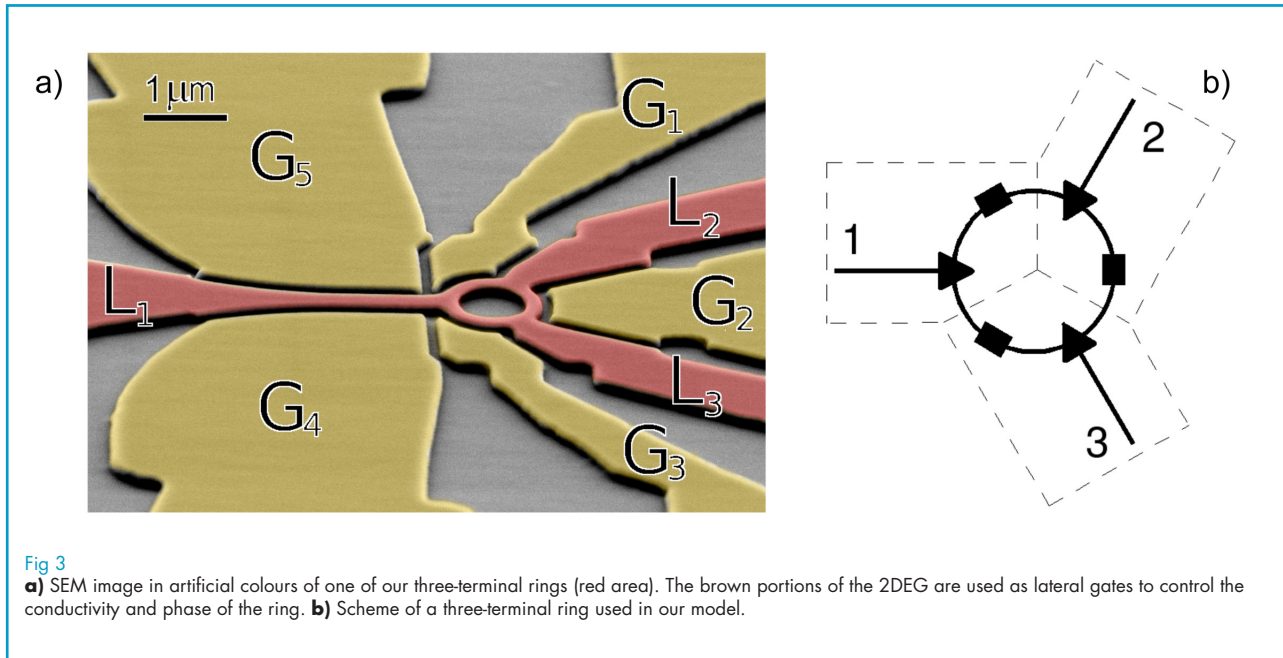
### SAW-driven flying qubits

SAW-driven single-electron wave packets can be used as *flying qubits* in 1D channels [5]. Within this scheme the qubit consists of two adjacent 1D channels, called the 0- and the 1-rail, respectively. The logical state  $|0\rangle$  ( $|1\rangle$ ) is determined by the presence of the SAW-driven single electron in the 0-rail (1-rail) [6]. Our approach exploits the Aharonov-Bohm (AB) effect to allow control on the phase of the electronic wavefunction at the outputs. Multiterminal Aharonov-Bohm rings were theoretically analyzed by means of scattering-matrix approaches in the Landauer-Büttiker framework, free

electron-like node equations, and displaced Gaussian wavefunctions [7,8]. At NEST we extended existing theories based on scattering-matrix approaches by including the effect of decoherence and classical (Lorentz) forces in the description of the system and carried out a comparison against experimental results on real devices by studying the low-temperature coherent-transport properties of three-terminal AB rings. Our analysis shows that the inclusion of these effects is necessary to fully understand the observed phenomenology.

Three-terminal AB rings were fabricated from a two-dimensional electron gas (2DEG) confined in a GaAs/AlGaAs heterostructure (Fig. 3a).

The second derivative of  $g_t = g_2 + g_3$  with respect to  $B$ , where  $g_i = I_i/V_{ex}$ ,  $I_i$  the output current from lead  $i$ , and  $V_{ex}$  the excitation signal applied to  $L_1$ , is reported in Fig. 4a as a function of  $B$  and  $V_{G2}$ , measured at a temperature of  $350$  mK.



It is symmetric with respect to  $B$  in the entire range of gate voltages explored. In the region between  $-0.1$  T and  $0.1$  T abrupt jumps of the oscillation phase from  $0$  to  $\pi$  can be seen at  $V_{G2} = 0.17$  V and  $V_{G2} = 0.125$  V, reminiscent of the phase-rigidity phenomena observed in two-lead,

closed rings [8]. At larger magnetic fields, these phase jumps become smoother, and evolve towards an almost continuous shift of the phase with gate bias. A remarkably different behaviour was observed in the evolution of the individual outputs as a function of  $B$  and  $V_{G2}$ , shown in Fig. 4b

and 4c. In this case, the phase of the oscillations of  $g_2$  evolves almost linearly with  $V_{G2}$  in the entire range of magnetic fields and gate voltages explored.  $g_3$  shows a similar behaviour, but with an opposite dependence of the phase evolution on  $V_{G2}$ .

We schematised our three-terminal rings with the three identical blocks shown in Fig. 3b, where triangles represent three-terminal scatterers and rectangles include the evolution of the wavefunction phase [9]. The effect of the Lorentz force is included

by introducing an asymmetry in the branching probability of each scatterer. Decoherence effects are modelled with absorbers located in the arms: with this approach our model is able to describe the evolution of the coherent part of the wavefunction.

A comparison between simulated and experimental total output of our ring is plotted in Fig. 4. Inspection of this Figure confirms the ability of our model to provide an accurate description of the experimental data.

#### References

- [1] A. Esslinger, A. Wixforth, R.W. Winkler, J. P. Kotthaus, H. Nickel, W. Schlapp, and R. Lsch, *Solid State Commun.* 84, 939 (1992).
- [2] M. Cecchini, G. de Simoni, V. Piazza, F. Beltram, H. E. Beere and D. A. Ritchie, *Appl. Phys. Lett.* 88, 212101 (2006).
- [3] J. M. Shilton, V. I. Talyanskii, M. Pepper, D. A. Ritchie, J. E. F. Frost, C. J. B. Ford, C. G. Smith and G. A. C. Jones, *J. Phys.: Condens. Matter* 8, L531 (1996); J. Cunningham, V. I. Talyanskii, J. M. Shilton, M. Pepper, A. Kristensen and P. E. Lindelof, *Phys. Rev. B* 62, 1564 (2000).
- [4] Giorgio De Simoni, Vincenzo Piazza, Lucia Sorba, Giorgio Biasiol, and Fabio Beltram, *Appl. Phys. Lett.* 94, 121103 (2009).
- [5] A. Bertoni, P. Bordone, R. Brunetti, C. Jacoboni, and S. Reggiani, *Phys. Rev. Lett.* 84, 5912 (2000); C. H. W. Barnes, J. M. Shilton, and A. M. Robinson, *Phys. Rev. B* 62, 8410 (2000).
- [6] R. Ionicioiu, G. Amaratunga, F. Udre, *Int.J.Mod.Phys. B* 15, 125 (2001).
- [7] C. H. Wu and D. Ramamurthy, *Phys. Rev. B* 65, 075313 (2002); 2 D. Ramamurthy, and C. H. Wu, *Phys. Rev. B* 66, 115307 (2002); S. Datta, M. Cahay, and M. McLennan, *Phys. Rev. B* 36, 5655 (1987); M. Cahay, M. McLennan, and S. Datta, *Phys. Rev. B* 37, 10125 (1988); C. H. Wu, and G. Mahler, *Phys. Rev. B* 43, 5012 (1991); B. Szafran and F. M. Peeters, *Europhys. Lett.* 70, 810 (2005).
- [8] A. Yacoby, R. Schuster, and M. Heiblum, *Phys. Rev. B* 53, 9583 (1996); A. Aharony, O. Entin-Wohlman, T. Otsuka, S. Katsumoto, H. Aikawa, and K. Kobayashi, *Phys. Rev. B* 73, 195329 (2006).
- [9] E. Strambini, V. Piazza, G. Biasiol, L. Sorba, and F. Beltram, *Phys. Rev. B* 79, 195443 (2009).

**Q**uantum cascade (QC) lasers [1] are semiconductor devices in which radiation is generated by electronic transitions within an artificial crystal, a so-called heterostructure. This heterostructure consists of alternating layers of two semiconductor materials, with the layer thickness determining the electronic states inside the crystal, and thereby the frequency of the emitted light as well as the electrical transport. The operation of QC lasers in the range of frequencies 1-10 THz was demonstrated in our laboratory, by employing superlattice active material and developing a waveguide concept based on interface modes called surface plasmons [2]. Here we present recent results in the implementation of THz QCLs into advanced photonic structures, allowing the emission of laser light from the surface of the semiconductor, and into external cavity set-ups for improved tuneability.

The present high level of interest in THz laser sources is driven by their many potential applications. These are found in fields such as gas sensing and spectroscopy, the provision of local oscillators for heterodyne detection in astronomy [3], and in advanced imaging techniques. Although each specific application has its own set of associated performance requirements, the majority require single mode laser light, with good beam quality and high powers. The Fabry-Perot cavities commonly used for THz QCLs tend to be intrinsically multi-mode and, equally important, their precise emission frequency cannot be determined a priori by device construction.

Distributed feedback (DFB) resonators were realized in recent past to achieve stable and predictable single mode emission. A number of different approaches were developed, all based on inserting a grating right at the top metal-semiconductor interface [4,5]. Surface-plasmon waveguides, in fact, present the nice feature of having the mode intensity peaked at the surface; any patterning of this interface is then bound to heavily affect the propagating mode. The use of higher order gratings is especially interesting for vertically emitting devices, which would otherwise be impossible, owing to the intersubband selection rules. This aspect is of relevance also to enhance the extraction of light from double-metal waveguides, which is typically quite low due to the impedance mismatch between

the guided mode and free space. We have now applied this concept to whispering gallery microdisk lasers, as exemplified in Fig. 1. By defining a circular second-order metal grating along the circumference, a single lasing whispering gallery mode can be selected and light collected in the vertical direction. Furthermore, the use of gratings with prime number circular symmetry forces the device to operate on the mode with highest vertical outcoupling, providing efficient vertical emission. The measured slope efficiency of 50 mW/A is in fact the largest observed to date for vertically emitting THz QC lasers. The beam profile is also circularly symmetric, which is an important feature for practical use in optical set-ups, and its divergence is mainly determined by the disk size [6].

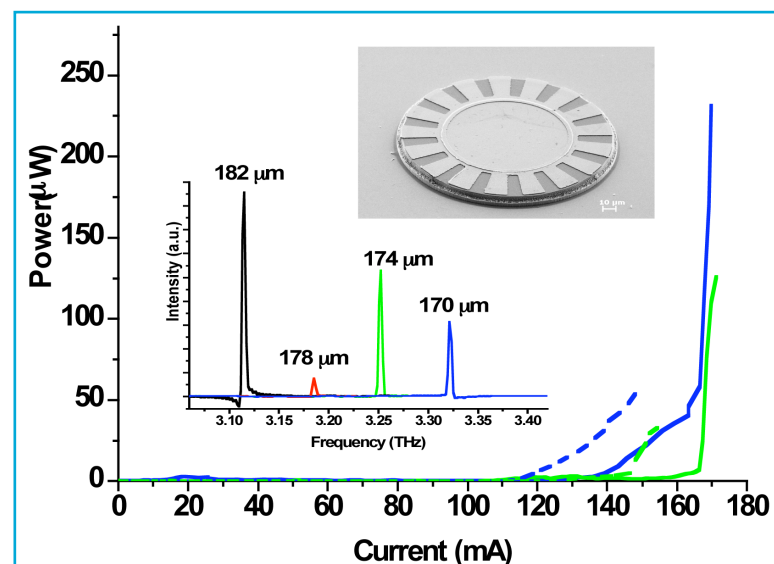
Alessandro Tredicucci

a.tredicucci@sns.it

### Collaborators

M.I. Amanti  
H.E. Beere  
F. Beltram  
R. Degl'Innocenti  
J. Faist  
R. Green  
G. Grosso  
T. Losco  
L. Mahler  
C. Mauro  
G. Pizzi  
A. Pohlkötter  
D.A. Ritchie  
H. Richter  
W. Schade  
A.D. Semenov  
M. Virgilio  
C. Walther  
U. Willer  
B. Witzigmann  
J. Xu

**Fig. 1** Light-current characteristics of  $\sim 3.2$  THz microdisk DFB lasers. Solid lines refer to disks with 17 grating periods, dashed lines to 16. The insets show a SEM picture of the finished device and single-mode emission spectra for disks with different diameter.



To optimize this aspect, we have then modeled and fabricated THz QCLs in a ring DFB resonator of much larger diameter [7]. A second order grating with a double slit configuration was found to offer the best compromise between electrical and optical properties of the top electrode.

Fig. 2 shows the I-L characteristics and the measured far-field of a fabricated device. Even without collection optics employed, the devices show peak powers up to 10 mW, with a slope efficiency of  $\sim 25$  mW/A, demonstrating the good radiative efficiency of this resonator and the directionality of the emitted power.

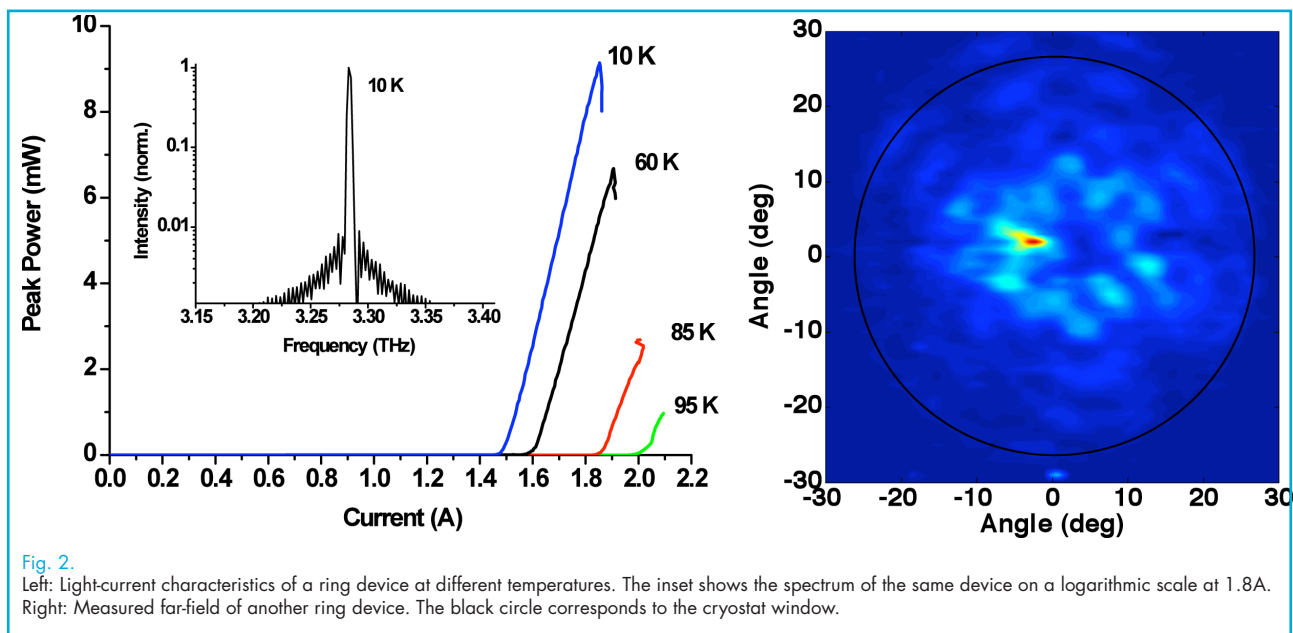


Fig. 2.

Left: Light-current characteristics of a ring device at different temperatures. The inset shows the spectrum of the same device on a logarithmic scale at 1.8 A. Right: Measured far-field of another ring device. The black circle corresponds to the cryostat window.

An alternative concept being investigated is based on quasi-periodic linear gratings generated with a deterministic rule [8]. Single-mode THz lasers have been realized employing a specially designed Fibonacci sequence. High-power collimated emission is achieved at an angle of nearly  $50^\circ$  from the surface normal, tailorable with grating design.

Tuning of the emission line is also an important aspect for spectroscopic applications. We have recently demonstrated the first THz QC lasers operating in an external cavity. A simple configuration with a controllable end mirror placed near the laser facet without collimating optics was adopted, and the emission tuned by changing the cavity length [9]. Typical performances are reported in Fig. 3 for a 4.7 THz laser. At the moment this configuration, while simple, allows tuning ranges of  $\sim 2\%$  of the emission frequency.

Interestingly, a similar set-up has also been used for the first measurement of the linewidth enhancement factor in a THz QC laser using a self-mixing technique [10]. The gain dynamics within the active region of THz QC lasers has been further studied through time-resolved pump-probe measurements of the gain recovery time. These were performed at the FELIX free electron laser source, monitoring the time evolution of the photocurrent induced by the THz pulses in a saturation regime of the transition [11]. The results were consistent with estimates of the electron transit time in the QC superlattice.

The efforts aiming at improving the temperature performance of the lasers are mostly focusing on exploring alternative active region materials. The absence in group IV semiconductors of the electron - longitudinal optical phonon scattering, presently considered the main source of

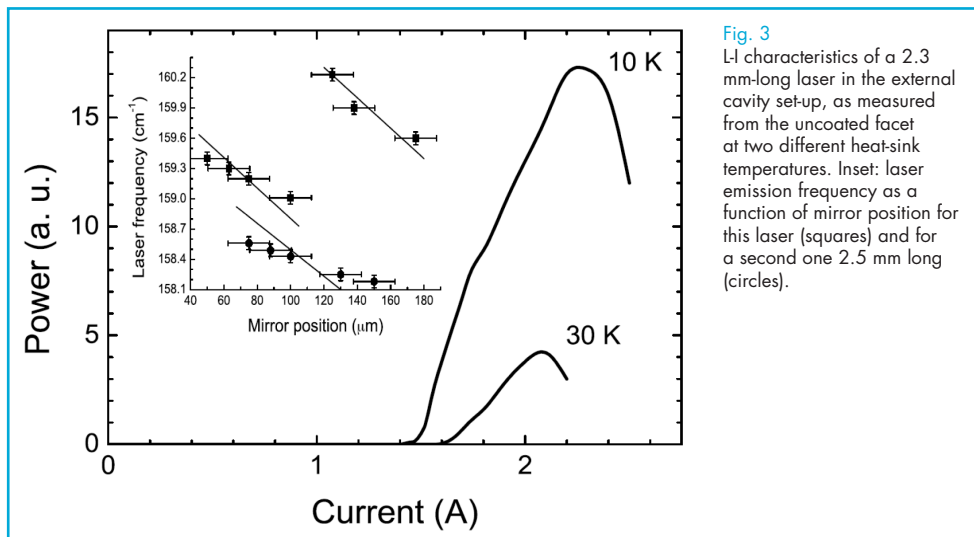


**Fig. 3**  
L-I characteristics of a 2.3 mm-long laser in the external cavity set-up, as measured from the uncoated facet at two different heat-sink temperatures. Inset: laser emission frequency as a function of mirror position for this laser (squares) and for a second one 2.5 mm long (circles).

non-radiative intersubband relaxation for electrons in III-V compounds, should considerably improve carrier lifetimes, leading to larger gain and higher operation temperature. So far, most of the efforts have been focused on hole-based (p-type) SiGe QCLs. This choice has been motivated by the easier procedure for obtaining Si-rich relaxed SiGe virtual substrates (VS), by the relatively high confining potential for holes, and by the smaller hole mass in the tunneling direction. The presence of three different hole subbands, however, makes the p-SiGe QCL design a challenging task. Owing to the much simpler conduction band structure, even in the presence of lattice strain, the concept of an electron-based (n-type) SiGe QCL is now attracting growing attention. As a first step towards the fabrication of a SiGe-based n-type THz QCL, NEST researchers have

evaluated the intersubband transitions in the conduction band of s-Si/SiGe [12] and s-Ge/SiGe [13] multi-QW structures (MQW). The measured absorption energies in the terahertz range are well interpreted by means of tight binding calculations which include self-consistent band-bending, depolarization effects, and provide the conduction band profile and the description of the electronic states throughout the whole Brillouin zone.

Finally, an important portion of THz research at NEST is now devoted to the development of practical applications of the THz quantum cascade technology through their implementation in sensing and imaging systems. In this framework, an imaging set-up based on a novel radiation-pressure detector employing a resonant tuning fork as sensitive element has recently been demonstrated [14].

#### References

- [1] J. Faist *et al.*, "Quantum cascade laser," *Science* 264, 553-556 (1994).
- [2] R. Köhler *et al.*, "Terahertz semiconductor-heterostructure laser," *Nature* 417, 156-159 (2002).
- [3] H. Richter, A. D. Semenov, S. G. Pavlov, L. Mahler, A. Tredicucci, H. E. Beere, D. A. Ritchie, K. S. Il'in, M. Siegel, and H.-W. Huebers, "Terahertz heterodyne receiver with quantum cascade laser and hot electron bolometer mixer in a pulse tube cooler," *Appl. Phys. Lett.* 93, 141108 (2008).
- [4] L. Mahler, A. Tredicucci, R. Köhler, F. Beltram, H.E. Beere, E.H. Linfield, D.A. Ritchie, "High performance operation of single mode terahertz quantum cascade lasers with metallic gratings," *Appl. Phys. Lett.* 87, 181101 (2005).
- [5] L. Mahler, A. Tredicucci, F. Beltram, C. Walther, H. E. Beere, and D. A. Ritchie, "Finite size effects in surface emitting terahertz quantum cascade lasers," *Opt. Express* 17, 6703 (2009).
- [6] L. Mahler, A. Tredicucci, F. Beltram, C. Walther, J. Faist, B. Witzigmann, H. E. Beere, and D. A. Ritchie, "Vertically emitting microdisk lasers," *Nature Photonics* 3, 46 (2009).

- [7] L. Mahler, M. I. Amanti, C. Walther, A. Tredicucci, F. Beltram, J. Faist, H. E. Beere, and D. A. Ritchie, "Distributed feedback ring resonators for vertically emitting terahertz quantum cascade lasers," *Opt. Express* 17, 13031 (2009).
- [8] L. Mahler, A. Tredicucci, R. P. Green, F. Beltram, C. Walther, J. Faist, H. E. Beere, and D. A. Ritchie, "Terahertz quantum cascade lasers with quasi-periodic resonators," *Physica E* 40, 2176 (2008).
- [9] J. Xu, J. M. Hensley, D. B. Fenner, R. P. Green, L. Mahler, A. Tredicucci, M. G. Allen, F. Beltram, H. E. Beere, and D. A. Ritchie, "Tunable terahertz quantum cascade lasers with an external cavity," *Appl. Phys. Lett.* 91, 121104 (2007).
- [10] R. P. Green, J. Xu, L. Mahler, A. Tredicucci, F. Beltram, G. Giuliani, H. E. Beere, and D. A. Ritchie, "Linewidth enhancement factor of terahertz quantum cascade lasers," *Appl. Phys. Lett.* 92, 071106 (2008).
- [11] R. P. Green, A. Tredicucci, N. Q. Vinh, B. Murdin, C. Pidgeon, H. E. Beere, and D. A. Ritchie, "Gain recovery dynamics of a terahertz quantum cascade laser," *Phys. Rev. B* 80, 075303 (2009).
- [12] G. Ciasca, M. De Seta, G. Capellini, F. Evangelisti, M. Ortolani, M. Virgilio, G. Grosso, A. Nucara, and P. Calvani, "THz intersubband absorption and conduction band alignment in n-type Si/SiGe multi-quantum wells," *Phys. Rev. B* 79, 085302 (2009).
- [13] M. De Seta, G. Capellini, Y. Busby, F. Evangelisti, M. Ortolani, M. Virgilio, G. Grosso, G. Pizzi, A. Nucara and S. Lupi, "Conduction-band intersubband transitions in Ge/SiGe quantum wells," *Appl. Phys. Lett.* 95, 051918 (2009).
- [14] U. Willer, A. Pohlkötter, W. Schade, J. Xu, T. Losco, R. P. Green, A. Tredicucci, H. E. Beere, and D. A. Ritchie, "Resonant tuning fork detector for THz radiation," *Opt. Express* 17, 14069 (2009).

## Transport phenomena in self-assembled nanowires

**S**elf-assembled nanowires (NWs) are emerging as a versatile and powerful tool for the study of transport phenomena at the nanoscale. NWs can be shaped in the form of complex axial and radial heterostructures in which normally incompatible materials can be combined into advanced – in some cases unprecedented – nanostructures. Such a level of flexibility makes it possible to explore innovative research directions. In particular, NW activities at NEST are presently focusing on the investigation of the interplay between nanomechanics and charge transport in self-assembled structures as well as Josephson coupling in devices combining superconductive elements and InAs/InP and InSb nanostructures.

NWs represent a promising example of the bottom-up approach to nanoscience and technology [1-4]. The vapor-liquid-solid growth mechanism at the basis of NW technology makes it possible to design and fabricate in a very controllable way complex nanometer-scale structures without the need of delicate patterning procedures typical of any top-down approach. This allows the parallel and large scale fabrication of high-quality nanostructures and opens the way to cheap production of advanced nanomaterials and nanodevices. Research activities on NWs started at NEST in 2008, in parallel with the installation of a chemical beam epitaxy facility (see Activity Report X.Y) dedicated to the growth of InAs/InP and InSb semiconducting NWs. Nanostructures are being experimentally studied with two main objectives: (i) investigate the interaction between nanomechanical degrees of freedom and charge transport; (ii) investigate charge and heat transport at the nanoscale.

The first aim has started to be pursued in mid 2008 at NEST thanks to the project "Acoustoelectrics in self-assembled one-dimensional semiconductors" funded by INFN-CNR. The research initiative led to the design and fabrication of InAs NW-based field effect transistors (FETs) on GaAs and LiNbO<sub>3</sub> piezoelectric substrates. These devices were used to investigate the influence of surface acoustic waves (SAWs) – excited on the substrate

by means of interdigital transducers – on charge transport in the NWs. A typical InAs FET on LiNbO<sub>3</sub> is visible in Fig.1a while an example of SAW-induced charge pumping can be seen in panel (b). In the studied devices both the piezoelectric potential associated to the SAW and the actual nanomechanical deformation of the NW can have an influence on free carriers in the nanostructure. Having successfully demonstrated the control of the NW electron system by SAW excitation [5], these results open the way to new single-electron pumping schemes which can have an impact for what concerns both metrology and the development of high-throughput single-photon sources. In order to reach these objectives, engineered InAs/InP nanostructures containing multiple barriers and quantum dots [6] are being investigated, in order to integrate them on LiNbO<sub>3</sub> and to achieve a precise quantization of the number of charges pumped per SAW cycle. Such advanced NW heterostructures are being routinely fabricated at the NEST Center thanks to its new facility for chemical beam epitaxy of III-V semiconductors [7].

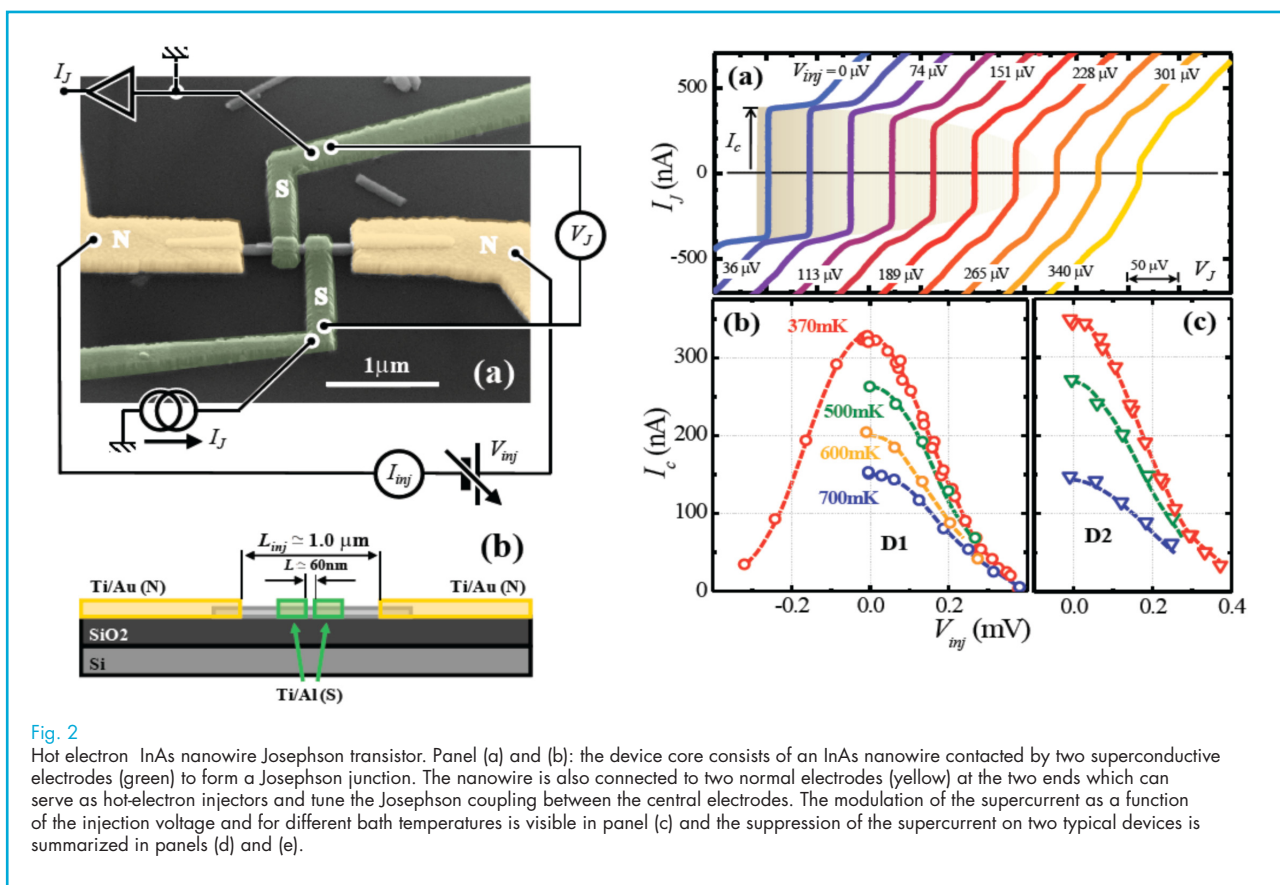
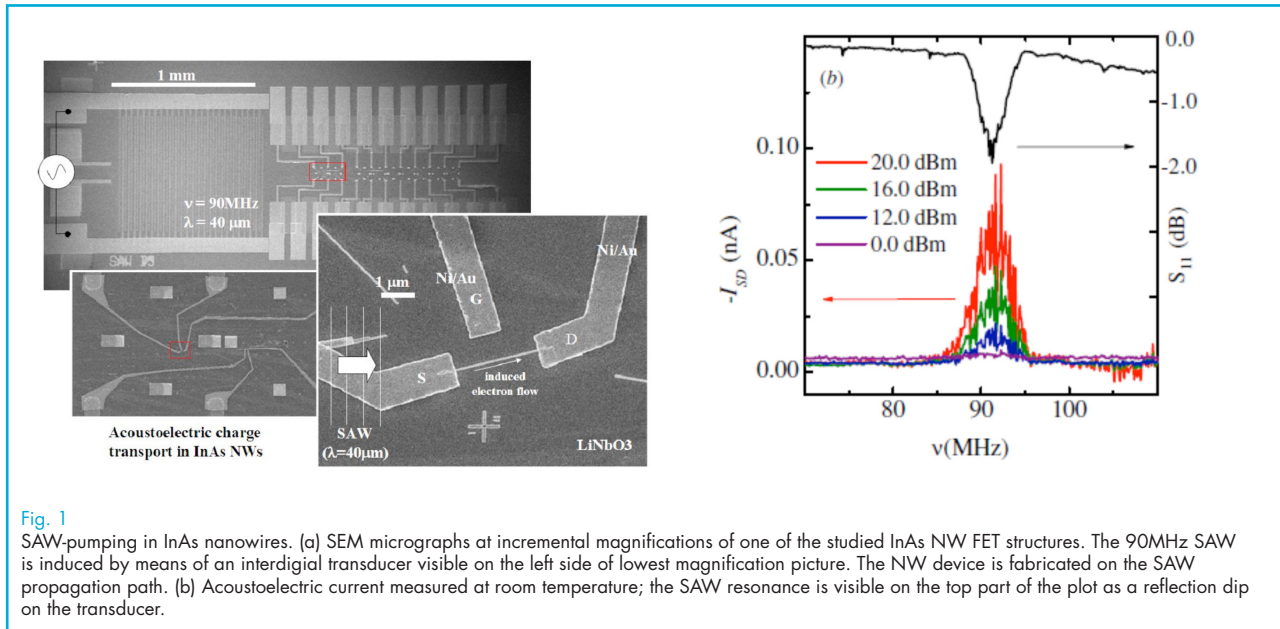
The second key target of the research activity – the study of charge and heat transport in nanoscale self-assembled structures – is being pursued by the development of hybrid devices combining InAs/InP and InSb NWs with superconductive elements. Figure 2a shows one of the concept devices which are being investigated at NEST: a hot-

Stefano Roddaro

s.roddaro@sns.it

### Collaborators

F. Beltram  
S. Biswas  
F. Giazotto  
A. Pescaglioni  
L. Romeo  
L. Sorba



electron Josephson transistor. The device, developed in 2009, consists of a Josephson junction which is formed by an InAs NW channel contacted by two superconductive leads (green) and which can be controlled

very efficiently by the injection of out-of-equilibrium carriers from normal-state control electrodes (yellow) fabricated at the two ends of the NW. Superconductive elements can play different crucial roles

in this sort of nanostructures [8]. When a superconductor is put in contact with a normal region through a transparent interface, pairing correlations leak out on the normal side and induce new transport properties and make it possible, for instance, to observe a Josephson current in a normal-state conductor, as in the case of Fig.2. In addition, superconductors can also play a key role as energy filters and as low-thermal conductivity electron leads.

In the device of Fig.2a they thus also allow to easily bring out of equilibrium the central section of the NW and to observe a marked suppression of the supercurrent for an injection voltage of barely few hundred of microVolts (see Fig.2b). These results are the basis of a wider research activity involving more advanced InAs/InP quantum systems, which open the way to a number of concept devices with an impact both in terms of fundamental physics and low-temperature applications [8].

#### References

- [1] C.M.Lieber "Nanoscale science and technology: Building a big future from small things", MRS Bulletin 28, 486 (2003).
- [2] M.T. Bjork *et al.* "One-dimensional steeplechase for electrons realized", Nano Lett. 2, 87 (2002).
- [3] S. Roddaro *et al.* "InAs nanowire metal-oxide-semiconductor capacitors", Appl. Phys. Lett. 92, 253509 (2008).
- [4] S. Roddaro *et al.* "Spin states of holes in Ge/Si nanowire quantum dots", Phys. Rev. Lett. 101, 186802 (2009).
- [5] S. Roddaro *et al.* "Charge pumping in InAs nanowires by surface acoustic waves", Semicond. Sci. Technol. 25, 024013 (2010).
- [6] J. Salfi *et al.* "Electronic properties of quantum dot systems realized in semiconductor nanowires" Semicond. Sci. Technol. 25, 024007(2010).
- [7] D. Ercolani *et al.* "InAs/InSb nanowire heterostructures grown by chemical beam epitaxy", Nanotech. 10, 505605 (2009).
- [8] F. Giazotto *et al.* "Opportunities for mesoscopics in thermometry and refrigeration: Physics and applications", Rev.Mod.Phys. 78, 217 (2006).



## Selective control of quantum Hall edge-channel trajectories by scanning gate microscopy

**E**lectronic Mach–Zehnder interferometers in the quantum Hall regime are currently discussed for the realization of quantum information schemes. A recently proposed device architecture employs interference between two co-propagating edge channels (see the report of V. Giovannetti). Here we demonstrate the precise control of individual edge-channel trajectories in quantum point contact devices in the quantum Hall regime. The biased tip of an atomic force microscope is used as a moveable local gate to pilot individual edge channels. Our results are discussed in light of the implementation of multi-edge interferometers.

Stefan Heun

stefan.heun@sns.it

### Collaborators

F. Beltram  
G. Biasiol  
N. Paradiso  
L.N. Pfeiffer  
S. Roddaro  
L. Sorba  
K.W. West

Interference phenomena are a fundamental manifestation of the quantum mechanical nature of electrons and have promising applications in solid-state quantum information technology. Two-dimensional electron systems (2DES) in the quantum Hall (QH) regime are especially suited for this purpose given the large electronic coherence length characteristic of edge-channel chiral transport. In particular, the realization of electronic Mach–Zehnder (MZ) interferometers in QH systems appears at present a sound technology for the implementation of quantum information schemes [1]. Despite this success, the edge topology of the single-channel MZ limits the complexity of these circuits to a maximum of two interferometers [2]. In order to overcome this constraint, new device architectures were recently proposed [3], where interference paths are built using two different parallel edge channels. In this configuration, control over the interaction between the different edge channels is challenging owing to the complexity of the edge structure. In order to address these issues we are exploring the use of scanning gate microscopy (SGM) to control the trajectory and interaction of edge channels based on our previous results on quantum point contact (QPC) devices in the QH regime [4–7]. In the present work, the two split gates of the QPC play a double role: they not only allow us to bring the edges in close

proximity, but they also provide the ability to select the edges that are sent to the center of the QPC.

Experiments were performed in the new SGM laboratory at NEST (Fig. 1a). The activity is aimed at combining our experience with transport properties of nanostructures with the opportunity of investigation offered by scanning probe microscopy operating at ultra-low temperature (300mK), in a magnetic field tunable up to 9T. The recently installed instrument allows to locally apply an electric potential by means of the conductive tip of an atomic force microscope (AFM) operating in non-contact mode. The



Fig. 1  
(a) The new SGM lab at NEST. (b) The AFM head for SGM measurements.

fundamental element of our SGM system is the AFM head (Fig. 1b). The upper part contains the sample holder with the wires for transport measurements. This is placed on a stack of piezo actuators providing the coarse and fine positioning of the sample, which allow sample movements of several millimeters with a sub-micron resolution and reproducibility. The lower part of the AFM head contains the tuning fork with the conductive tip, which allows us to both measure the sample topography and to apply a local potential. Our setup is also equipped with a STM head, which is capable of obtaining topographic images of conductive samples with atomic resolution. Both the AFM and the STM heads are non-magnetic (all the metallic parts are in titanium) and are designed to suitably work either at ultralow temperature or at room temperature. They are mounted to the cold finger of a 3He cryostat. The cryostat is inserted in a dewar suspended by means of springs in a soundproofed box in order to damp mechanical and acoustical noise. For low temperature operations a magnetic field up to 9 T is provided by a superconducting coil placed at the bottom of the dewar.

In order to validate our microscope setup we performed SGM measurements on QPCs at zero magnetic field. When the QPC conductance is quantized, the depletion spot induced by the tip causes a backscattering of electrons through the QPC [8,9]. When the tip is located above areas with high electron flow, the conductance is reduced by this effect,

while it remains constant over areas with small electron flow. Scanning the tip over the sample yields therefore images of electron flow. The conductance map in Fig. 2 shows the characteristic branched flow of electrons. These branches correspond to the paths of lowest energy for the electrons moving in the potential landscape of the 2DES. They extend over a length scale of about  $5\mu\text{m}$  due to the high mobility of the 2DES. The fringes decorating these structures are separated by half the Fermi wavelength. This can be better seen in the inset of Fig. 2 which shows a high-resolution image of one of the branches. The fringes are clearly resolved. They are due to the interference between time-reversed electron paths from the QPC and from the depletion spot generated by the AFM tip.

The present work is aimed at exploring the use of SGM to control the trajectory and the interaction of edge channels in the QH regime. The fundamental idea behind our experiments consists in exploiting the QPC not only to control the distance between counterpropagating edges (as in tunnelling experiments [6,7]) but also to set the number of edges flowing around each of the two split gates. An essential role here is played by the SGM tip, which is exploited first to determine the filling factor underneath the two split gates and then to put the selected edge states in interaction. All the experiments discussed in the following were performed at bulk 2DES filling factor  $\nu = 4$ . Since at this magnetic field the Zeeman splitting is too small to be observed in our experiment, we are studying two spin-degenerate edge channels here.

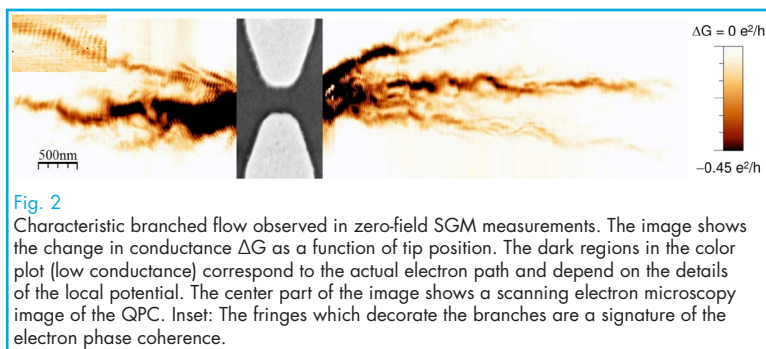
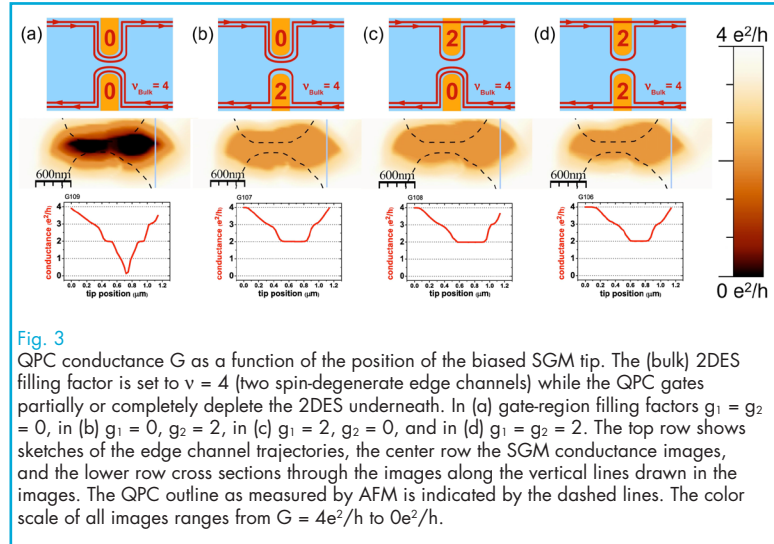


Fig. 3 shows the QPC conductance as a function of the position of the biased SGM tip. In the panel (a) the gate-region filling factors are  $g_1 = g_2 = 0$ . When the biased tip is brought close to the QPC, pairs of edge channels are backscattered one by one, and the conductance through the

QPC decreases in a step-like manner to 0. This clearly demonstrates the gating action of the tip even in the QH regime. Taking advantage of the high flexibility of our setup, we repeated the SGM measurements also in asymmetric configurations such as that shown in the panel (b) of Fig. 3, where  $g_1 = 0$  and  $g_2 = 2$ . In this case, only the pair of inner edge channels is backscattered by the local action of the tip, while the outer edge either flows far from the constriction (under the lower gate) or has no counterpart for the backscattering process to occur (upper gate). In this case, the conductance remains  $G = 2e^2/h$  even when the tip completely pinches off the constriction region. For the mirrored gate configuration in Fig. 3(c) with  $g_1 = 2$  and  $g_2 = 0$ , we obtained similar SGM images. We also studied the configuration depicted in Fig. 3(d) with identical filling factors  $g_1 = g_2 = 2$  under the split-gates. This situation is fundamentally different from the situations in Figs. 3(b) and (c), because here no unpaired edge channel is flowing through the QPC. The resulting SGM image, however, is similar to those shown in Figs. 3(b) and (c). These results clearly show that the lower bound for the conductance is determined by the number of paired edge channels which can be backscattered. We have obtained very similar results for other bulk 2DES



**Fig. 3** QPC conductance  $G$  as a function of the position of the biased SGM tip. The (bulk) 2DES filling factor is set to  $\nu = 4$  (two spin-degenerate edge channels) while the QPC gates partially or completely deplete the 2DES underneath. In (a) gate-region filling factors  $g_1 = g_2 = 0$ , in (b)  $g_1 = 0$ ,  $g_2 = 2$ , in (c)  $g_1 = 2$ ,  $g_2 = 0$ , and in (d)  $g_1 = g_2 = 2$ . The top row shows sketches of the edge channel trajectories, the center row the SGM conductance images, and the lower row cross sections through the images along the vertical lines drawn in the images. The QPC outline as measured by AFM is indicated by the dashed lines. The color scale of all images ranges from  $G = 4e^2/h$  to  $0e^2/h$ .

filling factors ( $\nu = 2$ , 2 spin-resolved edge channels; and  $\nu = 6$ , 3 spin-degenerate edge channels), which underlines the general validity of our findings to edge channels in the QH regime.

In conclusion, we have demonstrated a new method for the control of the trajectories of individual edge channels by the tip of the SGM. Our results can represent a crucial step for the implementation of multi-edge beam mixers and interferometers. We are now working on more refined device geometries to exploit this possibility for a control of the interaction of edge channels in QPC devices in the QH regime.

## References

- [1] Y. Ji, Y. Chung, D. Sprinzak, M. Heiblum, D. Mahalu, H. Shtrikman, *Nature* 422 (2003) 415.
- [2] I. Neder, N. Ofek, Y. Chung, M. Heiblum, D. Mahalu, V. Umansky, *Nature* 448 (2007) 333.
- [3] V. Giovannetti, F. Taddei, D. Frustaglia, R. Fazio, *Phys. Rev. B* 77 (2008) 155320.
- [4] S. Roddaro, V. Pellegrini, F. Beltram, G. Biasiol, L. Sorba, R. Raimondi, G. Vignale, *Phys. Rev. Lett.* 90 (2003) 046805.
- [5] S. Roddaro, V. Pellegrini, F. Beltram, G. Biasiol, L. Sorba, *Phys. Rev. Lett.* 93 (2004) 046801.
- [6] S. Roddaro, V. Pellegrini, F. Beltram, L.N. Pfeiffer, K. W. West, *Phys. Rev. Lett.* 95 (2005) 156804.
- [7] S. Roddaro, N. Paradiso, V. Pellegrini, G. Biasiol, L. Sorba, F. Beltram, *Phys. Rev. Lett.* 103 (2009) 016802.
- [8] M.A. Topinka, B.J. LeRoy, S.E.J. Shaw, E.J. Heller, R.M. Westervelt, K.D. Maranowski, A.C. Gossard, *Science* 289 (2000) 2323.
- [9] M.A. Topinka, B.J. LeRoy, R.M. Westervelt, S.E.J. Shaw, R. Fleischmann, E.J. Heller, K.D. Maranowski, A.C. Gossard, *Nature* 410 (2001) 183.



# Evidence for a first-order quantum phase transition of excitons in semiconductor bilayers

**W**hen dominated by quantum-mechanical fluctuations, ground state transformations display a tendency towards quantum criticality associated with collapse of the characteristic energy scale expressed by softening of low-lying excitation modes. In the presence of competing interactions and weak residual disorder the nature of the quantum phase transition is predicted to become discontinuous as the critical point is approached. The observation of these elusive effects require a fine tuning of the impact of the interaction terms that is difficult to achieve in experiments. We demonstrated that coupled electron bilayers realized in double quantum wells display excitonic and metallic ground states stabilized by different terms of electron interactions that can be tuned with high precision. This competition drives this soft-mode system to undergo a first-order quantum phase transition

Vittorio Pellegrini

vp@sns.it

Collaborators

B. Karmakar  
L. Pfeiffer  
A. Pinczuk  
K. West

In coupled electron bilayers confined in modulation-doped GaAs double quantum wells, the energy levels split into symmetric and anti-symmetric combinations separated by the tunnelling gap  $\Delta_{SAS}$ . In the presence of a quantizing perpendicular magnetic field and at total Landau level filling factor  $\nu_T = n_T 2\pi l_B^2 = 1$  ( $n_T$  is the total electron density in the bilayer and  $l_B$  is the magnetic length), the electron bilayer displays two distinct phases separated by a quantum phase transition (QPT). The two phases result from the competing impacts of inter- and intra-layer electron interaction [1,2] parameterized by  $d/l_B$ ,

where  $d$  is the distance between the two layers and by  $\Delta_{SAS}/E_c$ , where  $E_c = e^2/\epsilon l_B$  ( $\epsilon$  is the dielectric constant) is the intra-layer Coulomb energy [1,3].

At sufficiently low  $d/l_B$  or large  $\Delta_{SAS}/E_c$ , the ground states at  $\nu_T = 1$  are incompressible QH fluids [1,2]. A different phase occurs for low  $\Delta_{SAS}/E_c$  (at sufficiently large  $d/l_B$ ), when intra-layer correlations prevail on the inter-layer correlations. The compressible (non-QH) ground state of this phase is currently described as a Fermi metal of composite fermions (CFs) [4] (see Fig.1). The incompressible phase is also highly correlated and it is populated by coherent

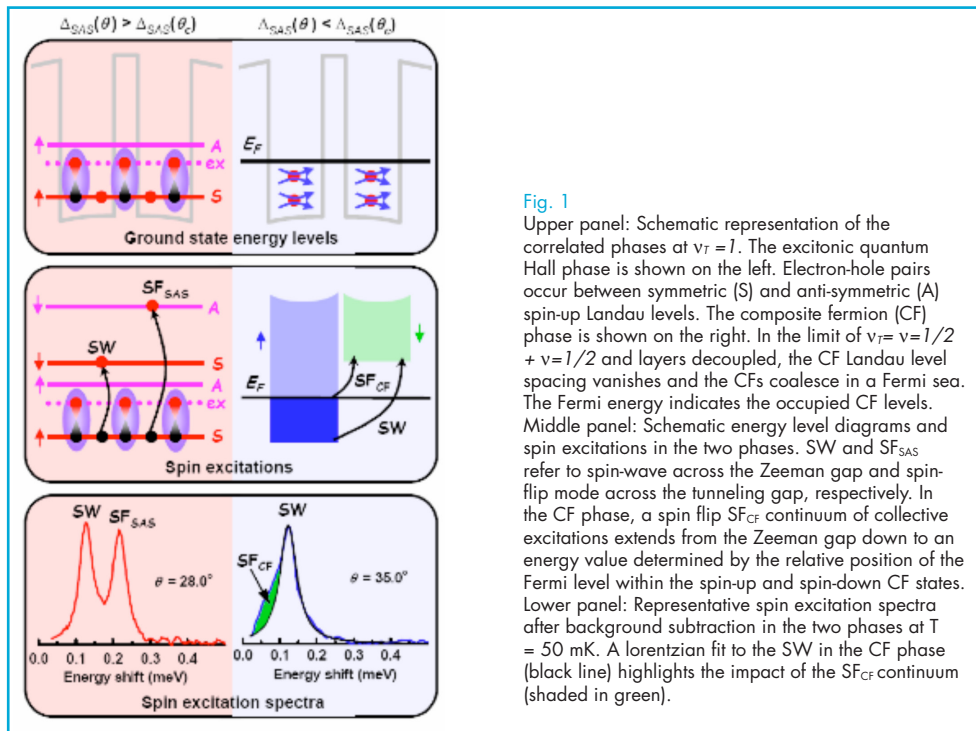
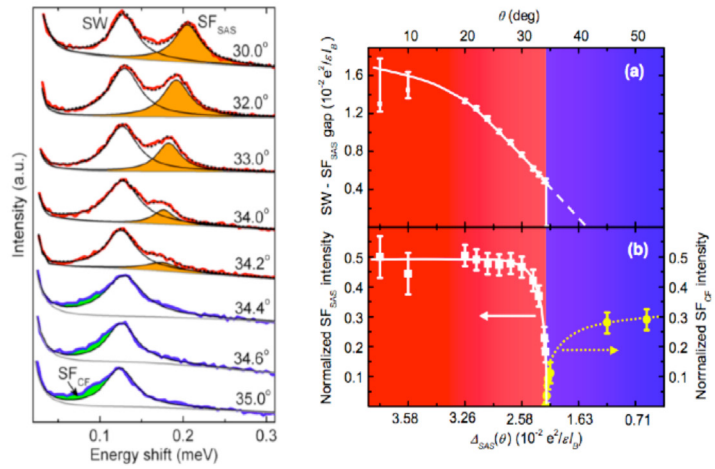


**Fig. 1**  
Upper panel: Schematic representation of the correlated phases at  $\nu_T = 1$ . The excitonic quantum Hall phase is shown on the left. Electron-hole pairs occur between symmetric (S) and anti-symmetric (A) spin-up Landau levels. The composite fermion (CF) phase is shown on the right. In the limit of  $\nu_T = \nu = 1/2 + \nu = 1/2$  and layers decoupled, the CF Landau level spacing vanishes and the CFs coalesce in a Fermi sea. The Fermi energy indicates the occupied CF levels. Middle panel: Schematic energy level diagrams and spin excitations in the two phases. SW and  $SF_{SAS}$  refer to spin-wave across the Zeeman gap and spin-flip mode across the tunneling gap, respectively. In the CF phase, a spin flip  $SF_{CF}$  continuum of collective excitations extends from the Zeeman gap down to an energy value determined by the relative position of the Fermi level within the spin-up and spin-down CF states. Lower panel: Representative spin excitation spectra after background subtraction in the two phases at  $T = 50$  mK. A Lorentzian fit to the SW in the CF phase (black line) highlights the impact of the  $SF_{CF}$  continuum (shaded in green).

Fig. 2

Left panel: Angular dependence of  $SF_{SAS}$  excitation intensity in the excitonic phase (in orange) and the spin-flip continuum  $SF_{CF}$  in the composite-fermion metallic phase (in green). Best fit results to the spectra (dotted lines) with two lorentzians (one in the CF phase) and the magneto-luminescence continuum and laser stray light (solid grey lines) are shown. Right panel: (a) Evolution of the correlated gap of the excitonic phase, i.e. the energy splitting between SW and  $SF_{SAS}$  excitations, as a function of tunnelling gap or tilt angle. The splitting remains finite at the phase boundary between the excitonic phase (red shaded) and the composite fermion metal (blue shaded). (b) Plot of integrated spin-flip excitation intensity. Data corresponds to the  $SF_{SAS}$  (white) and  $SF_{CF}$  (yellow) intensity (solid and dotted lines are guide for the eyes). The values are obtained after normalization with respect to the spin-wave SW intensity to take into account the angular dependence of oscillator strength of spin excitations.



electron-hole excitonic pairs across  $\Delta_{SAS}$  with a density that is a fraction of  $n_T/2$  (see Fig. 1) [5,6]. These two phases display remarkable manifestations in light scattering spectra as shown in Fig.1 lower panels.

We have employed the technique of resonant inelastic light scattering to study the spin excitations in the excitonic and CF phases, as shown in the middle panels of Fig.1 and determine the character of the QPT in bilayers. Measurements were performed on the sample mounted on a mechanical rotator in a dilution refrigerator with base temperatures below 100 mK under light illumination. The in-plane magnetic field reduces the tunnelling gap [7]. We reached a precision on angle of  $0.1^\circ$  (precision on  $\Delta_{SAS}/E_c$  of  $1 \times 10^{-4}$ ) enabling the investigation of the evolution of the correlated phases with unprecedented accuracy. Long wavelength spin excitations were measured following the procedure described in Refs. [4,5]. The sample studied in this work is a nominally symmetric modulation-doped  $Al_{0.1}Ga_{0.9}As/GaAs$  double quantum wells grown by molecular beam epitaxy with

$n_T = 1.1 \times 10^{11} \text{ cm}^{-2}$ , mobility above  $10^6 \text{ cm}^2/\text{Vs}$ ,  $d/l_B = 2.18$  ( $d = 25.5 \text{ nm}$  is the interlayer distance and the well width is  $18 \text{ nm}$ ) and  $\Delta_{SAS} = 0.36 \text{ meV}$ .

The data in Fig. 2 demonstrate a QPT linked to the disappearance of the  $SF_{SAS}$  excitation at a finite value of  $\Delta_{SAS}(\theta)$ , which is the correlated gap and order parameter of the excitonic phase [5]. These striking results offer evidence of a first-order character of the transformation [8]. Figure 2 right panel is revealing. The evolution of  $\Delta_{SAS}(\theta)$  in the excitonic phase suggests a continuous QPT at an angle slightly above  $40^\circ$ . There is, however, a marked discontinuity in the value of  $\Delta_{SAS}(\theta)$  (at the critical angle  $\theta_c = 34.2^\circ$ ) that points to a first-order QPT and to a subtle competition of the collective excitonic state with the CF metal phase. First-order transitions in the absence of disorder are predicted in QH insulators [9] in other condensed matter systems [10] and in particle physics [11]. One key property of the electron bilayer system studied here is that the roles of different electron correlation terms at the QPT can be tested by finely tuning their relative strength.

#### References

- [1] G.S. Boebinger, *et al.*, Phys. Rev. Lett. 64, 1793 (1990)
- [2] S.Q. Murphy, *et al.*, Phys. Rev. Lett. 72, 728 (1994)
- [3] K. Yang, *et al.*, Phys. Rev. Lett. 72, 732 (1994)
- [4] B. Karmakar, *et al.*, Solid State Comm. 143, 499 (2007)
- [5] S. Luin, *et al.*, Phys. Rev. Lett. 94, 146804 (2005)
- [6] J. Eisenstein and A. H. MacDonald, Nature 432, 691 (2004)
- [7] J. Hu and A. H. MacDonald, Phys. Rev. B 46, 12554 (1992)
- [8] B. Karmakar, *et al.* Phys. Rev. Lett. 102 036802 (2009)
- [9] L. Pryadko and S.C. Zhang, Phys. Rev. Lett. 73, 3282 (1994)
- [10] C.A. Marianetti, K. Koiliar and G. Ceder, Nature Materials 3, 627 (2004)
- [11] S. Coleman and E. Weinberg, Phys. Rev. D 7, 1888 (1973)

The interaction of light with material excitations has long attracted intense experimental and theoretical investigations. Thanks to the development of epitaxial growth techniques, it is now possible to realize monolithic microcavity structures in which both electrons and photons can be simultaneously confined and their interaction can be manipulated. In a microcavity, the photonic confinement deeply modifies light-matter interaction, and if the coupling strength is sufficiently large compared to the damping rates, new elementary excitations are formed which are mixed electronic and photonic states. The so-called “cavity polaritons” were first observed in solid-state systems employing excitonic states in semiconductors. Recently we demonstrated the strong coupling of the confined electromagnetic radiation with the transitions between the subbands in the conduction band of a GaAs-AlGaAs heterostructure, with the corresponding formation of “intersubband cavity polaritons” [1]. This system is very promising for the achievement of an unprecedented “ultra-strong coupling regime” of light-matter interaction, which is particularly interesting for the peculiar quantum nature of its eigenstates. Furthermore, theoretical predictions show that the ultrafast modulation of polariton coupling can result in the release of correlated photon pairs from the polariton ground state [2], in a process analogous to the dynamic Casimir effect and to Hawking black-hole radiation. Here we present evidence of cavity polaritons established between excited subbands and discuss the measurement of their dispersion [3]. First signatures of ultra-strong coupling contributions to the polariton energies are also reported [4] and non-adiabatic sub-cycle modulation of the coupling strength is demonstrated [5].

In an intersubband microcavity, the vacuum Rabi energy is a measure of the electromagnetic coupling and determines the polaritons energy splitting. It scales as the ratio  $\langle d_{ISBT} \rangle / \sqrt{L_{QW}}$  between the dipole matrix element  $\langle d_{ISBT} \rangle$  and the quantum well thickness  $L_{QW}$ . By judicious design, in larger quantum wells, one can have an increased using the transition from the first excited subband to the next higher subband (levels 2 and 3 in the inset of Fig.1), if the wells are doped so that the electron Fermi energy  $E_F$  is above level 2. The

angle-resolved reflectance measurements of a  $70^\circ$  prism-shaped sample with  $3.7 \times 10^{18} \text{ cm}^{-3}$  n-doped active region at liquid helium temperature are reported in Fig. 1. Two dips corresponding to the lower and upper polaritons are clearly observed, exhibiting a minimum splitting of about 40 meV, at an internal angle of about  $63.5^\circ$ . The splitting increases to about 52 meV at 300 K [3]. In order to extract precise information on the strength of the optoelectronic interaction, one should express the polariton dispersion

Alessandro Tredicucci

a. tredicucci@sns.it

### Collaborators

A. Anappara  
 A. Baranov  
 D. Barate  
 F. Beltram  
 G. Biasiol  
 C. Ciuti  
 R. Degl'Innocenti  
 S. De Liberato  
 J. Devenson  
 E. Gigliotti  
 G. Günter  
 J. Hees  
 R. Hüber  
 A. Leitenstorfer  
 A. Sell  
 L. Sorba  
 R. Teissier

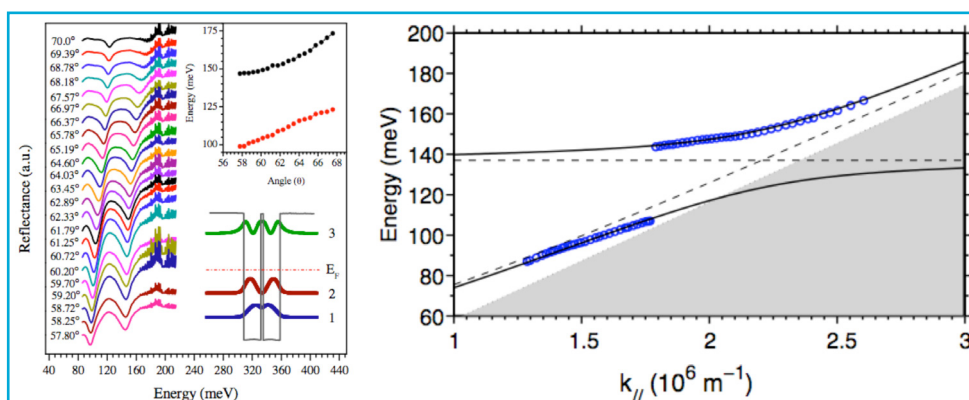
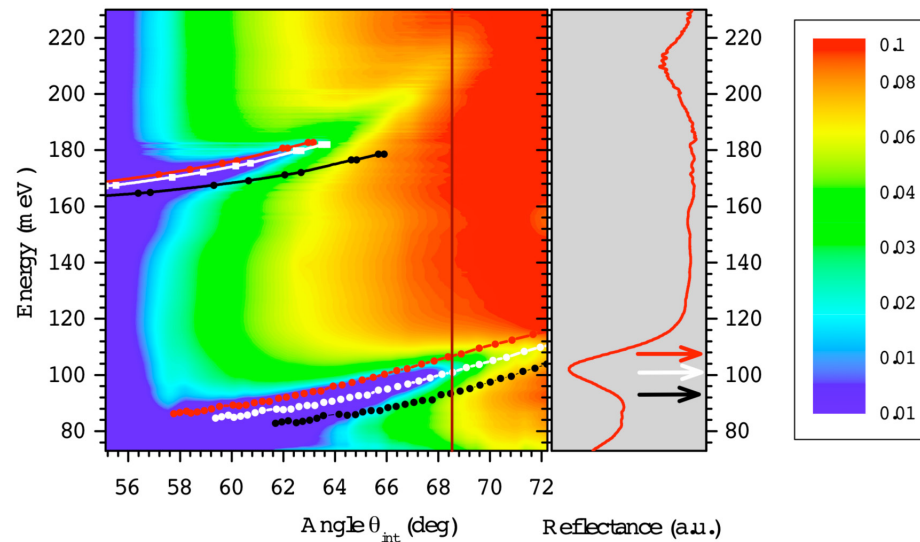


Fig. 1  
 Left: reflectance spectra of the microcavity sample resonant with the excited subband transition (2-3) as a function of incidence angle. Right: energy-wavevector dispersion; the dashed lines correspond to the uncoupled cavity and transition energies; experimental points are plotted as open circles; the shaded area outside the light cone is not accessible with the experiments.

Fig. 2

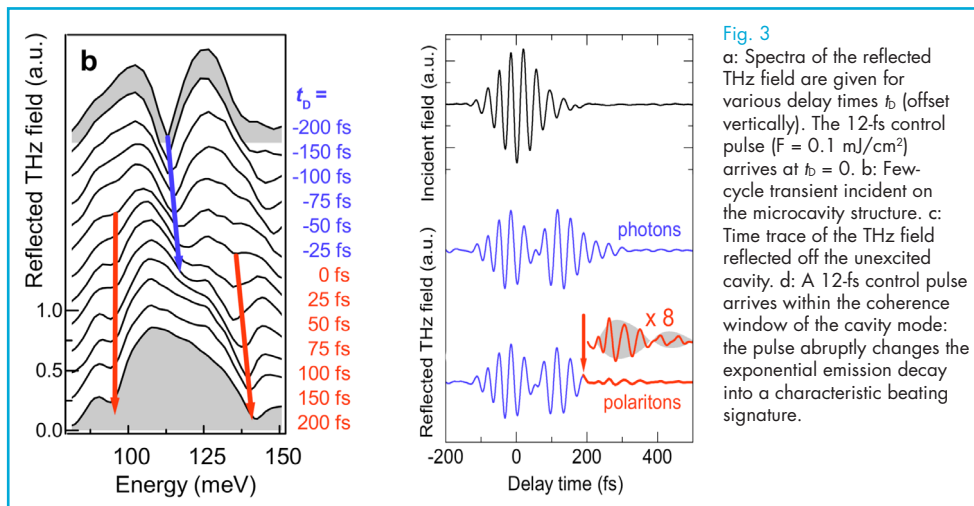
Angle-resolved reflectance of the intersubband microcavity displayed as contour plot (arb. units). The superimposed curves shown as circles are theoretical fits with the Rabi energy as the only free parameter. White curves were calculated using the full Hamiltonian, red ones without the anti-resonant term, and black ones with neither photon energy renormalization nor anti-resonant contributions. The right panel reports the reflectance spectrum corresponding to the internal angle of  $68.5^\circ$ . Arrows show the calculated lower-polariton energies for the three Hamiltonians detailed above.



as function of the in-plane wavevector  $k_{//}$ . The necessity arises from the fact that the polariton peaks at the same internal angle do not correspond to the same  $k_{//}$ . The actual energy-wavevector dispersion is reported in Fig. 1. As the lower polariton curve cannot be measured up to the anti-crossing point, an accurate fitting procedure is necessary in order to obtain the value of the vacuum-Rabi energy. The solid lines in Fig. 1 show the results of fitting the experimental data with the complete quantum-mechanical theory detailed in Ref. 2. The same procedure has also been performed on a different sample, operating though conventionally between the first two subbands. The measured reflectance is compared in Fig. 2 with the computed curves of the polariton dispersion [4]. Experimental data are shown as contour plot, while the polariton energies calculated from the full Hamiltonian are shown as white circles. A perfect agreement is found for a vacuum Rabi energy  $\hbar\Omega = 17$  meV, i.e.,  $\sim 11\%$  of the intersubband transition energy (152 meV). Black circles in Fig. 2 were instead obtained using the same value of  $\Omega$  but neglecting both *diamagnetic* and *anti-resonant* terms (defining the ultra-strong coupling), while the red ones excluding only the anti-resonant contribution but

including the photon renormalization. Though only small deviations appear for the upper polariton, the lower polariton dispersion calculated with either of the latter approximations is clearly incompatible with the experimental measurements, proving the relevance of these anomalous contributions [4].

As a consequence of the anti-resonant terms, the ground state of the system is a squeezed vacuum containing a finite number of virtual photons. Theory shows that non-adiabatic switching of  $\Omega_R$  may release these virtual quanta in correlated pairs [2]. As a matter of fact, non-adiabatic control poses an extreme experimental challenge: changes are required to be induced on a scale set by the cycle of light. We introduced then an all-optical scheme for femtosecond control of ultrastrongly coupled cavity polaritons – a first practical test-bed to target non-adiabatic QED phenomena [5]. Our sample contains undoped GaAs QWs, and radiative transitions between the subbands only become possible if electrons are injected extrinsically. We employ a 12-fs control pulse to excite electrons resonantly from the valence band into the first conduction subband, activating the intersubband field within femtoseconds. The eigenmodes of this system are then probed by resonant



reflection of a second mid-IR light pulse. Fig. 3a displays amplitude spectra recorded at various delay times  $t_b$ . The initial bare photon state is replaced by two coupled polariton branches appearing simultaneously at energy positions of 93 meV and 143 meV. Most remarkably, the new resonances do not gradually develop out of the bare cavity mode, but the cavity-intersubband coupling forms quasi-instantaneously.

The physics is most striking in the time domain. When a few-cycle multi-THz transient (time trace in Fig. 3b) impinges on the unexcited modulator structure, part of its energy is directly reflected off the cavity surface. A second portion is transmitted into the structure, prepares a coherent photon state in the resonator, and gets re-emitted subsequently contributing to

the overall reflected signal. This dynamics is encoded in a characteristic twin-pulse temporal structure of the reflected transient (Fig. 3c). The most intriguing situation is realized if we switch the eigenstates of the cavity while a coherent state of bare photons is still present (Fig. 3d): the incident THz transient first prepares a photon population in the unexcited cavity. During the free emission decay, the control pulse abruptly alters the eigenstates of the system. Remarkably, the decay of the bare cavity mode is interrupted on a time scale shorter than the oscillation cycle of light – a compelling proof of non-adiabaticity. The subsequent reemitted transient exhibits a characteristic two-mode beating in the time domain. The corresponding spectrum displays minima at photon energies of 93 meV and 143 meV - the hallmarks of both polariton branches.

## References

- [1] D. Dini, R. Köhler, A. Tredicucci, G. Biasiol, and L. Sorba, "Microcavity polariton splitting of intersubband transitions," *Phys. Rev. Lett.* **90**, 116401 (2003).
- [2] C. Ciuti, G. Bastard, and I. Carusotto, "Quantum vacuum properties of the intersubband cavity polariton field," *Phys. Rev. B* **72**, 115303 (2005); S. De Liberato, C. Ciuti, and I. Carusotto, "Quantum vacuum radiation spectra from a semiconductor microcavity with a time-modulated vacuum rabi frequency," *Phys. Rev. Lett.* **98**, 103602 (2007).
- [3] A.A. Anappara, A. Tredicucci, F. Beltram, G. Biasiol, L. Sorba, S. De Liberato, and C. Ciuti, "Cavity polaritons from excited subband transitions," *Appl. Phys. Lett.* **91**, 231118 (2007).
- [4] A.A. Anappara, S. De Liberato, A. Tredicucci, C. Ciuti, G. Biasiol, L. Sorba, and F. Beltram, "Signatures of the ultrastrong light-matter coupling regime," *Phys. Rev. B* **R79**, 201303 (2009).
- [5] G. Günter, A.A. Anappara, J. Hees, A. Sell, G. Biasiol, L. Sorba, S. De Liberato, C. Ciuti, A. Tredicucci, A. Leitenstorfer, and R. Huber, "Sub-cycle switch-on of ultrastrong light-matter interaction," *Nature* **458**, 178 (2009).



## Quantum properties of hybrid and superconducting structures

*In high critical temperature superconductors (HTS), and in general in complex oxides, electrons self-organize in ways qualitatively different from those of conventional metals and insulators, possibly generating unconventional phase transitions and novel forms of nanoscale ordering and quantum coherence. It is apparent that transport studies of nanoscale devices can be instrumental in clarifying the nature of the ground state, and to yield novel insights on dissipation and coherence in superconducting strongly correlated systems .*

*Here we report on robust macroscopic quantum behaviour in YBaCuO nanoscale junctions and rings, which also represent on a longer time scale the basic cell for novel superconducting/hybrid devices for solid state qubit architectures.*

An intense research activity has been focussed on the study of mesoscopic and macroscopic quantum properties in high critical temperature superconductor (HTS) junctions and nanostructures. The recent experiments on macroscopic quantum (MQ) effects in high critical temperature superconductor (HTS) junctions represent another significant step towards a Josephson platform, where important device functionalities are not anymore precluded to HTS junctions. The expected intrinsic limits due to dissipation and to still not completely identified low energy quasi-particles, have now to be reconsidered. Dissipation and coherence in unconventional d-wave systems with low energy quasi-particles on one hand, and nanoscale ordering on the other are the challenging objectives motivating these activities.

Nanoscale ordering and phase transition in complex oxides including HTS, where the electrons self-organize in ways qualitatively different from those of conventional metals and insulators, is one of the most outstanding problems in physics today. Strongly interacting electrons in the complex oxides have propensity to microscopically phase separate and to self-organize in patterns of lower dimension, and establish phase coherence between domains. This self assembly of electrons happens at a length scale of a few nanometers, with typical examples including the stripe ordering in

HTS. It is apparent that transport studies of nanoscale devices can be instrumental in discerning the nature of the ground state. The physics of superconductivity in structures with reduced dimensions is very intriguing and still unsettled, touching interesting arguments as quantum suppression of superconductivity in nanowires, the phase diagram of the superconductor-insulator transition, the dissipative dynamics induced by phase slips mechanism and, in perspective, the possibility of controlling the state – superconducting or insulating – of a nanowire by changing its environment.

Studies on quantum properties of Josephson junctions respond to the widespread need of expanding quantum technologies and in particular of developing quantum computation. In solid state qubit architectures, superconducting junctions can be considered as “atoms with wires”, which display energy-level quantization and strongly interact with electromagnetic environment. Hybrid systems encompassing superconductors, ultra-cold atoms degenerate gases,... seem to be the key for future quantum computer generations. HTS can offer specific qubit functionalities and unique read out protocols, and promote significant advances in the study of macroscopic quantum effects, coherence and dissipation in solid state systems.

We have realized various experiments on different systems, ranging from

Franco Carillo

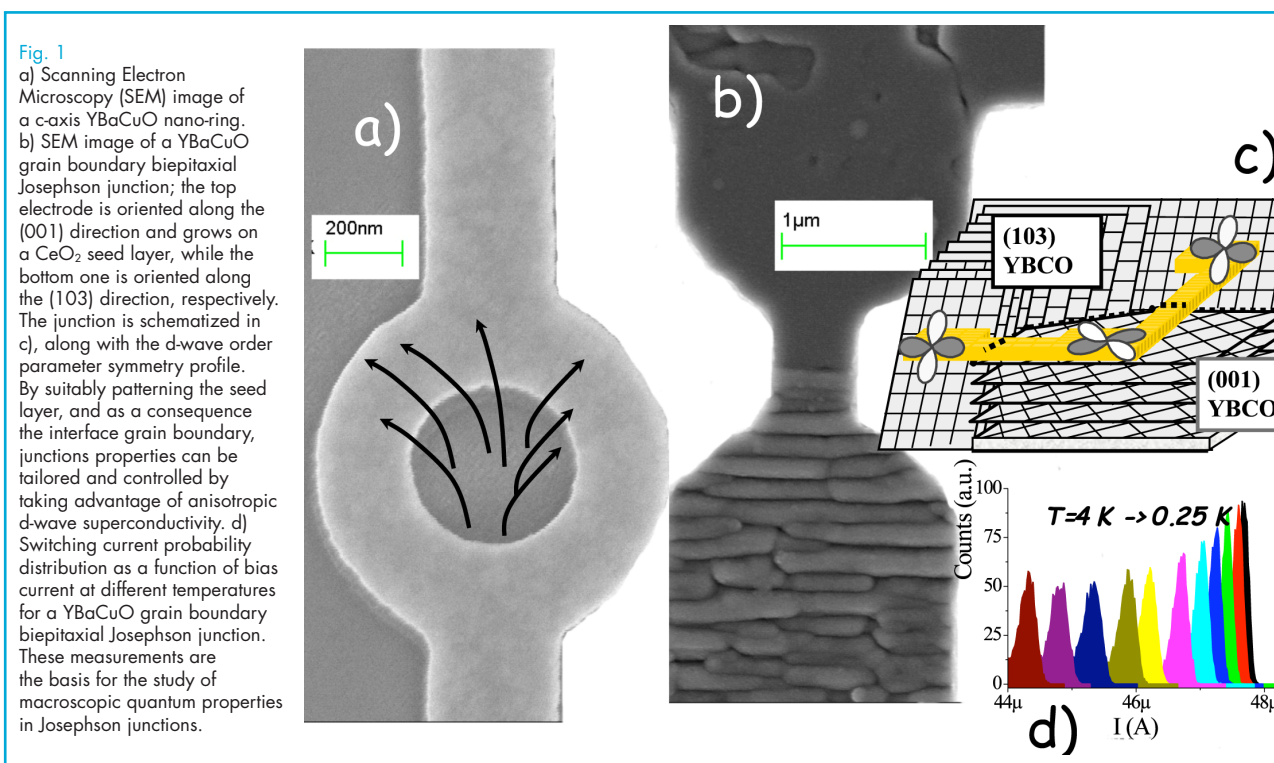
f.carillo@sns.it

### Collaborators

F. Beltram  
J. R. Kirtley  
D. Massarotti  
D. Montemurro  
G. Papari  
P. Pingue  
D. Stornaiuolo  
F. Tafuri

high quality YBaCuO biepitaxial grain boundary junctions and nano-structures [1,2,3,4,5] to HTS superlattices [6,7] and low critical temperature superconductor hybrid structures [8] and we have benefited of international collaborations such as Chalmers University of Technology

and IBM-Yorktown Heights/Stanford. Low-noise quantum measurements have been realized down to a few tenths of milliKelvin in the new low temperature facility developed at SUN/Napoli, being most of the samples designed and fabricated within CNR-INFM, SUN/Napoli and Pisa.



YBaCuO grain boundary biepitaxial junctions, for instance, are among the best available junctions. They are characterized by atomically flat grain boundary barriers [1], which have already allowed challenging experiments such as those on macroscopic quantum effects [2,4,1], on mesoscopic coherence [3], and are driving novel efforts. We have proved phase-coherent electronic transport in HTS grain boundary junctions incorporating superconducting correlations and resulting in a combination of Universal Conductance Fluctuations and Andreev reflection. Results on the first sub-micron junctions indicate improved reproducibility and features, which point to more uniform and tunnel-like barriers. This is a significant step in view of the ultimate limit of grain boundary nanostructures, which

is further supported by the realization of high quality YBCO nanowires of minimum width of 100 nm. They have shown excellent superconducting properties and intriguing collective behaviours [5].

We have realized one among the very first Little-Parks experiment on single HTS nano-rings, with evidence of non uniform vorticity [10]. This is the basic structure also for Aharonov-Bohm-like experiments in nano-structures in the underdoped regime, which are expected to shed light on the prominent categories of high-Tc models (preformed pairing, spin-charge separation, Bose condensation,...) by the direct measurement of the charge [11]. Hints on a fermionic scenario in Metal-Insulator Transition in HTS have been achieved through the direct measurement

of sheet resistance in superlattices and ultra-thin films with thickness down to 1 nm [6]. These ultra-thin film offer ideal conditions to investigate vortex quantum tunnelling phenomena and quantum phase transitions because of the extremely long extension of Pearl vortices [7,6].

In conclusion HTS nano-devices are the key for junctions with superior performances and reproducibility, for one dimensional YBaCuO wires, single electron transistors, nano-SQUIDs, relevant targets in view of a broader vision of integrated quantum electronics, and for future experiments based on the d-wave symmetry at the nanoscale.

#### References

- [1] F. Tafuri and J.R. Kirtley, *Rep. Prog. Phys.*, **68**, 2573 (2005); J.R. Kirtley and F. Tafuri, in "Treatise of Superconductivity" edited by Robert Schrieffer, pages 19-85 (Springer Verlag, 2007).
- [2] T. Bauch, T. Lindstrom, F. Tafuri, G. Rotoli, P. Delsing, T. Claeson, and F. Lombardi, *Science* **57**, 311 (2006); T. Bauch, F. Lombardi, F. Tafuri, A. Barone, G. Rotoli, P. Delsing, and T. Claeson, *Phys. Rev. Lett.* **94**, 087003 (2005).
- [3] A. Tagliacozzo, D. Born, D. Stornaiuolo, E. Gambale, D. Dalena, F. Lombardi, A. Barone, B.L. Altshuler, and F. Tafuri, *Phys. Rev. B* **75**, 012507 (2007); A. Tagliacozzo, F. Tafuri, E. Gambale, B. Jouault, D. Born, P. Lucignano, D. Stornaiuolo, F. Lombardi, A. Barone and B.L. Altshuler, *Phys. Rev. B* **79**, 024501 (2009)
- [4] G. Rotoli, T. Bauch, T. Lindstrom, D. Stornaiuolo, F. Tafuri and F. Lombardi, *Phys. Rev. B* **75**, 144501 (2007)
- [5] D. Stornaiuolo, E. Gambale, T. Bauch, D. Born, K. Cedergren, D. Dalena, A. Barone, A. Tagliacozzo, F. Lombardi and F. Tafuri, *Physica C* **468**, 310 (2008); G. Papari, F. Carillo, D. Born L. Bartoloni, E. Gambale, D. Stornaiuolo, P. Pingue, F. Beltram and F. Tafuri, to be published in *IEEE Trans. on Appl. Supercond.* (2009)
- [6] P. Orgiani, C. Aruta, G. Balestrino, D. Born, L. Maritato, P.G. Medaglia, D. Stornaiuolo, F. Tafuri and, A. Tebano, *Phys. Rev Lett.* **98**, 36401 (2007)
- [7] F. Tafuri, J.R. Kirtley, P.G. Medaglia, P. Orgiani and G. Balestrino, *Phys. Rev. Lett.* **92**, 157006 (2004); F. Tafuri, J.R. Kirtley, D. Born, D. Stornaiuolo P.G. Medaglia, P. Orgiani, G. Balestrino and V.G. Kogan, *Europhys. Lett.* **73**, 948 (2006)
- [8] F. Carillo, D. Born, V. Pellegrini, F. Tafuri, G. Biasiol, L. Sorba and F. Beltram, *Phys. Rev. B* **78**, 052506 (2008)
- [9] C. Tsuei and J. Kirtley, *Rev. Mod. Phys.* **72**, 969 (2000); H. Hilgenkamp and J. Mannhart, *Rev. Mod. Phys.* **74**, 485 (2002).
- [10] P. Papari, F. Carillo, D. Born, L. Bartoloni, E. Gambale, D. Stornaiuolo, P. Pingue, F. Beltram and F. Tafuri (2009 *IEEE Trans. On App. Superconductivity*, v. 19, n 3, (2009)
- [11] J.G. Bednorz and K.A. Muller *Rev. Mod. Phys.* **60**, 585 (1988); "Treatise of Superconductivity" edited by Robert Schrieffer, (Springer Verlag, 2007); P. Mohanty, J.Y.T. Wei, V. Ananth, P. Morales, W. Skocpol, *Physica C*, **408 - 410**, 666 (2004); J.A. Bonetti, D.S. Caplan, D.J. Van Harlingen, and M.B. Weissman, *Phys. Rev. Lett.*, **93**, 87002 (2008).



## Probing collective modes of correlated states of few electrons in quantum dots

**L**ow-lying collective excitations above highly correlated ground states of few interacting electrons confined in GaAs quantum dots (QDs) are probed by resonant inelastic light scattering. We highlight that separate studies of the changes in the spin and charge degrees of freedom offer unique access to the fundamental interactions. The case of QDs with four electrons is found to be determined by a competition between triplet and singlet ground states that is uncovered in the rich light scattering spectra of spin excitations. These light scattering results are described within a configuration-interaction framework that captures the role of electron correlation with quantitative accuracy. In these studies, inelastic light scattering methods emerge as powerful probes of collective phenomena and spin configurations in QDs.

Despite the large body of theoretical studies of the roles of correlation in QDs [1,2], probing experimentally the fundamental interactions underlying the emergence of a collective correlated state of few electrons in a QD represents a very demanding task. In our recent work we have shown that energies of low-lying spin and charge excitations of few electrons in nanofabricated GaAs QDs carry the signatures that identify electron correlation [3]. In the case of four electrons in the correlated regime the low-energy excitations manifest the formation of an electronic molecular state that has characteristic roto-vibrational modes [4]. These electron molecular excitations are revealed in the light scattering experiments, but are not directly accessible by transport methods nor in photoluminescence experiments. We recall that within time-dependent perturbation theory the resonant inelastic light scattering cross section incorporates two inter-band optical transitions close to the material band gap. Due to the conservation of energy, the energy difference between the incident and scattered photons is the energy of the QD excitation. Selection rules dictate that the active modes in light scattering experiments in QDs correspond to multipole inter-shell excitations (i.e., corresponding to even change in the angular momentum  $M$ ) between Fock-Darwin (FD) shells with the same orbital parity.

As in conventional molecules where the excitation spectra have a roto-vibrational character, in the strong-correlation regime where the Coulomb interaction rigidly fixes the relative positions of the electrons in the QD, the electronic excitations have character linked to either a vibrational configuration (associated with changes in the relative-motion wave function) or rotational state (with changes in the angular momentum). This is in contrast with the weak-correlation regime where the Coriolis force tends to mix the rotational and vibrational motions. A direct evidence for the formation of the electron molecule would be the independence of the vibrational modes from the rotational state of the electron system as a whole. To this end tuning of the ground state angular momentum  $M$  is needed to scan the roto-vibrational spectrum. To probe the ground state angular momentum we performed inelastic light scattering experiments on a QD array in a relatively small magnetic field perpendicular to the QD plane [4]. This procedure enables tuning the total angular momentum of the ground state from  $M = 0$  to  $M = 2$  (and from total spin  $S = 1$  to  $S = 0$ ) (see upper-right part of Fig.1). Samples were fabricated from a 25 nm wide, one-side modulation-doped  $\text{Al}_{0.1}\text{Ga}_{0.9}\text{As}/\text{GaAs}$  quantum well with measured low-temperature electron density  $n_e = 1.1 \cdot 10^{11} \text{ cm}^{-2}$  and a mobility of  $2.7 \cdot 10^6 \text{ cm}^2/\text{Vs}$ . QD arrays with sizes

Vittorio Pellegrini

vp@sns.it

### Collaborators

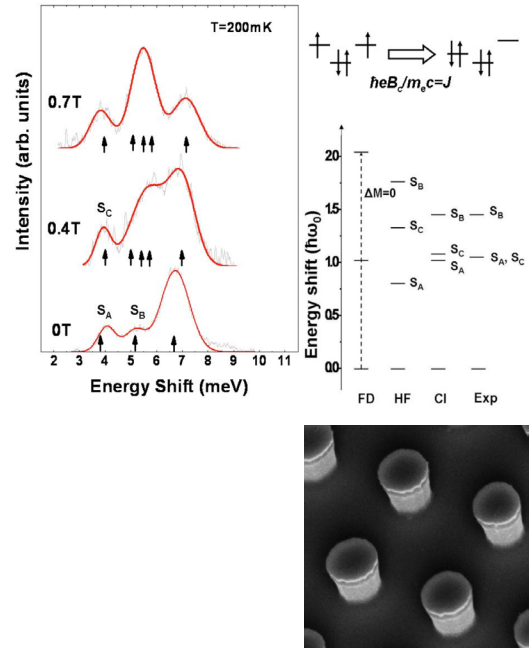
G. Goldoni  
M. Gurioli  
S. Kalliakos  
E. Molinari  
L. Pfeiffer  
A. Pinczuk  
M. Rontani  
A. Singha  
A. Vinattieri  
K. West

100 X 100 nm containing  $10^4$  identical single QD replica [5], were defined by

electron beam lithography and dry etching (see the SEM picture in Fig.1).

Fig. 1

Left panel: Light scattering spectra of spin excitations at different magnetic fields (the SEM picture of a quantum dot sample is also shown). Red lines are fits to the experimental data with Gaussians. At zero field the four-electron ground state is a spin triplet. As the magnetic field is turned on, when the cyclotron energy equals the exchange interaction contribution, the field induces a ground-state spin transition from the triplet ( $M=0, S=1$ ) to a singlet state ( $M=2, S=0$ ), (see top-right panel where the three lowest energy FD levels and electron occupation are shown). In our case, the transition occurs at  $\sim 0.27$  T. Lower right panel: Calculations of spin excitation energies. Within CI approach, both  $S_A$  and  $S_C$  transitions occur at  $\sim \hbar\omega_0$  (the energy quantum of the lateral harmonic potential, which is 3.75 meV in this particular case), and therefore strongly deviate from the Hartree-Fock calculation. The latter predicts a large exchange-energy splitting between  $S_A$  and  $S_C$  of  $J \sim (\hbar\omega_0)^{1/2}$  (around 1.5 meV).



We plot in Fig.1 the spin excitations at different magnetic fields. The calculated energies of the spin modes using the Configuration-interaction (CI) model are indicated as black arrows. At zero field, the spin excitation at  $\sim 5.2$  meV is identified as the Triplet-to-Singlet intershell monopole ( $\Delta M=0$ ) excitation (TS, here labeled  $S_B$ ) confirming the four-electron population in the QDs [3]. The large intensity increase of the TS mode beyond 0.3 T is due to the emergence of three closely spaced spin excitations from the new ground state (with total spin  $S = 0$  and  $M = 2$ ) and provides the evidence of the ground state transition from ( $M = 0, S = 1$ ) to ( $M = 2, S = 0$ ). The key finding is that the lowest-energy spin excitation, that is,  $S_A$  for the triplet ground state and  $S_C$  for the singlet ground state,

does not shift as we go through the ground-state transition. As pointed out above, this is precisely the molecular signature in the QD, where the rigid rotation of the electrons is decoupled from the relative-motion dynamics. This experimental result is in sharp contrast with that theoretically expected in the absence of correlation (see lower-right panel in Fig. 1).

These experimental results combined with refined theoretical analysis demonstrate the large sensitivity of inelastic light scattering methods in applications that uncover and monitor major impacts of electron-electron interactions in QDs with few-electrons. These are new venues that might provide much needed control of fundamental Coulomb interactions at the nanoscale.

#### References

- [1] S. M. Reimann, M. Manninen, Rev. Mod. Phys. 74 (2002) 1283.
- [2] A. Ghosal *et al.*, Nature Phys. 2 (2006) 336.
- [3] C. P. García *et al.*, Phys. Rev. Lett. 95 (2005) 266806.
- [4] S. Kalliakos *et al.*, Nature Phys. 4 (2008) 467.
- [5] S. Kalliakos *et al.*, Appl. Phys. Lett. 90, 181902 2007.

## Low-dimensional In-based semiconductor systems

Recent advances in the epitaxial growth of low-dimensional semiconductor systems with techniques such as molecular beam epitaxy (MBE) make it possible to form structures of various geometries. The composition profile and the vertical transport properties of self-assembled InAs/GaAs quantum dots (QDs) and quantum rings (QRs) are investigated by X-ray photoemission electron microscopy and conductive atomic force microscopy [1-3]. The resulting measurements give information on the mechanisms driving the formation of such low-dimensional structures. Furthermore, we have investigated the transport properties of two dimensional electron gases (2DEGs) in  $\text{In}_{0.75}\text{Ga}_{0.25}\text{As}$  quantum wells and found a correlation between the local indium concentration modulation, measured with X-ray photoemission electron microscopy, and the pronounced anisotropy observed in the low-temperature mobility of the 2DEG [4-5].

The self-organization of nanostructures represents a phenomenon of fundamental interest in material science, with great potential in various fields of technology. However, size, shape, and compositional distribution in strain-driven self-assembled nanostructures can be significantly modified by deposition of a capping layer. A striking example is the transformation of self-assembled QDs into QRs when a thin (few nm-thick) layer of barrier material is overgrown on the original islands under appropriate conditions.

QR samples were prepared in the high mobility MBE facility at the TASC laboratory in Trieste [2]. Topography and current maps of a QR sample were measured simultaneously by conductive atomic force microscopy (C-AFM) as shown in Fig. 1. The most significant feature exhibited in the current map is the lower conductivity (dark region) of the central QR hole compared to rim and wetting layer. Considering the presence of a surface oxide in the case of the C-AFM measurements, these results are consistent with data on the QR composition acquired with X-ray photoemission electron microscopy (XPEEM) [6]. For the topmost layer of the QR sample consisting of  $\text{In}_x\text{Ga}_{1-x}\text{As}$  with varying In content  $x$ , the XPEEM measurements show that the average In content is lowest in the capping layer ( $x = 0.53$ ) and gradually rises towards the central QR hole, where it reaches its maximum ( $x = 0.67$ ).

Two-dimensional electron gases (2DEGs)

based on  $\text{In}_x\text{Ga}_{1-x}\text{As}/\text{In}_x\text{Al}_{1-x}\text{As}$  quantum wells (QWs) with high In concentration offer potential advantages over  $\text{GaAs}/\text{Al}_x\text{Ga}_{1-x}\text{As}$  ones, both for studies in fundamental physics and for device applications, due to their peculiar properties such as low effective electron mass, large bare  $g$ -factor, large Rashba coupling, and highly transmissive metal-semiconductor interfaces for  $x \geq 0.75$ . The low temperature transport properties of  $\text{In}_{0.75}\text{Ga}_{0.25}\text{As}$  QWs manifest a strong mobility anisotropy that cannot be explained in terms of interface roughness scattering [4]. The identification of the mechanism limiting the mobility

Lucia Sorba

l.sorba@sns.it

### Collaborators

V. Baranwal  
G. Biasiol  
E. Cancellieri  
F. Carillo  
D. Ercolani  
S. Heun  
C. Jacoboni  
A. Locatelli  
R. Magri  
T.O. Mendes  
F. Noltling  
M.N. Orti  
M. Rosini  
P. Scherre

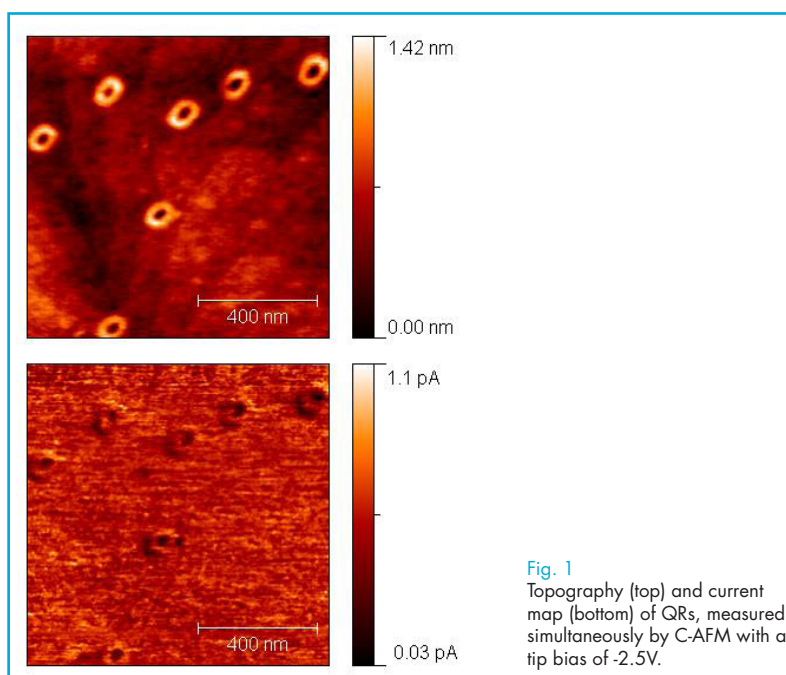
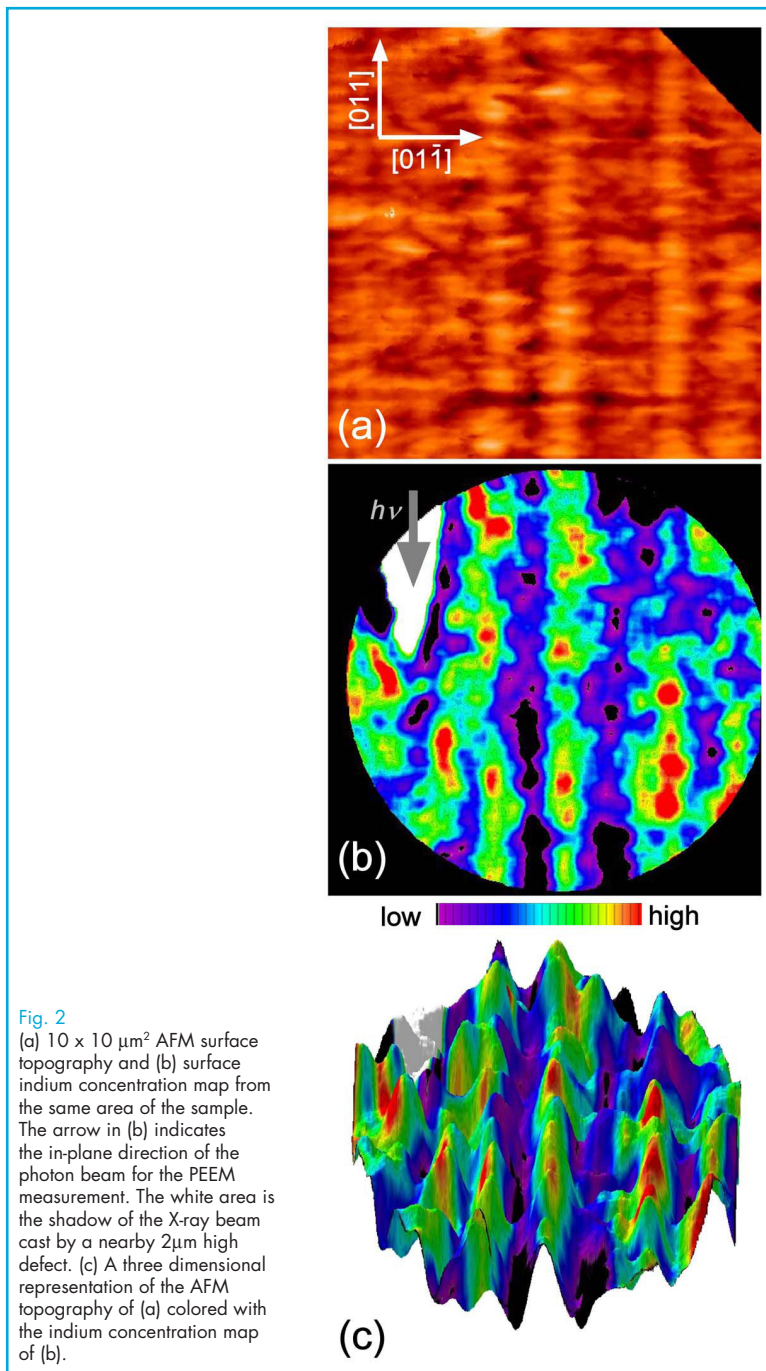


Fig. 1  
Topography (top) and current map (bottom) of QRs, measured simultaneously by C-AFM with a tip bias of -2.5V.

allows to design and grow higher quality 2DEGs, needed for high indium content InGaAs device fabrication. The surface concentration map obtained with XPEEM has allowed us to correlate, for the first time, the morphological properties of the sample surface measured by AFM shown in Fig. 2a with local variations in the indium concentration of the alloy (see Fig. 2b). In order to evaluate the

contribution of the local In fluctuations on the mobility, simulations were performed in collaboration with the University of Modena and Reggio Emilia [4] to verify if the transport asymmetry can be explained by a conduction band energy modulation correlated with the indium concentration. Good agreement was reached between the simulated and measured transport asymmetry. We have thus identified the main origin of the transport asymmetry to be a spatial modulation of the indium concentration in the QW.

These conclusions are confirmed by the increased mobility (in excess of  $50 \text{ m}^2/\text{V}\cdot\text{s}$ ) and reduced anisotropy of a QW sample containing a pure InAs layer.



#### References

- [1] G. Biasiol, S. Heun, G. B. Golinelli, A. Locatelli, T. O. Mentes, F. Z. Guo, C. Hofer, C. Teichert, and L. Sorba, "Surface compositional gradients of InAs/GaAs quantum dots", *Appl. Phys. Lett.* 87, 223106 (2005).
- [2] T. Mlakar, G. Biasiol, S. Heun, L. Sorba, V. T. Kumar, G. U. Kulkarni, V. Spreafico, and S. Prato, "Conductive Atomic Force Microscopy of InAs/GaAs Quantum Rings", *Appl. Phys. Lett.* 92, 192105 (2008).
- [3] V. Baranwal, G. Biasiol, S. Heun, A. Locatelli, T. Onur Mentes, M. Niño Orti, and L. Sorba, "Kinetics of the InAs/GaAs dot-to-ring evolution", *Phys. Rev. B* in press.
- [4] M. Rosini, E. Cancellieri, D. Ercolani, G. Biasiol, L. Sorba, and C. Jacoboni, "Transport anisotropy in InGaAs 2D electron gases", *Physica E* 40, 1392 (2008).
- [5] D. Ercolani, G. Biasiol, E. Cancellieri, M. Rosini, C. Jacoboni, F. Carillo, S. Heun, and L. Sorba, and F. Noltling, "Transport anisotropy in  $\text{In}_{0.75}\text{Ga}_{0.25}\text{As}$  two dimensional electron gases", *Phys. Rev. B* 77, 235307 (2008).
- [6] G. Biasiol, R. Magri, S. Heun, A. Locatelli, T. O. Mentes, and L. Sorba, "Surface compositional mapping of self-assembled InAs/GaAs quantum rings", *J. Crystal Growth* 311, 1764 (2009).

# Graphene

## Graphene and artificial graphene

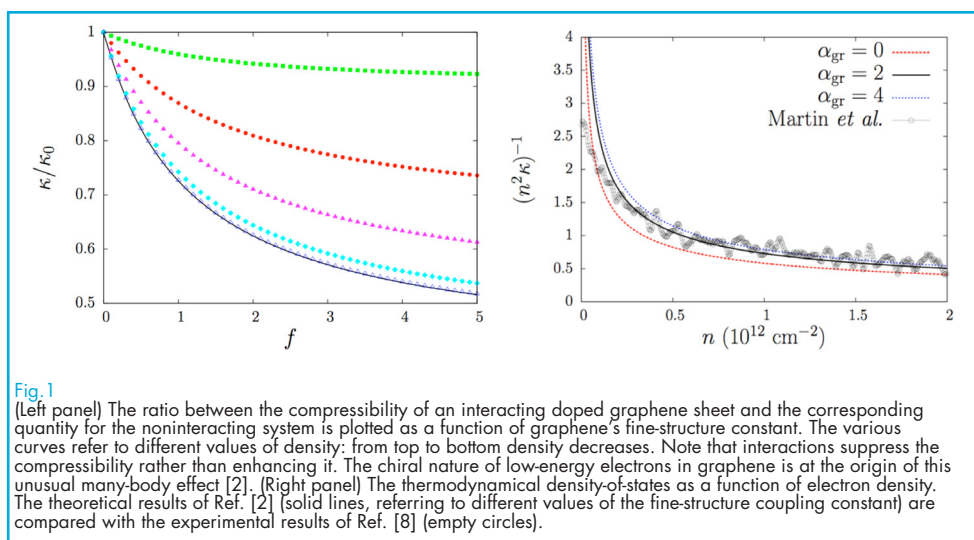
This area of research focuses on a novel class of two-dimensional (2D) electron liquids subjected to a lateral potential of honeycomb symmetry. During the years 2004-2005 a group in Europe (A. Geim and co-workers at the University of Manchester, UK) and one in the US (P. Kim and co-workers at the Columbia University, USA) have succeeded in the isolation of single- and few-layer graphene systems (see below) from graphite. Electrons in doped single-layer graphene behave like massless fermions. Graphene is a first remarkable and clean example of the impact of a potential with honeycomb structure on the electronic states and dynamics. In graphene the crystalline potential is determined by the spatial arrangement of Carbon atoms leading to linearly dispersing Dirac-cone bands and semimetallic behavior. When Coulombic electron-electron interactions are included, doped graphene represents a new type of many-electron problem, distinct from both an ordinary 2D electron gas and from quantum electrodynamics. Below we summarize some of the theoretical work done in this area of research. We also show that linearly-dispersing bands and massless-Dirac-fermion behavior can be induced in an ordinary 2D electron gas in GaAs/AlGaAs heterostructures when subjected to an external lateral potential with honeycomb symmetry that can be realized e.g. by nanofabrication.

Marco Polini

m.polini@sns.it

### Collaborators

G. Borghi  
F. Dolcini  
R. Fazio  
M. Gibertini  
B. Karmakar  
V. Pellegrini  
S. Peotta  
A. Principi  
D. Rainis  
A. Singha  
F. Taddei  
A. Tomadin



### Electron-electron interactions in doped graphene sheets

Graphene is a one-atom-thick electron system composed of Carbon atoms on a 2D honeycomb lattice, which has attracted an exceptional amount of interest in the scientific community [1]. We have investigated the interplay between chirality and electron-electron interactions in determining thermodynamic quantities

(such as compressibility - see Fig. 1 - and spin susceptibility) of doped graphene sheets [2]. We have also studied one-particle properties, carrying out calculations of the velocity renormalization [3], of the quasiparticle self-energy [3,4], and of the quasiparticle spectral function [4] (see Fig. 2). Similar studies have been carried out at finite temperature [5] and for bilayer graphene [6]. Finally, we have

also developed a Kohn-Sham-Dirac self-consistent scheme for graphene sheets that treats slowly-varying inhomogeneous external potentials and electron-electron interactions on an equal footing [7] (see Fig. 3).

#### Pseudospintronics with semiconductor and graphene bilayers

The layer degree-of-freedom in semiconductor quantum wells and in graphene bilayers can be viewed as a spin-1/2-like quantum degree-of-freedom. In particular this pseudospin quantum number gives rise to a collective mode analogous to the ferromagnetic resonance mode of a ferromagnet. In Ref. [9] we have outlined a many-body theory of the dependence of the energy and the damping of this mode on layer separation. Based on these results, we have discussed

the possibilities of realizing transport-current driven pseudospin-transfer oscillators in semiconductors, and of using the pseudospin-transfer effect as an experimental probe of intersubband plasmons. In Ref. [10] we have predicted that neutral graphene bilayers are pseudospin magnets in which the charge density-contribution from each valley and spin spontaneously shifts to one of the two layers. The band structure of this system is characterized by a momentum-space vortex, which is responsible for unusual competition between band and kinetic energies leading to symmetry breaking in the vortex core. We have also discussed the possibility of realizing a pseudospin version of ferromagnetic metal spintronics in graphene bilayers based on hysteresis associated with this broken symmetry.

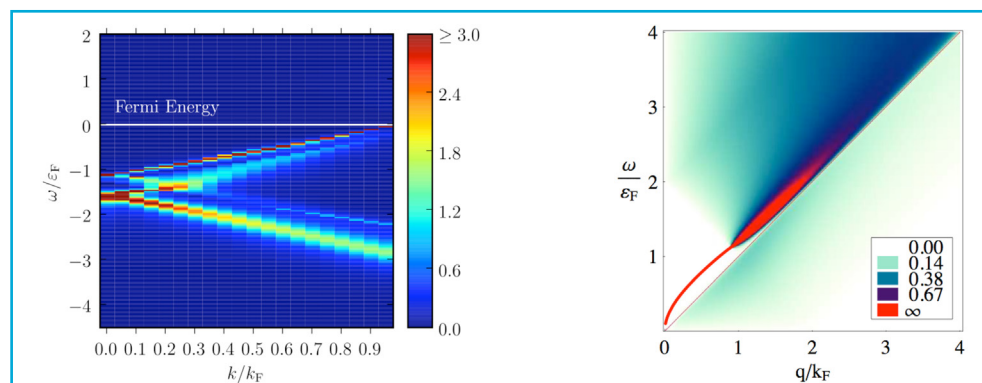
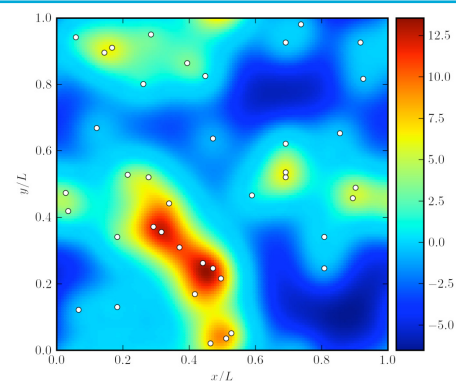


Fig. 2

(Left panel) A color plot of the spectral function of a n-doped graphene sheet as a function of momentum and energy [4]. For each value of momentum angle-resolved photoemission spectroscopy (ARPES) detects the portion of the spectral function with negative energy. The negative-energy ARPES spectra of a p-doped graphene sheet is identical to the positive-energy spectra of an n-doped sheet. (Right panel) The imaginary part of the inverse dielectric function is plotted as a function of momentum and energy. The plasmon collective mode is represented by the red line: it remains remarkably well defined even when it enters the interband electron-hole continuum.

Fig. 3

A color plot of the Kohn-Sham-Dirac [5] self-consistent ground-state density profile of a 2D system of interacting massless Dirac fermions in the presence of four randomly distributed Coulomb impurities (white circles) located away from the graphene plane. This particular result corresponds to a neutral-on-average graphene sheet. The ground-state density profile of weakly-doped graphene sheets is highly inhomogeneous, due to the random potential landscape created by the impurities, and is characterized by electron- and hole-rich puddles.



### Transport in hybrid graphene/superconductor junction

We have studied Andreev reflection in graphene nanoribbon/superconductor hybrid junctions [11]. By using a tight-binding approach and the scattering formalism we have shown that finite-size effects lead to notable differences with respect to the bulk graphene case. At subgap voltages, conservation of *pseudoparity*, a quantum number characterizing the ribbon states, yields either a suppression of Andreev reflection when the ribbon has an even number of sites in the transverse direction or perfect Andreev reflection when the ribbon has an odd number of sites. In the former case the suppression of Andreev reflection induces an insulating behavior even when the junction is biased; electron conduction can however be restored by applying a gate voltage. Finally, we have also checked that these findings remain valid in the case of *nonideal* nanoribbons in which the number of transverse sites varies along the transport direction.

### Dirac fermions in Gallium Arsenide: artificial graphene

In the following we report on the fabrication of a device from semiconducting heterostructures that has the potential to behave like graphene [12]. The starting material is a two-dimensional electron gas of very high purity confined in an AlGaAs/GaAs modulation-doped quantum well. On top of this, a honeycomb network of nanosized pillars analogous to carbon ions in the graphene lattice, modulates the electric potential in the two-dimensional electron gas. A SEM image of a typical sample is shown in Fig. 4 (left panel). The same figure shows (right panel) the calculated energy minibands for a muffin-tin potential with such honeycomb symmetry with the experimental parameters  $a=150$  nm,  $r=52.5$  nm, and with a chosen  $V_0 = -0.8$  meV, where  $V_0$  is the estimated strength of attractive potential experienced by the electrons in the nanosized regions of diameter  $2r=105$  nm.

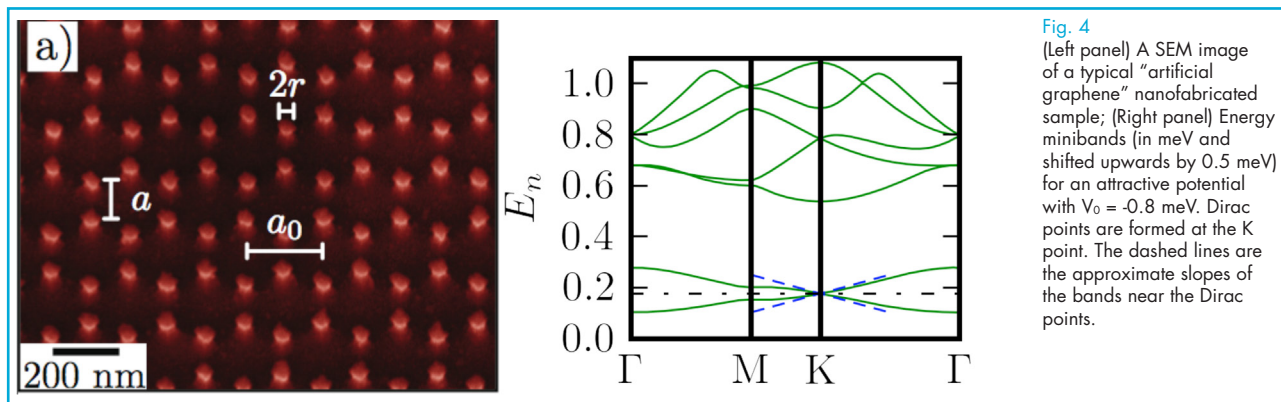


**Fig. 4**  
(Left panel) A SEM image of a typical "artificial graphene" nanofabricated sample; (Right panel) Energy minibands (in meV and shifted upwards by 0.5 meV) for an attractive potential with  $V_0 = -0.8$  meV. Dirac points are formed at the K point. The dashed lines are the approximate slopes of the bands near the Dirac points.

As dictated by symmetry and group theory, these minibands are characterized by the existence of two-fold degenerate points at the corners of the Brillouin zone. It is easy to show that states close to these points are effectively described by a two-component massless Dirac fermion Hamiltonian.

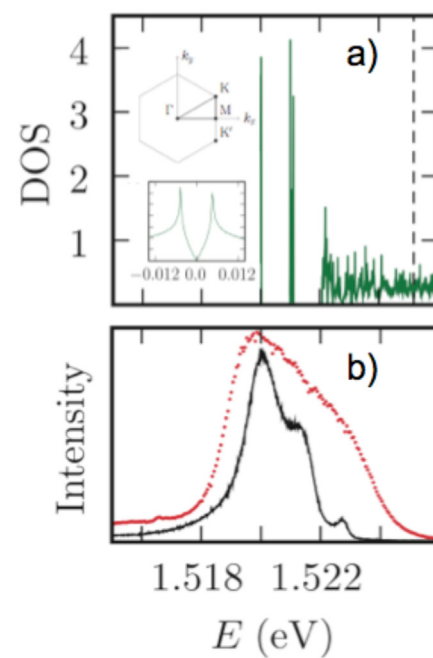
Figure 5 shows representative photoluminescence (PL) spectra at 2K both of the

unprocessed (red dotted curve) and processed (black solid curve) samples. In the unprocessed 2DEG case, the PL shape is determined by the density-of-states of the free electrons and equilibrium occupation factors of the 2DEG and photoexcited holes leading to an estimated electron density of around  $10^{11}$  cm<sup>-2</sup> in agreement with the transport results. The processed sample PL, on the contrary, displays a re-

markable change with the appearance of sharp structures on the high-energy side and an overall reduction of its linewidth, which are consistent with the modification of the conventional constant-in-energy DOS as shown in Fig. 5, provided that  $V_0$  is chosen appropriately ( $V_0 = -2.8$  meV in

this plot). The overall smaller linewidth of the PL suggests a reduction of the average electron density due to the impact of the etching process. Work is in progress to study the evolution of the cyclotron resonance in a magnetic field.

**Fig. 5**  
Panel a) Calculated density-of-states (DOS), in units of  $\text{eV}^{-1}\text{nm}^{-2}$ , as a function of energy for a muffin-tin potential with  $V_0 = -2.8$  meV,  $a=150$  nm, and  $r=52.5$  nm. The first structure in the DOS is fixed at the energy of the main photoluminescence (PL) peak (see panel b). The vertical dashed line denotes the Fermi level associated with the nominal density of  $1.1 \times 10^{11} \text{ cm}^{-2}$ . The insets to Fig. 5a show the Brillouin zone corresponding to the external periodic potential and a zoom of the DOS corresponding to the first structure in the main panel. The V-shaped DOS characteristic of MDFs is evident. Panel b) Low-temperature ( $T=2$  K) PL of the sample before (red dotted curve) and after (black solid curve) the processing.



Such artificially engineered 'graphene' may offer some advantages over its natural prototype, such as extremely high purity of samples, an ability to tune the parameters of the spectrum, and the possibility of

shaping the artificial graphene into geometries like ribbons with perfect edges, which are more useful in certain applications.

#### References

- [1] A.H. Castro Neto *et al.*, *Rev. Mod. Phys.* **81**, 109 (2009); A.K. Geim and A.H. MacDonald, *Phys. Today* **60** (8), 35 (2007); A.K. Geim and K.S. Novoselov, *Nature Mater.* **6**, 183 (2007).
- [2] Y. Barlas *et al.*, *Phys. Rev. Lett.* **98**, 236601 (2007).
- [3] M. Polini *et al.*, *Solid State Commun.* **143**, 58 (2007).
- [4] M. Polini *et al.*, *Phys. Rev. B* **77**, 081411(R) (2008).
- [5] M.R. Ramezani *et al.*, *J. Phys. A: Math. Theor.* **42**, 214015 (2009).
- [6] G. Borghi *et al.*, *Solid State Commun.* **149**, 1117 (2009).
- [7] M. Polini *et al.*, *Phys. Rev. B* **78**, 115426 (2008); see also A. Principi, M. Polini, and G. Vignale, *Phys. Rev. B* **80**, 075418 (2009).
- [8] J. Martin *et al.*, *Nature Phys.* **4**, 144 (2008).
- [9] S.H. Abedinpour *et al.*, *Phys. Rev. Lett.* **99**, 206802 (2007).
- [10] H. Min *et al.*, *Phys. Rev. B* **77**, 041407(R) (2008).
- [11] D. Rainis *et al.*, *Phys. Rev. B* **79**, 115131 (2009).
- [12] M. Gibertini *et al.*, *Phys. Rev. B* **79**, 241406(R) (2009).

## Electronic states and quantum transport in graphene ribbons

**G**raphene is a single atom thick sheet of carbon. For almost half century after the pioneering paper of Wallace, strictly two dimensional graphite was but a beautiful exercise for students of theoretical solid state physics and chemistry. Only recently high quality and stable under ambient conditions two dimensional carbon sheets have been isolated, and the potential of graphene-based electronics on the micro- and nano-metric scale has further magnified the interest toward this material. Graphene ribbons are infinitely extended in one direction and have two typical terminations in the orthogonal one: the zigzag and the armchair terminations. By means of the tight binding model for the description of the electronic states and the nonequilibrium Keldysh Green's function for quantum transport, we studied the electronic structure and current profiles of graphene ribbons. We show that charge manipulation in the engineering of graphene is conceptually possible by external gates and magnetic fields.

Graphene, neutral or controlled by external voltages, can be considered as a reservoir of massless relativistic particles. The peculiar relativistic-like dynamics of the charges involved in magnetotransport experiments have attracted great

interest and envisaged novel devices for nanoelectronics [1,2] and valley-valve filters [3].

Carrier density in graphene can be varied from electrons to holes using external local gates (see Fig. 1).

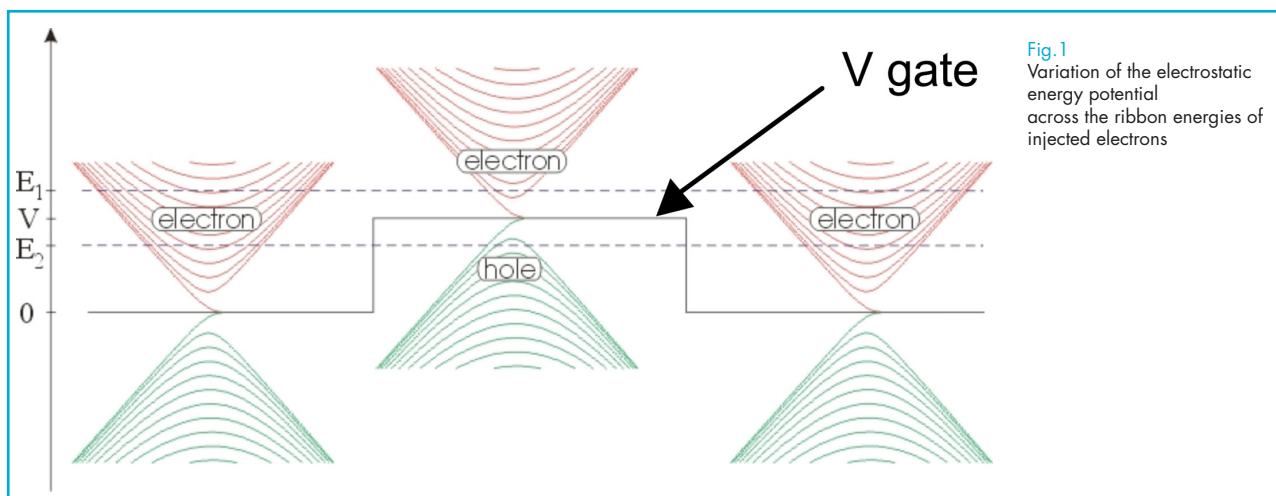
Giuseppe [Grosso](#)

[grosso@df.unipi.it](mailto:grosso@df.unipi.it)

**Collaborators**

A. Cresti

G. Pastori Parravicini



We have simulated stationary currents distribution [4,5] in graphene ribbons in the presence of magnetic fields and top gate potentials, by means of the nonequilibrium Keldysh-Green's function formalism within a tight-binding model. The exploited formalism allows imaging of local currents and evaluation of quantum shot noise. The Keldysh method, joint with the decimation-renormalization

technique, emerges as a very suitable tool for microscopic treatment of charge transport in the presence of superimposed potentials. This method, widely applied in the study of charge transport in conventional two-dimensional electron gases in square lattices, has been adapted to the honeycomb topology [4]. In the case of superimposed gates, it provides a real space view of the currents and suggest the way to realize their manipulation.

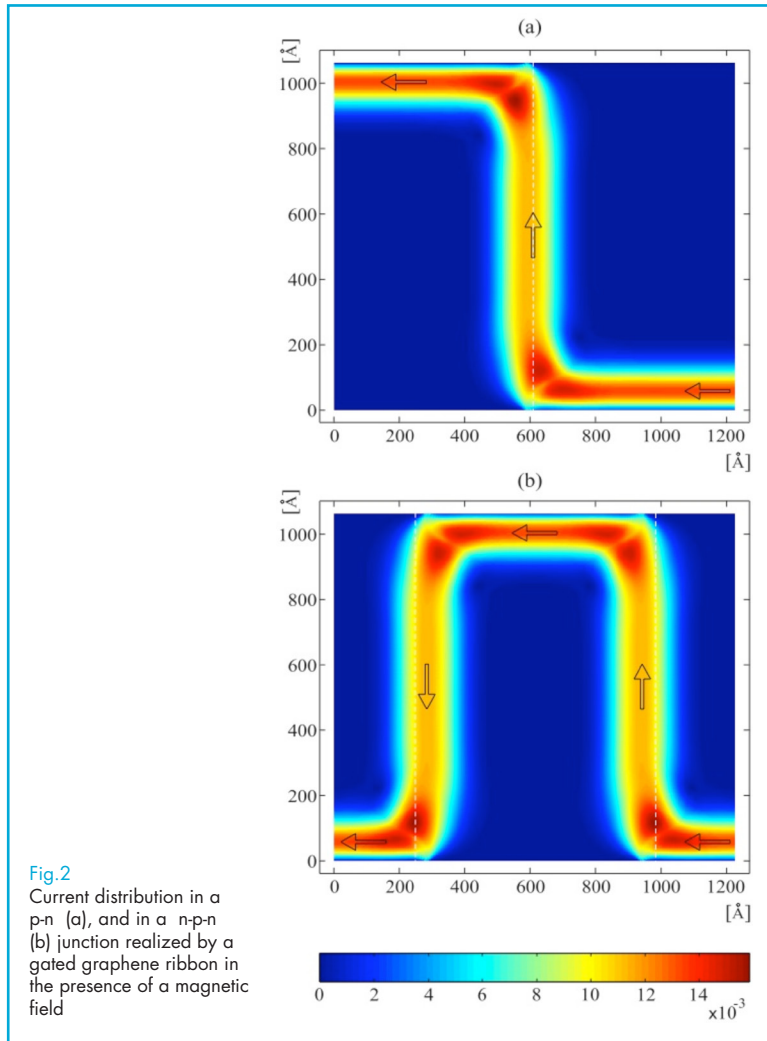


Fig.2  
Current distribution in a p-n (a), and in a n-p-n (b) junction realized by a gated graphene ribbon in the presence of a magnetic field

We have shown that in  $n$ - $p$ - $n$  devices, realized when the height of the gate potential barrier is larger than the energy of the injected carriers, electron particles turn into holes inside the barrier and turn back to electrons outside it. Imaging of current profiles (a) (see Fig.2) gives a vivid picture of the easy Klein tunneling through barriers by virtue of the electron-like or hole-like behavior of the relativistic particles in the  $n$ -doped and  $p$ -doped regions.

The current maps are of particular interest in the presence of magnetic fields since the spatial distribution of currents is sensitive to the nature of the carriers. In strong magnetic fields, electrons and holes flow along opposite edges of the sample and this shows that current manipulation is in principle possible by means of top gates.

Transport properties of graphene nanoribbons depend dramatically on their zigzag or armchair termination and on the presence of long range or short range disorder. Recently, it has been shown that a  $p$ - $n$  junction in a clean zigzag nanoribbon blocks the current completely if the number of carbon chains in the ribbon is even [3]. In the case of an odd number of chains, on the contrary, the system is almost transparent. We have evidenced this phenomenon by electronic transport simulations and have given an interpretation based on symmetry arguments [6].

The bipolar junction is obtained by means of a superimposed potential step with height  $V$  on the left region (Fig.3a), where the band structure turns out to be shifted by  $V$  (Fig.3b). We consider a potential that only varies along the longitudinal direction. If we inject the particles from the right side of the ribbon (red arrows) at an energy  $0 < E < V$ , the charges enter the system as electrons and are transmitted to the left as holes. As indicated in Fig.3b, in this range of energy the transport is realized by scattering from the K valley to the K' valley. In Fig.3c is reported the conductance  $G$  of a ribbon made up of  $N=100$  carbon chains for  $V = \Delta$ , where  $\Delta$  is the separation between the energy levels at K. In the region  $0 < E < V$  we have  $G = 0$ . For  $N=101$ , in the same region we have  $G = 2e^2/h$  [6].

To interpret this effect, we consider the spatial reflection symmetry of the zigzag nanoribbon with respect to the central plane along the longitudinal direction if  $N$  is even, or the reflection operation followed by a fractional translation for odd  $N$ . The energy bands can be classified as even or odd with respect to these spatial operations. To have intervalley scattering in the energy region where only one mode is active in both the  $p$  and  $n$  regions, the step potential must break the symmetry of the ribbon. It can be shown that the symmetry is respected when  $N$  is even,

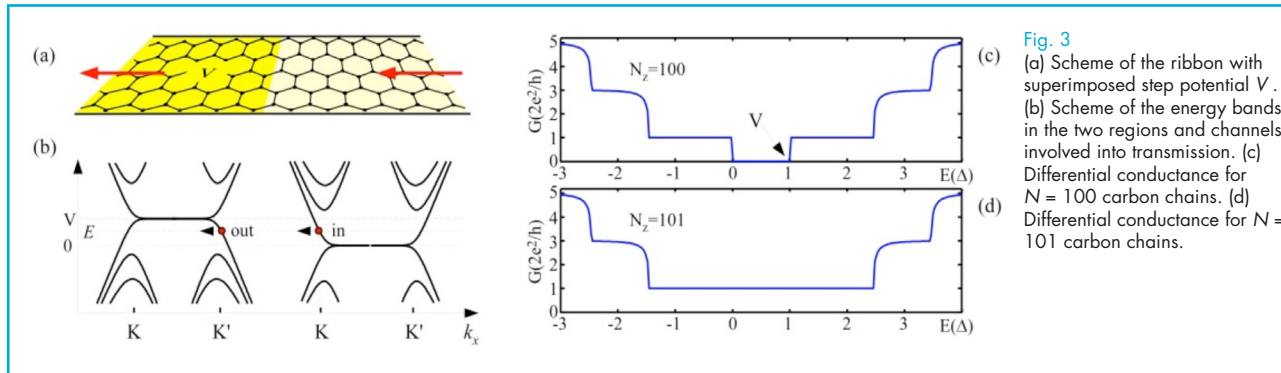


**Fig. 3** (a) Scheme of the ribbon with superimposed step potential  $V$ . (b) Scheme of the energy bands in the two regions and channels involved into transmission. (c) Differential conductance for  $N = 100$  carbon chains. (d) Differential conductance for  $N = 101$  carbon chains.

and no current transmission is allowed, while the symmetry is broken when  $N$  is odd. These general considerations are supported by direct calculations of the coupling between the crystalline wave functions of the ribbon induced by the superimposed step potential.

We have also investigated the transport properties of gated conjugated polymers of the polyacene series [7] as examples of ultranarrow zigzag graphene ribbons. Our simulations demonstrate that the polymeric system is insulating or

conducting according to the Fermi energy of the injected electrons, of the even or odd number of chains, and of the shape of the gate potential. In summary, we notice explicitly that for appropriate energy intervals to the right of the reference energy  $E = 0$ , all even ribbons are perfectly insulating. This behavior, appealing for electronic valve applications, was first observed for wide graphene ribbons. It occurs regardless of the two-valley band structure of graphene, and also holds for ultranarrow graphene ribbons. We have in fact shown that the origin of the effect are symmetry and topology.

#### References

- [1] K.S. Novoselov, A.K. Geim, S.V. Morozov, D. Jiang, M.I. Katsnelson, I.V. Grigorieva, S.V. Dubonos and A.A. Firsov, "Two-dimensional gas of massless Dirac fermions in graphene," *Nature* 438,197 (2005).
- [2] Y. Zhang, Y.-W. Tan, H.L. Stormer and P. Kim, "Experimental observation of the quantum Hall effect and Berry's phase in graphene," *Nature* 438, 201(2005).
- [3] A. Ricerz, J. Tworzydło and C.W.J. Beenakker, "Valley filter and valley valve in graphene," *Nature Phys.* 3, 177, (2007).
- [4] A. Cresti, G. Grosso and G. Pastori Parravicini, "Electronic states and magnetotransport in unipolar and bipolar graphene ribbons" *Phys. Rev. B* 77, 115408 (2008).
- [5] A. Cresti, G. Grosso and G. Pastori Parravicini "Numerical study of electronic transport in gated graphene ribbons" *Phys. Rev. B* 76, 205433(2007).
- [6] A. Cresti, G. Grosso and G. Pastori Parravicini, "Valley-valve effect and even-odd chain parity in p-n graphene junctions" *Phys. Rev. B* 77, 233402 (2008).
- [7] A. Cresti, G. Grosso and G. Pastori Parravicini "Field-effect resistance of gated graphitic polymeric ribbons" *Phys. Rev. B* 78, 115433 (2008).



## Interferometry and entanglement detection at the nanoscale

For many decades, interferometry has been a fundamental tool to disclose the classical and quantum properties of light. Optical interferometry is now also at the heart of a new quantum-based technologies with applications in metrology, imaging, and quantum information processing. In the solid state world, controlled quantum interference experiments appeared more recently when, thanks to the advances in fabrication, the wavelike nature of electrons could be tested in transport measurements. The observation of Aharonov–Bohm oscillations in the electric current and the Landauer–Büttiker formulation of quantum transport in terms of electronic transmission amplitudes signaled the beginning of quantum electronic interferometry. In this field we have recently initiated an intense investigation of interference effects in quantum Hall bars systems that led us to develop a novel architecture for edge-states interferometry. Within this context, our most recent research efforts focused on the manipulation of edge-state transport with the controlled introduction of artificial scattering centers. Our research activity in nanoscale-interferometry includes also the study of interference effects for the detection of electronic entanglement via current-noise correlations measurements, the study of excess noise and electron-electron interactions in quantum wires, as well as the study of interference effects in signaling processes implemented over quantum networks.

Among the different possible implementations of edge state interferometers, the adoption of chiral fractional quantum Hall channels offers intriguing perspectives thanks the non-trivial interaction mechanisms existing between edge excitations living at the boundary of different fractional quantum Hall states. Recent breakthroughs in the study of interference effects in quantum transport has been the experimental realization of electronic Mach–Zehnder (MZ) and Hanbury–Brown–Twiss (HBT) interferometers using edge states in a quantum Hall bar. Along this line we have proposed an alternative architecture for implementing electronic interferometry in quantum Hall bars which exploits scattering among parallel edge channels [1]. In contrast to previous developments, this one employs a simply connected mesa admitting serial concatenation of building elements closer to optical analogs. We have discussed the implementations of Mach–Zehnder and Hanbury–Brown–Twiss interferometers (Fig. 1) together with structures yet unexplored in quantum electronics.

Within this context, our most recent experimental activity has focused on a new strategy for the fabrication of tunable

point junctions between two quantum Hall edge states, one in the integer and one in the fractional regime [2]. Such junctions offer a valuable experimental feedback for understanding the mechanism of edge interaction between regions in the integer and fractional regime but they remained so far elusive and difficult to implement in practice. We realized our devices exploiting the concept of particle-hole duality that allowed circumventing some of

Vittorio Giovannetti

v.giovannetti@sns.it

### Collaborators

F. Beltram  
G. Biasiol  
F. Dolcini  
R. Fazio  
D. Frustaglia  
S. Heun  
N. Paradiso  
V. Pellegrini  
S. Pugnetti  
S. Roddaro  
L. Sorba  
F. Taddei  
T. Tufarelli

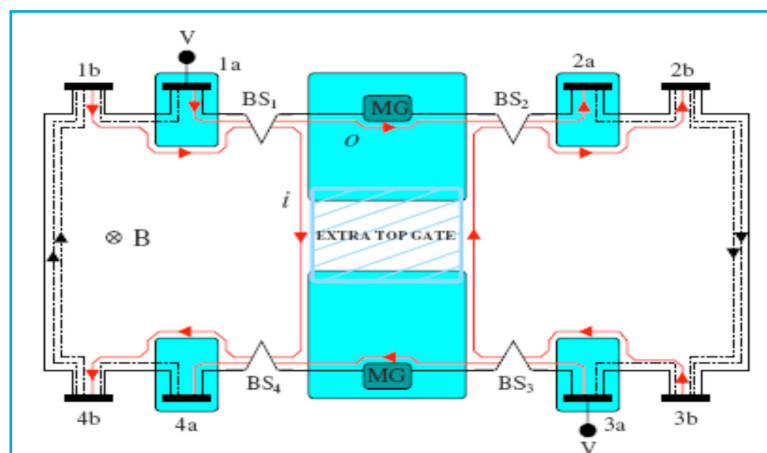


FIG. 1

Implementation of the Hanbury–Brown–Twiss interferometer with edge states. The shaded areas represent top gates that define regions of filling factor 1. In the rest of the sample, instead, we assume 2. Red lines represent the edge channels effectively taking part to the interferometer, BS1 and BS2 are beam splitters, while the gate MG is used to vary the shape and length of the outer edge channel.

the technical difficulties for the fabrication of the devices. The description of the setup and the SEM image of the junction are shown in Fig.2 panels c and d, respectively. We demonstrated that in a real quantum Hall junction transport is largely controlled by the local carrier density (i.e. filling factor) at the constriction point. These results provide relevant information for the realization of edge-state beam splitters of Ref. [1] in the fractional quantum Hall regime.

Another topic attracting a growing interest in the field of interferometry is related to entanglement characterization. On one hand, we have shown that current correlations at the exit ports of a beam splitter originated by crossing two nanowires (Fig. 2) can be used to detect electronic entanglement for a fairly general

input state [Fig. 3]. This includes the situation where electron pairs can enter the beam splitter from the same port, or be separated due to backscattering. The scheme that we have proposed allows to discriminate between occupation-number and degree-of-freedom entanglement. On the other hand, we have discussed an implementation of the entanglement witness, a method to detect entanglement with few local measurements, in systems where entangled electrons are generated both in the spin and orbital degrees of freedom [4]. We have addressed the efficiency of this method in various setups, including two different particle-hole entanglement structures, and we demonstrate that it can also be used to infer information on the possible dephasing afflicting the devices.

Fig. 2.

(a) Results of finite bias transport spectroscopy between an quantum Hall liquid at filling factor  $1/3$  and  $1$ . (b) Comparison between conduction curves at bias  $0$ ,  $200$ ,  $400$  and  $600$  microV and theoretical predictions for two selected limit cases: a discrete system of  $N_s$  (top axis) uncorrelated tunneling centers in the strong coupling regime (hollow blue circles); range of conductance  $G$  oscillation for a quantum Hall line junction. (c) Sketch of the device structure and (d) scanning electron picture of the junction region. From [2].

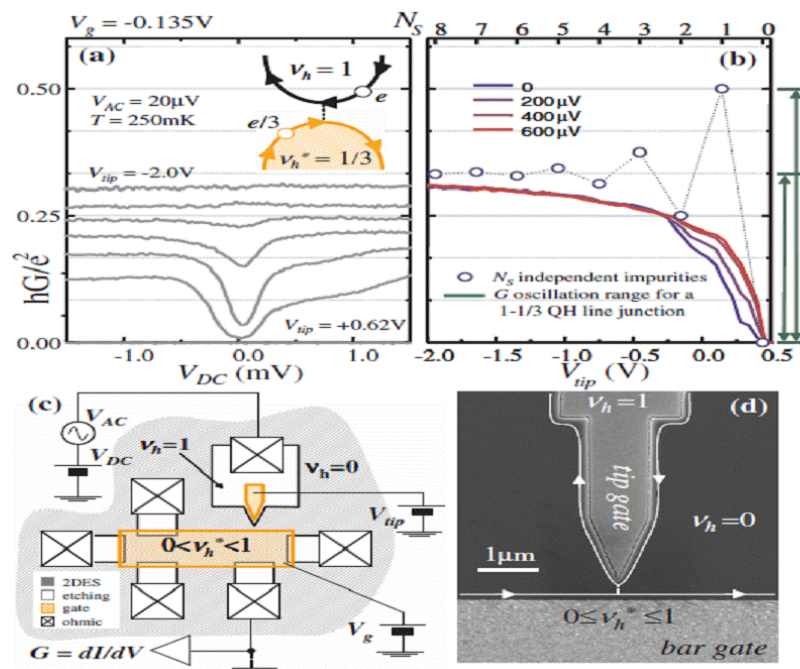
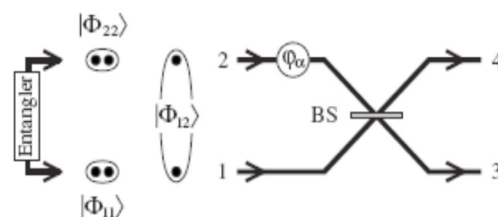


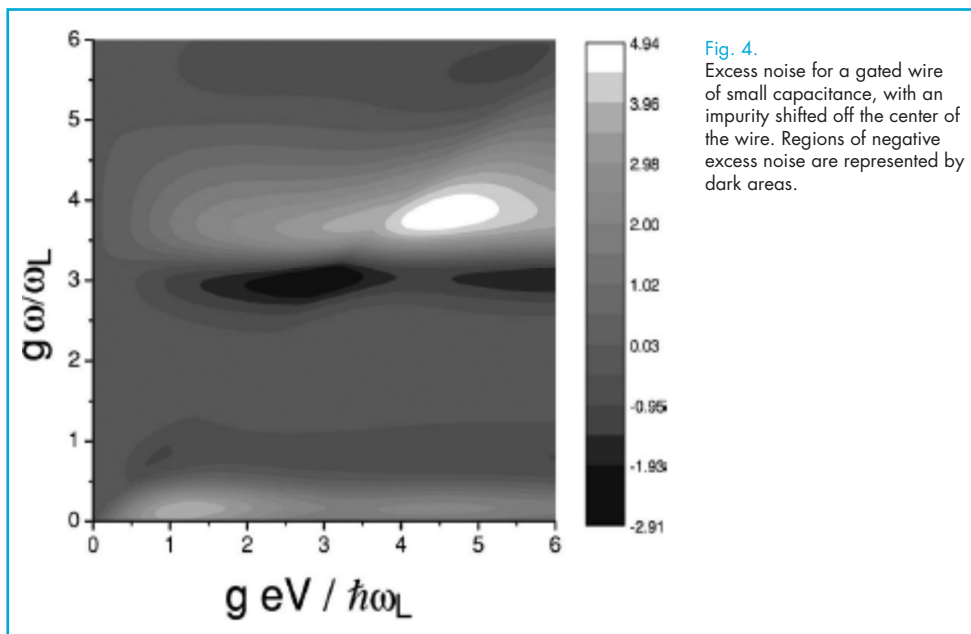
Fig. 3.

Sketch of the analyzer proposed in Ref. [3]. An external entangler prepares electron pairs and injects them into ports 1 and 2. The electrons are allowed to enter the analyzer from the same port and from different ports case, or in any superposition of the previous cases. Electrons propagating along lead 2 undergo an additional orbital or spin dependent controllable phase shift white circle in the figure, before impinging on a 50% beam splitter BS. Current correlations are measured at 3 and 4. From [3].



In our analysis of nanoscale interferometry we have also investigated the current noise of a quantum wire capacitively coupled to a gate in the quantum regime [5] and the conductance in a Fabry-Perot quantum wire configuration [6]. Specifically in the set-up analyzed in [5] both the shot noise and the finite-frequency noise have been analyzed in different regimes, ranging from large to small ratios between the geometrical and the quantum capacitance. In particular, we have demonstrated that the quantity

usually termed excess noise can become negative in various situations even at zero temperature (Fig. 4). Furthermore, we have estimated that such negative excess noise can be observed with state-of-the-art techniques using on-chip noise detection schemes. We therefore expect that these predictions can be verified in current experimental realizations of ballistic 1D conductors, such as quantum wires based on GaAs/AlGaAs heterostructures or single-wall carbon nanotubes.

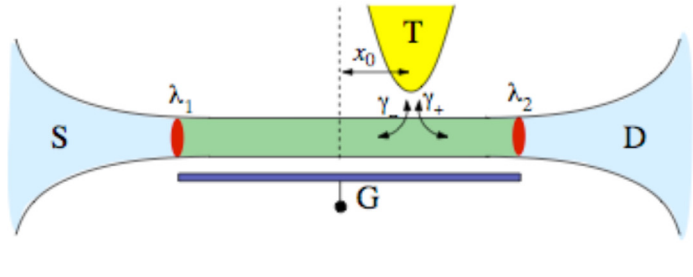


The scheme analyzed in [6] is schematically shown in Fig. 5. Here the wire is coupled to a third terminal (tip), and we allow for an asymmetry of the tip tunneling amplitudes of right and left moving electrons. For such set-up we analyze configurations where the tip acts as an electron injector or as a voltage-probe, and show that the transport properties of this three-terminal set-up exhibit very rich physical behavior. For a non-interacting wire we find that a tip in the voltage-probe configuration affects the source-drain transport in different ways, namely by suppressing the conductance, by modulating the Fabry-Perot oscillations, and by reducing their visibility. The combined effect of

electron electron interaction and finite length of the wire, accounted for by the inhomogeneous Luttinger liquid model, leads to significantly modified predictions as compared to models based on infinite wires. We show that when the tip injects electrons asymmetrically the charge fractionalization induced by interaction cannot be inferred from the asymmetry of the currents flowing in source and drain. Nevertheless interaction effects are visible as oscillations in the non-linear tip-source and tip-drain conductances. Important differences with respect to a two-terminal set-up emerge, suggesting new strategies for the experimental investigation of Luttinger liquid behavior.

Fig. 5.

Sketch of the set-up. A quantum wire is connected to metallic electrodes, denoted as source (S) and drain (D), respectively. A third electrode, denoted as tip (T), injects electrons into the wire at position  $x_0$ . The contact resistances are accounted for by two delta-like scatterers (red spots in the figure). From [6].

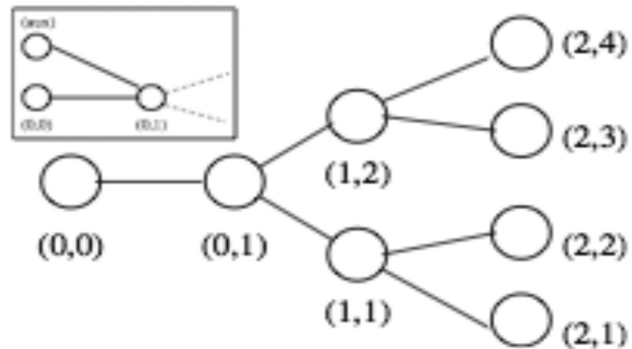


As mentioned in the introductory section, quantum interferometry plays also a fundamental role in efficiently routing the propagation of “signals” over networks of coupled quantum objects (say magnetic impurities). In a recent paper [7], we exploited this effect to improve the efficiency of excitation propagation in a binary-tree configurations (see Fig. 5). For a binary tree of order 2, a simple protocol

is presented which allows one to achieve arbitrary high transfer fidelity. It does not require fine-tuning of local fields and two-node coupling of the intermediate spins. Instead it assumes simple local operations on the intended receiving node: their role is to break the transverse symmetry of the network that induces an effective refocusing of the propagating signals.

Fig. 6.

Schematic of the set-up. Here a collection of spins are coupled via a ferromagnetic Heisenberg interaction according to the edge of the graph and the system is prepared into the ground state. At some initial time  $t$  an excitation is introduced in the system in the node  $(0,0)$  of the figure. The goal of the protocol is to be able to recover such excitation from a selected node on the right. From [7].



## References

- [1] V. Giovannetti, F. Taddei, D. Frustaglia, and R. Fazio, Phys. Rev. B 77, 155320 (2008).
- [2] S. Roddaro, N. Paradiso, V. Pellegrini, G. Biasiol, L. Sorba, F. Beltram Phys.Rev.Lett. 103, 016802 (2009).
- [3] V. Giovannetti, D. Frustaglia, F. Taddei, and R. Fazio, Phys. Rev. B 75, 241305(R) (2007).
- [4] L. Faoro and F. Taddei, Phys. Rev. B 75, 165327 (2007).
- [5] F. Dolcini, B. Trauzettel, I. Safi, and H. Grabert, Phys. Rev. B 75, 030404 (2007).
- [6] S. Pugnetti, F. Dolcini, D. Bercioux, H. Grabert, Phys. Rev. B 79, 035121 (2009).
- [7] T. Tufarelli, and V. Giovannetti, Phys. Rev. A 79, 022313 (2009).

**Q**uantum information allows to solve efficiently some problems which are believed to be intractable classically. Impact and advantages of quantum information protocols emerge in numerous situations and it is now believed that they will play a leading role in future technologies. Together with the ongoing development of more efficient schemes to solves new and old tasks in information science, a great deal of interest is devoted to select suitable physical systems where one can implement realize these ideas. Nanoelectronics is the natural arena to realize physical implementation of quantum hardware and superconducting nanocircuits have already proved to be ideal candidates for qubits. Our works in this period aimed at developing new quantum protocols in computation and communication as well as at the theoretical analysis of superconducting qubits.

Rosario Fazio

r.fazio@sns.it

### Collaborators

L. Amico  
D. Bose  
V. Brosco  
D. Burgarth  
T. Calarco  
F. Caruso  
D. Gerace  
A. Imamoglu  
S. Lloyd  
L. Maccone  
S. Montangero  
A. Osterloh  
D. Rossini  
S. Safaei  
V. Vedral

Among all possible applications of quantum mechanics to information science, communication is the branch that already is mature for technological applications. The paradigmatic approach to quantum communication assumes the possibility of encoding quantum information into mobile physical systems that are then transmitted from the sender of the messages to their intended receiver. This architecture finds its natural implementation in optics where photons, propagating in free-space or through fibers, carries the information from site to site. In [1] we have provided a rather comprehensive analysis of the physics of such channels introducing a general classification of the noise sources that affect them. The typical rates of coherence loss that photons suffer in these systems make it plausible to think at more complex strategies in which the signalling among distant parties is mediated by a network of quantum repeaters located at relatively short distances from each others [2]. Similar ideas have also been proposed to solve the scalability problem of quantum computation [3]. Inspired by such attempts we have developed cluster-like quantum computational and communication models [4,5] in which networks of coupled quantum memories (spin networks) are used as mediators for coordinating the action of otherwise independent, small size quantum computational devices.

The underlying idea of this approach is schematically illustrated in Fig. 1.

Spin networks proved also to be fundamental in designing efficient Quantum Random Access Memory (Qram) elements [6] and thus in addressing security problems such as the private querying of a remote database [7] (the latter being solved by employing our recently developed Quantum Private Query

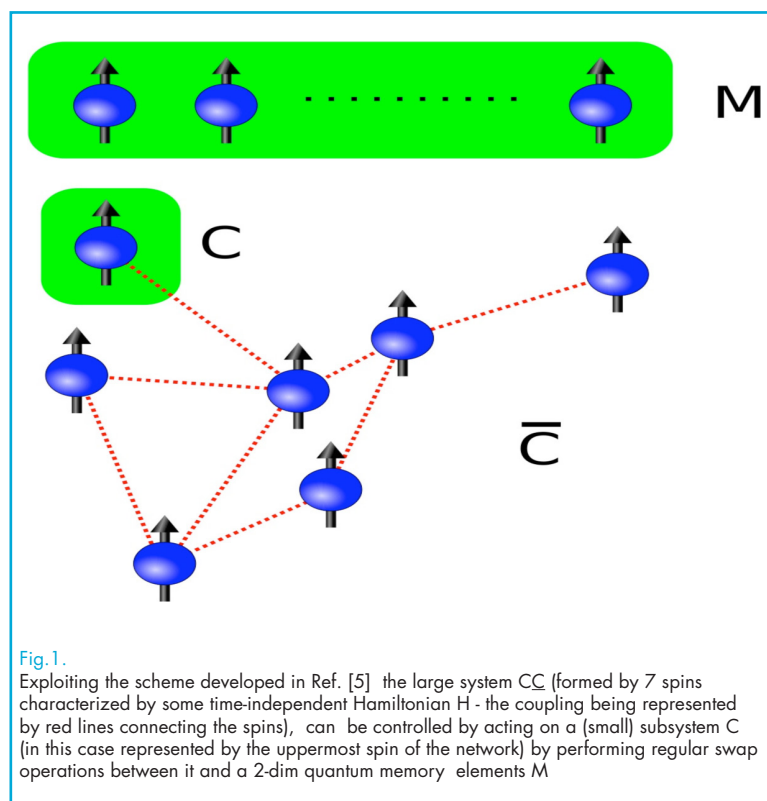


**Fig. 1.** Exploiting the scheme developed in Ref. [5] the large system  $CC$  (formed by 7 spins characterized by some time-independent Hamiltonian  $H$  - the coupling being represented by red lines connecting the spins), can be controlled by acting on a (small) subsystem  $C$  (in this case represented by the uppermost spin of the network) by performing regular swap operations between it and a 2-dim quantum memory elements  $M$

algorithm which exploits explicitly Qram-transformations). To test the feasibility and the efficiency of the above protocols we found it useful to refine our understanding of the mechanisms which superintend at the information flow in spin networks. To this aim we conducted an intense research on the way entanglement emerges in such systems [8-11] and its degradation due to the interaction with neighbouring elements [12].

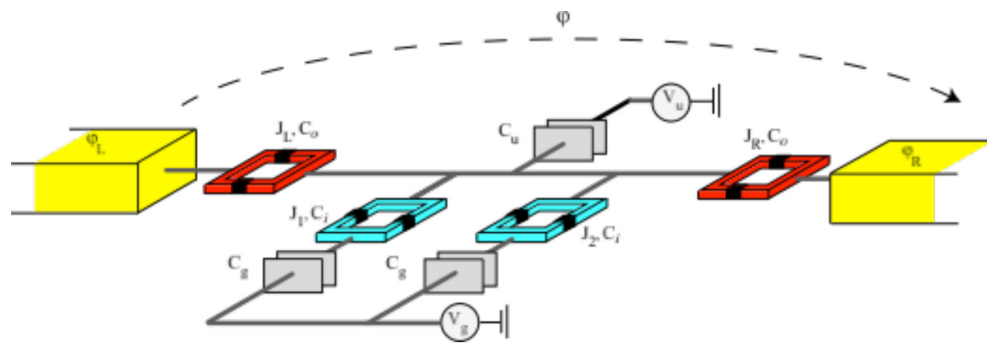
Our research on implementations of quantum information processing we concentrated on Josephson-junction qubits which are considered among the most promising due to their design flexibility and potential scalability. We applied optimal quantum control to superconducting charge qubits [12]. We analysed in detail the effect of noise and leakage, and we showed that optimisation yields a considerable improvement in gate fidelities even under such realistic conditions. Our protocol considerably increases the fidelity of the gate and, more important, it is quite robust in the disruptive presence of  $1/f$  noise. The improvement in the two-bit gate performances (errors of the order of  $10^{-3} \div 10^{-4}$  in realistic cases) allows to cross the fault tolerance threshold. The use of quantum optimal control theory to Josephson systems is not confined to the area of solid state quantum information. We recently applied to quantum pumping as well [13]. We showed that it is possible to obtain very accurate pumps in the non-adiabatic regime by a suitable choice of the shape of the gate voltage pulses (the

shape of these pulses being dictated by quantum optimal control theory). In the optimal case the error, with respect to the quantized value, can be as small as of the order of  $10^{-6} e$  ( $e$ =electron charge). In addition to their importance for metrological applications, Cooper pair pumps allow to study fundamental effects in quantum physics. It has been shown that the charge pumped during one cycle is related to the accumulated geometric phase. We showed that by proper designing the Cooper pair pump it is possible to investigate non-Abelian connections [14]. We derived an expression for the pumped charge in the presence of a degenerate spectrum and relate it to the non-Abelian connection of Wilczek and Zee. We proposed a superconducting network (see the scheme on Fig.2) where this relation can be tested and discuss two clear signatures of non-abelian holonomies.

First, under appropriate conditions, the pumped charge per cycle is quantized. Second and most important here the pumped charge depends both on the cycle and the point where the cycle starts. If tested experimentally this would be a clear proof of the non-Abelian nature of pumping.

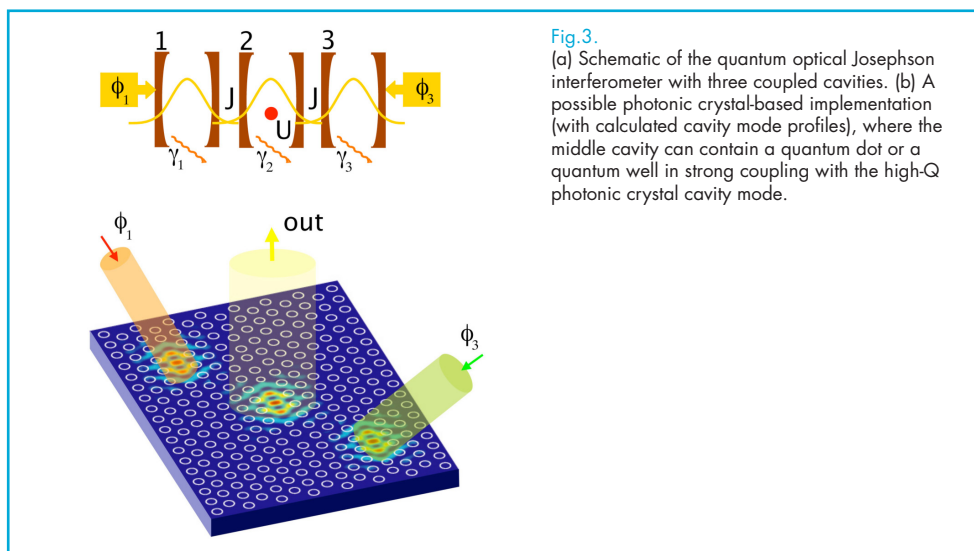
Within the research area on the quantum dynamics of superconducting nanocircuits we also investigated the exciting new area of circuit-QED. In this framework we study the properties of arrays of cavities and determined the phase diagram in the one-dimensional case [15]. Furthermore

Fig.2.  
Scheme for a non-Abelian  
Cooper pair pump.



we designed [16] an new devices that we termed the *Quantum optical Josephson interferometer*. It is shown in the Fig.3 and it consists of two coherently driven linear optical cavities connected via a central cavity with a single-photon nonlinearity. The interplay of tunneling and interactions is analyzed in the steady state of the system, when a dynamical equilibrium between driving and losses is established.

Strong photonic correlations can be identified clearly in the suppression of Josephson-like oscillations of the light emitted from the central cavity as the nonlinearity is increased. In the limit of a single nonlinear cavity coupled to two linear waveguides, we show that photon correlation measurements provide a unique probe of the crossover to the strongly correlated regime.



**Fig.3.** (a) Schematic of the quantum optical Josephson interferometer with three coupled cavities. (b) A possible photonic crystal-based implementation (with calculated cavity mode profiles), where the middle cavity can contain a quantum dot or a quantum well in strong coupling with the high-Q photonic crystal cavity mode.

## References

- [1] F. Caruso, J. Eisert, V. Giovannetti, A.S. Holevo, *New J. Phys.* 10, 083030 (2008).
- [2] J. I. Cirac, P. Zoller, H. J. Kimble and H. Mabuchi, *Phys. Rev. Lett.* 78, 3221 (1997); H.-J. Briegel, W. Dur, J. I. Cirac, and P. Zoller, *Phys. Rev. Lett.* 81, 5932 (1998).
- [3] L. Grover, e-print arXiv:quant-ph/9704012; R. Von Meter, K. Nemoto, and W. J. Munro, e-print arXiv:quant-ph/0701043.
- [4] D. Burgarth, V. Giovannetti, and S. Bose, *Phys. Rev. A* 75, 062327 (2007).
- [5] D. Burgarth and V. Giovannetti, *Phys. Rev. Lett.* 99, 100501 (2007).
- [6] V. Giovannetti, S. Lloyd, and L. Maccone *Phys. Rev. Lett.* 100, 160501 (2008).
- [7] V. Giovannetti, S. Lloyd, and L. Maccone *Phys. Rev. Lett.* 100, 230502 (2008).
- [8] L. Amico, R. Fazio, A. Osterloh, and V. Vedral, *Rev. Mod. Phys.* 80, 517 (2008).
- [9] D. Patane', R. Fazio and L. Amico, *New J. Phys.* 9, 322 (2007).
- [10] D. Binosi, G. De Chiara, S. Montangero, A. Recati, *Phys. Rev. A* 76, 140405 (2007).
- [11] D. Rossini, T. Calarco, V. Giovannetti, S. Montangero, and R. Fazio, *Phys. Rev. A* 75, 032333 (2007).
- [12] S. Montangero, T. Calarco and R. Fazio, *Phys. Rev. Lett.* 99, 170501 (2007).
- [13] S. Safaei, S. Montangero, F. Taddei and R. Fazio, *Phys. Rev. B* 77, 144522 (2008).
- [14] V. Brosco, R. Fazio, F.W.J. Hekking and R. Fazio, *Phys. Rev. Lett.* 100, 027002 (2008).
- [15] D. Rossini and R. Fazio, *Phys. Rev. Lett.* 99, 186401 (2007).
- [16] D. Gerace H. Tureci, A. Imamoglu, V. Giovannetti and R. Fazio, *Nat. Phys.* 5, 281 (2009)



## Silicon-Germanium heterostructures for optoelectronic devices

**S**ilicon and Germanium semiconductors are well known for electronic applications. However Si, Ge and their alloys were not been considered attractive as active materials in light emitting devices due to the indirect nature of fundamental interband transitions. The advent of epitaxial growth techniques, has encouraged many attempts to convert the indirect band gap into a direct band gap exploiting nanostructures engineering by means of control of growth conditions, system geometry, chemical composition, strain, bands alignment and external fields.

For this aim, the preliminary theoretical understanding and design of the complete structure is a key requirement.

We have investigated the electronic and optical properties of Si/SiGe and Ge/SiGe strained-layer multiple quantum wells grown on SiGe substrates with arbitrary alloy composition and strain. The good agreement with the experimental results demonstrates the effectiveness of the adopted theoretical approach based on the tight binding model, and its potential as precious tool to design realistic three dimensional heterostructures with desired electronic and optical properties.

Understanding of the electronic properties of semiconductor quantum-confined structures is a key requirement for the development of their potential applications in electronic and photonic devices. This is particularly relevant for heterostructures based on the SiGe system, in view of their compatibility with Si technology.

In particular, Ge has been playing an important role in Si-based photonics. Ge is a material largely compatible with Si processing, it is an indirect gap material but with the 0.8 eV direct transition at the  $\Gamma$  point not far above the indirect fundamental gap at 0.66 eV. This fact, together with the miscibility of Si and Ge over the whole concentration range, has led to a number of proposals for Si compatible Ge-based photonic device applications. Photo detectors made from epitaxial Ge layers on Si substrates, optical modulators based on the Franz-Keldysh effect, and most recently, optical modulators based on the quantum-confined Stark effect in strained Ge wells have been demonstrated. These results have motivated our objective to find a route toward an optoelectronics platform based on Si CMOS and Ge quantum wells. A  $sp^3d^5s^*$  tight-binding model has been adopted to evaluate the electronic properties and the interband and intraband optical transitions of a variety of low- and

rich- content Ge quantum wells between SiGe alloys barriers, grown along the [001] direction, under strain conditions imposed by a relaxed SiGe buffer alloy.

As first item we have investigated the possibility of achieving conduction intersubband transitions induced by normal incidence radiation in a n-type SiGe-based quantum well (QW) structure coherently grown on a SiGe substrate along the [001] direction [1]. The quest of normal incidence geometry, i.e. incident electric field polarized along the growth plane (TE polarization), is motivated by the technical simplifications it allows in fabrication of planar large array of infrared detectors for imaging applications. In fact quantum mechanical selection rules forbid coupling of radiation with electrons degree of freedom if the incident electric field has no component along the growth direction. In p-type QWs, due to the mixing of heavy hole, light hole and split off subbands, valence intersubband transitions are possible for whatever polarization of the incident radiation. In n-type QWs, we have to distinguish the case of isotropic conduction band minimum at the  $\Gamma$  point in direct gap structures and the case of indirect gap structures but with effective mass tensor diagonal with respect to the growth axis (Si-rich QW grown along

Giuseppe Grosso

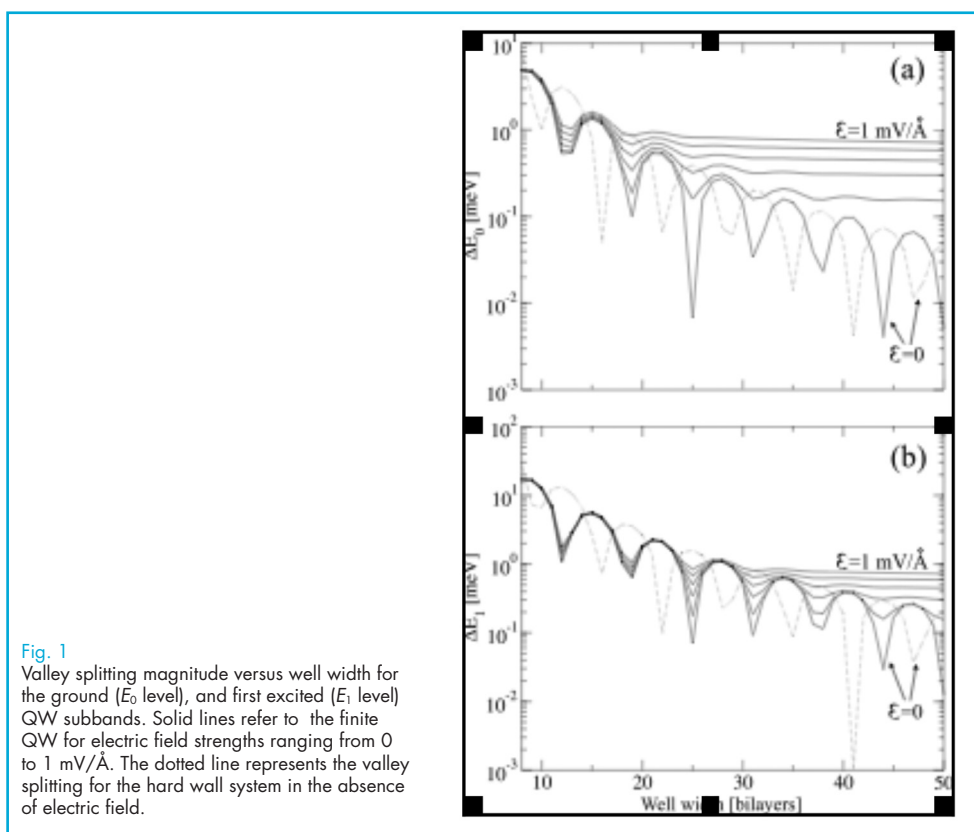
grosso@df.unipi.it

### Collaborators

F. Beltram  
M. Bonfanti  
D. Chrastina  
E. Grilli  
M. Guzzi  
G. Isella  
A. Tredicucci  
M. Virgilio  
H. von Känel

the [001] direction), from the case of conduction band ellipsoid minimum tilted with respect to the QW growth direction (Ge-rich QW grown along the [001] direction). We have demonstrated numerically that for the former class of structures normal incidence intersubband transitions are forbidden while they are allowed for the latter one [2, -4].

We have then analyzed the energy profile of the lowest conduction bands in Si and Ge QWs under different strain conditions [2, 4]. In particular we have investigated how the degeneracy of equivalent valleys in the bulk materials is resolved by uniaxial stress or other perturbations along the [001] axis, and how valley splitting depends from the well width or superimposed electric fields (see Fig. 1).



As second item we have studied interband optical transitions in Ge/SiGe MQWs with Ge-rich barriers [5,6]. Strain effects in the structure have been taken into account by means of elasticity theory and scaling the tight-binding hopping parameters according to the modified interatomic distances. Alloying in the barrier region was described by the virtual-crystal approximation.

To interpret the near-gap absorption, we show in the inset of Fig. 2 the band-edge profiles at the  $\Gamma$  and  $L$  points and the confined states obtained from

the diagonalization of the multilayer Hamiltonian. The arrows in Fig. 2 indicate the calculated transition energies between QW states at  $\Gamma$ , without excitonic effects. The peaks in the transmission spectra can thus be attributed to dipole allowed  $HHn-c\Gamma n$ ,  $LHn-c\Gamma n$ , and  $SO n-c\Gamma n$  transitions. Here,  $HHn$ ,  $LHn$ , and  $SO n$  indicate heavy- and light-hole and split-off valence states at  $\Gamma$ , respectively, and  $c\Gamma n$  indicate conduction states at  $\Gamma$ . All of them are confined in the Ge region with a type-I band-edge profile. In the transmission spectra, no clear evidence was found of

the expected indirect transitions at lower energies between confined hole states at  $\Gamma$  and conduction-band states at the  $L$  point.

We have also performed numerical investigations of the confined Stark effect in strained Ge quantum wells separated by  $\text{Si}_{0.15}\text{Ge}_{0.85}$  barriers [7]. Our simulations

(see Fig. 3) support the experimental results of Kuo *et al.* (Nature 437, 1334 (2005)) that this effect is robust even in group IV heterostructures involving Ge QWs provided that direct transitions at  $\Gamma$  are exploited. Excitonic effects below and above the interband threshold are also included in our calculations.

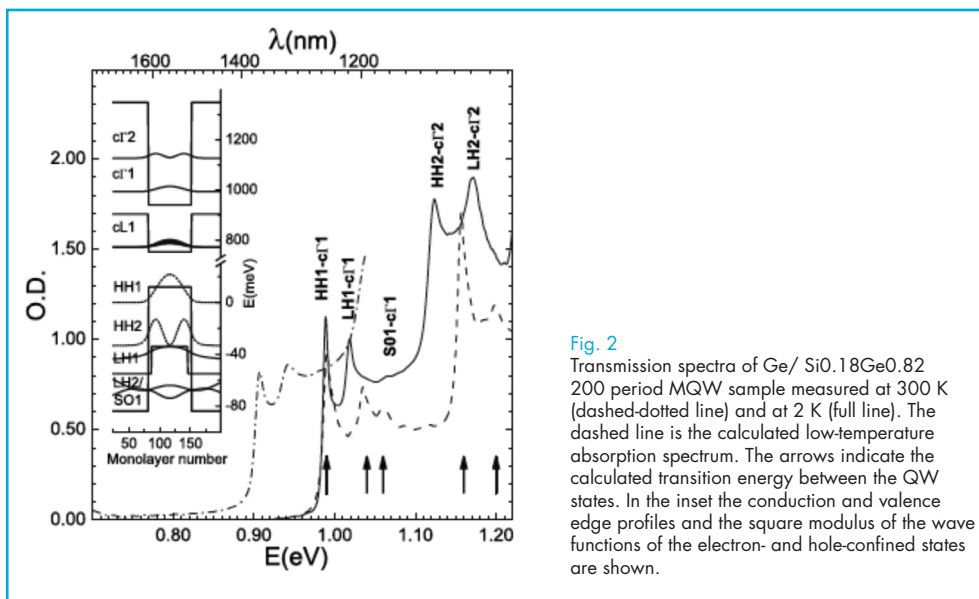


**Fig. 2**  
Transmission spectra of Ge/  $\text{Si}_{0.18}\text{Ge}_{0.82}$  200 period MQW sample measured at 300 K (dashed-dotted line) and at 2 K (full line). The dashed line is the calculated low-temperature absorption spectrum. The arrows indicate the calculated transition energy between the QW states. In the inset the conduction and valence edge profiles and the square modulus of the wave functions of the electron- and hole-confined states are shown.

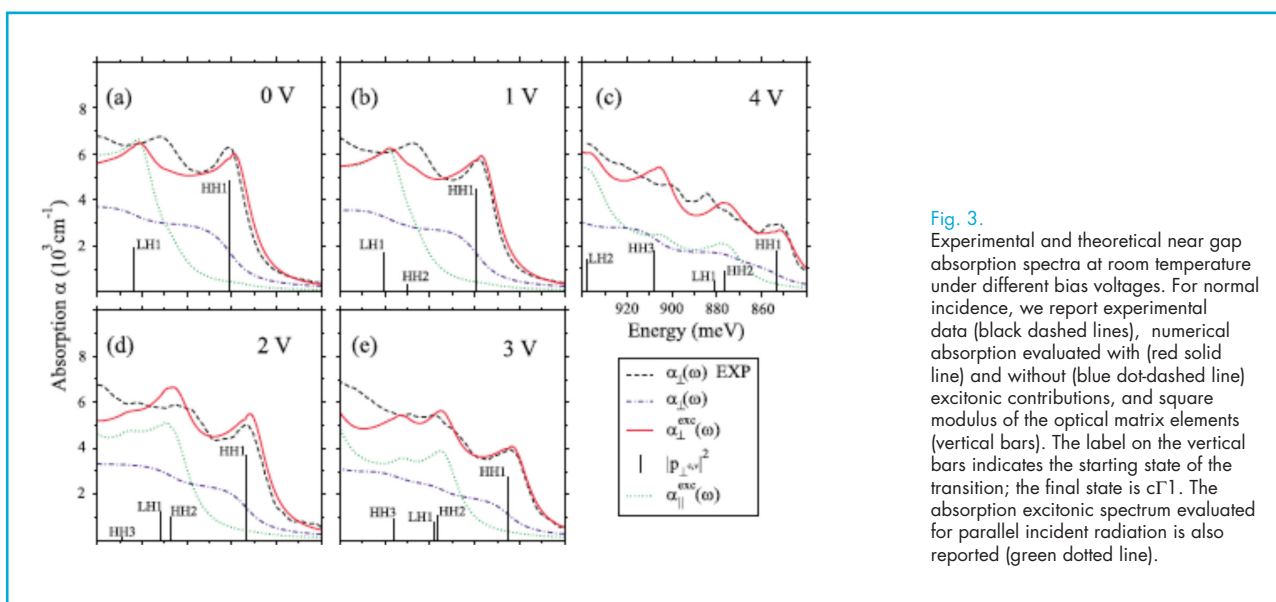


**Fig. 3.**  
Experimental and theoretical near gap absorption spectra at room temperature under different bias voltages. For normal incidence, we report experimental data (black dashed lines), numerical absorption evaluated with (red solid line) and without (blue dot-dashed line) excitonic contributions, and square modulus of the optical matrix elements (vertical bars). The label on the vertical bars indicates the starting state of the transition; the final state is  $c\Gamma_1$ . The absorption excitonic spectrum evaluated for parallel incident radiation is also reported (green dotted line).

## References

- [1] M. Virgilio, and G. Grosso "Conduction intersubband transitions at normal incidence in  $\text{Si}_{1-x}\text{Ge}_x$  quantum wells devices" *Nanotechnology* 18, 075402 (2007)
- [2] M. Virgilio, and G. Grosso "Optical transitions between valley split subbands in biased Si quantum wells" *Phys. Rev. B* 75, 235428 (2007)
- [3] M. Virgilio and G. Grosso "Valley splitting and selection rules for inter-doublets optical transitions in strained [001]-Si/SiGe heterostructures" *Physica E* 40, 2046 (2008).
- [4] M. Virgilio and G. Grosso "Valley splitting and optical intersubband transitions at parallel and normal incidence in [001]-Ge/SiGe quantum wells" *Phys. Rev. B* 79, 165310 (2009)
- [5] M. Bonfanti, E. Grilli, M. Guzzi, M. Virgilio, G. Grosso, D. Chrastina, G. Isella, H. von Känel and A. Neels "Optical transitions in Ge/SiGe multiple quantum wells with Ge-rich barriers" *Phys. Rev. B* 78, 041407(2008)
- [6] M. Virgilio, M. Bonfanti, D. Chrastina, A. Neels, G. Isella, E. Grilli, M. Guzzi, G. Grosso, H. Sigg and H. von Känel, "Polarization-dependent absorption in Ge/SiGe multiple quantum wells: theory and experiment", *Phys Rev. B* 79, 075323 (2009)
- [7] M. Virgilio, and G. Grosso "Quantum confined Stark effect in Ge/SiGe Quantum Wells: a tight-binding description" *Phys. Rev. B* 77, 165315 (2008)

## Thermal properties at the nanoscale: cooling and nonequilibrium

The understanding and the control of thermal properties is an interesting issue in nanoscale systems [1]. Due to their reduced sizes, out-of-equilibrium conditions can be reached and exploited once the energy relaxation mechanisms are under control. In this context electron cooling realized through electrostatic means is probably one of the most relevant aspects. The prototype refrigeration scheme, operating around or below 1K, is based on superconductors, which are characterized by a poor thermal conductivity in a well-defined energy window. This yielded substantial electron temperature reduction in metallic nanostructures. Our research interests in this field comprise both experimental and theoretical activities and focussed on different aspects: novel refrigeration schemes, manipulation of out-of-equilibrium conditions, study of relaxation mechanisms, and study of thermal transport properties in the presence of superconducting correlations.

Francesco Giazotto

f.giazotto@sns.it

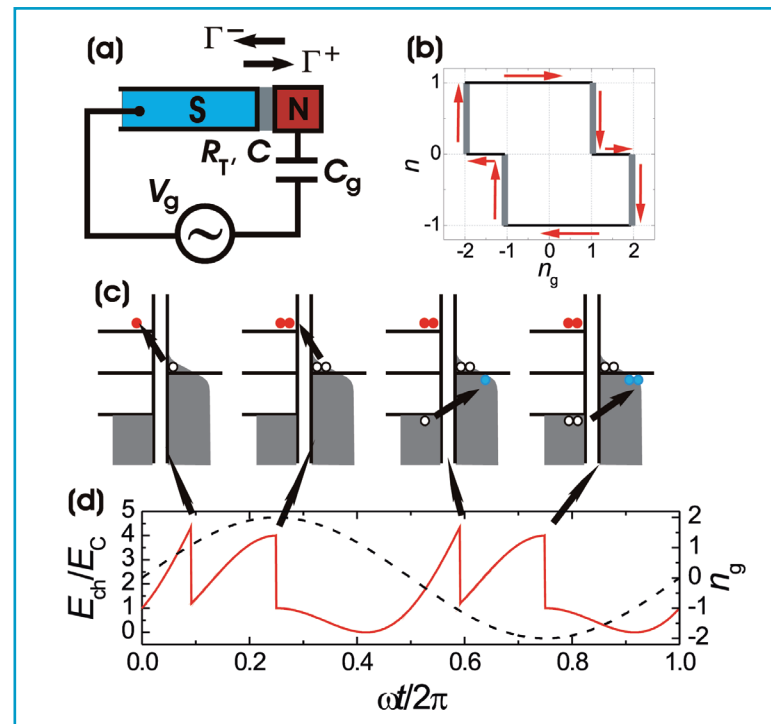
### Collaborators

F. Beltram  
O. Bourgeois  
R. Fazio  
C.P. Garcia  
S. Gasparinetti  
M. Governale  
H. Rabani  
J.P. Pekola  
O.P. Saira  
A. Savin  
F. Taddei  
S. Tirelli

Several important open questions concerning the cooling scheme based on superconductors have been addressed. On the experimental side, in the first instance we have proposed a cyclic refrigeration principle [2] which uses the sequential tunneling of electrons in a Coulomb-blockaded normal metal-superconductor single electron box (see Fig. 1). This results in a cooling power of about  $k_B T \times f$  at temperature  $T$  over a wide range of cycle frequencies  $f$ . Electrostatic work, done by the gate voltage source, removes heat from the Coulomb island with an efficiency of about  $k_B T / \Delta$ , where  $\Delta$  is the superconducting gap parameter. The performance is not affected significantly by nonidealities, for instance by offset charges. Secondly, we have conducted experiments [3] on a superconductor-normal-metal electron refrigerator in a regime where single-electron charging effects are significant. The system functions as a heat transistor; i.e., the heat flux out from the normal-metal island can be controlled with a gate voltage. A theoretical model developed within the framework of single-electron tunneling provides a full quantitative agreement with the experiment. This work serves as the first experimental observation of Coulombic control of heat transfer and, in particular, of refrigeration in a mesoscopic system. On the theoretical side, we have analyzed the influence of an ac drive on

heat transport in a hybrid normal metal-superconductor tunnel junction in the photon-assisted tunneling regime [4]. We have found that the useful heat flux out of the normal metal is always reduced as compared to its magnitude under static and quasi-static drive conditions. Our results are useful to predict the operative conditions for ac-driven superconducting electron refrigerators. Furthermore, we have proposed two novel refrigeration schemes. The first one starts from the consideration that when the cooling mechanism is based on a superconductor,

Fig. 1. (a) Single-electron box with a normal metal (N) island and a superconducting (S) lead. (b) The trajectory on the  $(n, n_g)$  plane for the cycle discussed here. (c) Sketch of energy band diagrams of the device showing the tunneling processes in this cycle. (d) The charging energy of the system (solid line, left scale), where discontinuities are observed as electrons tunnel. The gate cycle is shown by the dashed line (right scale).



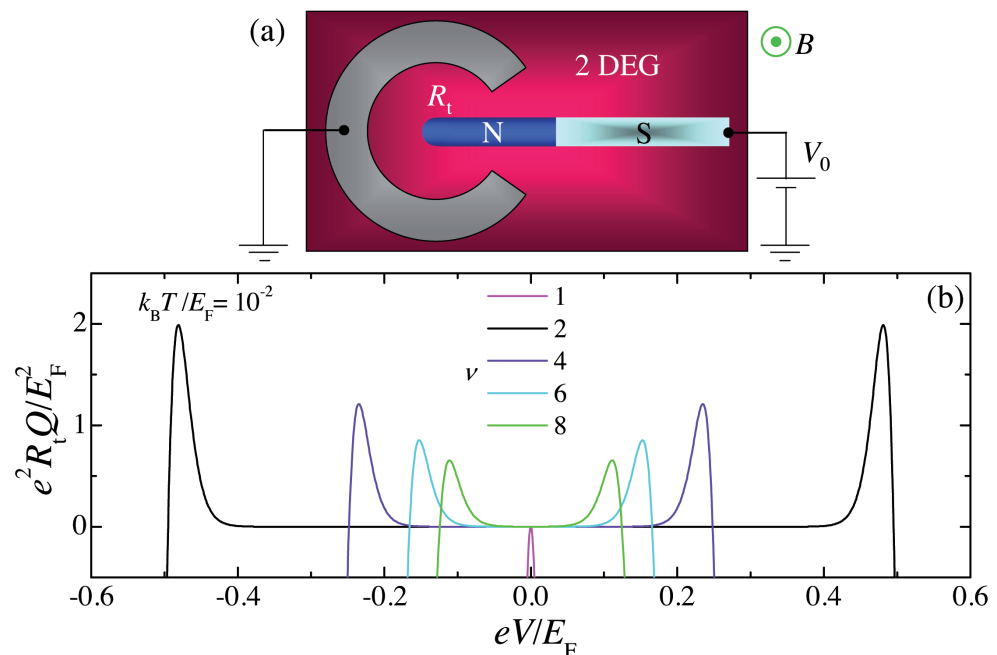
the cooling power at a given temperature is essentially determined by the value of the superconducting gap, which is fixed by the choice of the metal. Tunable gaps would be highly desirable in view of scalable applications. Motivated by this goal, we have proposed [5] a novel mechanism for refrigeration, based on *Landau-level quantization* (see Fig. 2). Analyzing thermal transport in two-dimensional electron gases (2DEGs) we have been able to show that heat can be efficiently extracted from a metallic nanostructure, thanks to the peculiar *bulk* DOS originating from Landau quantization. We find a large heat current through the system (about  $10^{-9}$  W) yielding a sizable electron cooling also at bath temperatures as high as a few kelvin. Moreover, the possibility to easily set the magnetic field value makes it possible to finely tune and optimize the performance available with this refrigeration principle under different operational conditions. As a further alternative refrigeration schemes, we have reconsidered a cooling principle, originally proposed in the 1930s but mostly unexploited so far, which is based on the adiabatic magnetization of a superconductor. We have presented [6]

a detailed dynamic description of the effect, computing the achievable final temperatures as well as the process time scales for different superconductors in various regimes. We have shown that, although in the experimental conditions explored so far the method is in fact inefficient, a suitable choice of initial temperatures and metals can lead to unexpectedly large cooling effect, even in the presence of dissipative phenomena. Our results suggest that this principle can be re-envisaged today as a performing refrigeration method to access the  $\mu\text{K}$  regime.

The understanding and manipulation of out-of-equilibrium conditions and their relation to heat dynamics in nanostructures is an important part of our research activity. In this direction we have performed several experiments. On the one hand, we have demonstrated [7] that manipulation of a Josephson current and its generation at temperatures above the critical one can be achieved by varying quasiparticle injection into a small superconducting Ti island tunnel coupled to four Al superconducting electrodes (see Fig. 3). Our results are successfully described within a model

Fig. 2.

(a) A normal metal island (N) is tunnel coupled to a 2DEG in an open pseudo Corbino disk geometry in the presence of a quantizing magnetic field. Grey region represents an ohmic contact to the 2DEG. (b) Heat current  $Q$  extracted from the N region versus voltage drop  $V$  across the barrier, for different filling factors  $\nu$ .



relating the superconducting state of the island to the heat flux originating from quasiparticle injection. From the practical point of view, our experiment demonstrates that quasiparticle injection can cool a metal wire from its normal state deep into the superconducting phase. On the other hand, we have studied quasiparticle energy relaxation at subkelvin temperatures by injecting hot electrons into an Al island and measuring the energy flux from quasiparticles into phonons both in the superconducting and in the normal state [8]. The data show strong reduction of the flux at low temperatures in the superconducting state, in qualitative agreement with the theory for clean superconductors. However, quantitatively the energy flux exceeds the theoretical predictions both in the superconducting and in the normal state, suggesting an enhanced or additional relaxation process. As far as theory is concerned, we have studied the role of the superconducting proximity effect on the electron-phonon energy exchange (a relevant relaxation mechanism for electrons in metals) in diffusive normal metals attached to superconductors [9].

The proximity effect modifies the local density of states in the normal metal leading to a weakening of the electron-phonon energy relaxation. We have shown that the effect is easily observable with modern thermometry methods and predicted that it can be tuned in structures connected to multiple superconductors by adjusting the phase difference between superconducting order parameters at the two NS interfaces.

Finally, we have theoretically investigated the influence of superconducting correlations on the electronic specific heat of a diffusive superconductor-normal metal-superconductor (SNS) Josephson junction [10,11]. We show that, thanks to proximity effect, the specific heat of the  $N$  region can be dramatically different from that in the absence of superconductivity (see Fig. 4). In particular, at low temperature, it is substantially suppressed with respect to the normal state and turns out to be largely tunable in magnitude by changing the phase difference between the  $S$  reservoirs. Such peculiarity of mesoscopic SNS Josephson junctions may have an impact for the implementation of devices, for instance,

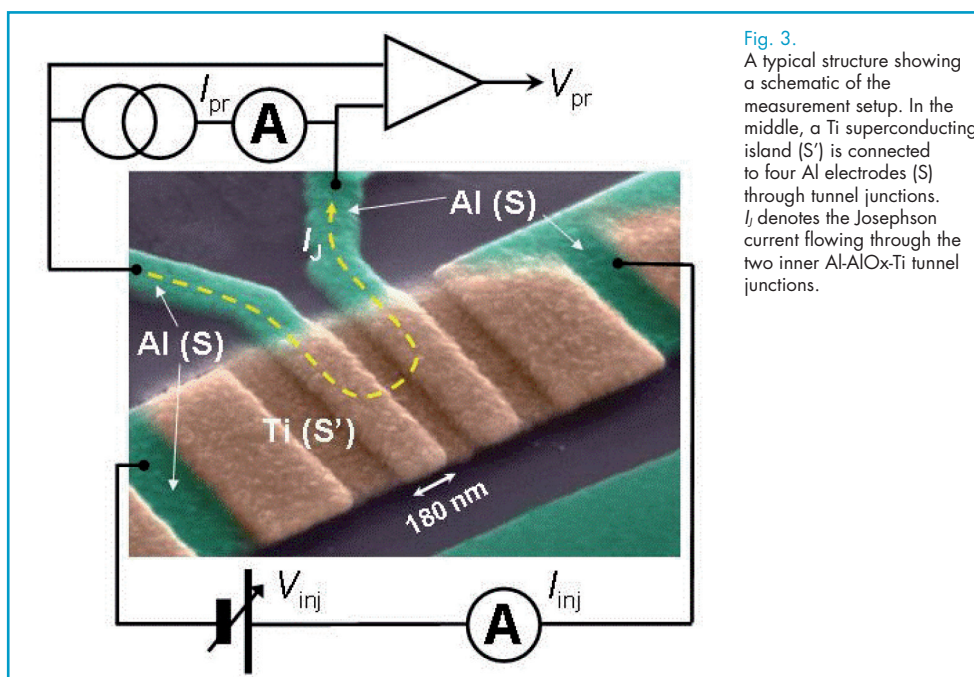


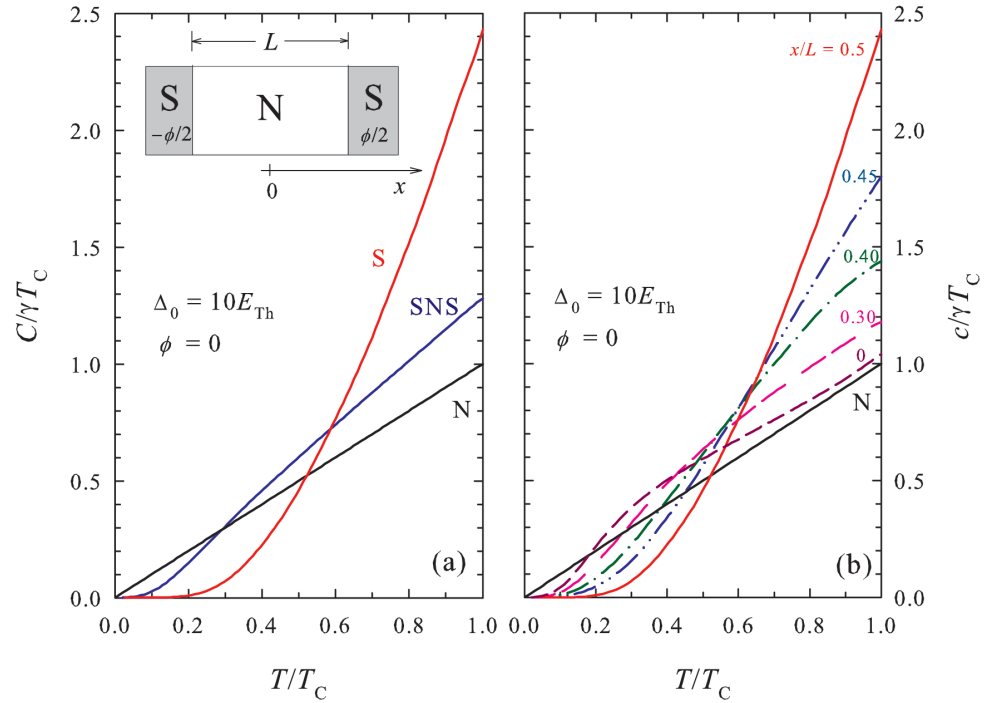
**Fig. 3.** A typical structure showing a schematic of the measurement setup. In the middle, a Ti superconducting island ( $S'$ ) is connected to four Al electrodes ( $S$ ) through tunnel junctions.  $I_J$  denotes the Josephson current flowing through the two inner Al-AlOx-Ti tunnel junctions.

ultrasensitive single-photon detectors based on proximity effect. We have also considered the influence of nonidealities occurring in an actual experiment, such

as the presence of barriers at the normal metal-superconductor interfaces, the spin-flip, the inelastic scattering in the N-metal region, and quasiparticle subgap states in the superconductors.

Fig. 4.

(a) Comparison of the SNS electronic specific heat  $C$  vs temperature  $T$  with that in the normal state (N) and in the superconductor (S) calculated for  $\Delta = 10 E_{\text{Th}}$  and  $\phi = 0$ . The inset shows a scheme of the SNS junction of length  $L$ . The point  $x = 0$  denotes the middle of the junction and the system is assumed quasi one dimensional. (b) Specific heat per unit length  $c$  vs  $T$  at different positions  $x$  along the N wire, calculated for  $\Delta = 10 E_{\text{Th}}$  and  $\phi = 0$ . Also shown is the specific heat in the absence of superconductivity (N).  $T_C$  is the critical temperature of the superconductor, and  $E_{\text{Th}}$  is the Thouless energy.



#### References

- [1] F. Giazotto, T. Heikkilä, A. Luukanen, A. M. Savin, J. P. Pekola, *Rev. Mod. Phys.* **78**, 217 (2006).
- [2] J. P. Pekola, F. Giazotto, O-P Saira, *Phys. Rev. Lett.* **98**, 037201 (2007).
- [3] O-P Saira, M. Meschke, F. Giazotto, A. M. Savin, M. Möttönen and J. P. Pekola, *Phys. Rev. Lett.* **99**, 027203 (2007).
- [4] N. B. Kopnin, F. Taddei, J. P. Pekola, F. Giazotto, *Phys. Rev. B* **77**, 104517 (2008).
- [5] F. Giazotto, F. Taddei, M. Governale, R. Fazio, and F. Beltram, *New J. Phys.* **9**, 439 (2007).
- [6] F. Dolcini and F. Giazotto, *Phys. Rev. B* **80**, 024503 (2009).
- [7] S. Tirelli, A. M. Savin, C. Pascual Garcia, J. P. Pekola, F. Beltram, and F. Giazotto, *Phys. Rev. Lett.* **101**, 077004 (2008).
- [8] A.V. Timofeev, C. Pascual Garcia, N. B. Kopnin, A. M. Savin, M. Meschke, F. Giazotto, and J. P. Pekola, *Phys. Rev. Lett.* **102**, 017003 (2009).
- [9] T. T. Heikkilä and F. Giazotto, *Phys. Rev. B* **79**, 094514 (2009).
- [10] H. Rabani, F. Taddei, O. Bourgeois, R. Fazio, and F. Giazotto, *Phys. Rev. B* **78**, 012503 (2008).
- [11] H. Rabani, F. Taddei, F. Giazotto, and R. Fazio, *J. Appl. Phys.* **105**, 093904 (2009).

## Quantum transport in hybrid normal-superconductor nanostructures

The quantum mechanical character of electronic transport can be accessed in nanoscale systems at low temperatures, typically below 1 K. Quantum behavior is of particular relevance in hybrid nanostructures, which are realized by putting into contact materials whose transport properties are different in nature, such as superconductors and normal metals (or semiconductors). While in the latter transport is due to essentially independent electrons, in superconductors electrons find themselves in a collective quantum state which yields transport without dissipation (supercurrent). In normal-superconductor hybrid nanostructures some superconducting properties are induced in the normal material giving rise to a large variety of phenomena, the most celebrated one being the Josephson effect. Our efforts in this field are directed both to experimental and theoretical aspects and comprise different issues such as spin-dependent effects, Josephson nanodevices and the characterization of entanglement.

Fabio Taddei

f.taddei@sns.it

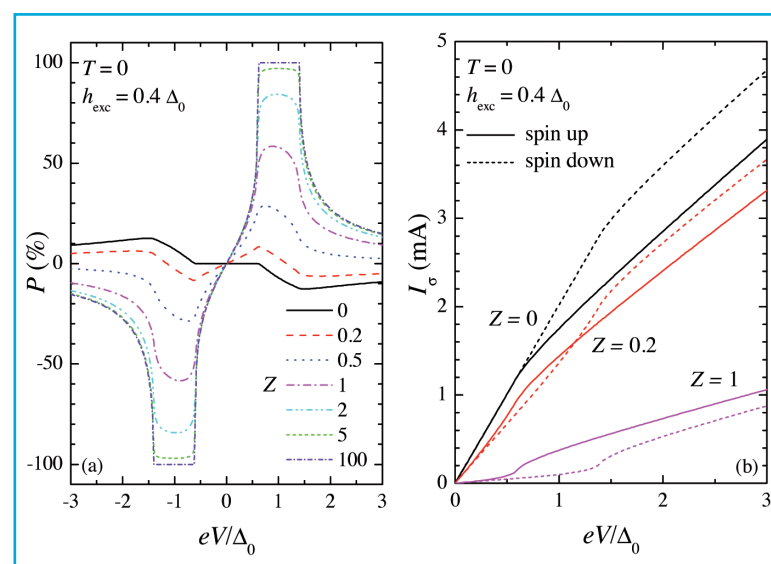
### Collaborators

F. Beltram  
P. D'Amico  
F. Dolcini  
R. Fazio  
C. P. García  
F. Giazotto  
S. Pugnetti  
J. Splettstoesser  
S. Tirelli

Spin-dependent properties, which are at the basis of spintronics devices, can be observed in hybrid systems. In this context we have analyzed the spin-dependent transport properties in systems composed of a normal region tunnel coupled to two superconductors with exchange fields induced by the proximity to thin ferromagnetic layers [1]. We have demonstrated that the quasiparticle distribution functions in the normal region depend on spin and are strongly sensitive to the relative angle between exchange fields in the two superconductors. As a result, the electric current flowing through the system is found to be strongly dependent on the relative angle between exchange fields, giving rise to a huge value of magnetoresistance. By tunnel coupling the normal region to an additional superconducting electrode, we have shown that it is possible to implement a spin-polarized current source of both spin species, depending on the bias voltages applied. Extraordinary large tunnel magnetoresistance, as large as 10<sup>6</sup>%, could be also obtained in a superconducting double spin valve device which takes advantage of the interplay between the spin-filtering effect of ferromagnetic insulators and superconductivity-induced out-of-equilibrium transport [2]. Importantly, magnetoresistance can be tuned over several orders of magnitude under voltage

biasing. Furthermore we have investigated the spin-polarized transport in normal metal–superconductor (NS) junctions as a function of interface transmissivity as well as temperature when the density of states of a superconductor is Zeeman-split in response to an exchange field [3]. Similarly to the “absolute spin-valve effect” predicted in Ref. [4], we have shown that NS junctions can be used to generate highly spin-polarized currents, in alternative to half-metallic ferromagnets. In particular, the spin-polarized current obtained is largely tunable in magnitude and sign by acting on bias voltage (Fig. 1). The effect can be enhanced by electron “cooling” provided by the superconducting gap.

Fig. 1. (a) Current polarization  $P$  vs bias voltage  $V$  for several values of interface transmissivity  $Z$  at  $T=0$ . (b) Spin-dependent electric current  $I_s$  vs  $V$  calculated for some  $Z$  values at  $T=0$ .

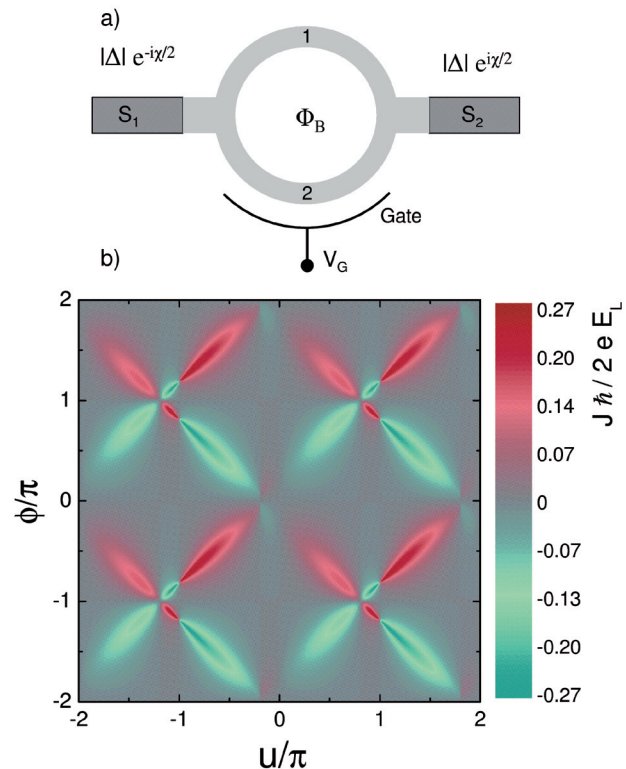


Another topic attracting a growing interest in the field of hybrid systems is the one concerning Josephson devices in which of interest is the supercurrent flowing between two superconducting regions separated by a weak link. On the theoretical side, we have demonstrated that when the weak link consists of a normal ballistic Aharonov-Bohm ring one can realize a fully controllable Josephson  $\pi$ -junction [5]: both the magnitude and the sign of the supercurrent can be tuned by the combined use of the magnetic flux threading the ring and the electrostatic gate located in one of the ring arms (Fig. 2). Estimates of the supercurrent for realistic implementations using InGaAs rings coupled to Nb electrodes lead to values of hundreds of nanoamperes, allowing to envisage this system as a promising realization of Josephson transistors. When the weak link is a single-walled metallic carbon nanotube we have analyzed the effects of the electron–electron interactions on the supercurrent within the Luttinger

liquid theory [6]. We have found that in the long junction limit the strong electronic correlations of the nanotube, together with its peculiar band structure, induce oscillations in the critical current as a function of the junction length and/or the nanotube electron filling. These oscillations represent a signature of the Luttinger liquid physics of the nanotube, for they are absent if the interaction is vanishing. This effect can be exploited to reverse the sign of the supercurrent, realizing a tunable  $\pi$ -junction. Out-of-equilibrium current has been investigated in the case where the weak link consists of a quantum dot. In particular, we have analyzed the effects of both Rashba and Dresselhaus spin-orbit couplings of the dot on the current-voltage characteristics, in the regime of strong dot-lead coupling [7]. The multiple Andreev reflection (MAR) subgap peaks are found to be modified, but not suppressed, by the spin-orbit interaction in a way that it strongly depends on the shape of the dot confining potential. In an isotropic dot

Fig. 2.

(a) Scheme of the Aharonov-Bohm Josephson junction. The light gray region indicates the normal metal ring, whereas dark green regions denote the superconducting leads. (b) Josephson current (in arbitrary units) as a function of gate voltage  $u=eV_G/E_L$  and normalized magnetic flux  $f$ , for a ring of 600nm long arms ( $E_L$  is the Thouless energy). Both magnitude and sign of the Josephson current can be tuned.



the MAR peaks are enhanced when the strength of Rashba and Dresselhaus terms are equal. In contrast, when the anisotropy of the dot confining potential increases, the dependence of the subgap structure on the Rashba-to-Dresselhaus spin-orbit angle decreases. Remarkably we have found that, when an in-plane magnetic field is applied to a strongly anisotropic dot, the peaks of the nonlinear conductance  $G$  oscillate as a function of the magnetic-field angle. This allows for a straightforward read-out of the spin-orbit angle through the location of maxima and minima of  $G$ . Regarding Josephson devices, we have conducted experimental investigation on two different nanosystems. The first one is a radiation detector based on a long superconductor-normal metal-superconductor Josephson junction [8]. The operation of this proximity Josephson sensor relies on large kinetic inductance variations under irradiation due to the exponential temperature dependence of the critical current. Coupled with a dc superconducting quantum interference

device readout, the device is able to provide a signal to noise ratio up to 1000 in the terahertz regime if operated as calorimeter, while very low electrical noise equivalent power at 200 mK can be achieved in the bolometer operation. The high performance together with the ease of fabrication make this structure attractive as an ultrasensitive cryogenic detector of terahertz electromagnetic radiation. The second system [9] consists of a planar V/Cu/V nanoscopic Josephson weak link (see Fig. 3). We have analyzed the low-temperature behavior of junctions of different length. The shorter junctions exhibit critical currents of several tens of microamperes at 350 mK, while Josephson coupling persists up to  $\sim 2.7$  K. Good agreement is obtained by comparing the measured switching currents to a model which holds in the diffusive regime. Our results demonstrate that V is an excellent candidate for the implementation of superconducting nanodevices operating at a few kelvins.

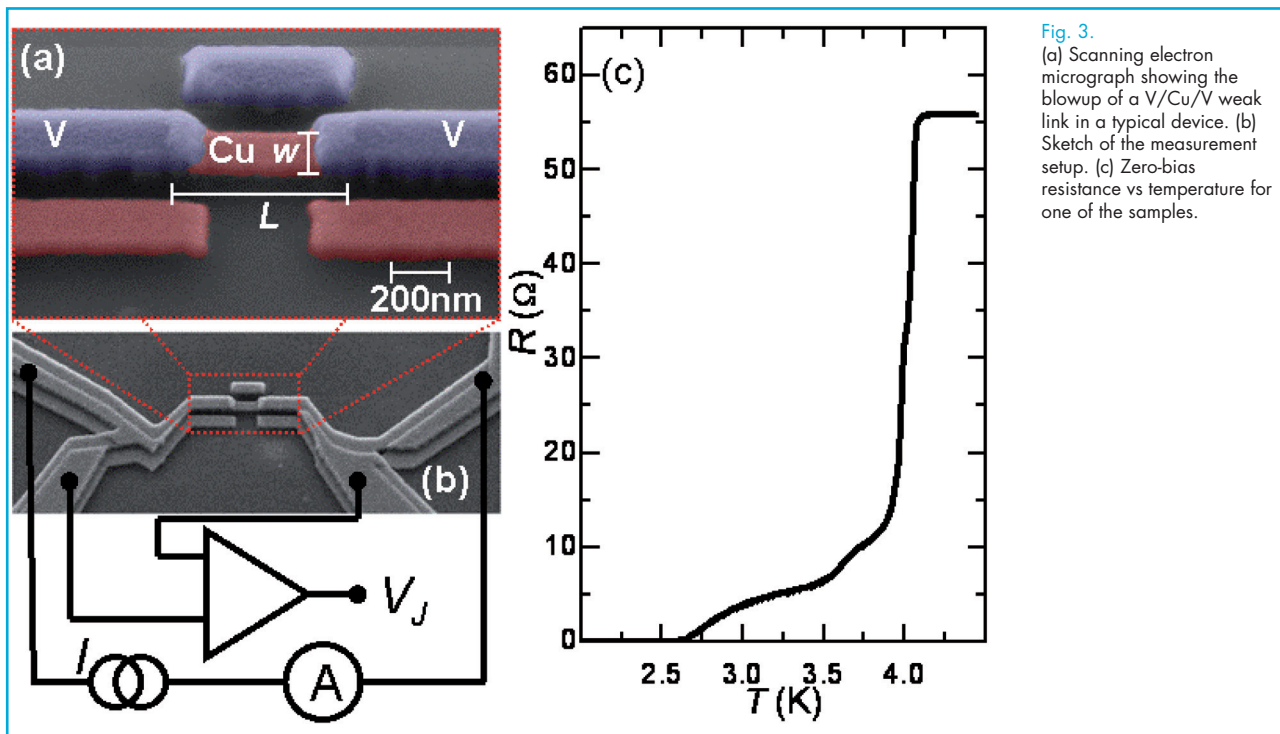


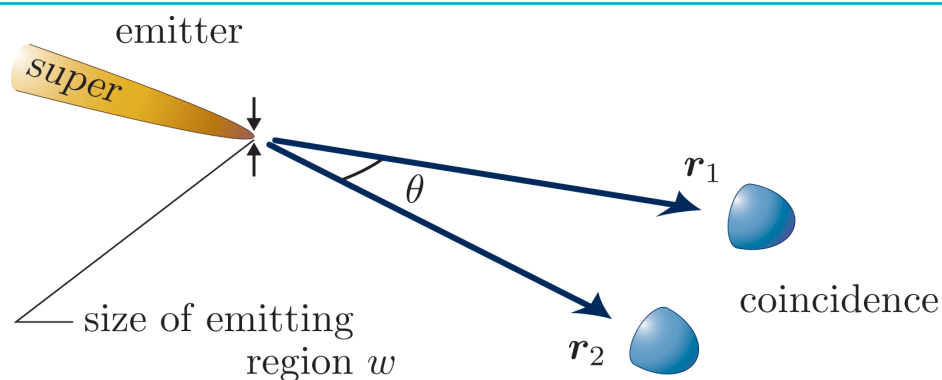
Fig. 3. (a) Scanning electron micrograph showing the blowup of a V/Cu/V weak link in a typical device. (b) Sketch of the measurement setup. (c) Zero-bias resistance vs temperature for one of the samples.

Finally, we have investigated the entanglement of electrons field-emitted from a superconducting tip into vacuum [10]. We have analyzed the nonlocal correlations by studying the coincidences of the field-emitted electrons (see Fig. 4) taking into account the interplay between

the bosonic nature of Cooper pairs and the fermionic nature of electrons. By orienting the detectors in opposite directions, we have shown that one can optimize the fraction of entangled electrons in order to perform a test of Bell's inequality.

Fig. 4.

(a) Field emission of electrons and coincident detections. The size of the emitting region at the tip is  $w$ , and two of the emitted electrons are detected at  $r_1$  and  $r_2$ .



#### References

- [1] F. Giazotto, F. Taddei, P. D'Amico, R. Fazio, F. Beltram, *Phys. Rev. B* **76**, 184518 (2007).
- [2] F. Giazotto, *Appl. Phys. Lett.* **95**, 042503 (2009)
- [3] F. Giazotto, F. Taddei, *Phys. Rev. B* **77**, 132501 (2008).
- [4] D. Huertas-Hernando, Yu. V. Nazarov, W. Belzig, *Phys. Rev. Lett.* **88**, 047003 (2002).
- [5] F. Dolcini, F. Giazotto, *Phys. Rev. B* **75**, 140511(R) (2007).
- [6] S. Pugnetti, F. Dolcini, R. Fazio, *Solid State Commun.* **144**, 551 (2007).
- [7] F. Dolcini, L. Dell'Anna, *Phys. Rev. B* **78**, 024518 (2008).
- [8] F. Giazotto, T. T. Heikkilä, G. P. Pepe, P. Helistö, A. Luukanen, J. P. Pekola, *Appl. Phys. Lett.* **92**, 162507 (2008).
- [9] C. Pascual Garcia, F. Giazotto, *Appl. Phys. Lett.* **94**, 132508 (2009).
- [10] K. Yuasa, P. Facchi, R. Fazio, H. Nakazato, I. Ohba, S. Pascazio, S. Tasaki, *Phys. Rev. B* **79**, 180503 (2009).

## Surface-acoustic-wave driven lab-on-chip technologies

The increasing demand for low-cost and portable devices for biomedical applications has stimulated the development of advanced micro-total-analysis systems ( $\mu$ TAS). The miniaturization of these devices led to better performance with respect to traditional analytical methods, since it involved smaller quantities of samples and reagents, allowing more reactions to occur in parallel on the same chip, more quickly and effectively, and with reduced manual intervention[1]. For a full exploitation of the advantages of microfluidics one needs highly controlled liquid flows into biochips. In the common case of hydrophobic capillaries, polar fluids must be forced into microchannels by means of active pumping elements, overcoming the large resistance to flow due to small microchannel sections. The existing pumping systems typically rely on external pressurized lines, which severely limit the portability of microfluidic systems. In the last years, the interaction between surface acoustic waves (SAWs) and liquids began to be studied as a pumping approach, relying on the streaming effect that drives the fluid flow in the direction of SAW propagation[2]. SAW methods have been mainly limited to mixing, localization or transport of droplets deposited on planar substrates, preferably patterned by regions of different wettability. The main issues of such open digitalized microfluidic architectures are the liquid evaporation and a remarkable sensitivity to surface contamination. Lab-on-a-Chip research activity at NEST lab aims to the design and realization of handheld, battery-operated biochips based on SAW-driven micropumps and closed microchannel networks suitable for automated, high-throughput, cost-effective diagnostics.

Marco Cecchini

m.cecchini@sns.it

### Collaborators

F. Beltram  
R. Cingolani  
S. Girardo  
L. Masini  
D. Pisignano  
I. Sanzari

Acoustic counterflow in hydrophobic microchannels

During 2007/2009 we investigated the application of SAW based pumping methods to microchannel environments fully compatible with  $\mu$ TAS applications, studying the flow of water and protein solutions in prototypical devices made by a piezoelectric lithium niobate ( $\text{LiNbO}_3$ ) substrate and elastomeric polymer patterns defining the capillary circuits.

We employed a combination of photo- and soft lithography to fabricate devices with different fluidic geometries. The basic layout consisted of two layers. The bottom layer was a  $\text{LiNbO}_3$  piezoelectric substrate, with two microfabricated interdigital transducers (IDTs) for SAW excitation and detection. The IDTs were composed by 20 pairs of 500- $\mu\text{m}$ -long Al fingers with 24  $\mu\text{m}$  periodicity ( $\sim$ 160 MHz resonance frequency on  $\text{LiNbO}_3$ ), placed at a distance of 3.4 mm. The upper layer was a patterned polydimethylsiloxane (PDMS) film. Channel geometries with lateral dimensions between 120 and 520  $\mu\text{m}$  and relative heights between

10 and 50  $\mu\text{m}$  were transferred onto PDMS replicas. Final devices were straightforwardly assembled by conformal bonding of the two layers (Fig. 1): the hybrid microchannels were thus defined by the  $\text{LiNbO}_3$  bottom wall and the PDMS lateral and top walls.

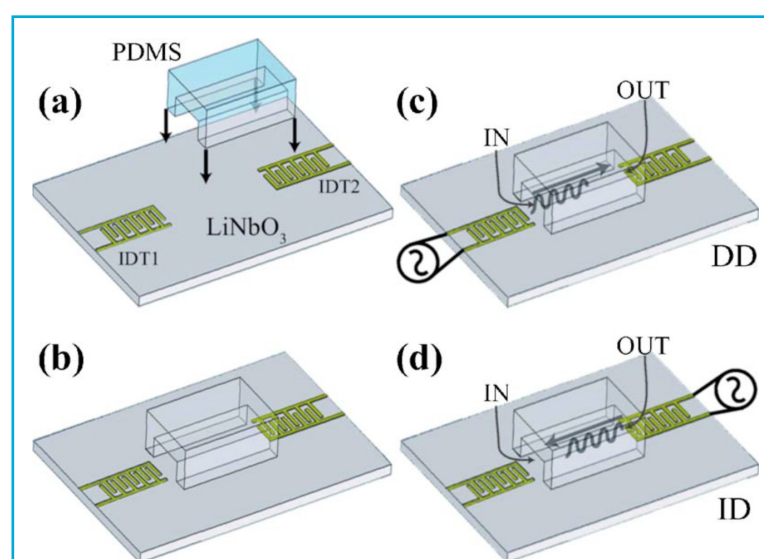
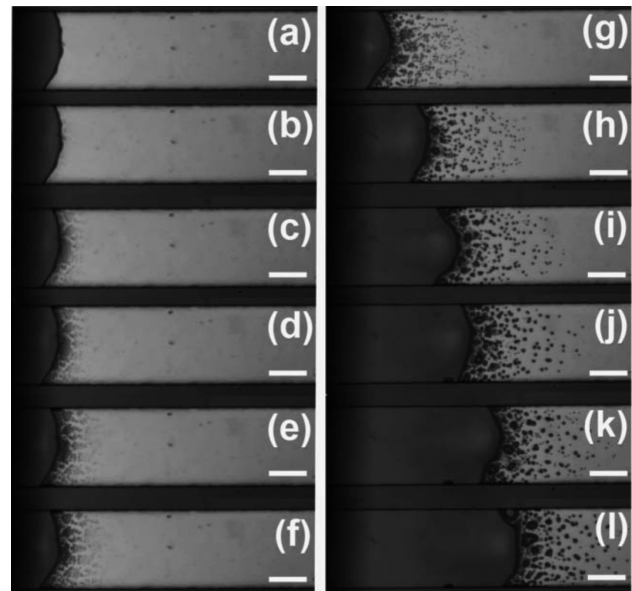


FIG. 1 Scheme for the assembling of microfluidic devices and the activation of the liquid motion into microchannels: (a) and (b) final devices were fabricated by the superposition of a PDMS textured element and a  $\text{LiNbO}_3$  substrate layer with IDTs for SAW excitation and detection; (c) DD and (d) ID experimental arrangements.

**FIG. 2**  
 Photographs of the water withdrawing micropumping at different times ( $t$ ). From (a) to (l):  $t = 0.00, 0.05, 0.06, 0.08, 0.09, 0.13, 0.53, 1.51, 2.46, 3.48, 4.49, \text{ and } 5.49$  s, respectively. Marker =  $100 \mu\text{m}$ .



The liquid reservoirs consisted in de-ionized water drops of about  $2 \mu\text{l}$  released at the entrance of the microchannels. Continuous SAWs were excited, and the position of the water-air interface within the channel was monitored as a function of time and power of the signal applied to the IDT ( $P_{\text{SAW}}$ ). We analyzed two different experimental arrangements. First, SAWs were excited from one IDT to the channel entrance and, hence, along the channel toward its outlet [direct drive (DD)] [Fig. 1(c)]. Second, the SAWs were launched in the opposite direction, i.e., from the other IDT, so that SAWs propagated from the channel outlet toward its inlet [inverted drive (ID)] [Fig. 1(d)]. In case of conventional DD, with increasing  $P_{\text{SAW}}$ , we observed droplet deformation caused by acoustic streaming and, finally, a rather slow movement of the liquid into the channel ( $P_{\text{SAW}} = 20$  dBm). At these power values, however, significant droplet atomization occurred that strongly affected the droplet outside the channel, where incoming SAW power was maximum. This led to fast evaporation of the water reservoir and prevented the filling of the microchannel.

ID showed a very different behavior[3]. For  $P_{\text{SAW}} > 14$  dBm, a fast liquid transfer from the reservoir droplet into the microchannel

(Fig. 2) was observed. We stress that the liquid was driven in the opposite direction with respect to the SAW propagation direction. In view of the known SAW-fluid interaction properties[2] so far leading to liquid drag only along the SAW direction, this phenomenon was quite unexpected. Figure 2 displays a typical filling process, where water nebulization was visible at the meniscus position. ID pumping is surprising in light of the fact that any momentum transfer to the liquid must be in the opposite direction with respect to actual fluid flow. Conventional acoustic-streaming physics, therefore, does not apply. In order to understand this dramatic difference between the ID and DD behaviors we must consider the different positions where the SAW-liquid interaction occurs. In the ID configuration, the interaction is maximum within the capillary and leads to a drastically enhanced water nebulization rate at the meniscus position. This atomization leads to the formation and growth of water particles sprayed off the main fluid drop within the channel (Fig. 2). The evolution of these droplets and their interaction with the liquid meniscus determine the observed pumping phenomenon: small droplet generation is followed by coalescence

and final merging with the meniscus. The latter phenomenon changes the position of the liquid-air interface, resulting in a net fluid movement in the opposite direction with respect to SAW propagation. The filling velocity ( $v_{\text{fill}}$ ) could be controlled up

to a maximum value of 1.24 mm/s (i.e., about 0.3 ml/min for the present channel geometry) by varying  $P_{\text{SAW}}$  up to 20 dBm, yielding rapid filling ( $t=0.9$  s) of the whole channel, without significant evaporation of the droplet reservoir.

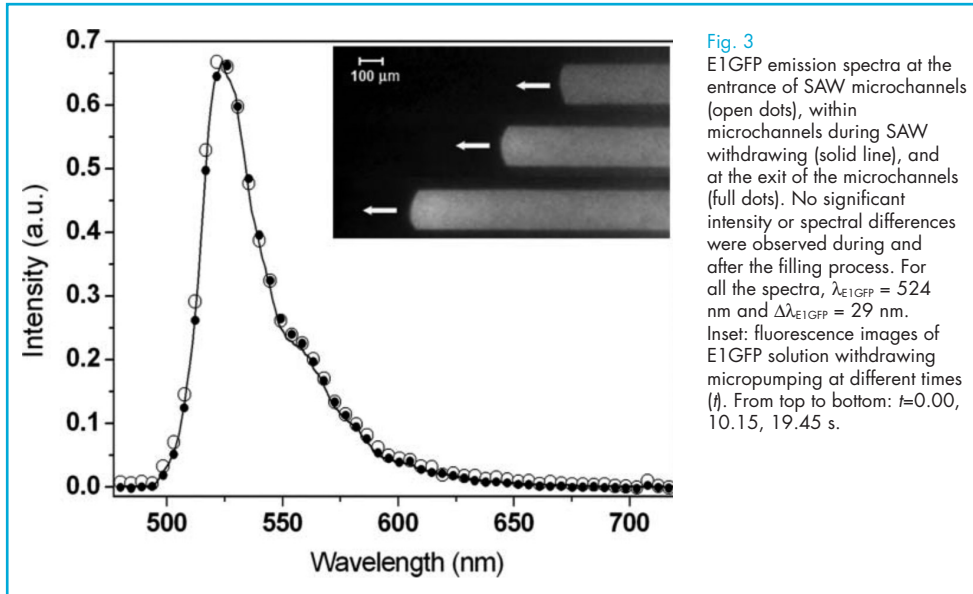


**Fig. 3** E1GFP emission spectra at the entrance of SAW microchannels (open dots), within microchannels during SAW withdrawing (solid line), and at the exit of the microchannels (full dots). No significant intensity or spectral differences were observed during and after the filling process. For all the spectra,  $\lambda_{\text{E1GFP}} = 524$  nm and  $\Delta\lambda_{\text{E1GFP}} = 29$  nm. Inset: fluorescence images of E1GFP solution withdrawing micropumping at different times ( $t$ ). From top to bottom:  $t=0.00$ , 10.15, 19.45 s.

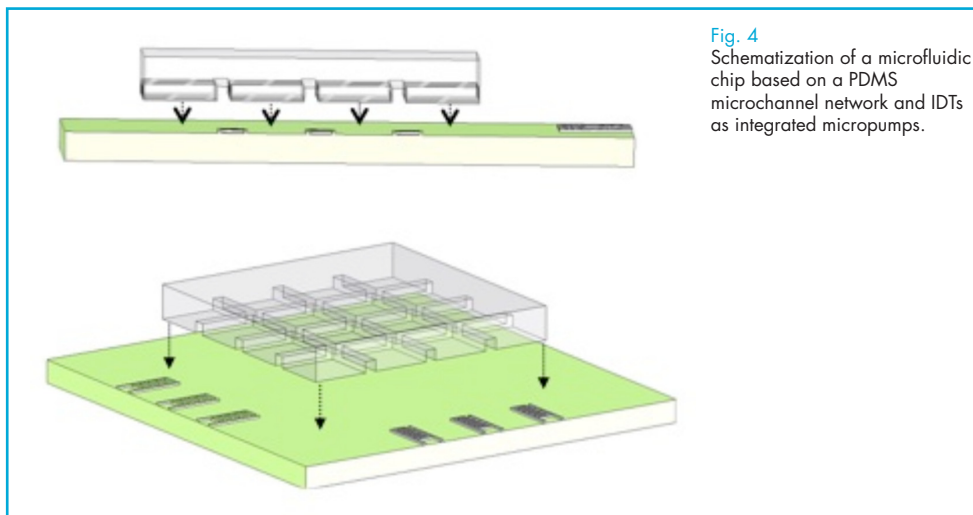


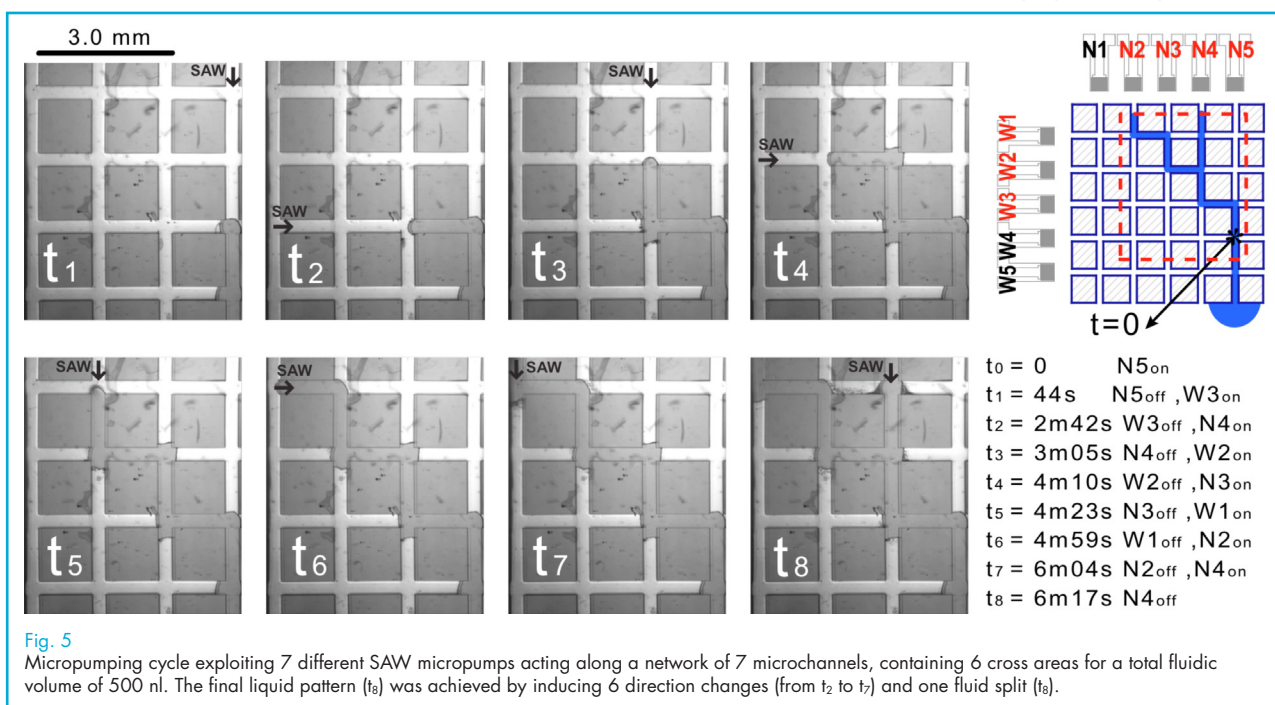
**Fig. 4** Schematization of a microfluidic chip based on a PDMS microchannel network and IDTs as integrated micropumps.

We also tested the compatibility of this pumping method with biological solutions[4]. Efficient microchannel filling was easily obtained also for solutions of fluorescent proteins (Fig. 3). For sake of example, in case of a channel with section  $200 \times 20 \mu\text{m}^2$  coupled to an IDT working at a resonance frequency of 151 MHz, a filling velocity of about  $50 \mu\text{m s}^{-1}$  was measured (for  $W = 21.5$  dBm). Important,

the protein fluorescence intensity and spectral characteristics (peak wavelength,  $\lambda_{\text{E1GFP}}$ , and emission full width at half maximum,  $\Delta\lambda_{\text{E1GFP}}$ ) were not significantly affected by the interaction with the SAW and with the hybrid channel during the entire filling process (Fig. 9). The unaltered protein fluorescence confirms the suitability of SAW withdrawing in microchannels for biological applications.

ID appears to be very promising for the fabrication of integrated micropumps for microfluidic chips and  $\mu$ TAS. Indeed, the present approach requires only an external signal generator set at the

IDT resonance frequency. Importantly, impedance matching and device geometry optimization (i.e., channel shape, IDT periodicity/aperture, IDT position, etc.) will enable battery-operated systems.



Work is in progress to extend this approach to more complex microfluidic networks by integrating several IDTs on the same chip to drive fluids along specific diagnostic paths (Fig. 4). SAW-based counterflows were successfully exploited to control liquids in hydrophobic microchannel arrays. The devices were formed by a  $5 \times 5$  orthogonal array of hybrid  $\text{LiNbO}_3$ /PDMS microchannels (20 input/output ports, 25 crossing areas) and

20 IDTs for SAW excitation and detection. SAW-induced acoustic counterflow was demonstrated to be capable of: i) filling discontinuous microchannels; ii) inducing  $90^\circ$  flow direction changes; iii) extracting fluid laterally from filled microchannels; and iv) flow splitting and simultaneous multichannel filling. Finally, one example of a complex filling sequence was given showing 6 direction changes and one fluid split (Fig. 5).

## References

- [1] T M Squires and S R Quake "Microfluidics: Fluid physics at the nanoliter scale" *Rev. Mod. Phys.* 77 977–1026 (2005); J Atencia and D J Beebe "Controlled microfluidic interfaces" *Nature* 437 648–655 (2005).
- [2] Z Guttenberg, H Muller, H Habermuller, A Geisbauer, J Pipper, J Felbel, M Kielinski, J Scriba and A Wixforth "Planar chip device for PCR and hybridization with surface acoustic wave pump" *Lab Chip* 5 308–317 (2005).
- [3] M Cecchini, S Girardo, D Pisignano, R Cingolani, and F Beltram "Acoustic-counterflow microfluidics by surface acoustic waves" *Appl. Phys. Lett.* 92 104103 (2008).
- [4] S Girardo, M Cecchini, F Beltram, R Cingolani and D Pisignano "Polydimethylsiloxane– $\text{LiNbO}_3$  surface acoustic wave micropump devices for fluid control into microchannels" *Lab-on-a-Chip* 8 1557–1563 (2008).
- [5] F Beltram, M Cecchini, R Cingolani, S Girardo, D Pisignano "Micro/nanofluidic channels structure fluid motion controlling device for chips (e.g. micromixers) for e.g. biological applications has polydimethylsiloxane structured volume, and piezoelectric substrate having active control mechanism" *International Patent WO2009013705-A1* (2007)

## Monitoring brain function by *in vivo* 2-photon microscopy

**T**he mission of the *in vivo* microscopy lab is to provide NEST with the ability of studying in anaesthetized animal models the function and structural plasticity of the brain and the physiological response to exogenously delivered agents. These techniques offer the capacity of studying at subcellular resolution and at high time resolution (1 Hz or better) the interactions between brain cells and nanofabricated devices.

The instrument at the core of this activity is the 2-photon microscope. This is a scanning microscope where the light source is provided by an ultrafast laser capable of delivering short light pulses (about 150 fs). Thanks to the high peak power, the near IR radiation provided by the pulsed laser is capable of exciting fluorophores that are normally excited at visible wavelength. The 2-photon microscope has several crucial advantages over the one-photon microscope: these features are instrumental in allowing imaging in thick samples:

1) 2-photon excitation is a non-linear phenomena that occurs only at the focal plane, therefore, there is no need for

a spatial filter to remove out of focus excitation with a consequent increase of detection efficiency.

2) Infrared excitation and its localisation at the focal plane decrease phototoxicity.

3) Infrared excitation is far less scattered by the tissue increasing the power that can be delivered at the focal plane, and the image contrast.

The implementation of this technique require the simultaneous solution of a wide variety of problems, ranging from the proper alignment and tuning of the microscope, to the design of custom systems for the maintenance of the animal under the microscope, to the application

Gian Michele Ratto

gimmi@in.cnr.it

### Collaborators

R. Brambilla  
L. Cancedda  
G. Carmignoto  
M. de Curtis  
C. Lodovichi  
G. Mandolesi  
I. Skalióra

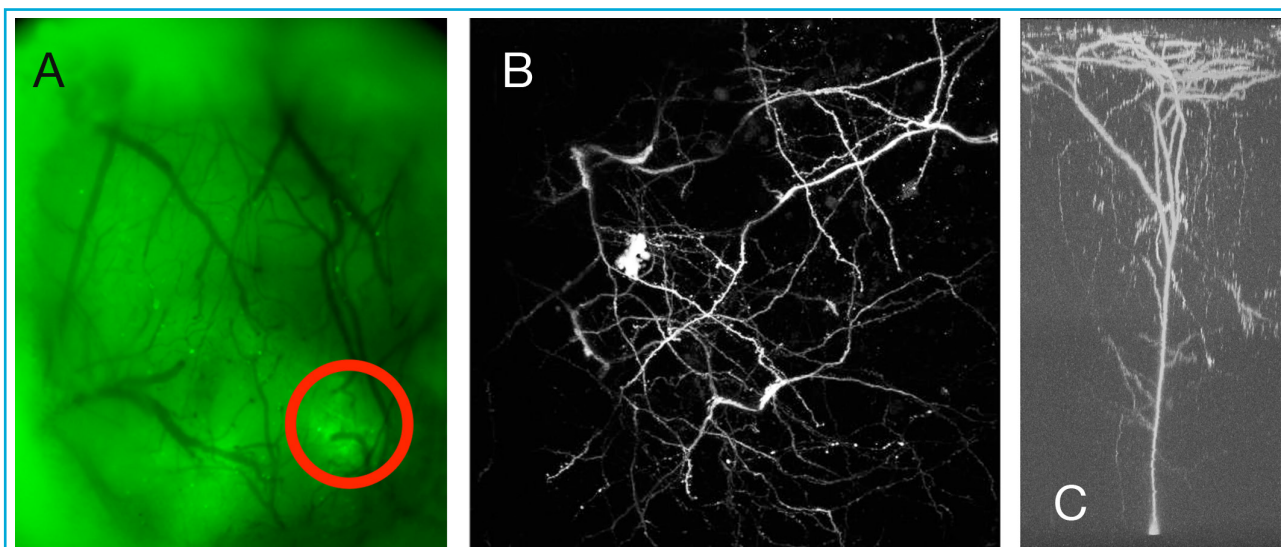


Fig. 1

A) Low magnification of the cortical surface. The pattern formed by the blood vessel is used to record the position of the imaged fields. This allow to record day after day changes occurring at specific cortical structures. The area marked by the red circle is shown at 2-photon excitation in B. C) transversal reconstruction of a brain neuron. The cell body is placed in cortical layer V at a depth of over 600 micron from the surface.

of proper procedures for the surgery and anaesthesia. Currently, we have devised protocols and the appropriate hardware components for *in vivo* imaging on visual and somatosensory cortices and on the olfactory bulb.

In figure 1 are shown examples of *in vivo* imaging of brain neurons in transgenic mice expressing the Green Fluorescent Protein GFP in a subset of cortical pyramidal cells. The optical access is obtained by implanting a recording chamber over the mouse skull. At the center of the opening a small craniotomy is cut in sterile conditions, the brain is exposed and then it is covered with a layer of transparent gel topped by a glass coverslip. In this way the recording chamber is sealed and can be kept on the mouse for days or even weeks. This procedure allows the longitudinal study of single identified features. We produced alternative designs of the imaging chambers to allow the

microinjection of pharmacological agents during the chronic imaging sessions.

Functional imaging is performed after the delivery to the cells, either by genetically encoded products or by microinjection, of fluorescent probes. In the example shown in figure 2 two fluorescent dyes are microinjected. The red fluorophore (Sulphorodhammine 101) selectively stain and identify a population of brain cells, the astrocytes. The green dye is the calcium indicator Oregon Green BAPTA 1, and provides a fluorescent signal proportional to the calcium load of each cell. The calcium indicator becomes fluorescent only after loading into healthy cells, and therefore the injecting microelectrode appears only red.

Imaging of the brain with Ca indicators is an especially powerful technique because electrical activity of neurons brings about an increase in Ca load. In

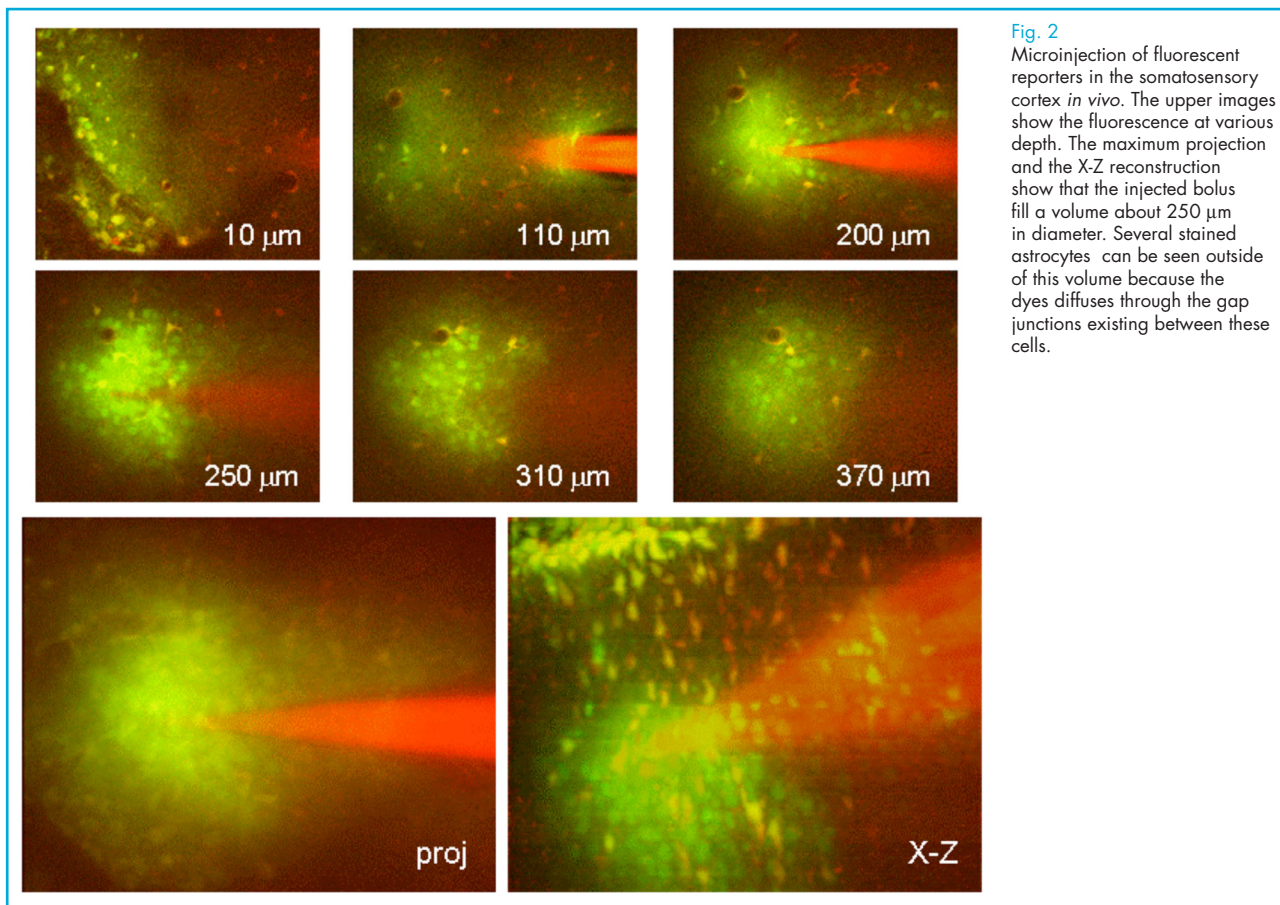
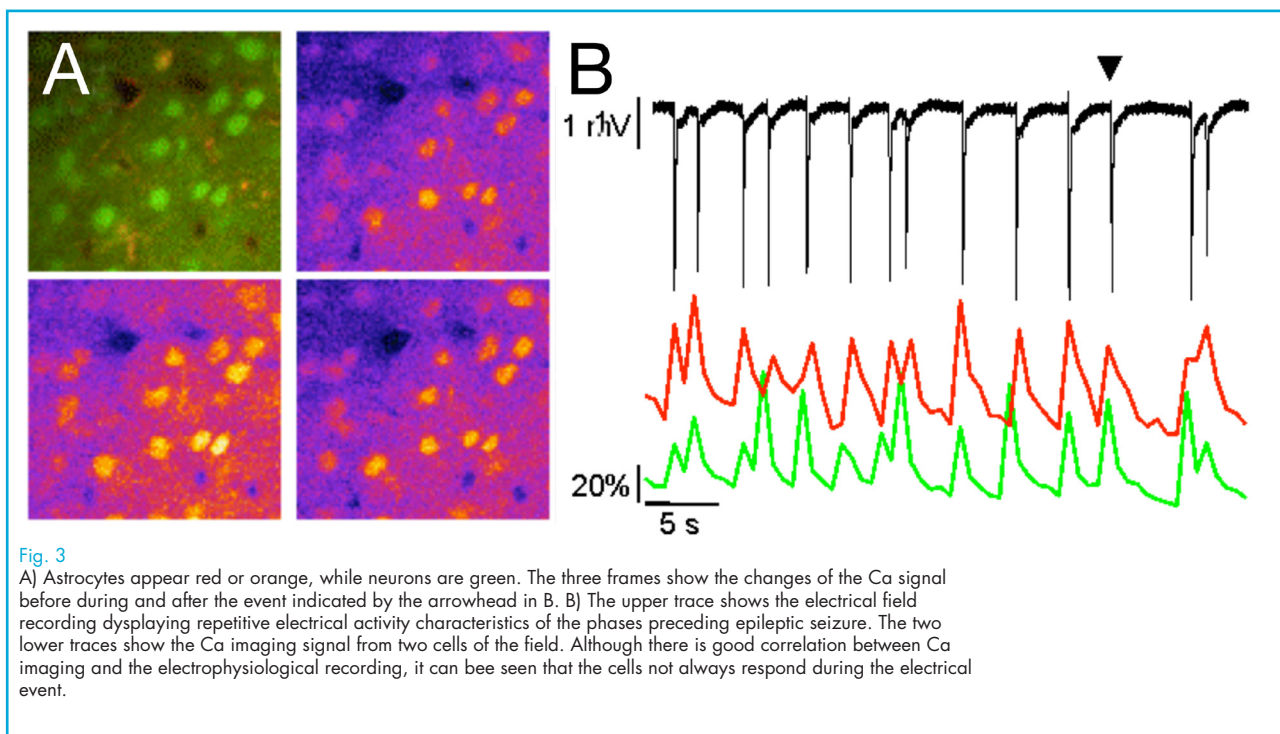


**Fig. 2**  
Microinjection of fluorescent reporters in the somatosensory cortex *in vivo*. The upper images show the fluorescence at various depth. The maximum projection and the X-Z reconstruction show that the injected bolus fill a volume about 250  $\mu\text{m}$  in diameter. Several stained astrocytes can be seen outside of this volume because the dyes diffuse through the gap junctions existing between these cells.

astrocyte, increase of Ca is associated to their activation with consequent release of neuro-active substances. Therefore, these experiments can return information shedding lights on processes as varied as cytotoxicity, neuronal computation, astrocyte physiology. Furthermore, we can combine the imaging with electrophysiological recordings obtained by a sharp electrode placed in the imagine volume. An example of such recording is provided in figure 3.

These techniques are crucial to study basic cellular mechanisms operating in

pathological conditions in mouse model of neurological diseases. Presently we are employing the combination of Ca imaging and electrophysiology to analyze the events at the basis of neuronal synchronisation during epileptic seizures. In this study, presently under review, we have demonstrated the existance of an excitatory loop between neurons and astrocytes that is instrumental for the onset of epileptic seizure. Furthermore, we have demonstrated that the pharmacological inhibition of this loop reduces the probability of enduring an epileptic seizure.





## E<sup>n</sup>GFP: protein nanodevices tailored for intracellular biosensing

Owing to their genetically encoded fluorescence, green fluorescent proteins (GFPs) have become an invaluable tool for the optical labeling and tracking of protein molecules in living cells at high spatial and temporal resolution. One of the ultimate challenges in microscopy is to devise GFP-based biosensors that combine the high resolution imaging property of luminescent probes with the functional information afforded by biochemical analysis. Here we present the development of new GFP-based biosensors for high-resolution intracellular pH and chloride sensing. The spectral properties of the E<sup>n</sup>GFP class (F64L/T203Y) were exploited for the design of a multiplex pH and chloride sensor, which overcame the limitations of existing methods to sense intracellular chloride concentration and pH.

### E<sup>1</sup>GFP as targeted biosensor of intracellular pH

The chromophore of E<sup>n</sup>GFP can exist in two optically distinguished forms (neutral and anionic) that are both fluorescent.<sup>1,2</sup> Such a dual fluorescence property makes possible the fabrication of ratiometric (i.e. concentration independent) pH sensors tailored to the 5-9 pH range.<sup>3,4</sup>

Intracellular pH (pH<sub>i</sub>) is a remarkable modulator of cell structure and function.<sup>4</sup> The genetically-encoded nature of GFP-pH<sub>i</sub> biosensors makes them the perfect fluorescent nanoreporters of intracellular H<sup>+</sup> concentration. In this field, we developed new E<sup>n</sup>GFP-based pH biosensor ratiometric by emission when excited at 405 nm (Fig. 1a), denoted as E<sup>1</sup>GFP (F64L/T203Y GFP).<sup>1</sup> By careful selection of the emission ranges in the ratiometric ratio, the working pH interval of E<sup>1</sup>GFP can be tuned from 6.0 up to neutrality, as displayed both *in vitro* and in cultured cells clamped to different pH values (Fig. 1b and d).<sup>4</sup> We demonstrated the ability of E<sup>1</sup>GFP to report dynamically on the pH of cell components by following the caveolin trafficking in the cell (Fig. 1e) and the gradual endosomal acidification associated with HIV Tat86 (fused to E<sup>1</sup>GFP) cell internalization.<sup>5</sup> The measurement of pH in endocytic vesicles is a way to monitor the progression of internalized exogenous molecules from their binding to receptors on the cell membrane down to their processing in specific cell compartments. After 4h Tat-E<sup>1</sup>GFP-stained

vesicles onto the plasma membrane showed a nearly neutral pH value, owing to their contact with the external buffer (Fig. 1f), whereas in the internalized pool we identified two endosomal subpopulations with two different pH values: ~6.5 and ~5.9 (Fig. 1f).<sup>4</sup> After 6h, the pH of each compartment significantly decreased. These findings are consistent with a gradual acidification associated with Tat internalization, indicating a prevalent endocytic mechanism of uptake.

### Simultaneous intracellular pH and chloride concentration measurements

Interestingly, the S65T mutation introduces a specific anion-binding site in E<sup>n</sup>GFP.<sup>4</sup> We thus decided to exploit this peculiarity in the development of a novel chloride sensor. Indeed Cl<sup>-</sup> participates in many physiological functions including stabilization of neuronal resting potential, charge balance in vesicular acidification, and regulation of cell volume.<sup>10</sup> Yet, processes regulating intracellular chloride concentration, [Cl<sup>-</sup>]<sub>i</sub>, are still widely unexplored mainly as a consequence of limiting methods to quantify chloride fluxes in living cells.

Our sensor was conceived as ratiometric, genetically-encoded and capable to simultaneously measure [Cl<sup>-</sup>]<sub>i</sub> and pH<sub>i</sub>. So, DsRed-monomer, which is insensitive to chloride and pH, was fused to E<sup>2</sup>GFP via a peptide linker as illustrated in Fig. 2A. The proposed sensor *in vitro* reversible (sub-second) response to mM

Daniele Arosio

d.arosio@sns.it

#### Collaborators

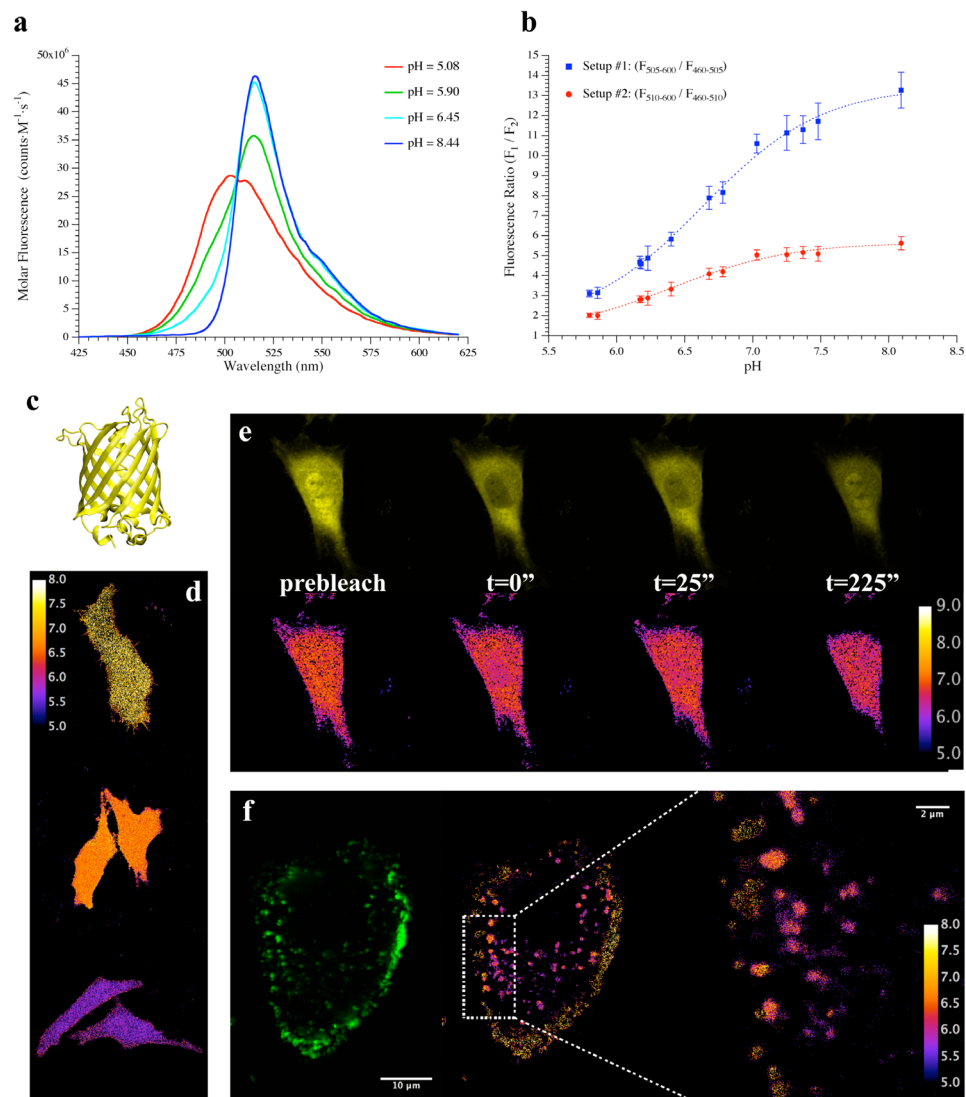
L. Albertazzi  
F. Beltram  
R. Bizzarri  
F. Cardarelli  
R. Gualdani  
S. Guidi  
S. Luin  
L. Marchetti  
R. Nifosi  
F. Ricci  
M. Serresi  
C. Viappiani

[Cl]<sub>i</sub> variation along with fast response to pH variations (< 1 ms) in the physiological pH range.<sup>3</sup> Green-to-red fluorescence ratio is regulated by [Cl]<sub>i</sub>; according to simple Langmuir isotherm (Fig. 2C) in the range from 1 to 300 mM. Subsequently, we demonstrated that the proposed sensor allows dynamic live imaging of [Cl]<sub>i</sub> in GABA-A receptor-triggered Cl<sup>-</sup> fluxes (Fig. 2C). Remarkably, by targeting the novel biosensor to the secretory pathway of neuroendocrine cells we provided an unprecedented quantification of the [Cl]<sub>i</sub> in large dense core vesicles (Fig. 2D).

The high-resolution characterization of the anion binding-site structure (Fig. 3) in E<sup>2</sup>GFP suggested further optimization of the chloride sensing GFP. Site directed mutagenesis allowed us to keenly control E<sup>n</sup>GFP chloride affinity (Fig. 3A). Remarkably, we engineered a new FP, E<sup>2</sup>GFP-V224L,<sup>11</sup> which bears the highest chloride affinity among FP. Thermodynamic and structural results together showed entropic origin of the increased chloride affinity owing to the presence of a water molecule in the binding pocket.

**Fig 1**

(a) Emission fluorescence of E<sup>1</sup>GFP at different pH by exciting at 405 nm; (b) Two ratiometric calibrations of E<sup>1</sup>GFP in HeLa cells clamped at different pH values: note that the ratiometric curve amplitude and linear range depend on the emission intervals; (c) typical b-barrel structure of E<sup>1</sup>GFP; (d) ratiometric pH maps of HeLa cells expressing E<sup>1</sup>GFP and clamped at pH 5.2 (lower panel), 6.7 (middle panel), and 8 (upper panel); (e) pH measured by E<sup>1</sup>GFP is not dependent on dynamic processes occurring in the cell: a diffusion-dependent fluorescence recovery in the nucleus is induced by bleaching (upper panel) but the measured pH is not biased by time dependent fluorescent changes (lower panel); (f) Real-time monitoring of endocytosis of Tat-E<sup>1</sup>GFP in HeLa cells at 4h: fluorescence is distributed on the cell membrane and internalized in endocytotic vesicles (left panel), whose pH is different (middle and right panel).



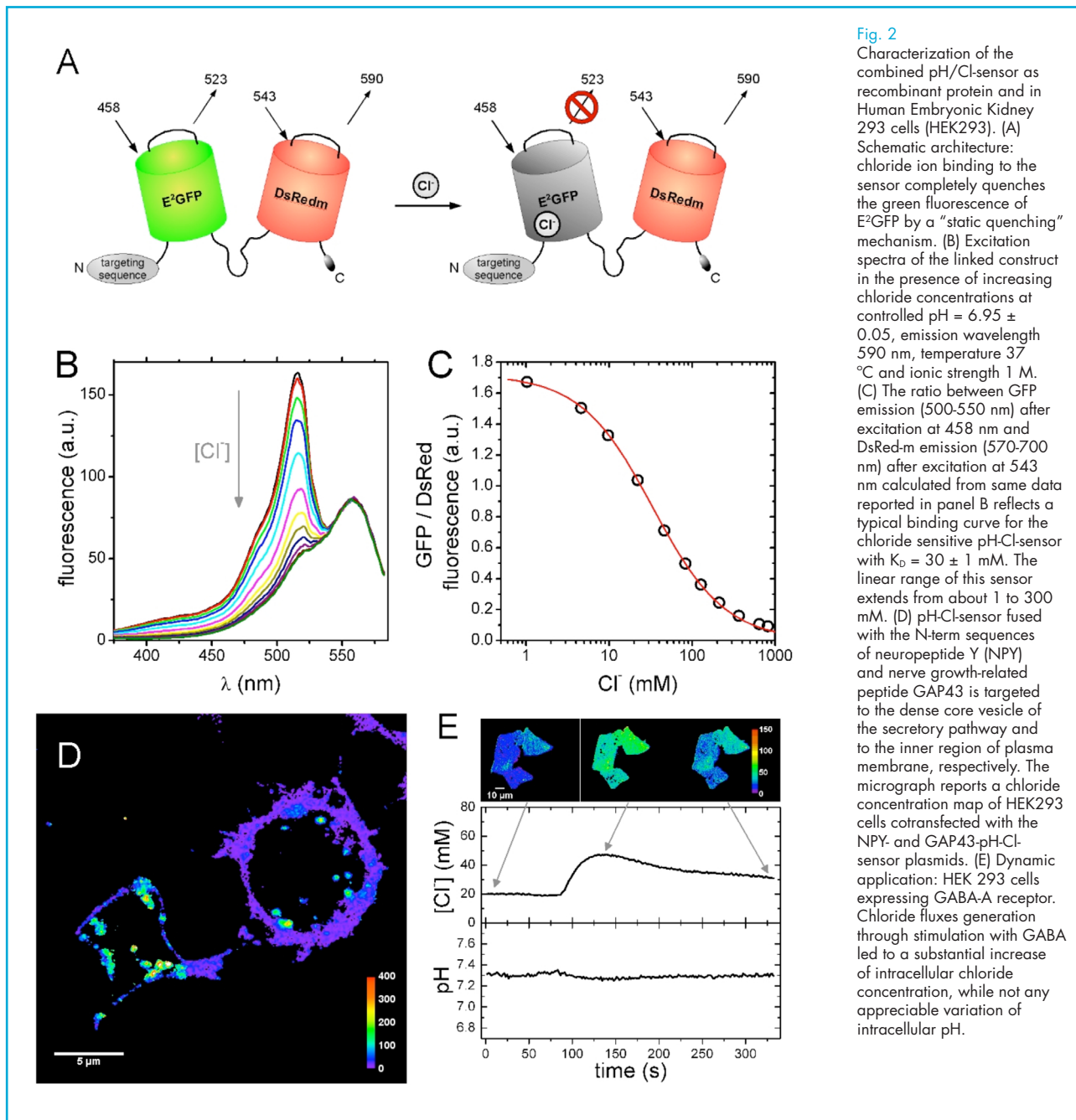


Fig. 2

Characterization of the combined pH/Cl<sup>-</sup> sensor as recombinant protein and in Human Embryonic Kidney 293 cells (HEK293). (A) Schematic architecture: chloride ion binding to the sensor completely quenches the green fluorescence of E<sup>2</sup>GFP by a "static quenching" mechanism. (B) Excitation spectra of the linked construct in the presence of increasing chloride concentrations at controlled pH = 6.95 ± 0.05, emission wavelength 590 nm, temperature 37 °C and ionic strength 1 M. (C) The ratio between GFP emission (500-550 nm) after excitation at 458 nm and DsRed-m emission (570-700 nm) after excitation at 543 nm calculated from same data reported in panel B reflects a typical binding curve for the chloride sensitive pH-Cl<sup>-</sup> sensor with K<sub>D</sub> = 30 ± 1 mM. The linear range of this sensor extends from about 1 to 300 mM. (D) pH-Cl<sup>-</sup> sensor fused with the N-term sequences of neuropeptide Y (NPY) and nerve growth-related peptide GAP43 is targeted to the dense core vesicle of the secretory pathway and to the inner region of plasma membrane, respectively. The micrograph reports a chloride concentration map of HEK293 cells cotransfected with the NPY- and GAP43-pH-Cl<sup>-</sup> sensor plasmids. (E) Dynamic application: HEK 293 cells expressing GABA-A receptor. Chloride fluxes generation through stimulation with GABA led to a substantial increase of intracellular chloride concentration, while not any appreciable variation of intracellular pH.

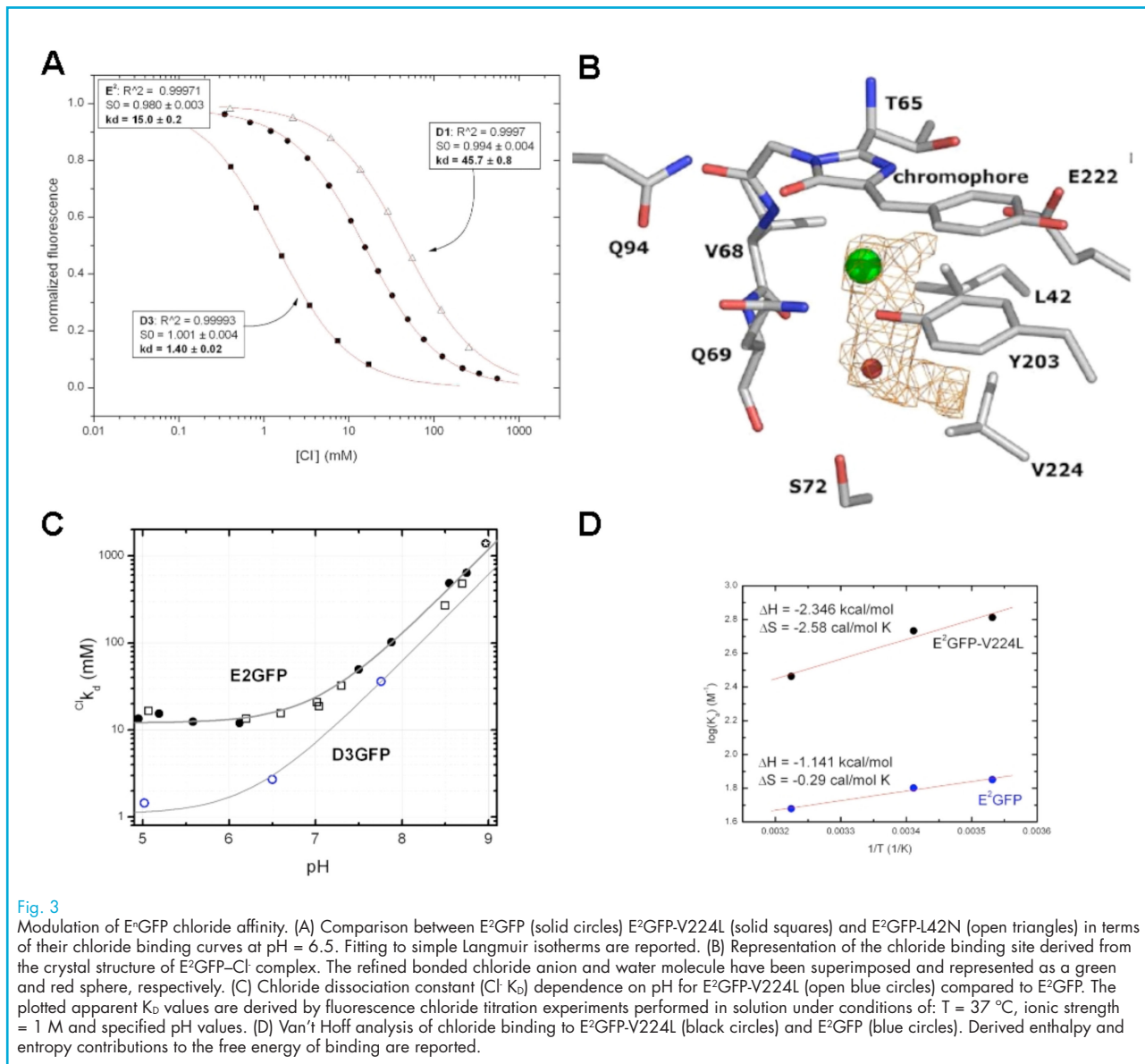


Fig. 3

Modulation of E<sup>2</sup>GFP chloride affinity. (A) Comparison between E<sup>2</sup>GFP (solid circles) E<sup>2</sup>GFP-V224L (solid squares) and E<sup>2</sup>GFP-L42N (open triangles) in terms of their chloride binding curves at pH = 6.5. Fitting to simple Langmuir isotherms are reported. (B) Representation of the chloride binding site derived from the crystal structure of E<sup>2</sup>GFP-Cl<sup>-</sup> complex. The refined bonded chloride anion and water molecule have been superimposed and represented as a green and red sphere, respectively. (C) Chloride dissociation constant (Cl<sup>-</sup> K<sub>d</sub>) dependence on pH for E<sup>2</sup>GFP-V224L (open blue circles) compared to E<sup>2</sup>GFP. The plotted apparent K<sub>d</sub> values are derived by fluorescence chloride titration experiments performed in solution under conditions of: T = 37 °C, ionic strength = 1 M and specified pH values. (D) Van't Hoff analysis of chloride binding to E<sup>2</sup>GFP-V224L (black circles) and E<sup>2</sup>GFP (blue circles). Derived enthalpy and entropy contributions to the free energy of binding are reported.

## References

- [1] Bizzarri, R.; Nifosi, R.; Abbruzzetti, S.; Rocchia, W.; Guidi, S.; Arosio, D.; Garau, G.; Campanini, B.; Grandi, E.; Ricci, F.; Viappiani, C.; Beltram, F. *Biochemistry* 2007, 46, 5494-5504.
- [2] Arosio, D.; Garau, G.; Ricci, F.; Marchetti, L.; Bizzarri, R.; Nifosi, R.; Beltram, F. *Biophys J* 2007, 93, 232-44.
- [3] Bizzarri, R.; Nifosi, R.; Abbruzzetti, S.; Rocchia, W.; Guidi, S.; Arosio, D.; Garau, G.; Campanini, B.; Grandi, E.; Ricci, F.; Viappiani, C.; Beltram, F. *Biophys. J.* 2007, 329A-329A.
- [4] Bizzarri, R.; Serresi, M.; Luin, S.; Beltram, F. *Anal Bioanal Chem* 2009, 393, 1107-1122.
- [5] Serresi, M.; Bizzarri, R.; Cardarelli, F.; Beltram, F. *Anal Bioanal Chem* 2009, 393, 1123-1133.

## Nanotechnology for guided cell differentiation

The morphogenesis of mammalian organs and tissues relies on the ability of individual cells to respond to a vast range of extracellular signals. Among these are gradients of soluble molecules such as growth factor and cell-secreted mitogens encoding for preferential directions over long distances. Much of the existing literature concerning guided cell differentiation focused on the identification and biological characterization of these molecules. In recent years an increasing body of evidence revealed that a second determinant of cell activity is provided by the chemical and physical properties of the extracellular matrix (ECM) in the cell proximity. These guidance cues are read by cells in a process that requires the activity of specific cell adhesion machineries and the remodeling of the cell shape. Several cellular responses such as polarization, migration, proliferation, and apoptosis are elicited by a direct cell-ECM interaction in virtually all cell types. A pivotal role in this process is played by the substrate nanotopography. In order to unravel the mechanisms by which differentiating cells read the local topography it is crucial to decouple its effects from those stemming from other chemical and physical stimuli. Thanks to recent advances in biomaterial nanofabrication, selected morphological aspects of the ECM are now reproducible in vitro through the realization of artificial scaffolds with controlled topography (Fig. 1). The related research activity at NEST lab follows two strategies: (i) improving the chemical and morphological properties of biomimetic two-dimensional (2D) scaffolds with nanostructured surface modifications (ii) understanding the cellular mechanisms regulating topographical guidance. Concerning line (i), during 2007-2008 we introduced original, biocompatible, nanostructured scaffolds for high-resolution time-lapse experiments made of standard tissue-culture polystyrene (TCPS) or cyclic olephine copolymer (COC), which were shown to induce efficient neurite guidance during neuronal differentiation. The effect of variation in the geometry of the topographical features was also investigated. Concerning line (ii) we studied the influence of anisotropic nanotopographies on neuronal differentiation and migration and revealed that neurite alignment and polarization are obtained via a geometrical constraint of cellular adhesions resulting in an angular modulation of neurite elongation and persistence. The involvement of cell-generated contractility and cytoskeletal remodeling in this process was also demonstrated.

### Nanostructured biomimetic scaffolds and applications

During 2007-2008 the possibility of imprinting anisotropic nano-textures (i.e. nanogratings, alternating lines of grooves and ridges of submicron size) on thermoplastic materials was successfully explored. Particular attention was paid to the physiological suitability of the resulting cell scaffold. To this aim tissue-culture polystyrene (TCPS) was initially chosen [1]. The desired topography could be induced by nanoimprint lithography (NIL) [1,2]. In these conditions no further surface chemical functionalization was added (Fig. 1A). The resulting imprinted substrates proved optimal for the growth of PC12 cells, a well-established model of neuronal differentiation [3]. The net

effect of cell-nanogratings interaction on TCPS substrates was investigated by means of live cell microscopy. Specifically two aspects were analysed; the efficiency of neurite alignment (Fig. 1B) and the cell polarity state (Fig. 1C-E) induced by nanogratings with varying geometries [1,2]. The tested geometries were the following: linewidths of 5  $\mu\text{m}$ , 2  $\mu\text{m}$ , 1  $\mu\text{m}$ , 750 nm and 500 nm and periodicities of 10  $\mu\text{m}$ , 4  $\mu\text{m}$ , 2  $\mu\text{m}$ , 1.5  $\mu\text{m}$  and 1  $\mu\text{m}$  respectively (Fig. 1B). As previously reported for other cell types, PC12 cells were only marginally affected by larger structures (>1  $\mu\text{m}$  linewidth) whereas sub-micron topography led to highly increased non-isotropic differentiation. Figure 1 displays the degree of axon outgrowth control determined by 750 and 500 nm

Aldo Ferrari

a.ferrari@sns.it

### Collaborators

F. Beltram  
M. Cecchini  
C. Di Rienzo  
P. Faraci  
D. Pisignano  
R. Sahai  
M. Serresi

linewidth gratings. The latter was found to be more effective, leading to over 90% of the axons aligning within 3° to the gratings, and almost 70% of axons aligned within 10°. For what concerns 750 nm linewidth substrates, 75% of axons were

aligned within 30° and the 36% within 10°. For comparison, the same analysis was performed on cells differentiating on flat, unpatterned TCPS: no preferential directionality was observed in this case (Fig. 1B).

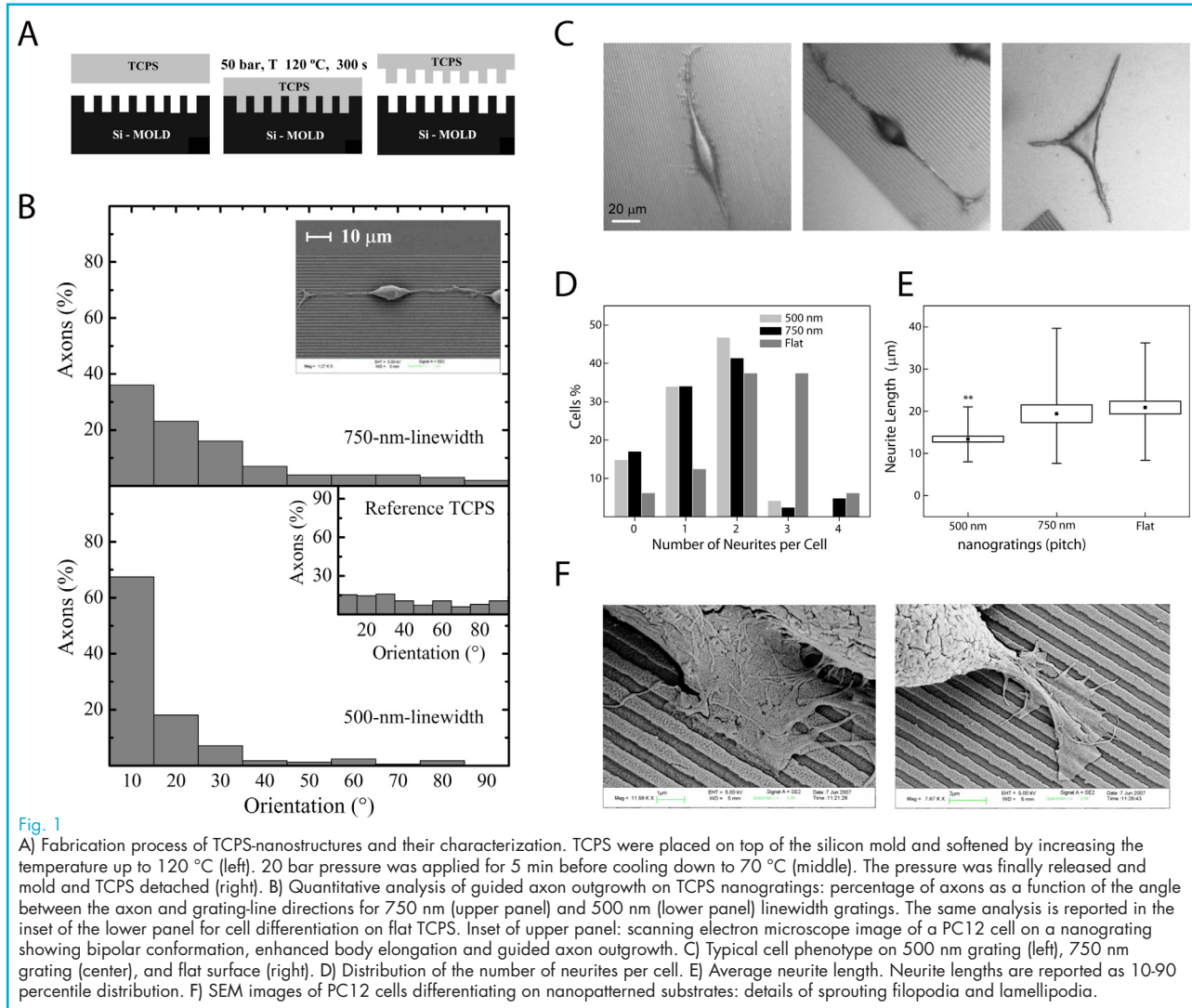


Fig. 1

A) Fabrication process of TCPS-nanostructures and their characterization. TCPS were placed on top of the silicon mold and softened by increasing the temperature up to 120 °C (left). 20 bar pressure was applied for 5 min before cooling down to 70 °C (middle). The pressure was finally released and mold and TCPS detached (right). B) Quantitative analysis of guided axon outgrowth on TCPS nanogratings: percentage of axons as a function of the angle between the axon and grating-line directions for 750 nm (upper panel) and 500 nm (lower panel) linewidth gratings. The same analysis is reported in the inset of the lower panel for cell differentiation on flat TCPS. Inset of upper panel: scanning electron microscope image of a PC12 cell on a nanograting showing bipolar conformation, enhanced body elongation and guided axon outgrowth. C) Typical cell phenotype on 500 nm grating (left), 750 nm grating (center), and flat surface (right). D) Distribution of the number of neurites per cell. E) Average neurite length. Neurite lengths are reported as 10-90 percentile distribution. F) SEM images of PC12 cells differentiating on nanopatterned substrates: details of sprouting filopodia and lamellipodia.

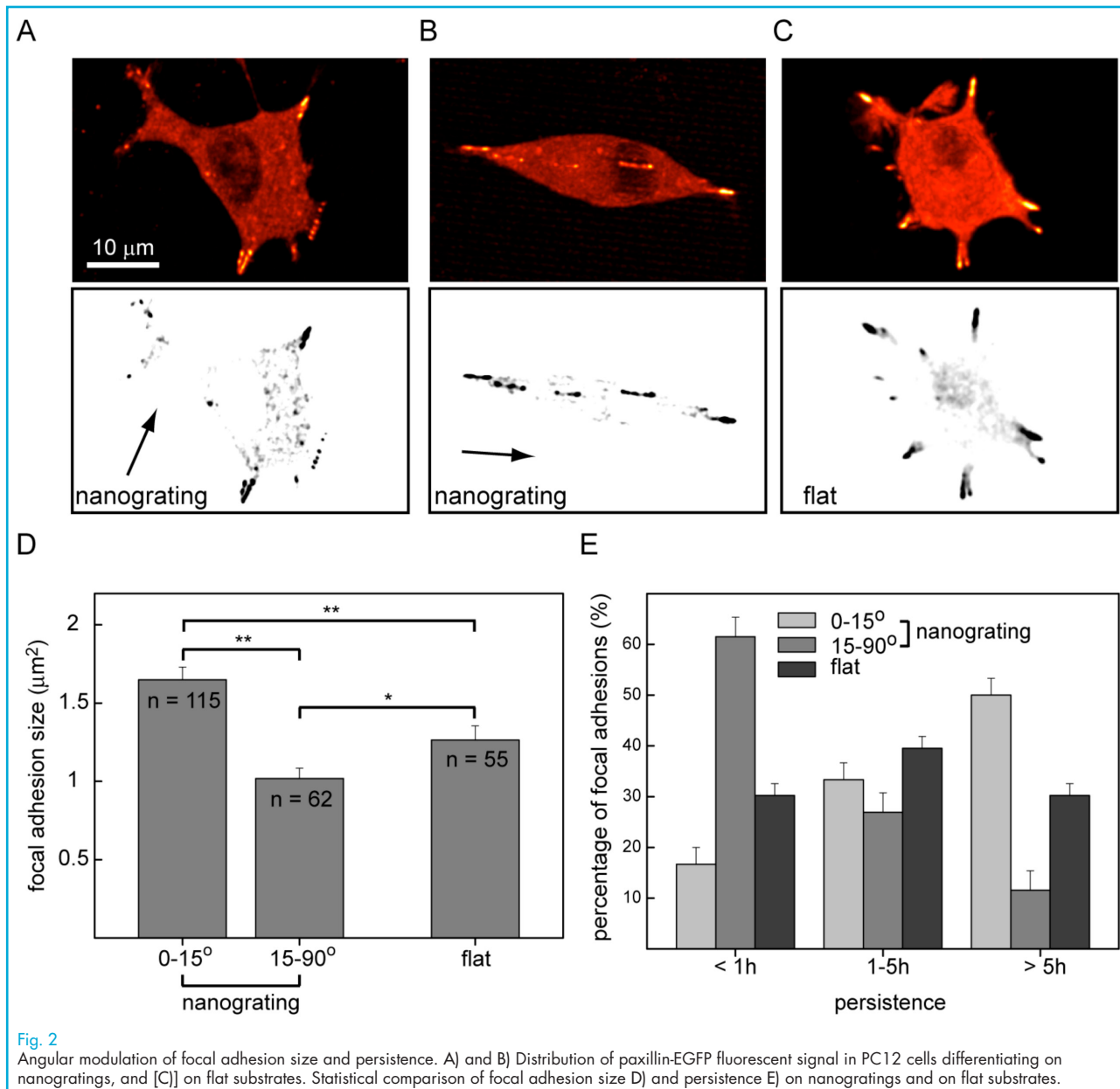
Nanogratings reduced to two the number of neurites produced by PC12 cells upon treatment with NGF (Fig. 1D). Neuronal bipolarity was correlated with an increased stretching of the cell body and a reduced length of the cell protrusions (Fig. 1E).

We next analysed the mechanisms governing the interaction between differentiating neuronal cells and our nanoimprinted topographies. Our work aimed at defining a biological link

between the topographical configuration of the substrate and the resulting cell polarity. For this activity we evaluated the use of new biocompatible materials with enhanced optical properties allowing the use of high-resolution live-cell microscopy in physiological conditions [4]. In this direction the nanoimprint protocol defined for TCPS could be further developed to obtain similar nanogratings imprinted on COC. Using these improved substrates we revealed the role played by integrin-

based adhesion complexes, the focal adhesions, during neuronal differentiation on anisotropic nanotopographies. First, we showed that during neuronal differentiation, topographical anisotropies control focal adhesion maturation. Modulation of adhesions was the driving mechanism that selected the properly aligned neurites. Notably, polarity selection via focal adhesion control was sufficient to induce a set of developmentally relevant changes, such as the transition

from a multipolar to a bipolar cell shape and the alignment of opposing neurites. Second, we demonstrated that a guiding topography can induce and consolidate a single polarity state by a patterned regulation of the cell differentiation machinery. Hence, differentiating neurons not only can 'read' the topographical guidance cues, but also can re-localize specific cellular activities along preferential directions and thus 'learn' achieving a committed differentiation.

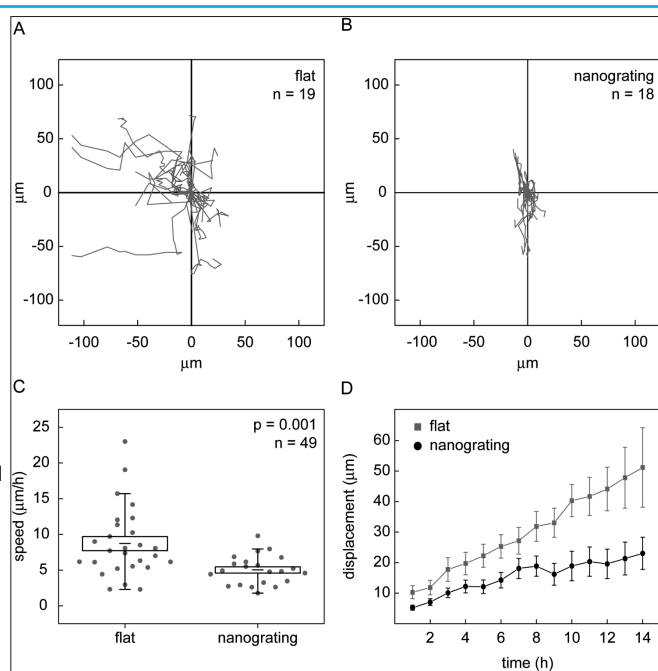


Moreover, we addressed the effect of nanogratings on the migration properties of differentiating PC12 cells and correlate their behavior with the polarity state induced by the substrate. During neuronal differentiation, cell-substrate interaction is sufficient to induce directional migration along the nanogratings (Fig. 3). Control cells contacting flat substrates migrated

freely in all directions while cells differentiating on nanogratings showed slower migration characterized by an angular restriction that confined cell movements. Finally, we showed that directional migration on nanogratings is linked to a specific organization of the cell cytoskeleton reflecting the nanograting directionality.

**Fig. 3**

Migration of PC12 cells differentiating on nanogratings or on flat substrates. A) Individual trajectories of PC12 cells (n=19) migrating on flat substrate. B) Individual trajectories of PC12 cells (n=18) migrating on nanogratings. For each trajectory (gray lines in panels A and B) the initial cell position was translated into the origin of the graph. C) Statistical analysis of cell speed during migration on nanogratings and flat substrates. The 5 to 95 percentile distribution (vertical line) was derived from individual data points (gray circles). The population mean is reported as a horizontal black line enclosed in a rectangular box whose length represents the standard error of the mean. The reported p-value was obtained performing a Mann-Whitney test. For this analysis 49 cells were considered. D) Cell displacement during migration. The average distance traveled from the origin is reported for cells migrating on flat substrates (gray squares) and on nanogratings (black circles) for each time of measure ( $t = 1$  h), for a total of 14 hours.



### References

- [1] M. Cecchini, G. Bumma, M. Serresi, F. Beltram, PC12 differentiation on biopolymer nanostructures. *Nanotechnology* 2007 Dec 19;18(50):-.
- [2] M. Cecchini, A. Ferrari, F. Beltram, PC12 polarity on biopolymer nanogratings. *Journal of Physics: Conference Series* 2008(1):012003.
- [3] D. Vaudry, P.J. Stork, P. Lazarovici, L.E. Eiden, Signaling pathways for PC12 cell differentiation: making the right connections. *Science* 2002 May 31;296(5573):1648-1649.
- [4] Cecchini M, Signori F, Pingue P, Bronco S, Ciardelli F, Beltram F. High-resolution poly(ethylene terephthalate) (PET) hot embossing at low temperature: thermal, mechanical, and optical analysis of nanopatterned films. *Langmuir* 2008 Nov 4;24(21):12581-12586.

## Fluorescent proteins for multiphoton and super-resolution imaging

**P**rogress in fluorescence imaging is enabling the study of biological events at unprecedented detail, thanks to novel microscopy techniques that provide imaging with nanoscale resolution. 3D imaging of living cells within intact tissues, organs, and whole animals, is accessible through multiphoton excitation. The remarkably rich photophysics of Fluorescent Proteins (FPs) makes them flexible enough to be used in conjunction with these advanced spectroscopic approaches. Here we report on our progress in understanding FPs multiphoton excitation spectra and in unraveling the photophysics behind photoactivation/deactivation of some FPs, a property enabling their use as fluorophores for nano-resolution imaging. This analysis allows us to develop new reversibly switchable FP mutants.

Stefano Luin

s.luin@sns.it

### Collaborators

S. Abbruzzetti  
P. Amat  
F. Beltram  
R. Bizzarri  
G. Lanza  
R. Nifosi  
M. Serresi  
V. Tozzini  
C. Viappiani  
V. Voliani

### Photoswitching and cis-trans photoisomerization

Recently, a novel approach to *in vivo* imaging has emerged with the development of new FPs that can be reversibly or irreversibly photoconverted between two optical states, adding a new temporal dimension to imaging of proteins at intracellular level. The most impressive results are obtained by using reversibly switchable FPs (RSFPs) [1,2], as they allow repeated activation events, thus prolonging the observation of biological dynamics, and the photo-labeling of several subcellular regions one after the other. Furthermore, RSFPs stand as excellent fluorophores for novel nano-resolution imaging techniques based on the regioselective activation/deactivation of emissive states at the nanoscale.

Based on computational modeling, we previously linked the photoswitching behavior of certain FPs to chromophore *cis-trans* photoisomerization [3]. As a further step to understanding the photophysics of photoswitching, we investigated the spectral and structural modification of synthetic chromophore analogues upon irradiation (Fig. 1). We found that *cis-trans* photoisomerization can be induced in all the chromophores and determined for the first time the optical, NMR and Raman spectra of neutral *trans* isomers (Fig1a-b, Fig2c), along with photoconversion quantum yields  $\phi_c$  by steady-state absorption measurements and by nanosecond laser-flash photolysis. Surprisingly,  $\phi_c$  ranged

from 0.1 to 1.0, demonstrating that photoconversion is a general and very efficient intrinsic photophysical mechanism of FP chromophores (Fig. 1c), whose efficiency is modulated by the mutant-specific protein environment [1,2].

Pre-resonant Raman experiments are able to determine the vibrational features of the chromophore also when embedded in the

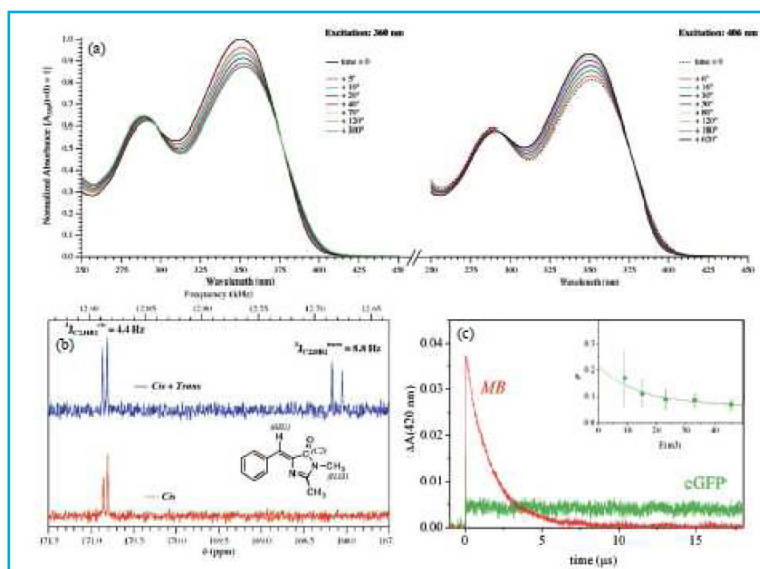


Fig. 1

The photochromic characteristics of chromophores are exemplified by the optical behavior of cBFPF upon irradiation. (a) Continuous irradiation at 360 nm leads to the time-dependent decrease and red-shift of the absorption spectrum due to the formation of a photoproduct (identified with the *trans* form tBFPF by NMR); (a, right panel) constant irradiation of photoconverted cBFPF at 406 nm, leads to the reversion of the absorption spectrum. (b)  $^{13}\text{C}$ -NMR spectra of native and photoconverted cBFPF while adopting selective decoupling between the methyl protons HA3 and C2: the detected  $^{13}\text{C}_{\text{C2,HB2}}$  values in the photoproduct correspond to those expected for the *cis* and *trans* isomers. (c) Single high-energy pulse irradiation at 355 nm of cGFP in methanol (OD=0.6) leads to a fast and irreversible absorption change (< 5 ns) detected at 420 nm (green line); methylene blue in water (OD=0.67) irradiated at the same wavelength shows a fast conversion to triplet state followed by slower (few  $\mu\text{s}$ ) decay to the ground singlet state because of quenching by molecular oxygen (red line). (inset) By using methylene blue as an actinometer, the comparative method yields  $\phi_c$  as a function of laser-pulse energy: extrapolation to zero energy gives the actual  $\phi_c$  value.

proteins (Fig. 2). We studied the Raman signatures of different chromophore states in GFP mutants and compared them to those of the isolated chromophores. Our experiments allowed us to demonstrate that the *cis-trans* isomerization is responsible for the photoswitching behaviour of at least two RSFPs, namely EYQ1 (a newly developed

GFP variant with T203Y E222Q) and BFPF (Y66F) [2]. In particular, for the case of EYQ1 we showed that at pH=8 the chromophore is anionic in the native form and neutral *trans* in the photoconverted form; it is neutral *cis* in the native form at lower pH. Our investigation highlights the relevance of Raman spectroscopy for the study of ground and metastable states of optically-active portions of proteins.

In order to develop more efficient RSFPs, we started by addressing those residues adjacent to the chromophore that can hinder its photochromic behaviour. Remarkably, we demonstrated that E222Q replacement induces reversible photoswitching in four GFPs otherwise differing in the mutation pattern, with switching 2-3 orders of magnitude faster than in any other reported photoswitchable GFPs.

We assessed the utility of the new RSFPs for intracellular studies by Fluorescence Recovery After Photobleaching to the -1, a technique that relies on the localized photoactivation of a fluorophore and the real-time monitoring of its subsequent dynamics. EYQ2 (S65T/T203Y/E222Q) was conjugated to a short peptide sequence that acts as a nuclear localization signal (NLS), i.e. it is recognized by the cellular importin system and actively transported to the nucleus [4]. Then, the dynamics of the nucleocytoplasmic shuttling of NLS-EYQ2 was determined by FRAP<sup>1</sup> (Fig. 2d). EYQ2 allowed for the long-term repetition of the experiment in the same cell, thus increasing the accuracy of kinetic measurements and ideally providing the correlation of transport dynamics with different cell states. FRAP<sup>1</sup> on NLS-EYQ2 yielded a shuttling time-constant ( $t=117\pm3$  s) in excellent agreement with the value measured by conventional FRAP on NLS-EGFP.

### Non-linear spectroscopy

We investigated the two-photon absorption (TPA) properties of various fluorescent proteins (BFP, CFP, GFP,

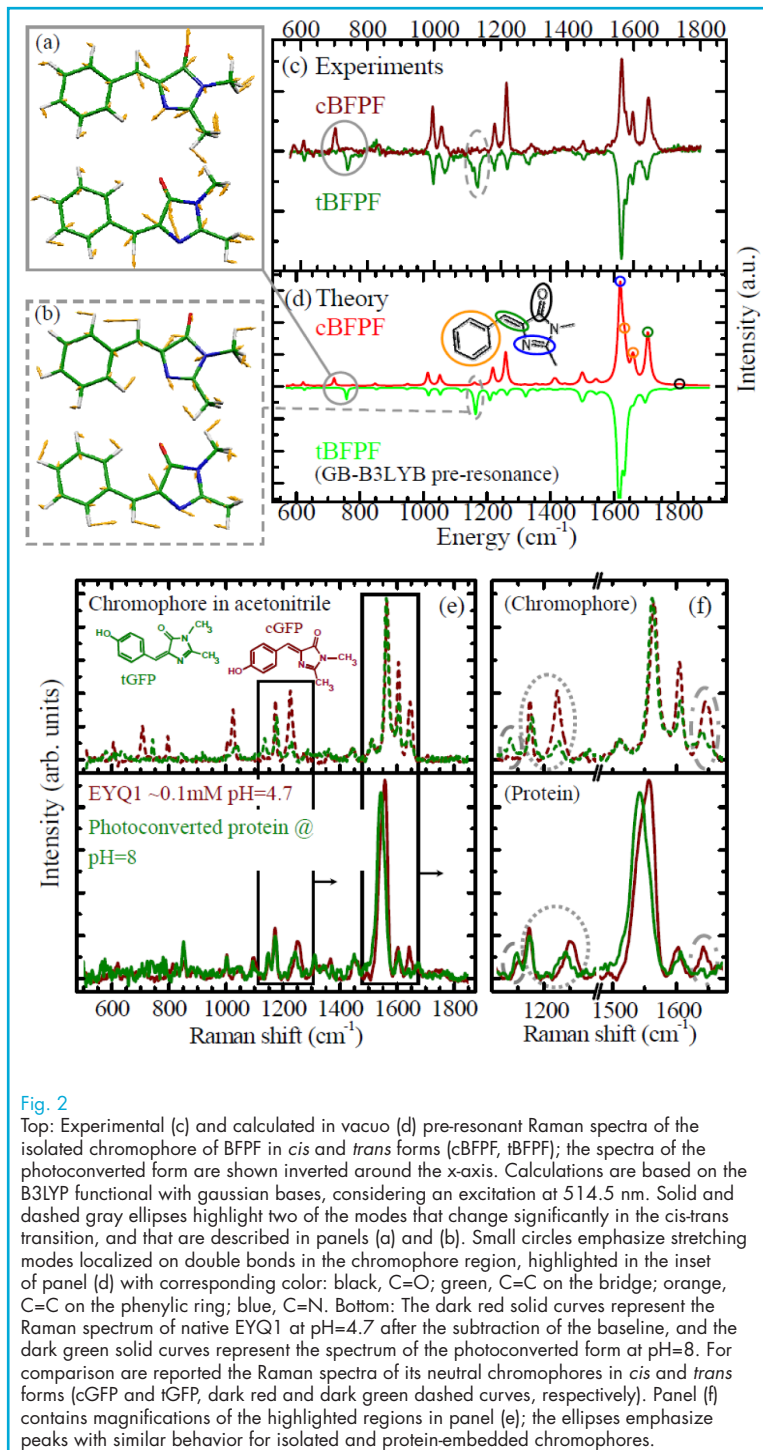
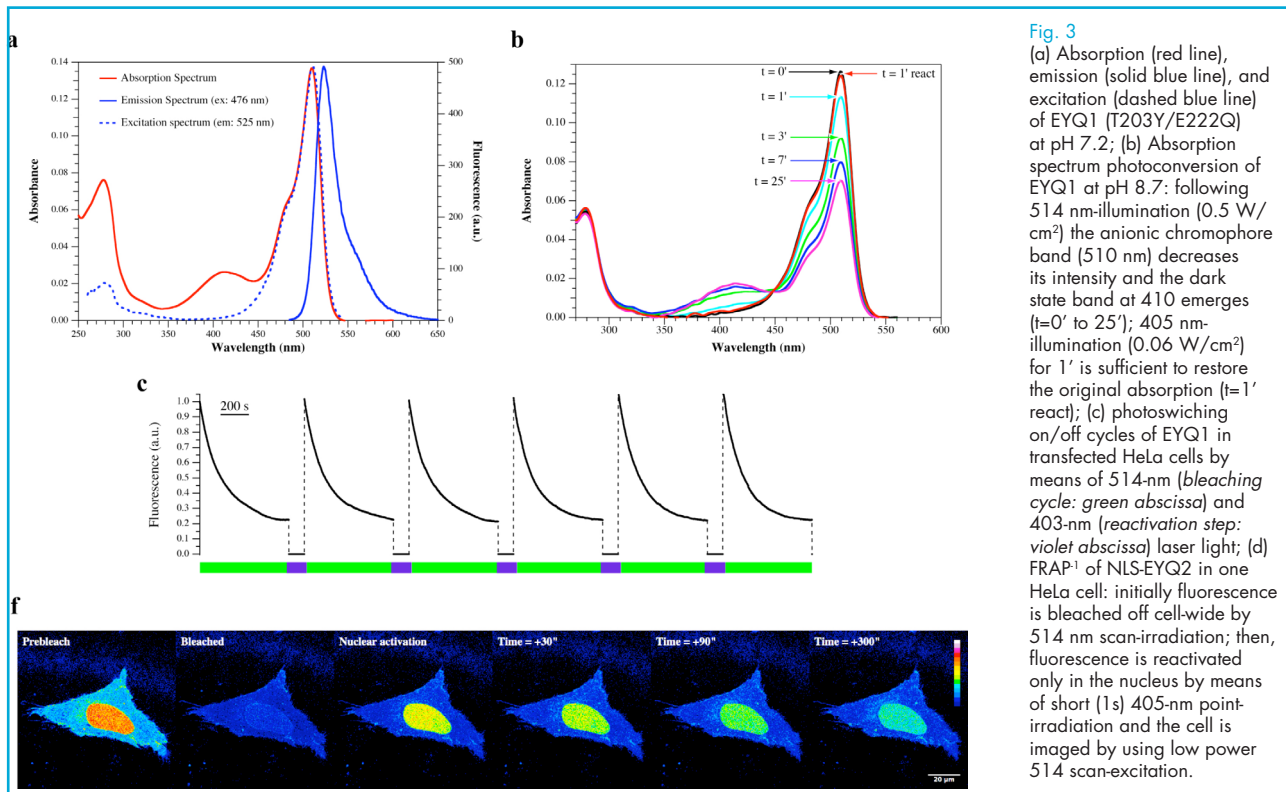


Fig. 2

Top: Experimental (c) and calculated in vacuo (d) pre-resonant Raman spectra of the isolated chromophore of BFPF in *cis* and *trans* forms (cBFPF, tBFPF); the spectra of the photoconverted form are shown inverted around the x-axis. Calculations are based on the B3LYP functional with gaussian bases, considering an excitation at 514.5 nm. Solid and dashed gray ellipses highlight two of the modes that change significantly in the *cis-trans* transition, and that are described in panels (a) and (b). Small circles emphasize stretching modes localized on double bonds in the chromophore region, highlighted in the inset of panel (d) with corresponding color: black, C=O; green, C=C on the bridge; orange, C=C on the phenyl ring; blue, C=N. Bottom: The dark red solid curves represent the Raman spectrum of native EYQ1 at pH=4.7 after the subtraction of the baseline, and the dark green solid curves represent the spectrum of the photoconverted form at pH=8. For comparison are reported the Raman spectra of its neutral chromophores in *cis* and *trans* forms (cGFP and tGFP, dark red and dark green dashed curves, respectively). Panel (f) contains magnifications of the highlighted regions in panel (e); the ellipses emphasize peaks with similar behavior for isolated and protein-embedded chromophores.

DsRed, mOrange, zFP and Kaede), and compared them with one-photon properties, using computational methods based on Density Functional Theory. This technique allowed us to calculate excitation wavelengths and cross sections for various model chromophores. A general relationship between excitation wavelength and structure was extracted,

based on the variation of electric dipole upon excitation, and ultimately connected with the extension of the  $\pi$ -conjugated system [5]. The two-photon calculations shed light on the peculiar TPA features of DsRed (Fig. 3a) [6], and predicted the presence of high-energy (500-700 nm) TPA bands in several other FPs [7]. These excitation bands, later confirmed



**Fig. 3** (a) Absorption (red line), emission (solid blue line), and excitation (dashed blue line) of EYQ1 (T203Y/E222Q) at pH 7.2; (b) Absorption spectrum photoconversion of EYQ1 at pH 8.7: following 514 nm-illumination ( $0.5 \text{ W/cm}^2$ ) the anionic chromophore band (510 nm) decreases its intensity and the dark state band at 410 emerges ( $t=0'$  to  $25'$ ); 405 nm-illumination ( $0.06 \text{ W/cm}^2$ ) for  $1'$  is sufficient to restore the original absorption ( $t=1'$  react); (c) photoswitching on/off cycles of EYQ1 in transfected HeLa cells by means of 514-nm (bleaching cycle: green abscissa) and 403-nm (reactivation step: violet abscissa) laser light; (d) FRAP<sup>1</sup> of NLS-EYQ2 in one HeLa cell: initially fluorescence is bleached off cell-wide by 514 nm scan-irradiation; then, fluorescence is reactivated only in the nucleus by means of short (1s) 405-nm point-irradiation and the cell is imaged by using low power 514 scan-excitation.

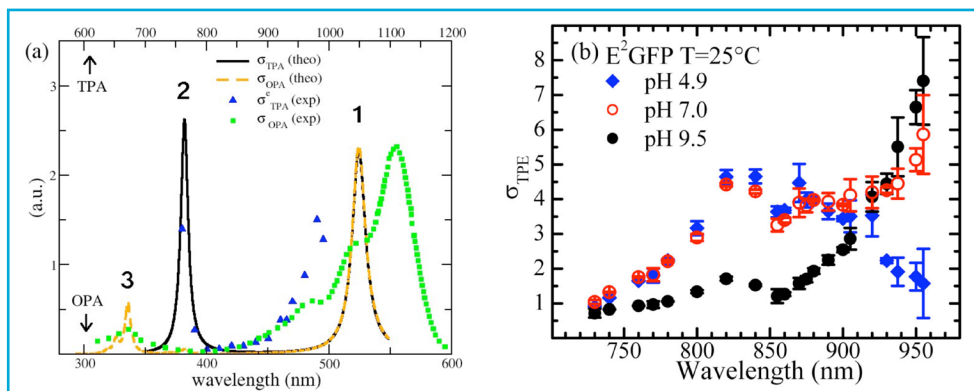


**Fig. 4** (a): Comparison between experimental and theoretical spectra of DsRed. The two-photon measured cross section (blue triangles) displays a strong increase below 800 nm (band 2), whereas the one photon spectrum (green squares) is rather featureless in that region. The calculated TPA cross section (black solid line) reproduces this band, as due to excitation at a higher excited state. The blue shift between the theoretical and experimental 1 band is due to having considered the isolated model chromophore instead of the entire protein, to intrinsic errors of the theory, and to neglect of vibronic features. (b): 2-photon-action cross-sections  $\sigma_{TPE}$  in GM units ( $1 \text{ GM}=10^{-50} \text{ cm}^4 \text{ s/photon}$ ) of E<sup>2</sup>GFP (at pH = 4.9, 7.0 and 9.5) over the 730–960 nm excitation range, with fluorescence emission in the range 450–650 nm. Error bars are estimated as standard deviations of the results of 4 to 10 measurements, often at different excitation intensities.

by experiments, can provide researchers with useful, and yet unexploited, spectral windows for two-photon imaging.

We are currently performing detailed measurements of two-photon excitation

and photoconversion spectra in selected proteins. Preliminary results demonstrated the suitability of E<sup>2</sup>GFP (F64L S65T T203Y) as a two-photon pH ratiometric indicator (Fig. 3b) [8].

#### References

- [1] V. Voliani, R. Bizzarri, R. Nifosi, S. Abbruzzetti, E. Grandi, C. Viappiani, F. Beltram, "Cis-trans photoisomerization of fluorescent-protein chromophores", *J. Phys. Chem. B.* 112, 10714-22 (2008)
- [2] S. Luin, V. Voliani, G. Lanza, R. Bizzarri, R. Nifosi, P. Amat, V. Tozzini, M. Serresi, F. Beltram, "Raman Study of Chromophore States in Photochromic Fluorescent Proteins", *J. Am. Chem. Soc.* 131, 96-103 (2009)
- [3] R. Nifosi, A. Ferrari, C. Arcangeli, V. Tozzini, V. Pellegrini and F. Beltram, "Photoreversible dark state in a tristable Green Fluorescent Protein variant", *J. Phys. Chem. B* 107, 1679 (2003)
- [4] F. Cardarelli, M. Serresi, R. Bizzarri, M. Giacca, F. Beltram, *Mol Ther* 2007, 15, 1313-22.
- [5] R. Nifosi, P. Amat, V. Tozzini, "Variation of spectral, structural and vibrational properties within the Intrinsically Fluorescent Proteins family: a Density Functional Study", *J. Comput. Chem.* 28, 2366-2377 (2007)
- [6] R. Nifosi, Y. Luo, "Predictions of Novel Two-Photon Absorption Bands in Fluorescent Proteins", *J. Phys. Chem. B.* 111, 14043-14050 (2007)
- [7] R. Nifosi, Y. Luo, "The origin of the anomalous Two-Photon absorption in Fluorescent Protein DsRed" *J. Phys. Chem. B (letter)* 111, 505-507, (2007)
- [8] R. Bizzarri, M. Serresi, S. Luin, F. Beltram, "Green Fluorescent Protein-based pH indicators for in vivo use: a review", *Anal. Bioanal. Chem.* 393, 1107-1122 (2009)

## Modeling macro-biomolecules

**B**iological matter is characterized by an overwhelming complexity: In order to “live” an organism must undergo a variety of events that occur on different scales of length and time. These range from a few Å, the size of the active site of proteins, where the ultra-fast triggering steps of the biochemical reactions take place, up to the level of the cells and organs, where the macroscopic physiological effects are detectable by the naked eye, and involve the nano- and micro- scale as intermediates. This hierarchical organization is responsible for the complexity, because each single process inherently involves a cascade of events occurring on different scales.

In the period 2005-2006 we developed and tested modeling methodologies tailored to address the nano-micro scale typical of the macromolecular aggregates, namely the Coarse Grained models. In the subsequent period (2007-2009), we extended those models and applied them to specific problems (fundamental steps of HIV replication and in general of DNA replication, and the Fluorescent Proteins structural and optical properties). In addition, we started a process of integration of the CG models within a more general multi-scale approach, which, we believe, is essential for a coherent description and a deep understanding of any biological processes.

The HIV protease (HIV pr) is a virus-specific enzyme whose action is essential for the virus maturation: it cleaves the Gag viral poly-protein in functional parts that will be structural and functional elements of the new viral particles. In 2005-2006 we developed a CG model for HIV pr based on the one-interacting-center-per-amino-acid description (one-bead (OB) model[1]). The model was shown to accurately describe the protein dynamics on time scales large enough to address the slow ( $\mu$ sec-msec) process of the active site opening[2], that is the first step of the action mechanism of this enzyme. In 2007-2008, we applied the model to the study of the whole cleavage process: the model was able to clarify some details of the binding with a model substrate (a part of the Gag poly-peptide) and of the product release after cleavage[3] (Fig. 1 (a)). A similar simulation study with the whole Gag poly-protein is currently in progress. These studies are relevant to indicate novel therapeutic strategies exploiting the HIV pr inhibition. Additionally we studied the interactions of HIV pr with currently used inhibitor drugs[4] (Fig. 1 (b)). In this case a multi-scale approach involving also all-atom simulations was adopted in order to address the more chemically complex

interactions occurring with non-peptide ligands.

The same methodology was also applied to the study of HIV-Integrase – an enzyme responsible for the viral DNA integration into the cell nucleus. Since the acetylation of some of its specific Lysine residues is involved in the process, using molecular recognition and docking methodologies, we built models of Integrase complexed with the two acetyl transferases (HATs) p300 and GCN5 (Fig 2). We showed that the obtained models are compatible with experimental observations and possess stereochemical quality. On the basis of the models we hypothesize that the residue which is more likely to be acetylated by both HATs is Lys 273. Finally, we applied an Essential Dynamics analysis to both models which outlined two critical regions of Integrase which can provide possible allosteric sites on the enzyme for the inhibition of the viral genome integration in the host cell [5].

The one-bead model was then extended to nucleic acids, for which a one-bead-per-nucleotide model was developed. In particular our DNA model is able to accurately predict the dynamics of supercoiling and local denaturation of torsionally stressed DNA nanorings

Valentina Tozzini

v.tozzini@sns.it

### Collaborators

P. Amat  
S. Bonella  
A. Di Fenza  
G.N. Embrapa  
J.A. McCammon  
R. Nifosi  
W. Rocchia  
F. Trovato  
J. Trylska  
K. Voltz

Fig. 1

Modeling the HIV pr action mechanism. (a) In red-blue-green: subsequent snapshots taken from the simulation of the model-substrate (in green) capture, cleavage and product release by the HIV pr (red-blue). The orange rectangle highlights the snapshot where the substrate HIV-1 pr complex is formed. The same portion of the HIV-1 pr (green) complexed with the Gag (white-yellow) is enclosed in the 3D orange parallelepiped. The cleaved yellow part undergoes a structural transformation before becoming a structural part of the capsid. The complex within the envelope of the immature virion is also pictorially represented in the left lower corner. (b) The multiscale simulation of the binding of an antiviral drug to HIV pr. In the first snapshot two steps of the approaching phase of the drug to the active site from a CG simulation are shown. The following four snapshots are taken from the all-atom MD simulation of the capture phase.

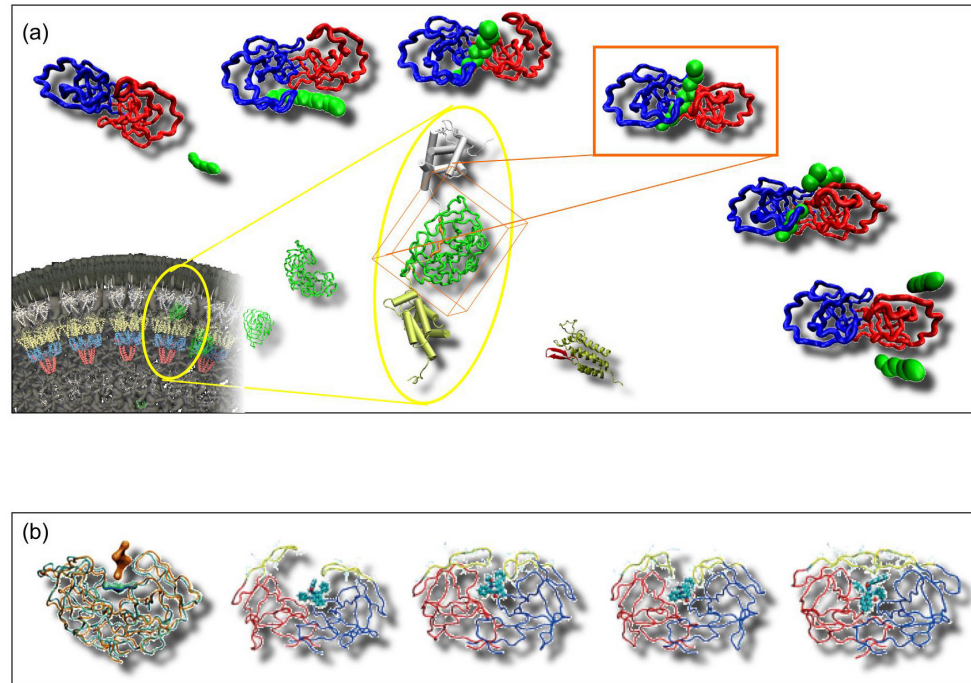
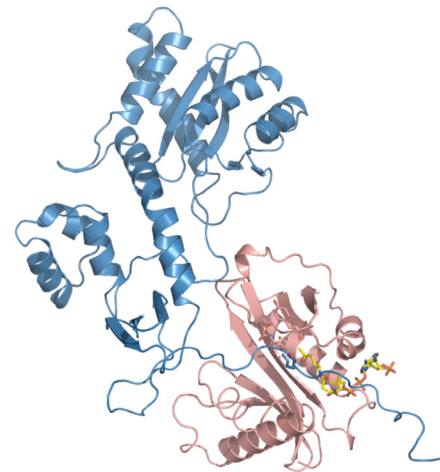


Fig 2

Cartoon view of the complex between HIV-1 Integrase (blue) and the acetyltransferase GCN5 (pink). The residue which undergoes acetylation (Lys 273), the co-factor molecule (AcetylCoA, yellow) are shown as sticks together with the residues of the catalytic site.



and of entire small plasmids [6] (Fig 3). This study indicates that the torsional stress physiologically present in DNA has an important role in the regulation of the interplay between compaction-decompaction and duplication of DNA, that requires the strand separation. A simplified version of the model was integrated with the one-bead models for proteins [7] and used within a multi-scale approach [8] to study the wrapping-unwrapping of DNA around the core proteins in the nucleosomes [9] (Fig 4).

The surface representation of biomolecules, consisting in defining a biomolecule by means of its solvent accessible surface, can be placed at the "very coarse" extreme in the multi-scale approaches. Surface representations are widely used in the docking and molecular recognition methodologies. Having in mind the idea of building an integrated framework for multi-scale approaches, the accurate and efficient representation of the electrostatics has an important role. In order to make some steps forward in this field, the

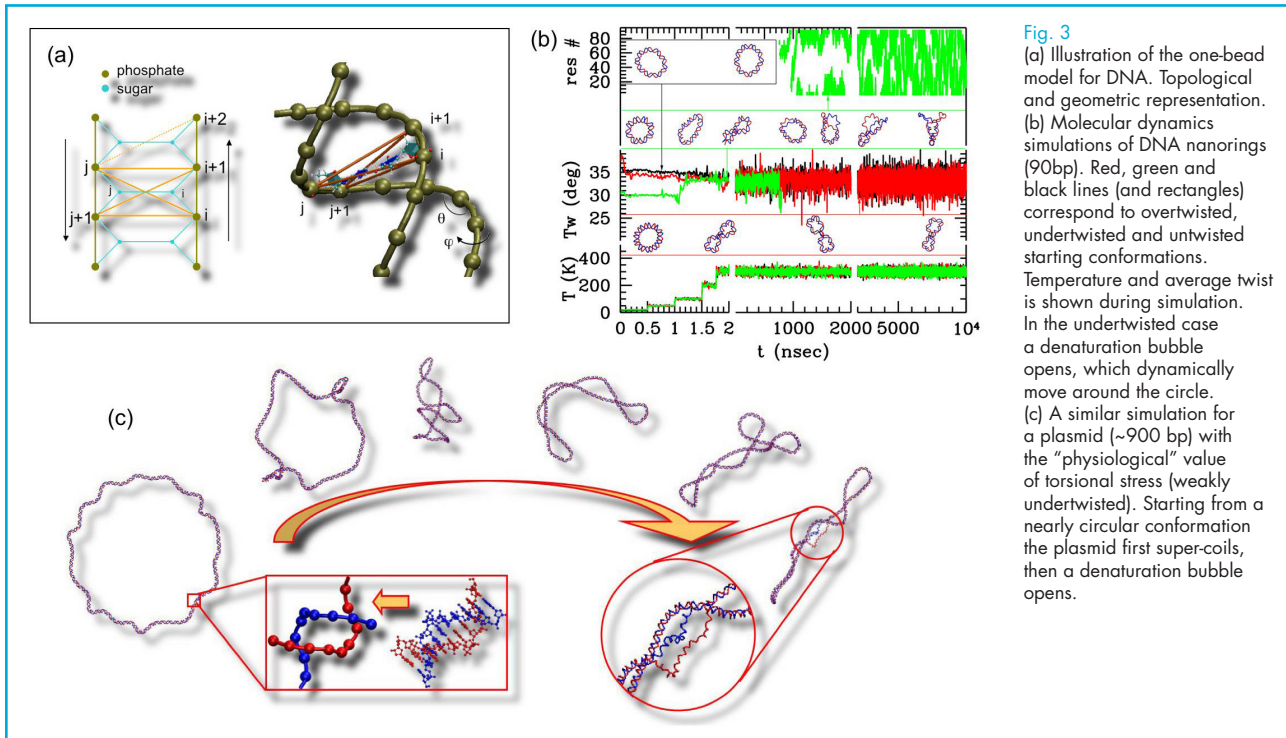


**Fig. 3**  
 (a) Illustration of the one-bead model for DNA. Topological and geometric representation. (b) Molecular dynamics simulations of DNA nanorings (90bp). Red, green and black lines (and rectangles) correspond to overtwisted, undertwisted and untwisted starting conformations. Temperature and average twist is shown during simulation. In the undertwisted case a denaturation bubble opens, which dynamically move around the circle. (c) A similar simulation for a plasmid (~900 bp) with the "physiological" value of torsional stress (weakly undertwisted). Starting from a nearly circular conformation the plasmid first super-coils, then a denaturation bubble opens.

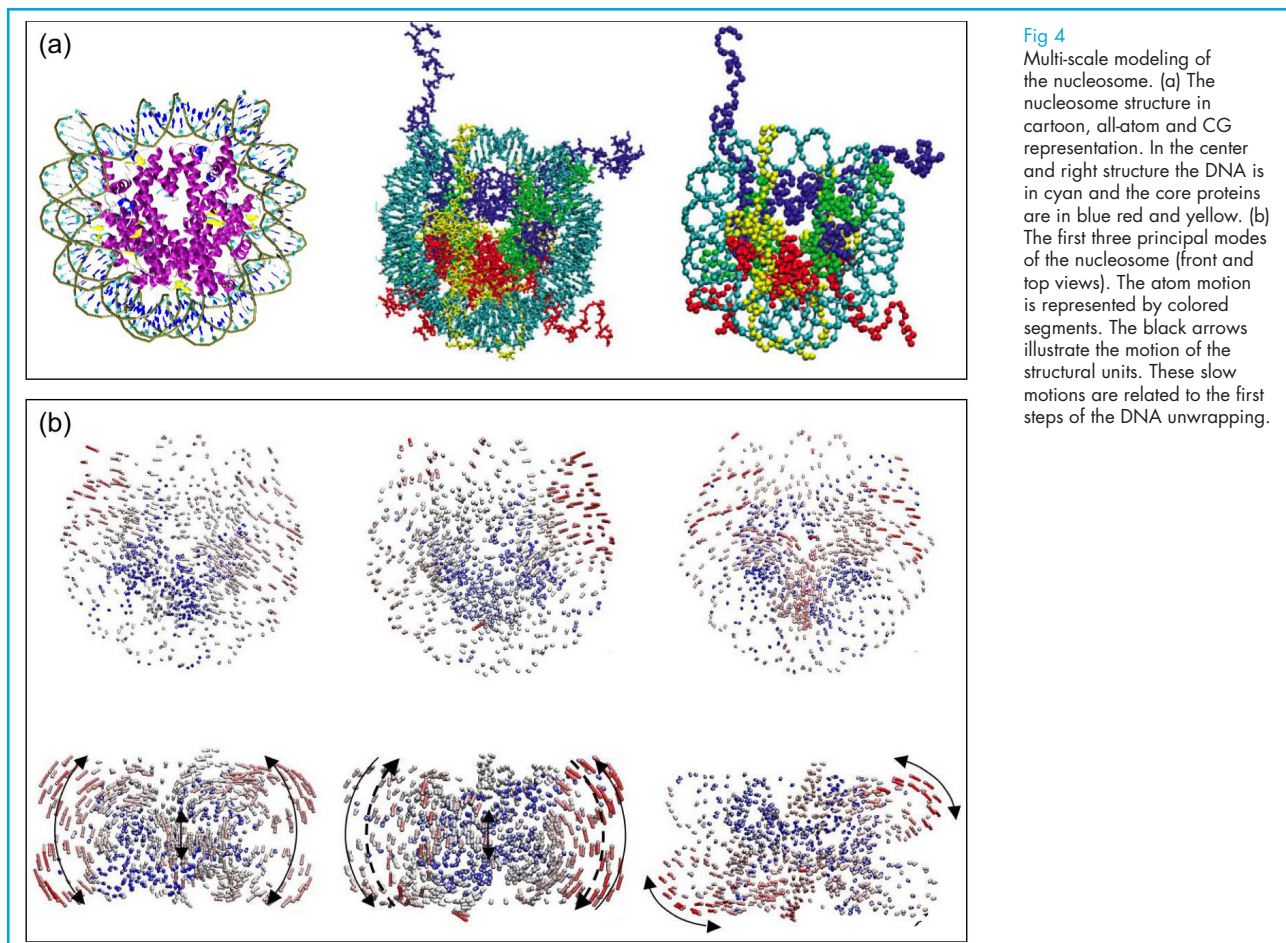


**Fig 4**  
 Multi-scale modeling of the nucleosome. (a) The nucleosome structure in cartoon, all-atom and CG representation. In the center and right structure the DNA is in cyan and the core proteins are in blue red and yellow. (b) The first three principal modes of the nucleosome (front and top views). The atom motion is represented by colored segments. The black arrows illustrate the motion of the structural units. These slow motions are related to the first steps of the DNA unwrapping.

electrostatic potential generated by all the existing PDB structures was calculated and stored in a relational DataBase in order to identify new patterns for predicting interesting structural properties related to molecular recognition[10].

An extensive description of the coarse grained and atomic based approaches for proteins and of their integration with atomic-based models in multi-scale approaches was proposed in a review paper[11], that also illustrates these methods on two very important example-systems, namely the green fluorescent proteins (GFP) and the proteins involved in the replication of HIV. The foremost relevance of these two biomolecular systems was confirmed by the assignment of two of the Nobel prizes in 2008: in chemistry for the discovery of GFP and in medicine for the discovery of HIV.

An extensive description of the coarse grained and atomic based approaches

for proteins and of their integration with atomic-based models in multi-scale approaches was proposed in a review paper[11], which also illustrates these methods on two very important example-systems, namely the proteins involved in the replication of HIV and the green fluorescent proteins (GFP). The foremost relevance of these two biomolecular systems was confirmed by the assignment of two of the Nobel prizes in 2008: in medicine for the discovery of HIV and in chemistry for the discovery of GFP. Further molecular modeling activity on the latter system include a study of the oligomerization propensity of Fluorescent proteins using a novel statistical algorithm[12] and an investigation on photophysical properties for specific imaging applications reported in the section: "Fluorescent proteins for multiphoton and super-resolution imaging".

#### References

- [1] V. Tozzini and J.A. McCammon *One-Bead Coarse Grained Models for Proteins* in "Coarse-graining of condensed Phase and Biomolecular Systems", G.A. Voth Ed, Taylor & Francis/CRC press, Chapter 19 (2008)
- [2] V. Tozzini, J. Trylska, C-E Chang, J.A. McCammon *Flap opening dynamics in HIV-1 protease explored with a coarse-grained model* J Struct Biol, 157 606-615 (2007)
- [3] J. Trylska, V. Tozzini, C.-E. Chang, J.A. McCammon *HIV-1 protease substrate binding and product release pathways explored with coarse-grained molecular dynamics* Biophys J, 92 4179-4187 (2007)
- [4] C.-E. Chang, J. Trylska, V. Tozzini, J.A. McCammon *Binding pathways of ligands to HIV-1 Protease: Coarse-grained and atomistic simulations* Chem Biol Drug Des, 69 5-13 (2007)
- [5] A. Di Fenza, W. Rocchia, V. Tozzini *Complexes of HIV-1 integrase with HAT proteins: multi-scale models, dynamics and hypotheses on allosteric site of inhibition* Proteins 76, 946-958 (2009)
- [6] F. Trovato, V. Tozzini *Supercoiling and Local Denaturation of Plasmids with a Minimalist DNA Model* J Phys Chem B 112, 13197-13200 (2008)
- [7] K. Voltz, T. Wocjan, K. Klenin, J. Trylska, V. Tozzini, V. Kurkal, J. Smith, J. Langowski *DNA dynamics on the nucleosome simulated by coarse-grained models* Biophys J, Suppl S 540A-540A (2007)
- [8] K. Voltz, J. Trylska, V. Tozzini, V. Kurkal-Siebert, J. Langowski, J. Smith, *Coarse-grained force field for the nucleosome from self-consistent multiscaling* J Comput Chem 29, 1429-1439 (2008)
- [9] K. Voltz, J. Trylska, V. Tozzini, V. Kurkal-Siebert, J. Smith, and J. Langowski *Global motions in the nucleosome explored using a coarse-grained model* NIC Series 40, 141-144 (2008)
- [10] W. Rocchia, G. Neshich *Electrostatic potential calculation for biomolecules - creating a database of pre-calculated values reported on a per residue basis for all PDB protein structures* Genetics and Molecular Research 6, 923-936 (2007)
- [11] V. Tozzini *Multi-Scale Modeling of Proteins* Acc Chem Res, DOI: 10.1021/ar9001476
- [12] Bonella, W. Rocchia, P. Amat, R. Nifosí and V. Tozzini *SPDhound, a mutual information based method to investigate specificity determining positions* Algorithms 2, 764-789 (2009)

## Nanotechnology for intracellular delivery and targeting of drugs, nanoreporters and nanoactuators

**T**he selective permeability of the plasma membrane prohibits most exogenous agents from gaining cellular access. A very effective class of transporters for the internalization of drugs, biosensors and imaging agents are cell penetrating peptides (CPPs), a group of short cationic sequences with a remarkable capacity for membrane translocation. Cell-penetrating peptides guarantee high delivery yield, low toxicity and the possibility to enter a wide range of target cells. Moreover they can act as molecular carriers for delivery of cargoes (e.g. proteins and nucleic acids) to relevant sub-cellular domains (mitochondria, endosomal vesicles and nucleus). This report describes recent advances in the use of Tat arginin-rich peptides and provides further information on the controversial mechanism of its nuclear entry. Nuclear localization is particularly significant, as it is one of the fundamental steps for gene-therapy approaches and can open the way to probe and modify cellular processes of utmost importance.

Peptide-mediated delivery of bioactive molecules appears to be a new biotechnology tool that in many aspects is superior to commonly used delivery agents (liposomes, microinjection, electroporation, viral systems). Cell penetrating peptides typically consist of short basic peptide sequences that could cross the plasma membrane and deliver their cargo directly into the cell. Among CPPs we focused our attention on the arginine-rich motif derived from the HIV transactivator of transcription protein Tat (residues 47-57 YGRKKRRQRRR of HIV-Tat protein full length). In order to elucidate the entrance pathway and to identify the intracellular trafficking properties of Tat-based vector, we engineered a recombinant fusion protein consisting of Tat sequence fused to the green fluorescent protein (GFP). The purified protein added to the culture medium first attaches to the cell membranes - presumably by ionic interactions - and then permeates cells by endocytosis. An array of endocytosis assays had demonstrated that Tat enters living HeLa cells using both clathrin-dependent pathway and macropinocytosis and progressively translocates into low-pH endosomes.

Once we had identified Tat protein as a vector system capable to cross cell membranes and elucidated its mechanism of internalization, we focused upon the investigation of the ability of Tat-derived

peptides to transduce cargoes of different size in specific sub-cellular compartments. Cell penetrating properties depend upon the integrity of Tat arginine-rich motif, YGRKKRRQRRR, corresponding to a putative nuclear localization sequence (NLS) and the trans-activation responsive region-binding domain of the entire Tat protein.

To assess the nucleus/cytoplasm shuttling properties driven by Tat peptide we engineered green fluorescent protein (GFP)-based fusion proteins of different molecular size, both below and above the passive diffusion size limit through the nuclear pore (NP). These constructs represented a benchmark for intracellular passive diffusion behavior when expressed in cells and were also used as cargoes for prototypical active import by fusing them to the NLS (Nuclear Localization Sequence) of SV40. The behavior of these two classes of constructs was compared with the same GFP-cargoes fused to the Tat peptide. *In vivo* imaging allowed us to study Tat peptide-intracellular localization and dynamics (FRAP analysis). Our findings support a passive diffusion mechanism directing Tat movement across the nuclear envelope (NE) (Fig. 1).

The identification of this limitation of Tat peptide as a nuclear delivery vector prompted us to improve Tat functionality for the correct translocation of cargoes to the

Michela Serresi

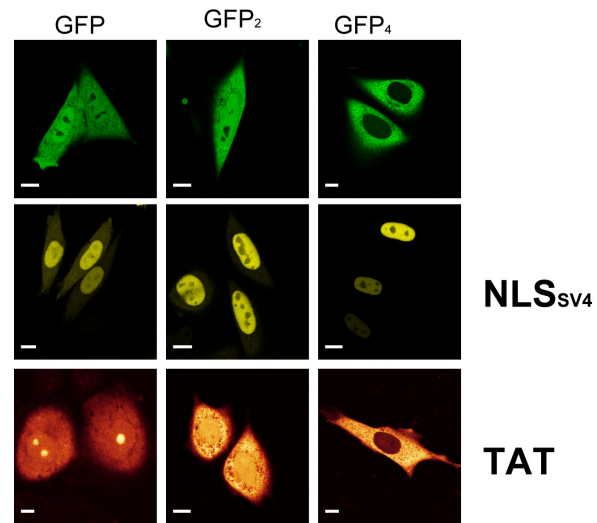
m.serresi@sns.it

### Collaborators

A. Albanese  
L. Albertazzi  
F. Beltram  
R. Bizzarri  
F. Cardarelli  
F. Salomone

Fig. 1

Cargo-dependent sub-cellular localization. As untagged constructs (above panel), Tat-GFP and Tat-GFP<sub>2</sub> are uniformly distributed between nucleus/cytoplasm compartments; Tat-GFP<sub>4</sub> is completely excluded from the nucleus (below panel). In contrast, NLS-tagged cargoes are predominantly localized in the nucleus of HeLa cells (middle panel).

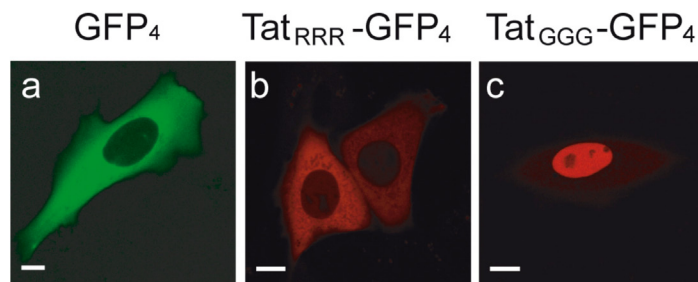


nucleus. To accomplish this goal, we focused our study on the rational mutagenesis of the Tat peptide to afford variants with finely tuned intercompartmental dynamics and controllable nuclear transport mechanism. By mutagenesis of the carboxy-terminal stretch "RRR" of Tat sequence into "GGG" (not-charged residues), we engineered a novel variant of Tat peptide, Tat<sub>GGG</sub>-EGFP with well-defined nuclear active transport properties. Remarkably, the Tat<sub>GGG</sub> fused

to GFP<sub>4</sub>-cargo (110 Kda, exceeding the size-threshold value for passive diffusion through nuclear pore) was predominantly detected into the nucleus (Fig. 2 c): this indicates that the Tat<sub>GGG</sub> sequence does determine active nuclear import of large cargoes. Conversely, the wild-type Tat peptide is not able to drive the active nuclear import of the same cargo, and is completely excluded from the nucleus (Fig 2 b), as untagged GFP<sub>4</sub> (Fig.2a).

Fig. 2

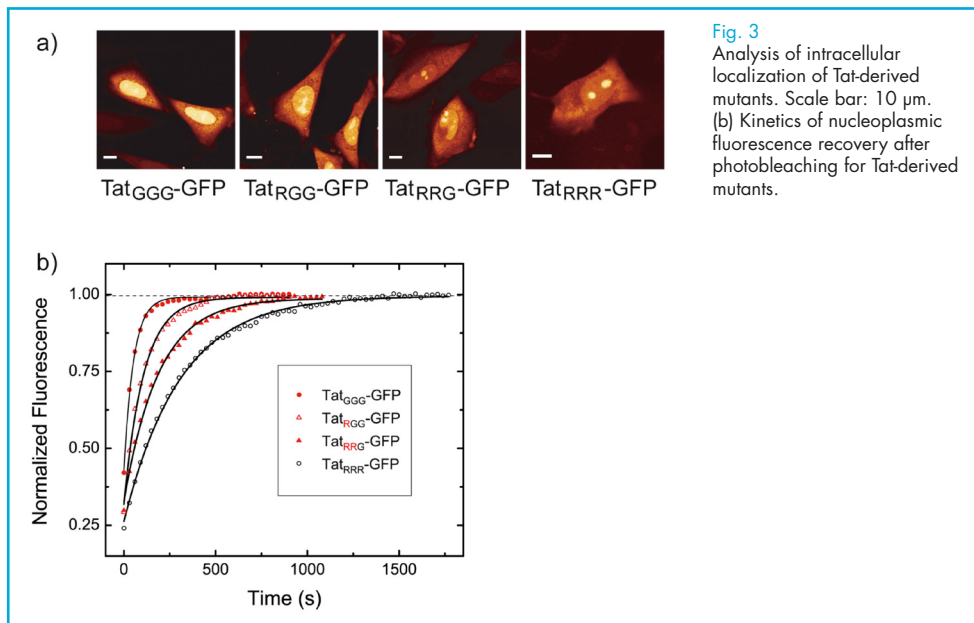
Tat<sub>GGG</sub>-mediated active nuclear accumulation of GFP<sub>4</sub> cargo, while Tat<sub>RRR</sub> shown the same behavior of untagged GFP<sub>4</sub>



Since the substitution of 'RRR' residues with 'GGG' allowed us to switch on and off the Tat-peptide nuclear-import properties, we explored the degree of tunability yielded by the variation of the number of positively charged C-terminal arginine residues. By *in vivo* imaging we found that the one-by-one replacement of glycine residues to wild-type Tat sequence gradually increases the effective nuclear accumulation of constructs in comparison with Tat<sub>RRR</sub>-GFP

(Fig.3a). Collected recovery curves by FRAP-analysis show that the addition of glycine residues can progressively accelerate the intercompartment mobility of Tat<sub>RRR</sub>-derived mutants (Fig.3b)<sup>2</sup>.

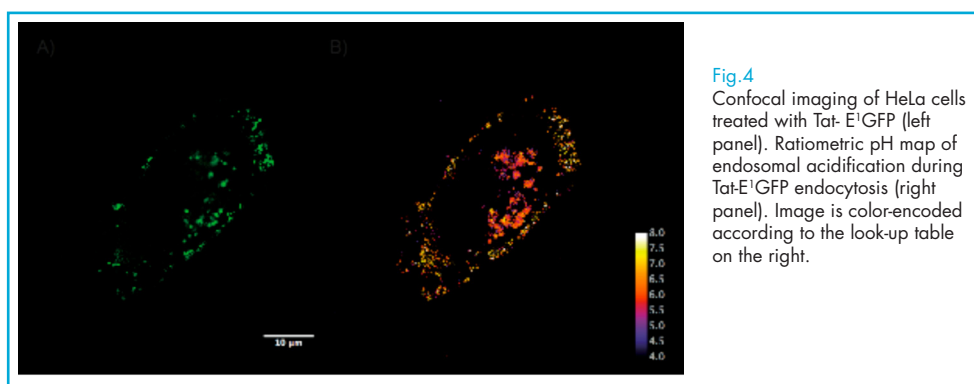
Our data on the intracellular properties of TAT<sub>GGG</sub> confirmed our choice of this mutant as a major candidate for drug/nanoactuators delivery into the nuclear compartment. Indeed, analogously to the wild-type precursor, TAT<sub>GGG</sub> fused



to cargoes molecules were shown to translocate through the cell membranes and internalize within endosomes.

As a first implementation of a Tat-driven nanoreporter we showed the intracellular delivery of a genetically encoded pH-reporter conjugated to Tat protein. E<sup>1</sup>GFP is a pH-sensitive fluorescent protein with a  $pK_a$  close to 6.0 that is suitable for *in vivo* ratiometric emission pH-measurements. By fusing E<sup>1</sup>GFP to Tat sequence we were able to monitor in real time the changes

in vesicles pH starting from its initial cell surface value through the intracellular endocytic network. After 4 hours of internalization we observed that Tat-E<sup>1</sup>GFP accumulated in two subpopulations of endosomes: the first accumulated in bright patches close to the plasma-membrane with a  $\text{pH}$  of  $6.77 \pm 0.13$  and a second population represented by few clusters of vesicles embedded in the cytoplasm with a  $\text{pH}$  value of  $5.78 \pm 0.08$  (Fig.4)<sup>3</sup>



Based on these results a part of our recent research activity was devoted to engineering multifunctionalized nanoactuators endowed with cell-penetrating properties. PAMAM dendrimers represent an exciting new class of macromolecular architecture and they

are very promising tools for therapeutic and diagnostic purposes. Unlike classical polymers, dendrimers have a high degree of molecular uniformity, narrow molecular weight distribution, specific size and shape characteristics, and a highly-functionalized terminal surface. The hyperbranched

architecture of these nanostructures allows us to include: 1) a biocompatible scaffold for functionalization; 2) a vector (i.e. TAT peptides derived thereof) for intracellular

delivery and nuclear targeting of cargoes; 3) a fluorescence sensing-molecule that allows *in vivo* imaging.

#### References

- [1] F. Cardarelli, M. Serresi, R. Bizzarri, M. Giacca, and F. Beltram. *In vivo* studies of HIV-1 Tat Arginine-rich motif unveils its transport characteristics *Mol. Ther.* 15(7), 1313-1322 (2007)
- [2] F. Cardarelli, M. Serresi, R. Bizzarri, and F. Beltram. Tuning the transport properties of HIV-1 Tat arginine-rich motif in living cells *Traffic* 9(4), 528-539 (2008)
- [3] M. Serresi, R. Bizzarri, F. Cardarelli and F. Beltram. Real time measurement of endosomal acidification by a novel genetically encoded biosensor *Anal Bioanal Chem* Feb;393(4):1123-33. Nov 27 Epub 2008 (2009)

This area of research focuses on the study of equilibrium phase diagrams and nonequilibrium dynamics of cold atoms. These systems offer a large degree of tunability and are essentially disorder-free [1]. One can thus address experimentally a number of fundamental questions without having to face the typical complications of solid-state environments. The work reported below has been done in collaboration with several people, including K. Capelle (IFSC, Brazil), M. Cazalilla (CSIC-UPV/EHU, Donostia-San Sebastian, Spain), C. Kollath (Ecole Polytechnique, France), X. Gao (Zhejiang Normal University, China), and G. Vignale (University of Missouri-Columbia, USA).

Marco Polini

m.polini@sns.it

Collaborators

R. Fazio  
D. Rainis  
M. Rizzi  
A. Tomadin  
M.P. Tosi

### Equilibrium phase diagrams

In Ref. [2] we have studied by means of the density-matrix renormalization-group (DMRG) technique a two-component atomic Fermi gas with *attractive* interactions inside a 1D optical lattice. We have demonstrated how this system exhibits phases characterized by atomic-density waves (ADWs), and we have shown how the existence of ADWs can be detected by measuring the light-scattering diffraction pattern. In Ref. [3] we

have studied a similar system, but in the presence of a finite spin polarization. By means of the DMRG we have computed the pairing correlations in the whole range from weak to strong coupling. We have demonstrated that pairing correlations exhibit quasi-long range order and oscillations at the wave number expected from the Fulde-Ferrell-Larkin-Ovchinnikov (FFLO) theory and we have shown that charge and spin degrees of freedom are coupled already for small spin polarization.

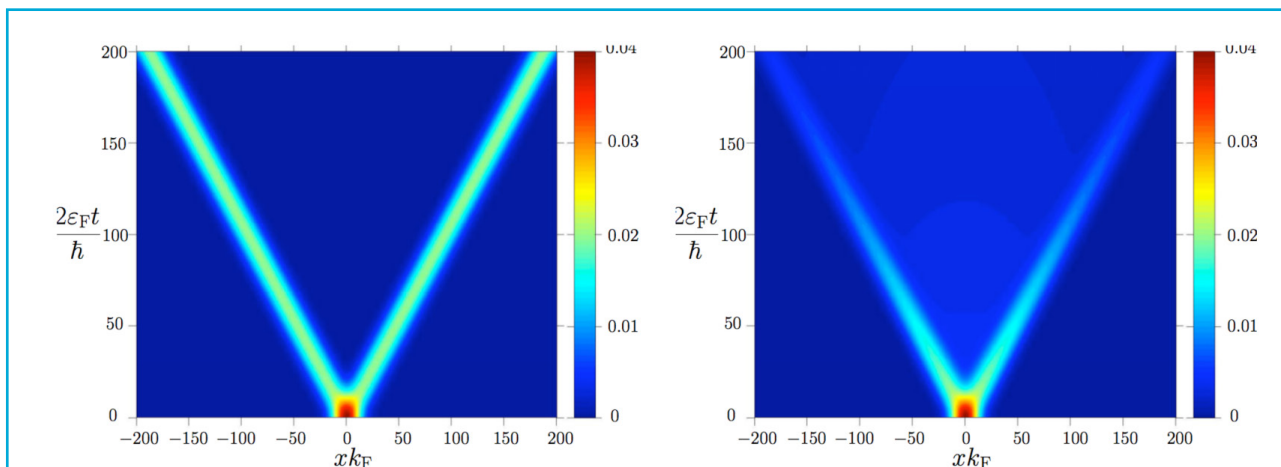


Fig. 1

(Left panel) Space-time evolution of a spin packet in the ballistic limit (no spin-drag). The left and right components of the packet propagate at the Fermi velocity and their width does not change. (Right panel) Same as in the left panel but in the presence of a finite spin-drag relaxation time [4]. Notice the spreading and attenuation of the packet as time progresses.

### Non-equilibrium dynamics

Low-energy spin and charge excitations of 1D interacting fermions are completely decoupled and propagate with different velocities. These modes however can decay due to several possible mecha-

nisms. In Ref. [4] we have exposed a new facet of spin-charge separation: not only the speeds but also the damping rates of spin and charge excitations are different. While the propagation of long-wavelength charge excitations is essentially ballistic, spin propagation is

intrinsically damped and diffusive (see Fig. 1). We have also suggested that cold Fermi gases trapped inside a tight atomic waveguide offer the unique opportunity to measure the spin-drag relaxation rate that controls the broadening of a spin packet.

In Ref. [5] we have presented detailed investigations of the nonequilibrium dynamics of spin-polarized cold Fermi gases following a sudden switching-on of the atom-atom pairing coupling strength. Within a time-dependent mean-field approach we have shown that on increasing the imbalance it takes longer for pairing to develop, the period of the nonlinear oscillations lengthens, and the maximum value of the pairing amplitude decreases. As expected, dynamical pair-

ing is suppressed by the increase of the imbalance. Eventually, for a critical value of the imbalance the nonlinear oscillations do not even develop. Finally, we have pointed out an interesting temperature-reentrant behavior of the exponent characterizing the initial instability (see Fig. 2).

Finally, in Ref. [6] we have presented a fully-microscopic theory to study the dynamics in 1D cold Fermi gas following a quench. Our approach, which is based on time-dependent current-density-functional theory, is applicable well beyond the linear-response regime and produces both spin-charge separation and spin-drag-induced broadening of the spin packets (see Fig. 3).

Fig. 2

(Left panel) The instability exponent as a function of spin-polarization and reduced temperature [5]. A finite instability exponent implies the development of pairing. A re-entrant region is clearly visible. (Right panel) Time-evolution of the distribution of condensed particles. As time evolves it pulses in synchronism with the nonlinear oscillations of the pairing function [5].

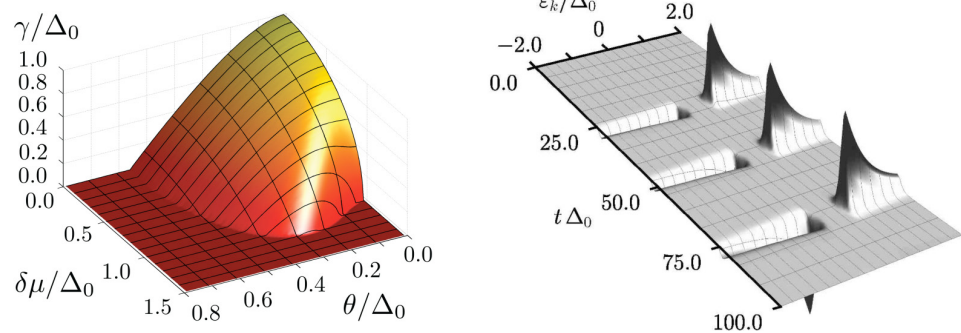
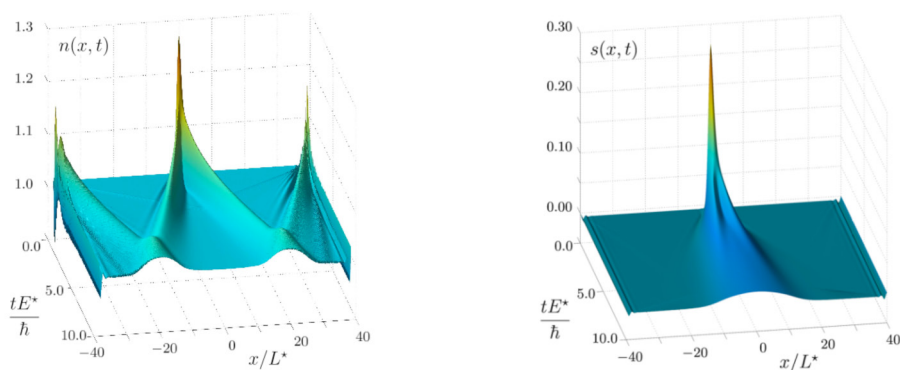


Fig. 3

(Left panel) A 3D plot of the space-time evolution of a density packet after a local quench [6]. Note that already at short times some density waves appear, coming from the sharp edges of the waveguide (Friedel oscillations): at larger time they mix with the original packet. (Right panel) Same as in the left panel but for a spin packet. We clearly see how the propagation in the spin channel is essentially diffusive [4,6].



#### References

- [1] For a recent review see I. Bloch, J. Dalibard, and W. Zwerger, *Rev. Mod. Phys.* 80, 885 (2008).
- [2] X.-L. Gao *et al.*, *Phys. Rev. Lett.* 98, 030404 (2007).
- [3] M. Rizzi *et al.*, *Phys. Rev. B* 77, 245105 (2008).
- [4] M. Polini and G. Vignale, *Phys. Rev. Lett.* 98, 266403 (2007); D. Rainis *et al.*, *Phys. Rev. B* 77, 035113 (2008).
- [5] A. Tomadin *et al.*, *Phys. Rev. A* 77, 033605 (2008).
- [6] X.-L. Gao *et al.*, *Phys. Rev. Lett.* 101, 206402 (2008); W. Li *et al.*, *Phys. Rev. B* 78, 195109 (2008).

## New experimental techniques

Differential Near Field Scanning Optical Microscope (DNSOM)	101
Growth of semiconductor nanowires	103



## Differential Near Field Scanning Optical Microscope (DNSOM)

Recently, Ozcan and coworkers demonstrated in the visible wavelength range the principle of a new type near field microscopy termed differential Near Field Scanning Optical Microscopy (DNSOM)<sup>1</sup>. It involves scanning a relatively large rectangular aperture in the near-field of an object and recording detected power as a function of the scanning position. The image reconstruction is achieved by taking a two-dimensional derivative of the recorded power map. Unlike conventional NSOM, the size of the rectangular aperture does not determine the resolution in DNSOM; instead, the resolution is practically

determined by the sharpness of the corners of the rectangular aperture.

In our lab we implemented the first DNSOM set-up in medium infrared and THz regime, employing for the first time in near field microscopy a quantum cascade laser as a THz source.

In Fig. 1(a) we show the DNSOM experimental setup together with a schematic picture of the system configuration adopted (Fig. 1(b)) while in Fig. 1(c) we report the visible image of a test metallic square (30  $\mu\text{m}$  side) aligned within a 100  $\mu\text{m}$  side squared metallic aperture.

Fabio Beltram  
Riccardo Degl'Innocenti  
Vincenzo Piazza  
Pasqualantonio Pingue  
Alessandro Tredicucci

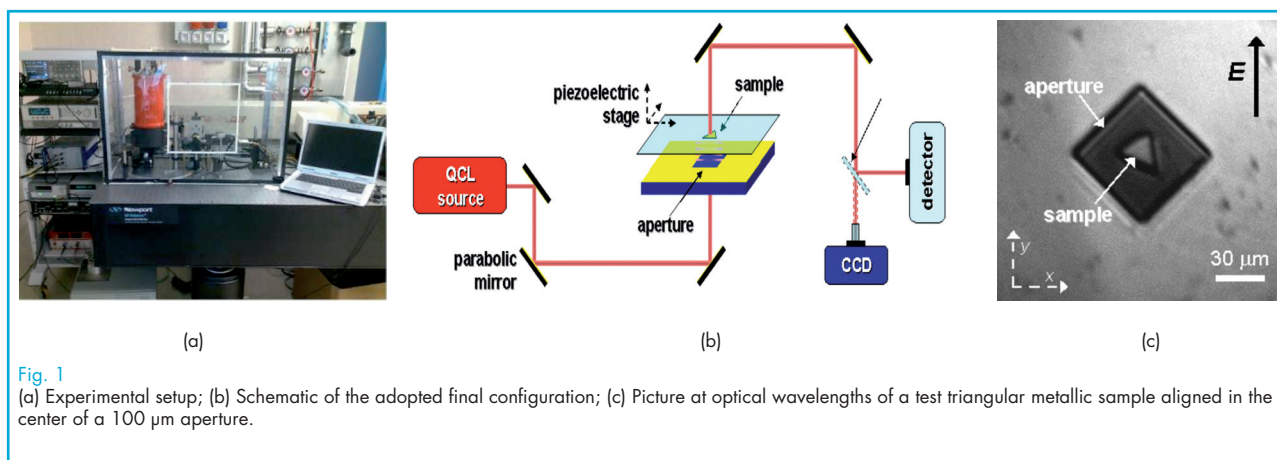
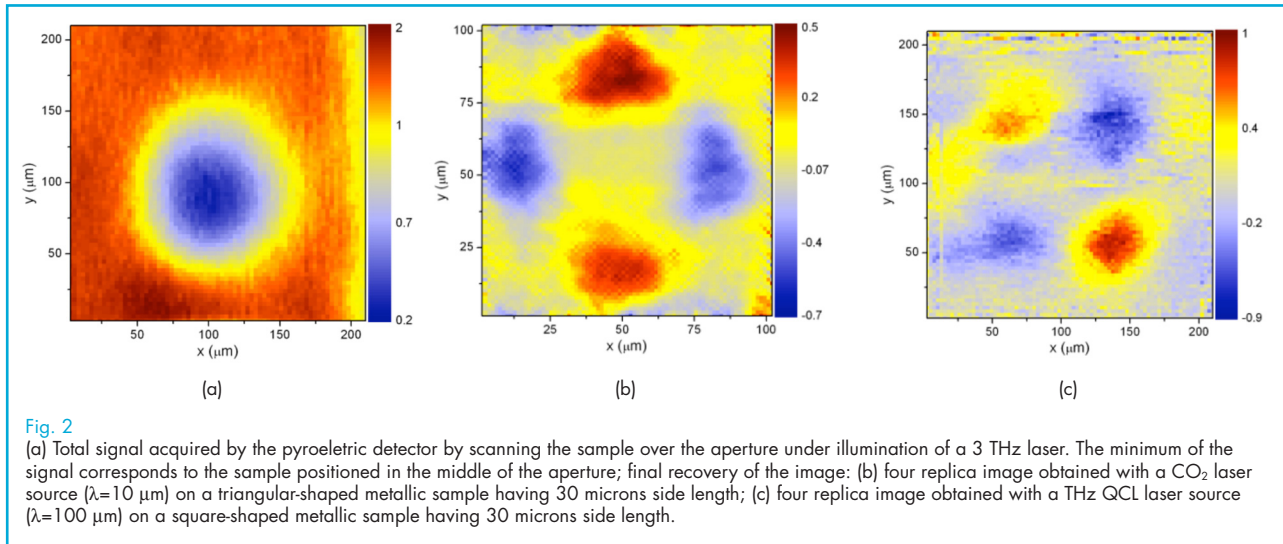


Fig. 1 (a) Experimental setup; (b) Schematic of the adopted final configuration; (c) Picture at optical wavelengths of a test triangular metallic sample aligned in the center of a 100  $\mu\text{m}$  aperture.

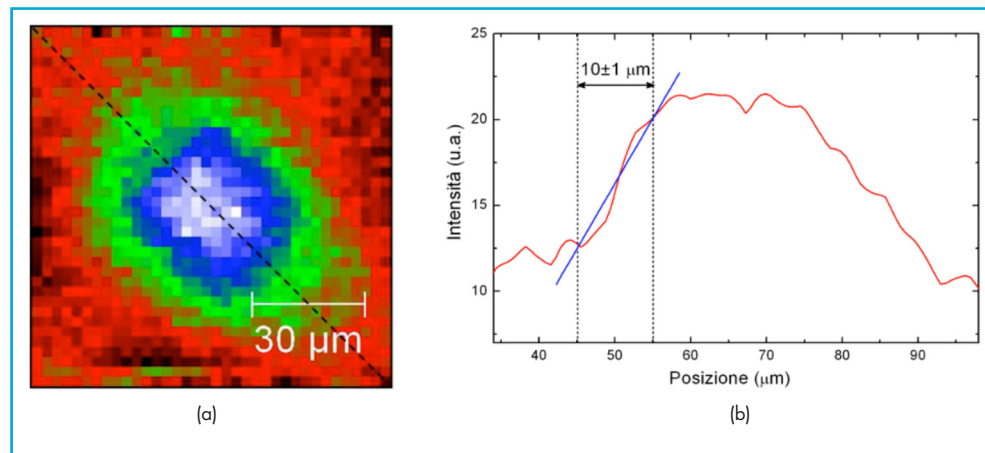
The typical corresponding spatially resolved signal acquired scanning the sample over the aperture is reported in Fig. 2(a). In order to recover the image of the sample, one has to perform the second derivative  $\partial^2/\partial x\partial y$  of the total

signal, obtaining in this way four replica of the imaged sample. Some experimental results on metallic patterns are shown in Fig. 2(b) when a  $\text{CO}_2$  laser was employed as source and in Fig. 2(c) in the case of a THz QCL radiation.

<sup>1</sup> Aydogan Ozcan, Ertugrul Cubukcu, Alberto Bilenca, Kenneth B. Crozier, Brett E. Bouma, Federico Capasso, and Guillermo J. Tearney, *Nano Lett.*, 2006, 6 (11), pp 2609–2616.



**Fig. 3**  
 (a) Same picture as in Fig. 2(c), bottom right corner; (b) analysis of the intensity profile along the dashed line of (a).



Actually, the experimental resolution achievable with the system is about  $10\ \mu\text{m}$  for 3 THz light [1], corresponding to  $\sim \lambda/10$ , as exemplified in Fig. 3. Some tests on biological sample as patterned DNA and cells are under way.

Major improvements will be pursued in the future using a different detector (cooled bolometer), decreasing the aperture/sample distance and increasing the average power of the laser source (using a high-power, ultra-low-vibration closed-cycle cryostat).

#### References

- [1] R. Degl'Innocenti, M. Montinaro, J. Xu, V. Piazza, P. Pingue, A. Tredicucci, F. Beltram, H.E. Beere, D.A. Ritchie, Differential Near-Field Scanning Optical Microscopy with THz quantum cascade laser sources, OPTICS EXPRESS Vol. 17, No. 26, pag. 23785 (2009).

## Growth of semiconductor nanowires

A Riber Compact-21 CBE system was recently installed in the NEST laboratory. This system is equipped with 3 injectors: one each for the group III elements (In, Ga) given by trimethylindium (TMIn) and triethylgallium (TEGa), one each for the

group V elements given by tributylarsenic (TBAs) and tributylphosphur (TBP), and one for sources such as tributylselenium (TBSe) for n-doping of the nanowires and trisdimethylaminoantimony (TDMASb) for InSb nanowires growth.

Daniele Ercolani  
Ang Li  
Lorenzo Lugani  
Lucia Sorba

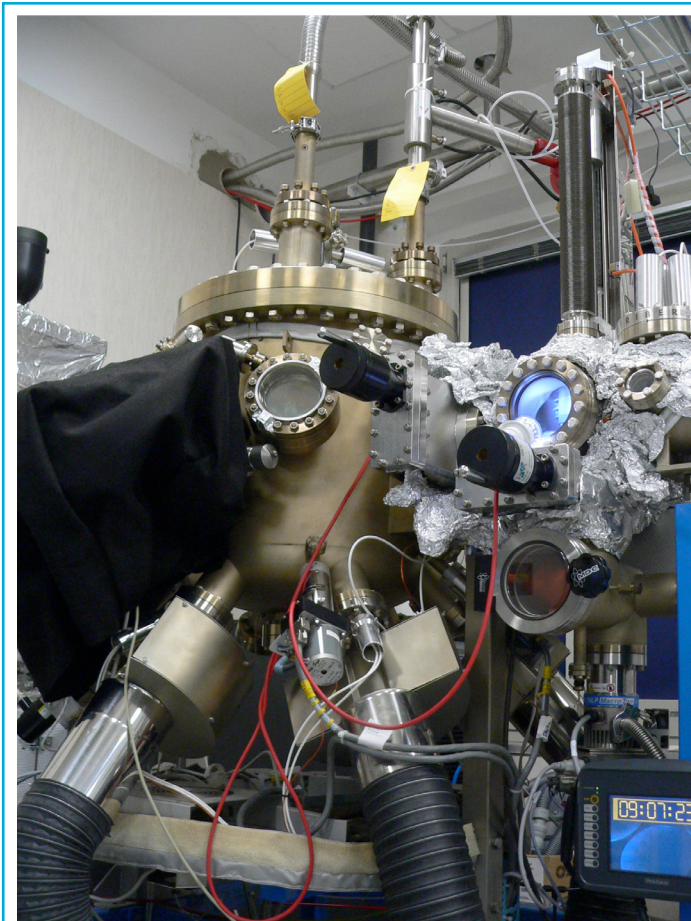
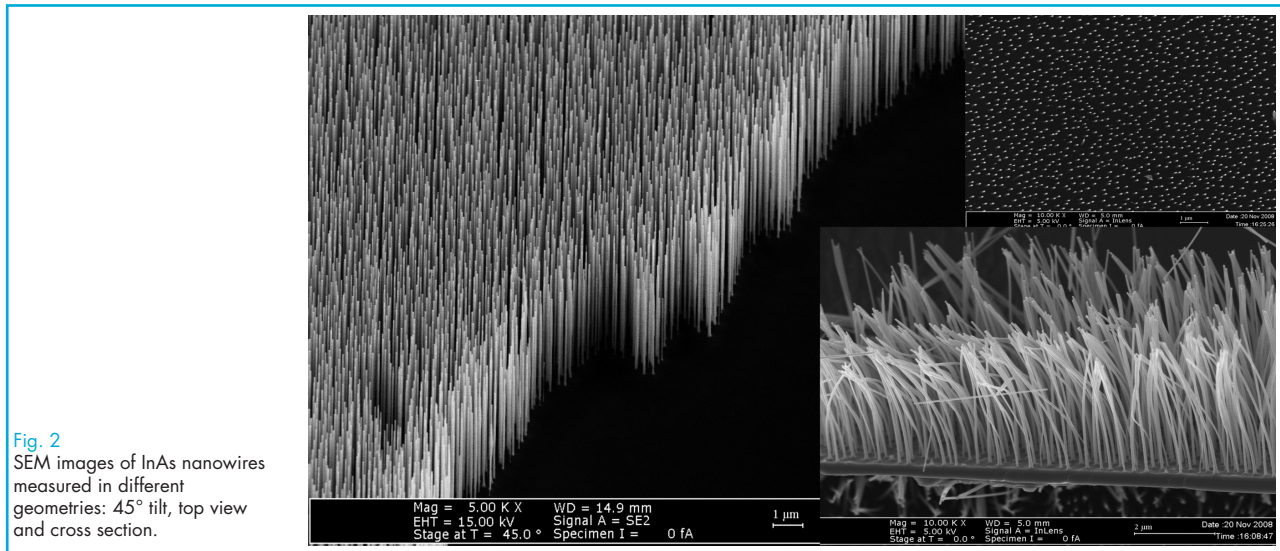


Fig. 1  
Photograph of the CBE growth chamber at NEST laboratory

The synthesis of InAs nanowires is realized through a bottom-up approach based on the catalysis from metallic particles [1]. The liquid alloy with the substrate material is generally obtained through metal nanoparticles (in general gold), as shown in Fig. 2. Using the CBE technique, on InAs(111)B substrates we have synthesized InAs nanowires of diameters ranging from 10 to 100 nm, with lengths of several microns and a precision in their lateral dimensions

comparable to fluctuations of a single atomic plane (see Fig. 2). Furthermore, axial and radial heterostructure InAs-InP nanowires have been synthesized with elevated crystalline quality and with variable layer thickness. Due to the very peculiar properties such as low bandgap, high Landé g-factor, small effective mass and high thermopower we are also carrying out a research activity focused on the growth of InSb-InAs nanowire heterostructures.



Furthermore, part of the research activity is focusing on the integration of semiconductor nanowires in functional superconductor devices. In particular, we aim at the investigation of the Josephson junctions based on III-V nanowires coupled to superconducting leads. The Josephson coupling will be studied both in equilibrium and non-equilibrium conditions. The latter regime will be accomplished thanks to multi terminal devices (see Fig.3) where some of the contact electrodes will be used as current injectors while others

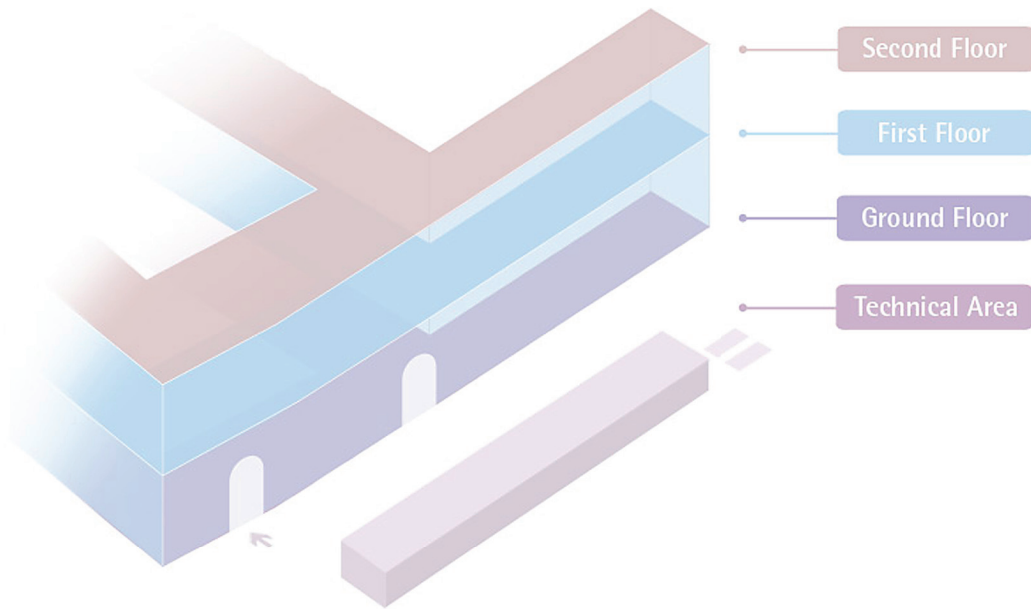
will allow the detection of changes in the superconductive properties of the proximized nanowire. Andreev physics will be more in general studied as a function of the interface quality in superconductor-nanowire mesoscopic structures realized using different semiconductor (InAs, InSb) and superconductor (Al, Ti, V) materials. We acknowledge financial support from Monte dei Paschi di Siena with the project "Implementazione del laboratorio di crescita dedicato alla sintesi di nanofili a semiconduttore".

**Fig. 3**  
SEM image of an InAs nanowire connected to four Ti/Al superconductor nanofingers. The gap between consecutive electrodes is about 50 nm.

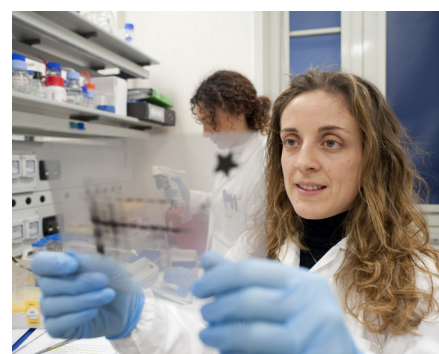


## NEST facilities



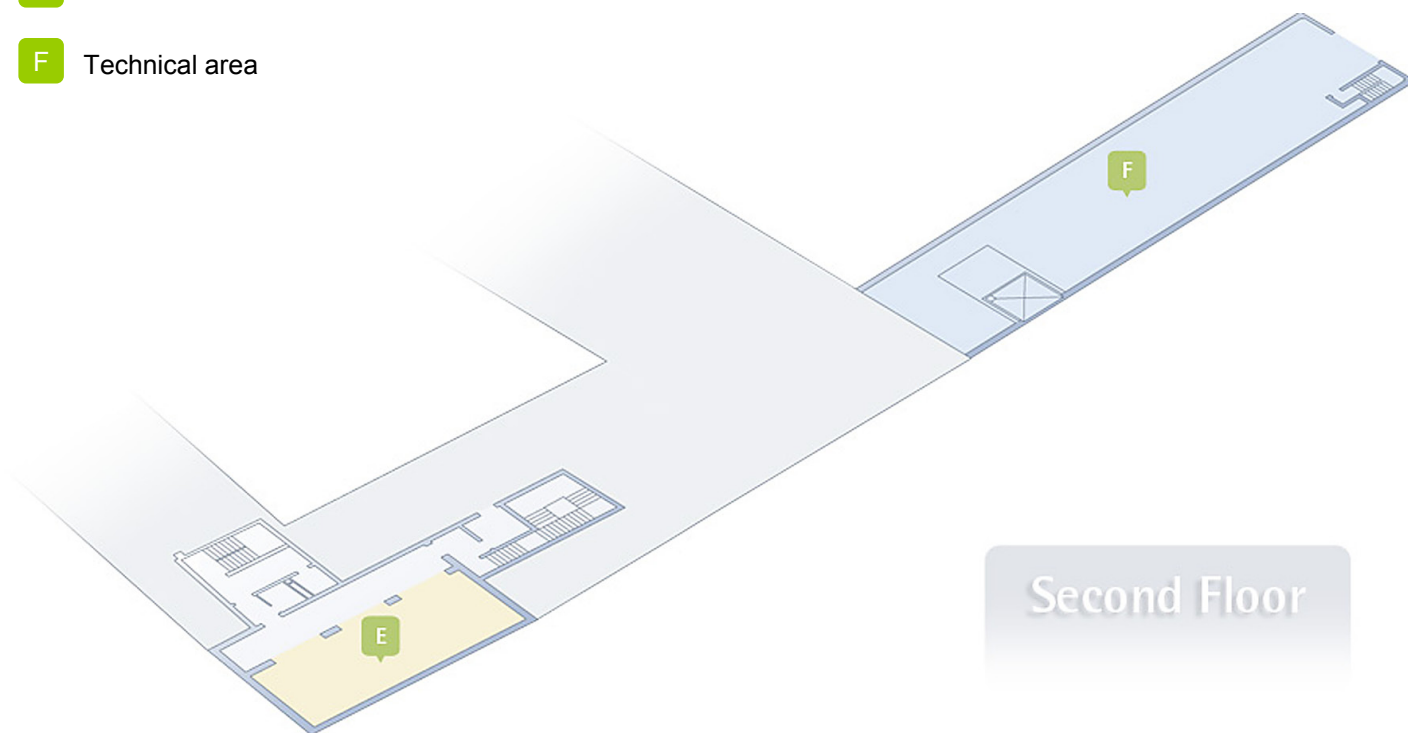


- 1.1** Clean Room Facility
- 1.2** Wedge bonding
- 1.3** Spatially-resolved Raman and two-photon microscopy
- 1.4** MIR and Ultrafast spectroscopy
- 1.5** Confocal Microscopy
- 1.6** THz Quantum Cascade Lasers and DNSOM
- 1.7** Nuclear Magnetic Resonance
- 1.8** BSL2 Facility
- 1.9** Synthesis Facility
- 1.10** Hot Room
- 1.11** Tissue Culture
- 1.12** Bio Chemistry and Molecular Biology
- 1.13** Technical Bio Services
- 1.14** Lab-on-a-chip Technology
- 1.15** In vivo Two Photon Imaging



E Offices

F Technical area





## Publications



## Publications

### 2009

- G. Papari, F. Carillo, D. Born, L. Bartoloni, E. Gambale, D. Stornaiuolo, P. Pingue, F. Beltram, F. Tafuri, *YBCO Nanobridges: Simplified Fabrication Process by Using a Ti Hard Mask*, *Applied Superconductivity* 19, 183-186 (2009)
- S. Montangero, D. Frustaglia, T. Calarco, R. Fazio, *Quantum billiards in optical lattices*, *EuroPhys. Lett.* 88, 30006 (2009)
- S. Safaei, S. Montangero, F. Taddei, R. Fazio, *Optimized single-qubit gates for Josephson phase qubits*, *Phys. Rev. B* 79, 064524 (2009)
- S. Pugnetti, Y.M. Blanter, F. Dolcini, R. Fazio, *Detection of Tiny Mechanical Motion by Means of the Ratchet Effect*, *Phys. Rev. B* 79, 174516 (2009)
- V. Giovannetti, D. Burgarth, S. Mancini, *Communication Through a Quantum Link*, *Phys. Rev. A* 79, 012311 (2009)
- V. Giovannetti, S. Lloyd, L. Maccone, J.H. Shapiro, *Sub-Rayleigh Quantum Imaging*, *Phys. Rev. A* 79, 013827 (2009)
- T. Tufarelli and V. Giovannetti, *High fidelity state transfer in binary tree networks*, *Phys. Rev. A* 79, 022313 (2009)
- V. Giovannetti, S. Montangero, M. Rizzi, R. Fazio, *Homogeneous MERA states: an information theoretical analysis*, *Phys. Rev. A* 79, 052314 (2009)
- D. Patanè, A. Silva, L. Amico, R. Fazio, G. E. Santoro, *Adiabatic dynamics of a quantum critical system coupled to an environment: Scaling and kinetic equation approaches*, *Phys. Rev. B* 80, 024302 (2009)
- S. Montangero, M. Rizzi, V. Giovannetti, R. Fazio, *Critical exponents of one-dimensional quantum critical models by means of MERA tensor network*, *Phys. Rev. B* 80, 113103 (2009)
- K. Yuasa, D. Burgarth, V. Giovannetti, H. Nakazato, *Efficient generation of a maximally entangled state by repeated on- and off-resonant scattering of ancilla qubits*, *New J. Phys.* 11, 123027 (2009)
- S. Montangero, R. Fazio, P. Zoller, G. Pupillo, *Dipole oscillations of confined lattice bosons in one dimension* *Phys. Rev. A* 79, 041602(R) (2009)
- H. Lignier, A. Zenesini, D. Ciampini, O. Morsch, E. Arimondo, S. Montangero, G. Pupillo, R. Fazio, *Trap modulation spectroscopy of the Mott-insulator transition in optical lattices*, *Phys. Rev. A* 79, 041601(R) (2009)
- D. Burgarth, S. Bose, C. Bruder, V. Giovannetti, *Local controllability of quantum networks*, *Phys. Rev. A* 79, 060305(R) (2009)
- F. De Martini, V. Giovannetti, S. Lloyd, L. Maccone, E. Nagali, L. Sansoni, F. Sciarrino, *Experimental Quantum Private Queries with linear optics* *Phys. Rev. A* 80, 010302(R) (2009)
- T. Caneva, M. Murphy, T. Calarco, R. Fazio, S. Montangero, V. Giovannetti, G. E. Santoro, *Optimal Control at the Quantum Speed Limit*, *Phys. Rev. Lett.* 103, 240501 (2009)
- D. Gerace, H. E. Tureci, A. Imamoglu, V. Giovannetti and R. Fazio, *The quantum optical Josephson interferometer*, *Nature Physics* 5, 281 (2009)
- E.V. Deviatov, B. Marquardt, A. Lorke, G. Biasiol, L. Sorba, *Interference effects in transport across a single incompressible strip at the edge of the fractional quantum Hall System*, *Phys. Rev. B* 79, 125312 (2009)
- B. Karmakar, V. Pellegrini, A. Pinczuk, L.N. Pfeiffer, K.W. West, *Quantum phase transition of a quantum Hall excitonic state in electron bilayers*, *International Journal of modern physics B* 23, 2607 (2009)
- M. Gibertini, A. Singha, V. Pellegrini, M. Polini, G. Vignale, A. Pinczuk, L. N. Pfeiffer, K. W. West, *Engineering artificial graphene in a two-dimensional electron gas*, *Phys. Rev. B* 79, 241406 (2009)
- B. Karmakar, V. Pellegrini, A. Pinczuk, L.N. Pfeiffer, K. W. West, *First-Order Quantum Phase Transition of Excitons in Quantum Hall Bilayers*, *Phys. Rev. Lett.* 102, 036802 (2009)
- A. Singha, V. Pellegrini, S. Kalliakos et al, *Optical anisotropy of electronic excitations in elliptical quantum dots*, *Appl. Phys. Lett.* 94, 073114 (2009)
- S. Roddaro, N. Paradiso, V. Pellegrini, G. Biasiol, L. Sorba, F. Beltram, *Tuning nonlinear charge transport between integer and fractional quantum Hall states*, *Phys. Rev. Lett.* 103, 016802 (2009)
- S. Kalliakos, M. Rontani, V. Pellegrini, A. Pinczuk, A. Singha, C.P. Garcia, G. Goldoni, E. Molinari, L. N. Pfeiffer, K. W. West, *Probing collective modes of correlated states of few electrons in semiconductor quantum dots*, *Solid State Communications*, 149, 1436 (2009)
- B. Karmakar, V. Pellegrini, A. Pinczuk, L. N. Pfeiffer, K. W. West, *Evidence of interlayer correlation in spin excitations of quantum Hall bilayers with negligible tunnelling*, *Phys. Rev. B Rapid Comm* 80, 241312 (2009)

- L. Mahler, A. Tredicucci, F. Beltram, C. Walther, J. Faist, B. Witzigmann, H.E. Beere, D.A. Ritchie, *Vertically emitting microdisk lasers*, Nature Photon. 3, 46 (2009)
- G. Günter, A. A. Anappara, J. Hees, A. Sell, G. Biasiol, L. Sorba, S. De Liberato, C. Ciuti, A. Tredicucci, A. Leitenstorfer, R. Huber, *Sub-cycle switch-on of ultrastrong light-matter interaction*, Nature 458, 178 (2009)
- L. Mahler, A. Tredicucci, F. Beltram, C. Walther, H.E. Beere, D.A. Ritchie, *Finite size effects in surface emitting Terahertz quantum cascade lasers*, Opt. Express 17, 6703 (2009)
- A.A. Anappara, S. De Liberato, A. Tredicucci, C. Ciuti, G. Biasiol, L. Sorba, F. Beltram, *Signatures of the ultrastrong light-matter coupling regime*, Phys. Rev. B 79, 201303(R) (2009)
- L. Mahler, M.I. Amanti, C. Walther, A. Tredicucci, F. Beltram, J. Faist, H.E. Beere, D.A. Ritchie, *Distributed feedback ring resonators for vertically emitting terahertz quantum cascade lasers*, Opt. Express 17, 13031 (2009)
- R.P. Green, A. Tredicucci, N.Q. Vinh, B. Murdin, C. Pidgeon, H.E. Beere, D.A. Ritchie, *Gain recovery dynamics of a terahertz quantum cascade laser*, Phys. Rev. B 80, 075303 (2009)
- U. Willer, A. Pohlkötter, W. Schade, J. Xu, T. Losco, R. P. Green, A. Tredicucci, H.E. Beere, D.A. Ritchie, *Resonant tuning fork detector for THz radiation*, Opt. Express 17, 14069 (2009)
- A. Tredicucci, *Quantum dots: long life in zero dimensions*, Nature Mater. 8, 775 (2009)
- J. M. Hensley, J. Montoya, M. G. Allen, J. Xu, L. Mahler, A. Tredicucci, H. E. Beere, D. A. Ritchie, *Spectral behavior of a terahertz quantum-cascade laser*, Opt. Express 17, 20476 (2009)
- A. Tredicucci and A. Di Carlo, *Terahertz Technology: An ultrafast amplifier*, Nature Photon. 3, 681 (2009)
- S. Cibella, M. Ortolani, R. Leoni, G. Torrioli, L. Mahler, J.H. Xu, A. Tredicucci, H.E. Beere, D.A. Ritchie, *Wide dynamic range terahertz detector pixel for active spectroscopic imaging with quantum cascade lasers*, Appl. Phys. Lett. 95, 213501 (2009)
- R. Degl'Innocenti, M. Montinaro, J. Xu, V. Piazza, P. Pingue, A. Tredicucci, F. Beltram, H. E. Beere, D. A. Ritchie, *Differential Near-Field Scanning Optical Microscopy with THz quantum cascade laser sources*, Opt. Express 17, 23785 (2009)
- V. Baranwal, G. Biasiol, S. Heun, A. Locatelli, T. O. Montes, M. N. Orti, L. Sorba, *Kinetics of the evolution of InAs/GaAs quantum dots to quantum rings: A combined x-ray, atomic force microscopy, and photoluminescence study*, Phys. Rev. B 80, 155328 (2009)
- S. Roddaro, P. Caroff, G. Biasiol, F. Rossi, C. Bocchi, K. Nilsson, L. Fröberg, J.B. Wagner, L. Samuelson, L.E. Wernersson, L. Sorba, *Growth of vertical InAs nanowires on heterostructured substrates*, Nanotech 20, 285393 (2009)
- D. Ercolani, F. Rossi, A. Li, S. Roddaro, V. Grillo, G. Salvati, F. Beltram, L. Sorba, *InAs/InSb nanowire heterostructures grown by chemical beam epitaxy*, Nanotech. 20, 505605 (2009)
- S. Roddaro, N. Paradiso, V. Pellegrini, G. Biasiol, L. Sorba, F. Beltram, *Tuning Nonlinear Charge Transport between Integer and Fractional Quantum Hall States*, Phys. Rev. Lett. 103, 016802 (2009)
- A. Tagliacozzo, F. Tafuri, E. Gambale, B.Jouault, D.Born, P.Lucignano, D. Stornaiuolo, F.Lombardi, A. Barone, B.L. Altshuler, *Mesoscopic conductance fluctuations in YBCO grain boundary Junction at low temperature*, Phys. Rev. B 79, 024501 (2009)
- T. Bhuvana, L. Gregoratti, S. Heun, M. Dalmiglio, G. U. Kulkarni, *Electron resist behaviour of Pd hexadecanethiolate examined using x-ray photoelectron spectroscopy with nanometric lateral resolution*, Langmuir 25, 1259-1264 (2009)
- G. Biasiol, R. Magri, S. Heun, A. Locatelli, T. O. Montes, L. Sorba, *Surface compositional mapping of self-assembled InAs/GaAs quantum rings*, J. Crystal Growth 311, 1764-1766 (2009)
- A. Ferrari, M. Cecchini, R. Degl'Innocenti, F. Beltram, *Directional PC12 Cell Migration along Plastic Nanotracks*, IEEE Transaction on biomedical Engineering, Letters Vol.56, No.11, 2692-2696 (2009)
- F. Cardarelli, R. Bizzarri, M. Serresi, L. Albertazzi, F. Beltram, *Probing nuclear localization signal-importin alpha binding equilibria in living cells*, J Biol Chem. 2009 Dec 25, 284(52):36638-46, Epub 2009 Oct 26 (2009)
- L. Comelli, L. Marchetti, D. Arosio, S. Riva, G. Abdurashidova, F. Beltram, A. Falaschi, *The homeotic protein HOXC13 is a member of human DNA replication complexes*, Cell Cycle 2009 8:3, 1-6; 1 February.
- B. Baragatti, M. Laniado-Schwartzman, D. Angeloni, F. Scebba, E. Ciofini, D. Sodini, V. Ottaviano, S. Nencioni, A. Paolicchi, J. P. Graves, D. C. Zeldin, K. H. Gotlinger, S. Luin, F. Cocceani, *EDHF function in the ductus arteriosus: evidence against involvement of epoxyeicosatrienoic acids (EETs) and 12S-hydroxyeicosatetraenoic (12S-HETE)*, Am. J. Physiol. Heart Circ. Physiol. 297(6), H2161-8 (2009). Doi:10.1152/ajpheart.00576.2009
- A. Di Fenza, W. Rocchia, V. Tozzini, *Complexes of HIV-1 integrase with HAT proteins: Multiscale models, dynamics, and hypotheses on allosteric sites of inhibition*, Proteins, 76(4), 946-958 (2009)

- S. Bonella, W. Rocchia, P. Amat, R. Nifosì and V. Tozzini, *SDPhound, a Mutual Information-Based Method to Investigate Specificity-Determining Positions*, Algorithms, 2, 764-789 (2009)
- L. Salassa, C. Garino, G. Salassa, C. Nervi, R. Gobetto, C. Lamberti, D. Gianolio, R. Bizzarri, P.J. Sadler, *Ligand-Selective Photodissociation from [Ru(bpy)(4AP)(4)](2+): a Spectroscopic and Computational Study*, Inorg. Chem. 48(4), 1469-1481 (2009)
- E. Alpi, E. Landi, M. Barilari, M. Serresi, P. Salvadori, A. Bachi, L. Dente, *Channel-interacting PDZ protein "CIPP" interacts with proteins involved in cytoskeletal dynamics*, Biochem J, Apr 15, 419(2), 289-300 (2009)
- S. Luin, V. Voliani, G. Lanza, R. Bizzarri, R. Nifosì, P. Amat, V. Tozzini, M. Serresi, F. Beltram, *Raman Study of chromophore states in photochromic intrinsically fluorescent proteins*, J Am Chem Soc. Jan 14, 131(1), 96-103 (2009). Doi: 10.1021/ja804504b
- M. Serresi, R. Bizzarri, F. Cardarelli, F. Beltram, *Real-time measurement of endosomal acidification by a novel genetically encoded biosensor*, Anal Bioanal Chem. 393(4): 1123-1133 (2009)
- R. Bizzarri, M. Serresi, S. Luin, F. Beltram, *Green fluorescent Protein-based pH indicator for in vivo use: a review*, Anal Bioanal Chem. 393(4), 1107-1122 (2009)
- H. Rabani, F. Taddei, F. Giazotto, R. Fazio, *Influence of interface transmissivity and inelastic scattering on the electronic entropy and specific heat of diffusive SNS Josephson junctions*, J. App. Phys. 105, 093904 (2009)
- S. Pugnetti, F. Dolcini, D. Bercioux, H. Grabert, *Electron tunneling into a quantum wire in the Fabry-Perot regime*, Phys. Rev. B 79, 035121 (2009)
- F. Dolcini and F. Giazotto, *Adiabatic Magnetization of Superconductors as a High-Performance Cooling Mechanism*, Phys. Rev B 80, 024503 (2009)
- K. Yuasa, P. Facchi, R. Fazio, H. Nakazato, I. Ohba, S. Pascazio, S. Tasaki, *Nonlocality of Field-Emitted Electrons from a Superconductor*, Phys. Rev. B 79, 180503 (R) (2009)
- G. Borghi, M. Polini, R. Asgari, A.H. MacDonald, *Dynamical response functions and collective modes of bilayer grapheme*, Phys. Rev. B 80, 241402 (R) (2009)
- M. Polini and G. Vignale, *Spins in cold atoms - what a drag!* Physics 2, 87 (2009)
- A. Principi, M. Polini and G. Vignale, *Linear response of doped graphene sheets to vector potentials*, Phys. Rev. B 80, 075418 (2009)
- D. Rainis, F. Taddei, F. Dolcini, M. Polini, R. Fazio, *Andreev reflection in graphene nanoribbons*, Phys. Rev. B 79, 115131 (2009)
- M.R. Ramezani, M.M. Vazifeh, R. Asgari, M.R. Rahimi Tabar, M. Polini, A.H. MacDonald, *Finite-temperature screening and the specific heat of doped graphene sheets*, J. Phys. A: Math. Theor. 42, 214015 (2009)
- G. Borghi, M. Polini, R. Asgari, A.H. MacDonald, *Fermi velocity enhancement in monolayer and bilayer graphene*, Solid State Commun. 149, 1117 (2009)
- M. Gibertini, A. Singha, V. Pellegrini, M. Polini, G. Vignale, A. Pinczuk, L.N. Pfeiffer, K.W. West, *Engineering artificial graphene in a two-dimensional electron gas*, Phys. Rev. B 79 241406(R) (2009)

## 2008

- S. Roddaro, *Trasporto in nanofili di semiconduttore*, Nuovo Saggiatore 24, 28 (2008)
- O. Karlström, A. Wacker, K. Nilsson, G. Astromskas, S. Roddaro, L. Samuelson, L.E. Wernersson, *Analysing the capacitance-voltage measurements of vertical wrapped-gated nanowires*, Nanotech 19, 435201 (2008)
- S. Roddaro, K. Nilsson, G. Astromskas, L. Samuelson, L.E. Wernersson, O. Karlström, A. Wacker, *InAs nanowires metal-oxide-semiconductor capacitors*, Appl. Phys. Lett. 92, 253509 (2008)
- S. Roddaro, A. Fuhrer, P. Brusheim, C. Fasth, H.Q. Xu, L. Samuelson, X. J., C. M. Lieber, *Spin States of Holes in Ge/Si Nanowire Quantum Dots*, Phys. Rev. Lett. 101, 186802 (2008)
- P. Gallo, M. Felici, B. Dwir, K. A. Atlasov, K.F. Karlsson, A. Rudra, A. Mohan, G. Biasiol, L. Sorba, E. Kapon, *Integration of Site-Controlled Pyramidal Quantum Dots and Photonic Crystal Membrane Cavities*, Appl. Phys. Lett. 92, 263101 (2008)
- F. Carillo, D. Born, V. Pellegrini, F. Tafuri, G. Biasiol, L. Sorba, F. Beltram, *Relevant energy scale in hybrid mesoscopic Josephson junctions*, Phys. Rev. B 78, 052506 (2008)
- G. Bimonte, D. Born, E. Calloni, G. Esposito, U. Huebner, E. Il'ichev, L. Rosa, F. Tafuri, R. Vaglio, *Low noise cryogenic system for the measurement of the Casimir energy in rigid cavities*, J. Phys. A: Math. Theor. 41, 164023 (2008)
- R. Fittipaldi, A. Vecchione, R. Ciancio, S. Pace, M. Cuoco, D. Stornaiuolo, D. Born, F. Tafuri, E. Olsson, S. Kittaka, H. Yaguchi, Y. Maeno, *Superconductivity in Sr(2)RuO(4)-Sr(3)Ru(2)O(7) eutectic crystals*, Europhys. Lett. 83, 27007 (2008)
- D. Stornaiuolo, E. Gambale, T. Bauch, D. Born, K. Cedergren, D. Dalena, A. Barone, A. Tagliacozzo, F. Lombardi, F. Tafuri, *Underlying physical aspects of fluctuations in YBa2Cu3O7-d grain boundary Josephson junctions*, Physica C 468, 310 (2008)
- F. Tafuri, A. Tagliacozzo, D. Born, D. Stornaiuolo, E. Gambale, D. Dalena, P. Lucignano, B. Jouault, F. Lombardi, A. Barone, B.L. Altshuler, *Coherent quasiparticle transport in grain boundary junctions employing high-Tc superconductors*, Microelectronics Journal 39, 1066 (2008)
- L. Amico, R. Fazio, A. Osterloh, V. Vedral, *Entanglement in Many-Body Systems*, Rev. Mod. Phys. 80, 517 (2008)
- V. Giovannetti, S. Lloyd, L. Maccone, *Quantum Private Queries*, Phys. Rev. Lett. 100, 230502 (2008)
- V. Giovannetti, S. Lloyd, L. Maccone, *Quantum Random Access Memory*, Phys. Rev. Lett. 100, 160501 (2008)
- V. Giovannetti, S. Montangero, R. Fazio, *Quantum MERA channels*, Phys. Rev. Lett. 101, 180503 (2008)
- S.-H. Tan, B. I. Erkmen, V. Giovannetti, S. Guha, S. Lloyd, L. Maccone, S. Pirandola, J. H. Shapiro, *Quantum illumination with Gaussian states*, Phys. Rev. Lett. 101, 253601 (2008)
- D. Patanè, A. Silva, L. Amico, R. Fazio, G. E. Santoro, *Adiabatic Dynamics in Open Quantum Critical Many-Body Systems*, Phys. Rev. Lett. 101, 175701 (2008)
- V. Giovannetti, S. Lloyd, L. Maccone, *Architectures for a quantum random access memory*, Phys. Rev. A 78, 052310 (2008)
- T. Caneva, R. Fazio, G.E. Santoro, *Adiabatic quantum dynamics of the Lipkin-Meshkov-Glick model*, Phys. Rev. B 78, 104426 (2008)
- D. Urban, J. Koenig, R. Fazio, *Coulomb-Interaction Effects in Full Counting Statistics of a Quantum-Dot Aharonov-Bohm Interferometer*, Phys. Rev. B 78, 075318 (2008)
- D. Rossini, R. Fazio and G.E. Santoro, *Photon and polariton fluctuations in arrays of QED-cavities*, Europhys. Lett. 83, 47011 (2008)
- D. Rossini, V. Giovannetti, S. Montangero, *Spin chain model for correlated quantum channels*, New J. Phys. 10, 115009 (2008)
- F. Caruso, J. Eisert, V. Giovannetti, A.S. Holevo, *Multi-mode bosonic Gaussian channels*, New J. Phys. 10, 083030 (2008)
- F. Caruso, V. Giovannetti, C. Macchiavello, Mary Beth Ruskai, *Qubit channels with small correlations*, Phys. Rev. A 77, 052323 (2008)
- V. Giovannetti and A. S. Holevo, *Quantum Shared Broadcasting*, Quantum Information Processing 7, 55 (2008)
- M. Häfner, J.K. Viljas, D. Frustaglia, F. Pauly, M. Dreher, P. Nielaba and J.C. Cuevas, *Theoretical study of the conductance of ferromagnetic atomic-sized contacts*, Phys. Rev. B 77, 104409 (2008)
- M. Rizzi, S. Montangero and G. Vidal, *Simulation of time evolution with multiscale entanglement renormalization ansatz*, Phys. Rev. A 77, 052328 (2008)
- D. Rossini, P. Facchi, R. Fazio, G. Florio, D. A. Lidar, S. Pascazio, F. Plastina and P. Zanardi, *Bang-Bang control of a qubit coupled to a quantum critical spin bath*, Phys. Rev. A 77, 052112 (2008)

- L. Dell'Anna and F. Dolcini, *Multiple Andreev reflections in a quantum dot coupled to superconductors: Effects of spin-orbit coupling*, Phys. Rev. B 78, 024518 (2008)
- F. Taddei and F.W.J. Hekking, *Measuring the distribution of current fluctuations through a Josephson junction with very short current pulses*, Europhys. Lett. 83, 47009 (2008)
- H. Rabani, F. Taddei, O. Bourgeois, R. Fazio, and F. Giazotto, *Phase-Dependent Electronic Specific Heat in Mesoscopic Josephson Junctions*, Phys. Rev. B 78, 012503 (2008)
- F. Dolcini and L. Dell'Anna, *Multiple Andreev reflections in a quantum dot coupled to superconducting leads: effect of spin-orbit coupling*, Phys. Rev. B 78, 024518 (2008)
- M. E. Kordesch and S. Heun, *Synchrotron radiation photoemission electron microscopy in Encyclopedia of Surface and Colloid Science*, Editors: Ponisseril Somasundaran and Arthur Hubbard, Taylor & Francis (2008)
- T. Vijaykumar, G. Raina, S. Heun, and G. U. Kulkarni, *Catalytic behaviour of individual Au nanocrystals in the local anodic oxidation of Si surfaces*, J. Phys. Chem. C 112, 13311-13316 (2008)
- D. Ercolani, G. Biasiol, E. Cancellieri, M. Rosini, C. Jacoboni, F. Carillo, S. Heun, L. Sorba, and F. Nolting, *Transport anisotropy in In<sub>0.75</sub>Ga<sub>0.25</sub>As two-dimensional electron gases induced by indium concentration modulation*, Phys. Rev. B 77, 235307 (2008)
- F. Ratto, S. Heun, O. Moutanabbir, and F. Rosei, *In situ nanoscale mapping of the chemical composition of surfaces and 3D nanostructures by photoelectron spectromicroscopy*, Nanotechnology 19, 265703 (2008)
- T. Mlakar, G. Biasiol, S. Heun, L. Sorba, T. Vijaykumar, G. U. Kulkarni, V. Spreafico, and S. Prato, *Conductive atomic force microscopy of InAs/GaAs quantum rings*, Appl. Phys. Lett. 92, 192105 (2008)
- F. Ratto, T. W. Johnston, S. Heun, and F. Rosei, *A numerical approach to quantify self-ordering among self-organized nanostructures*, Surf. Sci. 602, 249-258 (2008)
- A. Candini, F. Carillo, G. Biasiol, P. Pingue, M. Affronte, L. Sorba, *Magnetic field sensitivity of In<sub>0.75</sub>Ga<sub>0.25</sub>As Hall nanoprobes*, Materials Science And Engineering B-Solid State Materials For Advanced Technology, 147, 148-151 (2008)
- N. Coluccelli, G. Galzerano, L. Bonelli, A. Di Lieto, M. Tonelli, P. Laporta, *Diode-pumped passively mode-locked Yb : YLF laser*, Optics Express, 16, 2922-2927 (2008)
- F. Pellegrini, S. Montangero, G.E. Santoro, R. Fazio, *Adiabatic quenches through an extended quantum critical region*, Physical Review B 77, 140404 (2008)
- S. Safaei, S. Montangero, F. Taddei, R. Fazio, *Optimized cooper pair pumps*, Physical Review B 77, 144522 (2008)
- V. Giovannetti, F. Taddei, D. Frustaglia, R. Fazio, *Multichannel architecture for electronic quantum Hall interferometry*, Physical Review B 77, 155320 (2008)
- F. Haupt, F. Cavaliere, R. Fazio, M. Sassetti, *Suppression of the Fano factor in nanoelectromechanical systems*, Physica E-Low-Dimensional Systems & Nanostructures 40, 1267-1269 (2008)
- R. Fazio, *Condensed-matter physics - Opposite of a superconductor*, Nature 452, 542-543 (2008)
- F. Dolcini, F. Giazotto, *The electro-magnetostatic Aharonov-Bohm effect as a tool to tune the Josephson current*, Physica E-Low-Dimensional Systems & Nanostructures 40, 2091-2092 (2008)
- F. Giazotto, F. Taddei, *Superconductors as spin sources for spintronics*, Physical Review B 77, 132501 (2008)
- F. Giazotto, T.T. Heikkila, G.P. Pepe, P. Heliö, A. Luukanen, J.P. Pekola, *Ultrasensitive proximity Josephson sensor with kinetic inductance readout*, Applied Physics Letters 92, 162507 (2008)
- V.S. Khrapai, A.A. Shashkin, M.G. Trokina, V.T. Dolgoplov, V. Pellegrini, F. Beltram, G. Biasiol, L. Sorba, *Filling factor dependence of the fractional quantum hall effect gap*, Physical Review Letters 100, 196805 (2008)
- S. Kalliakos, C.P. Garcia, V. Pellegrini, A. Pinczuk, B.S. Dennis, L.N. Pfeiffer, K.W. West, M. Rontani, G. Goldoni, E. Molinari, *Correlated states and spin transitions in nanofabricated AlGaAs/GaAs few-electron quantum dots probed by inelastic light scattering*, Physica E-Low-Dimensional Systems & Nanostructures 40, 1867-1869 (2008)
- B. Karmakar, S. Luin, V. Pellegrini, A. Pinczuk, B.S. Dennis, L.N. Pfeiffer, K. W. West, *Signatures of composite-fermion metals in electron bilayers at  $\nu(T)=1$* , Physica E-Low-Dimensional Systems & Nanostructures 40, 1312-1314 (2008)
- S. Kalliakos, V. Pellegrini, C.P. Garcia, A. Pinczuk, L.N. Pfeiffer, K. W. West, *Optical control of energy-level structure of few electrons in AlGaAs/GaAs quantum dots*, Nano Letters 8, 577-581 (2008)
- G. Turri, V. Sudesh, M. Richardson, M. Bass, A. Toncelli, M. Tonelli, *Temperature-dependent spectroscopic properties of Tm<sup>3+</sup> in germanate, silica, and phosphate glasses: A comparative study*, Journal of Applied Physics 103, 093104 (2008)

- T.H. My, P. Goldner, O. Guillot-Noel, M. Tonelli, F. Bretenaker, *Single-frequency operation of an orange avalanche upconversion laser for high-resolution laser spectroscopy*, European Physica Journal-Applied Physics 42, 121-124 (2008)
- L. Mahler, A. Tredicucci, R.P. Green, F. Beltram, C. Walther, J. Faist, H.E. Beere, D.A. Ritchie, *Terahertz quantum cascade lasers with quasi-periodic resonators*, Physica E-Low-Dimensional Systems & Nanostructures 40, 2176-2178 (2008)
- T. Losco, J.H. Xu, R.P. Green, A. Tredicucci, H.E. Beere, D.A. Ritchie, *THz quantum cascade designs for optimized injection*, Physica E-Low - Dimensional Systems & Nanostructures 40, 2207-2209 (2008)
- V. Brosco, R. Fazio, F. W. J. Hekking, and A. Joye, *Non-Abelian superconducting pumps*, Phys. Rev. Lett. 100, 027002 (2008)
- N. B. Kopnin, F. Taddei, J. P. Pekola, and F. Giazotto, *Influence of photon-assisted tunneling on heat flow in a normal metalsuperconductor tunnel junction*, Phys. Rev. B 77, 104517 (2008)
- M. Rizzi and A. Imambekov, *Pairing of 1D Bose-Fermi mixtures with unequal masses*, Phys. Rev. A 77, 023621 (2008)
- A. Tomadin, M. Polini, M.P. Tosi and R. Fazio, *Nonequilibrium pairing instability in ultracold Fermi gases with population imbalance*, Phys. Rev. A 77, 033605 (2008)
- R.P. Green, J.H. Xu, L. Mahler, A. Tredicucci, F. Beltram, G. Giuliani, H. E. Beere and D. A. Ritchie, *Linewidth enhancement factor of terahertz quantum cascade lasers*, Appl. Phys. Lett. 92, 071106 (2008)
- L. Gridneva, A. Persson, M. Á. Nino, J. Camarero, J. J. de Miguel, R. Miranda, C. Hofer, C. Teichert, T. Bobek, A. Locatelli, S. Heun, S. Carlsson, and D. Arvanitis, *Experimental investigation of the spin reorientation of Co/Au based magnetic nanodot arrays*, Phys. Rev. B 77, 104425(2008)
- A. Anappara, A. Tredicucci, F. Beltram, L. Sorba, G. Biasiol, *Tailoring light-matter interaction in intersubband microcavities*, Physica E 40, 1906 (2008)
- A. J. M. Giesbers, U. Zeitler, D. Reuter, A. D. Wieck, G. Biasiol, L. Sorba, and J. C. Maan, *Aharonov-Bohm effect of quantum Hall edge channels*, Physica E 40, 1470 (2008)
- M. Rosini, E. Cancellieri, D. Ercolani, G. Biasiol, L. Sorba and C. Jacoboni, *Transport anisotropy in InGaAs 2D electron gases*, Physica E 40, 1392 (2008)
- M. Virgilio and G. Grosso, *Valley splitting and selection rules for inter-doublets optical transitions in strained [001]-Si/SiGe heterostructures*, Physica E 40, 2046-2048 (2008)
- A. Cresti, G. Grosso and G. Pastori Parravicini, *Current profiles in gated graphene ribbons*, Physica E 40, 1712-1714 (2008)
- A. Cresti, G. Grosso and G. Pastori Parravicini, *Electronic states and magnetotransport in unipolar and bipolar graphene ribbons*, Phys. Rev. B 77, 115408-115416 (2008)
- M. Virgilio, and G. Grosso, *Quantum confined Stark effect in Ge/SiGe Quantum Wells: a tight-binding description*, Phys. Rev. B 77, 165315-165321 (2008)
- S. Barsanti, F. Cornacchia, A. Di Lieto, A. Toncelli, M. Tonelli, P. Bicchi, *Nd<sup>3+</sup>-doped fluoride film grown on LiYF<sub>4</sub> substrate by pulsed laser deposition*, Thin Solid Films 516, 2009-2013 (2008)
- S. Abbruzzetti, S. Bruno, S. Faggiano, L. Ronda, E. Grandi, A. Mozzarelli, C. Viappiani, *Characterization of ligand migration mechanisms inside haemoglobins from the analysis of geminate rebinding kinetics*, Methods in Enzymology - Globins and other NO-reactive Proteins in Microbes, Plants and Invertebrates, 329-345 (2008)
- L. Ronda, S. Abbruzzetti, S. Bruno, S. Bettati, A. Mozzarelli, C. Viappiani, *Ligand-Induced Tertiary Relaxations During the T-to-R Quaternary Transition in Hemoglobin*, J. Phys. Chem. B, 112, 127901-12794 (2008)
- V. Voliani, R. Bizzarri, R. Nifosi, S. Abbruzzetti, E. Grandi, C. Viappiani, F. Beltram, *Cis-Trans Photoisomerization of Fluorescent-Protein Chromophores*, J. Phys. Chem. B, 12, 10714-10722 (2008)
- L. Ronda, S. Bruno, S. Abbruzzetti, C. Viappiani, S. Bettati, *Ligand reactivity and allosteric regulation of hemoglobin-based oxygen carriers*, Biochimica et Biophysica Acta - Proteins and Proteomics, 1784, 13651377 (2008)
- M. Cecchini, F. Signori, P. Pingue, S. Bronco, F. Ciardelli and F. Beltram, *High-resolution poly(ethylene terephthalate) (PET) hot embossing at low-temperature: thermal, mechanical and optical analysis of nanopatterned films*, Langmuir, 24, 12581-12586 (2008)
- S. Girardo, M. Cecchini, F. Beltram, R. Cingolani and D. Pisignano, *Polydimethylsiloxane-LiNbO<sub>3</sub> surface acoustic wave micropump devices for fluid control into microchannels*, Lab-on-a-Chip 8, 1557 (2008)
- M. Cecchini, A. Ferrari and F. Beltram, *PC12 polarity on biopolymer nanogratings*, Journal of Physics: Conference Series, 100, 012003 (2008)
- L. Albertazzi, D. Arosio, L. Marchetti, F. Ricci, F. Beltram, *Quantitative FRET Analysis With the EGFP-mCherry Fluorescent Protein Pair*, Photochem. Photobiol. (2008)

- F. Trovato, V. Tozzini, *Supercoiling and Local Denaturation of Plasmids with a Minimalist DNA Model*, J. Phys Chem B 112 13197-13200 (2008)
- K. Voltz, J. Trylska, V. Tozzini, V. Kurkal-Siebert, J. Smith and J. Langowski, *Global motions in the nucleosome explored using a coarse-grained model*, NIC Series, 40, 141-144 (2008)
- F. Cardarelli, M. Serresi, Bizzarri R., Beltram F., *Tuning the transport properties of HIV-1 tat arginine-rich motif in living cells*, Traffic 9, 528-539 (2008)
- M. Cecchini, S. Girardo, D. Pisignano, R. Cingolani, F. Beltram, *Acoustic-counterflow microfluidics by surface acoustic waves*, Applied Physics Letters 92, 104103 (2008)
- M. Marchi, M. Becucci, P. Tognini, M. Maffei, N. Landsberger, G.M. Ratto, M. Costa, *Epigenetic drugs modulate MeCP2 dynamics in living cells*, Cellular Oncology 30, 264-265 (2008)
- V. Tozzini, J.A. McCammon, *One-Bead Coarse Grained Models for Proteins*, in "Coarse-graining of condensed Phase and Biomolecular Systems" G A Voith Ed, Taylor & Francis/CRC press, Chapter 19 (2008)
- K. Voltz, J. Trylska, V. Tozzini, V. Kurkal-Siebert, J. Langowski, J. Smith, *Coarse-grained force field for the nucleosome from self-consistent multiscaling*, J Comput Chem 29, 1429-1439 (2008)
- G. Xianlong, M. Polini, D. Rainis, M.P. Tosi, and G. Vignale, *Time-Dependent Current-Density-Functional Theory of Spin-Charge Separation and Spin Drag in One-Dimensional Ultracold Fermi Gases*, Phys. Rev. Lett. 101, 206402 (2008)
- G. Xianlong, M. Polini, M.P. Tosi, and B. Tanatar, *Effect of disorder on the interacting Fermi gases in a one-dimensional optical lattice*, Int. J. Mod. Phys. B 22, 4500 (2008)
- W. Li, G. Xianlong, C. Kollath, and M. Polini, *Collective excitations in one-dimensional ultracold Fermi gases: Comparative study*, Phys. Rev. B 78, 195109 (2008)
- M. Polini, A. Tomadin, R. Asgari and A.H. MacDonald, *Density-functional theory of graphene sheets*, Phys. Rev. B 78, 115426 (2008)
- A.I. Mese, P. Capuzzi, Z. Akdeniz, S.E. Okan e M.P. Tosi, *Coulomb crystallites from harmonically confined charged bosons in two dimensions*, J. Phys.: Condens. Matter 20, 335222-335227 (2008)
- M. Rizzi, M. Polini, M.A. Cazalilla, M.R. Bakhtiari, M.P. Tosi, and R. Fazio, *Fulde-Ferrell-Larkin-Ovchinnikov pairing in one-dimensional optical lattices*, Phys. Rev. B 77, 245105 (2008)
- A. Tomadin, M. Polini, M.P. Tosi, and R. Fazio, *Nonequilibrium pairing instability in ultracold Fermi gases with population imbalance*, Phys. Rev. A 77, 033605 (2008)
- M. Polini, R. Asgari, G. Borghi, Y. Barlas, T. Pereg-Barnea, and A. H. MacDonald, *Plasmons and the spectral function of graphene*, Phys. Rev. B 77, 081411(R) (2008)
- Z. Akdeniz, Z. Cicek Önem, R. Ruberto, G. Pastore e M.P. Tosi, *Molecular clusters in gaseous and liquid AlCl<sub>3</sub>*, Phys. Chem. Liquids 46, 1-8 (2008)
- H. Min, G. Borghi, M. Polini and A.H. MacDonald, *Pseudospin magnetism in graphene*, Phys. Rev. B 77, 041407(R) (2008)
- D. Rainis, M. Polini, M.P. Tosi and G. Vignale, *Spin-drag relaxation time in one-dimensional spin-polarized Fermi gases*, Phys. Rev. B 77, 035113 (2008)

## 2007

- B. Karmakar, S. Luin, V. Pellegrini, A. Pinczuk, B.S. Dennis, L.N. Pfeiffer, K.W. West, *Metamorphosis of a quantum Hall bilayer state into a composite fermion metal*, Solid State Communications 143, 499-503 (2007)
- S. Kalliakos, C.P. Garcia, V. Pellegrini, M. Zamfirescu, L. Cavigli, M. Gurioli, A. Vinattieri, A. Pinczuk, B.S. Dennis, L.N. Pfeiffer, K.W. West, *Photoluminescence of individual doped GaAs/AlGaAs nanofabricated quantum dots*, Applied Physics Letters 90, 181902 (2007)
- V. Pellegrini, S. Luin, B. Karmakar, A. Pinczuk, B.S. Dennis, L.N. Pfeiffer, K.W. West, A. Vinattieri, A. Pinczuk, B.S. Dennis, L.N. Pfeiffer, K.W. West, *Seeing emergent phases in quantum Hall double layers*, Journal Of Applied Physics 101, 081718 (2007)
- D. Prevosto, S. Napolitano, P. Pingue, S. Capaccioli, M. Lucchesi, *Investigation of structural relaxation and surface modification of ultrathin films of poly(ethylene terephthalate)*, European Physical Journal- Special Topics 141, 193-198 (2007)
- S. Bigotta, A. Di Lieto, A. Toncelli, M. Tonelli, D. Seletskiy, M.P. Hasselbeck, M. Sheik-Bahae, R.I. Epstein, *Laser cooling of solids: New results with single fluoride crystals*, Nuovo Cimento della Società Italiana di Fisica, B-General Physics Relativity Astronomy and Mathematical Physics and Methods 122, 685-694 (2007)
- C. Mauro, R.P. Green, A. Tredicucci, F. Beltram, H.E. Beere, D.A. Ritchie, *Amplification of terahertz radiation in quantum cascade structures*, Journal of Applied Physics 102, 063101 (2007)
- Y. N. Ovchinnikov, A. Barone, A.A. Varlamov, *Macroscopic quantum tunneling in "Small" josephson junctions in a magnetic field*, Phys. Rev. Lett. 99 037004 (2007)
- T. Bauch, K. Cedergren, J. Johansson, G. Rotoli, F. Tafuri and F. Lombardi, *Dynamics of d-wave YBa<sub>2</sub>Cu<sub>3</sub>O<sub>7-x</sub> dc SQUIDs*, Supercond. Science and Technology 20, S98 (2007)
- F. Tafuri, A. Tagliacozzo, D. Born, D. Stornaiuolo, E. Gambale, D. Dalena and F. Lombardi, *Mesoscopic conductance fluctuations in High-T<sub>c</sub> grain boundary Josephson junctions: coherent quasiparticle transport*, Physica C 460-462, 343 (2007)
- F. Lombardi, T. Bauch, K. Cedergren, J. Johansson, T. Lindström, F. Tafuri, G. Rotoli, P. Delsing and T. Claeson, *Energy level quantization in a YBaCuO Josephson Junction*, Physica C 460-462, 335 (2007)
- A. Tagliacozzo, D. Born, D. Stornaiuolo, E. Gambale, D. Dalena, F. Lombardi, A. Barone, B. L. Altshuler and F. Tafuri, *Observation of mesoscopic conductance fluctuations in YBaCuO grain boundary Josephson Junctions*, Phys. Rev. B 75, 12507 (2007)
- F. Lombardi, T. Bauch, G. Rotoli, T. Lindström, J. Johansson, K. Cedergren, F. Tafuri and T. Claeson, *Dynamics of a LC shunted YBa<sub>2</sub>Cu<sub>3</sub>O<sub>7-d</sub> Josephson junction*, IEEE Trans. on Appl. Supercond. 17, 653 (2007)
- D. Stornaiuolo, D. Born, D. Dalena, E. Gambale, G. Rotoli, T. Bauch, A. Tagliacozzo, A. Barone, F. Lombardi and F. Tafuri, *Advances in YBa<sub>2</sub>Cu<sub>3</sub>O<sub>7-d</sub> Grain Boundary Biepitaxial Josephson Junctions: Transport Properties and Mesoscopic Effects*, IEEE Trans. on Appl. Supercond. 17, 3581 (2007)
- D. Born, D. Stornaiuolo, F. Tafuri, P. G. Medaglia, P. Orgiani, G. Balestrino, F. Lombardi, J. R. Kirtley and V. G. Kogan, *CaBaCuO Ultrathin Films and Junctions*, IEEE Trans. on Appl. Supercond. 17, 3581 (2007)
- P. Orgiani, C. Aruta, G. Balestrino, D. Born, L. Maritato, P. G. Medaglia, D. Stornaiuolo, F. Tafuri and A. Tebano, *Direct measurement of sheet resistance R in cuprate systems: evidence of fermionic scenario in Metal-Insulator Transition*, Phys. Rev Lett. 98, 36401 (2007)
- J. R. Kirtley and F. Tafuri, *Tunneling Measurements of the cuprate superconductors*, in "Treatise of Superconductivity" edited by Robert Schrieffer, 19-85 (2007)
- G. Rotoli, T. Bauch, T. Lindstrom, D. Stornaiuolo, F. Tafuri and F. Lombardi, *Classical resonant activation of a Josephson junction embedded in an LC-circuit*, Phys. Rev. B 75, 144501 (2007)
- G. Bimonte, D. Born, E. Calloni, G. Esposito, U. Hubner, E. Il'ichev, L. Rosa, O. Scaldaferrri, F. Tafuri, R. Vaglio, *The Aladin2 experiment: Sensitivity study*, Nuclear Instruments and Methods in Physics Research A 572, 515 (2007)
- D. Stornaiuolo, D. Born, R. Fittipaldi, A. Vecchione, F. Tafuri and Y. Maeno, *Transport measurements on Sr<sub>2</sub>RuO<sub>4</sub> - Sr<sub>3</sub>Ru<sub>2</sub>O<sub>7</sub> eutectic crystals*, Physica C 460-462, 526 (2007)
- D. Born, D. Stornaiuolo, F. Tafuri, J. R. Kirtley, V. G. Kogan, P. G. Medaglia, P. Orgiani, G. Balestrino, T. Bauch, F. Lombardi, *Transport measurements on ultra-thin CaBaCuO films*, Physica C 460-462, 845 (2007)
- S. Tsuchiya, F. Dalfovo, C. Tozzo, L. Pitaevskii, *Stability and excitations of solitons in 2D Bose-Einstein condensates*, J. Low Temp. Phys. 148, 393 (2007)
- F. Pellegrini and S. Montangero, *Fractal fidelity as a signature of quantum chaos*, Phys. Rev. A 76, 052327 (2007)

- D. Binosi, G. De Chiara, S. Montangero, A. Recati, *Increasing entanglement through engineered disorder*, Phys. Rev. A 76, 140405 (2007)
- D. Burgarth and V. Giovannetti, *Mediated Homogenization*, Phys. Rev. A 76, 062307 (2007)
- A. A. Anappara, A. Tredicucci, F. Beltram, G. Biasiol, L. Sorba, S. De Liberato, and C. Ciuti, *Cavity polaritons from excited-subband transitions*, Appl. Phys. Lett. 91, 231118 (2007)
- G. De Chiara, A. Lozinski, G. Massimo Palma, *Berry phase in open quantum systems: a quantum Langevin equation approach*, Eur.Phys. J. D. 41, 179-183 (2007)
- M.A.Cirone, G. Compagno, G. M. Palma, R. Passante, F.S. Persico, *Casimir-Polder potentials as entanglement probe*, Europhysics Letters, 78, 30003 (2007)
- M.Paternostro, M.S.Kim, G.M.Palma, *Accumulation of Entanglement in a Continuous Variable Memory*, Phys. Rev. Lett. 98, 140504 (2007)
- F. Ciccarello, G. M. Palma, M. Zarccone, Y. Omar and V. R. Vieira, *Effect of static disorder in an Electron Fabry-Perot interferometer with two quantum scattering centers*, Laser Physics 17, 889 (2007)
- G.Benenti and G. M. Palma, *Reversible and irreversible dynamics of a qubit interacting with a small environment*, Phys. Rev. A 75, 052110 (2007)
- F. Ciccarello, G. M. Palma, M. Zarccone, Y. Omar and V R Vieira, *Electron Fabry-Perot interferometer with two entangled magnetic impurities*, J. Phys. A 40 7993-8008 (2007)
- F.Ciccarello, G. M.Palma, and M.Zarccone, *Entanglement-induced electron coherence in a mesoscopic ring with two magnetic impurities*, Phys.Rev.B 75, 205415 (2007)
- G. De Chiara, C. Brukner, R. Fazio, G.M. Palma and V. Vedral, *Can entanglement be extracted from many body systems?* International Journal of Quantum Information, 5, 125-130 (2007)
- U. Messina e G. M. Palma, *Entanglement swapping in a Franson interferometer setup*, Journal of Modern Optics, special issue in honour of the sixtieth birthday of Professor Sir Peter Knight, 54, 2297-2306 (2007)
- C. Di Franco, G. M. Palma, M. Paternostro, M. S. Kim, *Information-flux approach to multiple-spin dynamics*, Phys. Rev. A 76, 042316 (2007)
- S. Bellucci, F. Carillo, P. Onorato, *Spin separation in a T ballistic nanojunction due to lateral-confinement-induced spin-orbit coupling*, Journal of Physics: Condensed Matter, Volume 19, Issue 39, 395018 (2007)
- A. Cresti, *Electronic conductance in open quantum dots*, Nanotechnology 18, 055403 (2007)
- A. Cresti, G. Grosso and G. Pastori Parravicini, *Numerical study of electronic transport in gated graphene ribbons*, Phys. Rev. B 76, 205433-205440 (2007)
- M. Virgilio and G. Grosso, *Optical transitions between valley split subbands in biased Si quantum wells*, Phys. Rev. B 75, 235428-235433 (2007)
- M. Virgilio and G. Grosso, *Conduction intersubband transitions at normal incidence in Si<sub>1-x</sub>G<sub>x</sub> quantum wells devices*, Nanotechnology 18, 075402-075406 (2007)
- V. Toccafondo, A. Cerqueira S., Jr., S. Faralli, E. Sani, A. Toncelli, M. Tonelli and F. Di Pasquale, *Er<sup>3+</sup>-doped BaY<sub>2</sub>F<sub>8</sub> crystal waveguides for broadband optical amplification at 1.5 μm*, Journal of Applied Physics 101, 023104 (2007)
- D. Gatti, G. Galzerano, A. Toncelli, M. Tonelli, P. Laporta, *Actively mode-locked Tm-Ho:LiYF<sub>4</sub> and Tm-Ho:BaY<sub>2</sub>F<sub>8</sub> lasers*, Appl. Phys. B 86, 269-273 (2007)
- G. Galzerano, P. Laporta L. Bonelli, A. Toncelli and M. Tonelli, *Single-frequency diode-pumped Yb:KYF<sub>4</sub> laser around 1030 nm*, Optics Express 15, 3257 (2007)
- F. Cornacchia, A. Toncelli, M. Tonelli, E. Favilla, K. A. Subbotin, V. A. Smirnov, D. A. Lis, A. M. Prokhorov, E. V. Zharikov, *Growth and spectroscopic characterization of Er<sup>3+</sup>:CaWO<sub>4</sub>*, Journal of Applied Physics 101, 123113 (2007)
- S. Bigotta, A. Toncelli, M. Tonelli, E. Cavalli, E. Bovero, *Spectroscopy and energy transfer parameters of Tm<sup>3+</sup>- and Ho<sup>3+</sup>-doped Ba<sub>2</sub>NaNb<sub>5</sub>O<sub>15</sub> single crystals*, Optical Materials 30, 129-131 (2007)
- F. Cornacchia, R. Simura, A. Toncelli, M. Tonelli, A. Yoshikawa, T. Fukuda, *Spectroscopic properties of Y<sub>3</sub>Sc<sub>2</sub>Al<sub>3</sub>O<sub>12</sub> (YSAG) single crystals grown by micro-PD technique*, Optical Materials 30, 135-138 (2007)
- L. Bonelli, A. Toncelli, A. Di Lieto, M. Tonelli, *Spectroscopic analysis of 10% Yb<sup>3+</sup>:KYF<sub>4</sub> crystal*, Journal of Physics and Chemistry of Solids 68 2381-2386 (2007)
- A. Romito, S. Montangero and R. Fazio, *Transport properties of a periodically driven superconducting single electron transistor*, Phys. Rev. B 75, 184528 (2007)
- P. Vignolo, R. Fazio and M.P. Tosi, *Quantum vortices in optical lattices*, Phys. Rev. A 76, 023616 (2007)
- D. Rossini, V. Giovannetti, and R. Fazio, *Information transfer rates in spin quantum channels*, Int. J. Quant. Inf. 5, 439 (2007)

- S. Pugnetti, F. Dolcini and R. Fazio, *dc Josephson Effect in Metallic Single-Walled Carbon Nanotubes*, Sol. St. Comm. 144, 551 (2007)
- F. Dolcini, B. Trauzettel, I. Safi, and H. Grabert, *Negativity of the excess noise in a quantum wire capacitively coupled to a gate*, Phys. Rev. B 75, 030404 (2007)
- F. Dolcini and F. Giazotto, *Switching the sign of Josephson current through Aharonov-Bohm interferometry*, Phys. Rev. B 75, 140511(R) (2007)
- D. Rossini, T. Calarco, V. Giovannetti, S. Montangero and R. Fazio, *Decoherence by engineered quantum baths*, J. Phys. A: Math. Theor. 40, 8033 (2007)
- D. Patanè, R. Fazio and L. Amico, *Bound entanglement in the XY model*, New J. Phys. 9, 322 (2007)
- D. Burgarth and V. Giovannetti, *The generalized Lyapunov Theorem and its application to quantum channels*, New J. Phys. 9, 150 (2007)
- D. Rossini, T. Calarco, V. Giovannetti, S. Montangero and R. Fazio, *Decoherence induced by interacting quantum spin baths*, Phys. Rev. A 75, 032333 (2007)
- D. Burgarth, V. Giovannetti and S. Bose, *Optimal quantum chain communication by end gates*, Phys. Rev. A 75, 062327 (2007)
- F. Caruso and V. Giovannetti, *Qubit quantum channels: a characteristic function approach*, Phys. Rev. A. 76, 042331 (2007)
- T. Caneva, R. Fazio and G.E. Santoro, *Adiabatic quantum annealing dynamics in a random Ising chain*, Phys. Rev. B 76, 144427 (2007)
- G. Xianlong, M. Rizzi, M. Polini, R. Fazio, M.P. Tosi, V.L. Campo Jr., K. Capelle, *Luther-Emery Phase and Atomic-Density Waves in a Trapped Fermion Gas*, Phys. Rev. Lett. 98, 030404 (2007)
- D. Burgarth and V. Giovannetti, *Full control by locally induced relaxation*, Phys. Rev. Lett. 99, 100501 (2007)
- S. Montangero, T. Calarco and R. Fazio, *Robust optimal quantum gates for Josephson charge qubits*, Phys. Rev. Lett. 99, 170501 (2007)
- D. Rossini and R. Fazio, *Mott insulating and glassy phases of polaritons in arrays of coupled cavities*, Phys. Rev. Lett. 99, 186401 (2007)
- S. Roddaro, P. Pingue, V. Piazza, V. Pellegrini, F. Beltram, *The optical visibility of graphene: Interference colors of ultrathin graphite on SiO<sub>2</sub>*, Nano Letters 7(9), 2707-2710 (2007)
- R. Green, L. Mahler, C. Mauro, T. Losco, J. Xu, A. Tredicucci, F. Beltram, H. Beere and D. Ritchie, *Tailoring the emission of terahertz quantum cascade lasers*, Terahertz Frequency Detection and Identification of Materials and Objects, 41-54 (2007)
- J. Xu, J. M. Hensley, D. B. Fenner, R. P. Green, L. Mahler, A. Tredicucci, M. G. Allen, F. Beltram, H. E. Beere and D. A. Ritchie, *Tunable terahertz quantum cascade lasers with an external cavity*, Appl. Phys. Lett. 91, 121104 (2007)
- C. Mauro, R. P. Green, A. Tredicucci, F. Beltram, H. E. Beere and D. A. Ritchie, *Amplification of terahertz radiation in quantum cascade structures*, J. Appl. Phys. 102, 063101 (2007)
- M. D'Acunto, S. Napolitano, P. Pingue, P. Giusti and P. Rolla, *Fast formation of ripples induced by AFM. A new method for patterning polymers on nanoscale*, Materials Letters, 61, 3305-3309 (2007)
- Napolitano S., Prevosto D., Lucchesi M., Pingue P., D'Acunto M., Rolla P., Langmuir, *Influence of a Reduced Mobility Layer on the Structural Relaxation Dynamics of Aluminum Capped Ultrathin Films of Poly (ethylene terephthalate)*, (Research Article), 23(4), 2103-2109 (2007)
- S. Roddaro, P. Pingue, V. Piazza, V. Pellegrini and F. Beltram, *The Optical Visibility of Graphene: Interference Colors of Ultrathin Graphite on SiO<sub>2</sub>*, Nano Lett., 7 (9), 2707-2710 (2007)
- L. Faoro and F. Taddei, *Entanglement detection for electrons via witness operators*, Phys. Rev. B 75, 165327 (2007)
- J. Splettstoesser, M. Governale, J. König, F. Taddei and R. Fazio, *Pumping through a quantum dot in the proximity of a superconductor*, Phys. Rev. B 75, 235302 (2007)
- V. Giovannetti, D. Frustaglia, F. Taddei and R. Fazio, *Characterizing electron entanglement in multiterminal mesoscopic conductors*, Phys. Rev. B 75, 241305(R) (2007)
- F. Giazotto, F. Taddei, M. Governale, R. Fazio, F. Beltram, *Landau Cooling in Metal-Semiconductor Nanostructures*, New J. Phys. 9, 439 (2007)
- F. Taddei, P. D'Amico, Rosario Fazio, F. Beltram, Phys. Rev. B 76, 184518 (2007)
- T. Schmidt, T. Clausen, J. I. Flege, S. Gangopadhyay, A. Locatelli, T. O. Menten, F. Z. Guo, S. Heun and J. Falta, *Adsorbate induced self-ordering of germanium nanoislands on Si(113)*, New Journal of Physics \*9\* 392 (2007)

- V. S. Khrapai, A. A. Shashkin, M. G. Trokina, V. T. Dolgoplov, V. Pellegrini, F. Beltram, G. Biasiol, L. Sorba, *Direct measurements of the gap in the fractional quantum Hall effect*, Phys. Rev. Lett. 99, 086802 (2007)
- A. Candini, G.C. Gazzadi, A. di Bona, M. Affronte, D. Ercolani, G. Biasiol and L. Sorba, *Focused ion beam patterned Hall nano-sensors*, J. Magn. Magn. Mater. 310, 2752 (2007)
- A. Maione, M. Macucci, G. Iannaccone, G. Basso, B. Pellegrini, M. Lazzarino, L. Sorba, and F. Beltram, *Probing Pauli Blocking with shot noise in resonant tunneling diodes: experiment and theory*, Phys. Rev. B 75, 125327 (2007)
- A. A. Anappara, D. Barate, A. Tredicucci, J. Devenson, R. Teissier and A. Baranov, *Giant intersubband polariton splitting in InAs/AlSb microcavities*, Solid State Commun. 142, 311 (2007)
- N. Beverini, G. Carelli, A. De Michele, A. Moretti, L. Mahler, A. Tredicucci, H. E. Beere and D. A. Ritchie, *Frequency characterization of a terahertz quantum-cascade laser*, IEEE Trans. Instrum. Meas. 56, 262 (2007)
- H. W. Hübers, S. G. Pavlov, H. Richter, A. D. Semenov, L. Mahler, A. Tredicucci, H. E. Beere and D. A. Ritchie, *Molecular Spectroscopy with TeraHertz Quantum Cascade*, Lasers J. Nanoelectron. Optoelectron. 2, 101 (2007)
- A. A. Anappara, A. Tredicucci, F. Beltram, G. Biasiol and L. Sorba, *Controlling polariton coupling in intersubband microcavities*, Superlatt. Microstruct. 41, 308 (2007)
- F. Dolcini, B. Trauzettel, I. Safi and H. Grabert, *Negativity of the excess noise in a quantum wire capacitively coupled to a gate*, Phys. Rev. B 75, 030404 (2007)
- R. Bizzarri, R. Nifosi, S. Abbruzzetti, W. Rocchia, S. Guidi, D. Arosio, G. Garau, B. Campanini, E. Grandi, F. Ricci, C. Viappiani, F. Beltram, *Thermodynamic and kinetic characterization of protonation exchanges in GFPs: a way to mutants with tailored optical properties*, Biophysical Journal 329A-329A, Suppl. S (2007)
- M. Cecchini, G. Bumma, M. Serresi, F. Beltram, *PC12 differentiation on biopolymer nanostructures*, Nanotechnology 18, 505103 (2007)
- W. Rocchia, G. Neshich, *Electrostatic potential calculation for biomolecules - creating a database of pre-calculated values reported on a per residue basis for all PDB protein structures*, Genetics and Molecular Research 6, 923-936 (2007)
- C. Viappiani, S. Bruno, S. Faggiano, A. Mozzarelli, S. Abbruzzetti, E. Grandi, E. Cacciatori, P. Dominici, *Ligand migration in class-1 non symbiotic hemoglobin from Arabidopsis thaliana*, Biophysical Journal, 538A-538A Supplement: Suppl. S (2007)
- R. Nifosi, Y. Luo, *Predictions of Novel Two-Photon Absorption Bands in Fluorescent Proteins*, J. Phys. Chem. B. 111, 14043-14050 (2007)
- S. Bruno, S. Faggiano, F. Spyraakis, A. Mozzarelli, E. Cacciatori, P. Dominici, E. Grandi, S. Abbruzzetti, C. Viappiani, *Different roles of protein dynamics and ligand migration in non symbiotic hemoglobins AHb1 and AHb2 from Arabidopsis thaliana*, Gene 398, 224-233 (2007)
- S. Abbruzzetti, E. Grandi, S. Bruno, S. Faggiano, F. Spyraakis, A. Mozzarelli, P. Dominici and C. Viappiani, *Ligand migration in non symbiotic hemoglobin AHb1 from Arabidopsis thaliana*, Journal of Physical Chemistry B 111, 12582-12590 (2007)
- M. Marchi, A. Guarda, A. Bergo, N. Landsberger, C. Kilstup-Nielsen, G.M. Ratto, M. Costa, *Spatio-Temporal Dynamics and Localization of MeCP2 and Pathological Mutants in Living Cells*, Epigenetics, Sep, 2(3):187-97. Epub Sep 18 (2007)
- E. Putignano, G. Lonetti, L. Cancedda, G.M. Ratto, M. Costa, L. Maffei, T. Pizzorusso, *Developmental downregulation of histone posttranslational modifications regulates visual cortical plasticity*, Neuron. 2007 Mar 1;53(5):747-59. Erratum in: Neuron. 2007 Apr 5;54(1):177
- F. Cardarelli, M. Serresi, R. Bizzarri, M. Giacca, F. Beltram, *In Vivo Study of HIV-1 Tat Arginine-rich Motif Unveils Its Transport Properties*, Mol Ther, 15: 1313-1322 (2007)
- R. Nifosi, P. Amat, V. Tozzini, *Variation of spectral, structural, and vibrational properties within the intrinsically fluorescent proteins family: a density functional study*, Journal of Computational Chemistry, Volume 28, Issue 14, 2366-2377 (2007)
- D. Arosio, G. Garau, F. Ricci, L. Marchetti, R. Bizzarri, R. Nifosi, F. Beltram, *Spectroscopic and Structural Study of Proton and Halide Ion Cooperative Binding to GFP*, Biophysical Journal 93: 232-244 (2007)
- R. Bizzarri, R. Nifosi, S. Abbruzzetti, W. Rocchia, S. Guidi, D. Arosio, G. Garau, B. Campanini, E. Grandi, F. Ricci, C. Viappiani, F. Beltram, *Green fluorescent protein ground states: The influence of a second protonation site near the chromophore*, Biochemistry 46 (18): 5494-5504 May 8 (2007)
- R. Nifosi and Y. Luo, *Origin of the anomalous two-photon absorption in fluorescent protein DsRed*, Journal of Physical Chemistry B 111 (3): 505-507 Jan 25 (2007)
- K. Voltz, T. Wocjan, K. Klenin, J. Trylska, V. Tozzini, V. Kurkal, J. Smith, J. Langowski, *DNA dynamics on the nucleosome simulated by coarse-grained models*, Biophys J, Suppl S 540A-540A (2007)

- J. Trylska, V. Tozzini, C.E. Chang, J. A. McCammon, *HIV-1 protease substrate binding and product release pathways explored with coarse-grained molecular dynamics*, *Biophys J*, 92 4179-4187 (2007)
- C. E. Chang, J. Trylska, V. Tozzini, J. A. McCammon, *Binding pathways of ligands to HIV-1 Protease: Coarse-grained and atomistic simulations*, *Chem Biol Drug Des*, 69 5,13 (2007)
- V. Tozzini, J. Trylska, C. E. Chang, J. A. McCammon, *Flap opening dynamics in HIV-1 protease explored with a coarse-grained model*, *J Struct Biol*, 157, 606-615 (2007)
- R. Ruberto, G. Pastore, Z. Akdeniz and M.P. Tosi, *Structure and diffusion in aluminium and gallium trihalide melts from simulations based on intramolecular force laws*, *Molec. Phys.* 105, 2383-2392 (2007)
- S. H. Abedinpour, M. Polini, A.H. MacDonald, B. Tanatar, M.P. Tosi and G. Vignale, *Theory of the Pseudospin Resonance in Semiconductor Bilayers*, *Phys. Rev. Lett.* 99, 206802 and arXiv:0706.1702v1 (2007)
- P. Karaman, Z. Akdeniz, M.P. Tosi, *Z. Naturforsch, Transferable deformation-dipole model for ionic materials*, 62°, 265-269 (2007)
- P. Vignolo, R. Fazio, M.P. Tosi, *Quantum vortices in optical lattices*, *Phys. Rev. A* 76, 023616.1-4 (2007)
- E. Goat, R. Ruberto, G. Pastore, Z. Akdeniz, M.P. Tosi, *From molecular clusters to liquid structure in AlCl<sub>3</sub> and FeCl<sub>3</sub>*, *Phys. Chem. Liquids* 45, 487-501 (2007)
- M.P. Tosi, *Quantum mechanics at work*, *Concepts of Physics* 4, 471-484 (2007)
- S.H. Abedinpour, R. Asgari, M. Polini and M.P. Tosi, *Analytic theory of pair distribution functions in symmetric electron-electron and electron-hole bilayers*, *Solid State Commun.* 144, 65 (2007)
- Y. Barlas, T. Pereg-Barnea, M. Polini, R. Asgari and A.H. MacDonald, *Chirality and correlations in graphene*, *Phys. Rev. Lett.* 98, 236601 (2007)
- M. Polini and G. Vignale, *Spin-drag and spin-charge separation in cold Fermi gases*, *Phys. Rev. Lett.* 98, 266403 (2007)
- M. Polini, R. Asgari, Y. Barlas, T. Pereg-Barnea, and A.H. MacDonald, *Graphene: a pseudochiral Fermi liquid*, *Solid State Commun.* 143, 58 and cond-mat/07043786 (2007)
- S.H. Abedinpour, M. Polini, X. L. Gao, M. P. Tosi, *Density-functional theory of inhomogeneous electron systems in thin quantum wires*, *Eur. J. Phys. B* 56, 127 (2007)
- P. Capuzzi, I.A. Howard, N.H. March, M.P. Tosi, *First-order density matrices in one dimension for independent fermions and impenetrable bosons in harmonic traps*, *Phys. Lett. A* 361, 261 (2007)
- S.H. Abedinpour, M. Polini, X.L. Gao, M.P. Tosi, *Emergence of Wigner molecules in one-dimensional systems of repulsive fermions under harmonic Confinement*, *Phys. Rev. A* 75, 015602 (2007)
- X.-L. Gao, M. Rizzi, M. Polini, R. Fazio, M.P. Tosi, V.L. Campo Jr., K. Capelle, *Luther-Emery phase and atomic density waves in a trapped fermion gas*, *Phys. Rev. Lett.* 98, 030404 (2007)
- S.H. Abedinpour, M.R. Bakhtiari, X.-L. Gao, M. Polini, M. Rizzi, M.P. Tosi, *Phase behaviors of strongly correlated Fermi gases in one-dimensional confinements*, *Laser Phys.* 17, 162 (2007)